Structural modelling of the complex Cenozoic zone of the Levant Basin offshore Lebanon

Ramadan Ghalayini

Université Pierre et Marie Curie

Ecole doctorale Géoscience Ressources naturelles et Environnement

Institut de Sciences de la Terre de Paris, ISTeP

Structural modelling of the complex Cenozoic zone of the Levant Basin offshore Lebanon

Par Ramadan Ghalayini

Thèse de doctorat de Géoscience

Présentée et soutenue publiquement le 9 Juillet 2015

Devant un jury composé de :

Dominique FRIZON de LAMOTTE	Professeur U. Cergy-Pontoise (Rapporteur)
Olivier DAUTEUIL	Directeur de recherche CNRS, U. Rennes (Rapporteur)
Eric BARRIER	Chargé de recherche CNRS, Sorbonnes Universités Paris VI (Examinateur)
Sylvie LEROY	Directeur de recherche CNRS, Sorbonnes Universités Paris VI (Examinatrice)
Christian BLANPIED	TOTAL (invité)
Catherine HOMBERG	Maître de conférence, Sorbonnes Universités Paris VI (Directrice de thèse)
Jean-Marc DANIEL	IFPEN (Co-Directeur de thèse)
Fadi Henry NADER	IFPEN (Co-Directeur de thèse)

STRUCTURAL MODELLING OF THE COMPLEX CENOZOIC ZONE OF THE LEVANT BASIN OFFSHORE LEBANON

Ramadan Ghalayini

__ *"All faith is false, all faith is true;*
truth is the shattered mirror strewn
in myriad bits; while each believes
his little bit the whole to own" __

Sir Richard Burton, *The Kasidah*

I dedicate this work to my family

Acknowledgements

My first and most earnest acknowledgement goes to Fadi Nader for his help, support and advices for the past few years. An unexpected meeting with Fadi at the Geological Society of London in February 2011 has set the path for this project and initiated a long lasting passion in the geology of this complicated Middle East region. I also deeply acknowledge my supervisor at Paris VI, Catherine Homberg, for her constant support, guidance and advices throughout the past three years. Jean-Marc Daniel is greatly acknowledged for his constant assistance and advices knowing his very tight schedule. His enthusiasm and practicality made work with him a pleasure. I appreciate everything I learnt from my supervisors during this project.

This work was sponsored by TOTAL of which I would like to kindly thank Anne Lesueur and Charlotte Nielsen for their kind support and advices. I am also indebted for PGS for providing the seismic data, and particularly to Per Helge Semb for his help and John Comstock for his enthusiasm and the discussion we had. The Lebanese petroleum administration in general and Wissam Chbat in particular are greatly acknowledged for their support.

I am very thankful for the members of the examining committee: Dominique Frizon Delamotte, Olivier Dauteuil, Eric Barrier and Sylvie Leroy who accepted to be part of the jury and attended the final presentation. Special thanks to the reviewers of the articles published within this study, and mainly Prof. Chris Jackson for his comments and insights in the course of this project. I would like to thank Lucien Montadert for his insights, advices and fruitful discussions we had on Mediterranean geology. His enthusiasm is inspiring. I also owe a debt of gratitude to Maroun Ijreiss from the American University of Beirut for his kindness and help throughout the past few years, finding every old and rare manuscript, thesis and map on the geology of the Middle East he has in his priceless library at his office. Far too many people to mention individually have assisted me in many ways during my work at IFPEN. Special thanks to Jean-Marie Mengus and Romain Darnault for their help and guidance during analogue modelling. I also acknowledge Marie-Claude Lynch for her friendliness and help scanning the models.

Many people are thanked throughout the last three years for their friendship and the unforgettable time we spent together. Perhaps my warmest regards go to the friends at CIUP: Andrea and Andrea, Oli, Pietro, Eduardo, Olivier, Regina, Sabrina, Thi Minh, Wassim, Sarah, Sandy, the garden team, the classical music buddies and many many others for the good moment cooking in the kitchen or partying every weekend in the houses of the cité. Special thanks to all the residents of the cité universitaire who made those three years remarkable and rich in experiences from every part and corner of the world. The music, operas, art and museums nights will stay forever in my heart for no better artistic experience can be found in a city other than the city of lights Paris. I will never forget all the concerts I attended at opera Garnier and Bastille and those I performed at in many places. Thanks for Ali Ayoubi and the Murex people for the continuous outing we had in Paris eating out and laughing next to the Eiffel Tower. For Lamia keeping up with my nagging in the last few years, motivating me and pushing me to be better, thank you for your understanding and for everything. A PhD is a selfish activity indeed.

My office mates are warmly regarded for the fun times spent at IFPEN and UPMC and the smart discussions we had. Felipe, Laura, Julia, Maelianna, Marine, Josselin, Vassylis, Richard, Anouk, Dante, Camille, Virginie, Lucas, Nikolaus and Nicolas and many others of whom I apologize if I didn't mention them for they are so many. For the interns who worked on the Levant Basin and other projects, even though they stayed for a short time but their presence was remarkable: France, Cyprian, Katreine, Nemo and Aurely. We spent wonderful and exciting times with Vincent and Elodie working for the AAPG student chapter and with the following year's committee organizing trips abroad and field excursions together. Exciting times were spent in Hungary and other countries in the framework of AAPG looking at the local geology and culture. For this, I warmly thank Orsolya Gyori for her exciting enthusiasm in carbonate sedimentology and diagenesis, especially when trying to explain the local geology and pursuing me to abandon structural geology and shift to carbonates. Although this will never happen, but I do acknowledge however that I hold more appreciation to carbonates now.

Lastly and most importantly, I am very grateful and indebted to my family. Thank you for getting me this far in life, supporting me and motivating me. Thank you for your love, encouragement and never-ending support.

Abstract

The Levant Basin is located at the easternmost Mediterranean at the intersection of three major tectonic plates (Africa, Arabia, Eurasia and the smaller Anatolian microplate). The Levant Fracture System (Arabia-Africa plate boundary) borders the basin to its east and represents a 1000 km long left-lateral transform system linking rifting in the Red Sea with plate convergence along the Taurus Mountains (Arabia-Eurasia plate boundary). The Levant Basin is bordered to the north by the Cyprus Arc (Africa-Eurasia plate boundary). The interaction between these tectonic plates had important consequences on the evolution of the Levant Basin whereby its eastern boundary has been affected by deformation along the Levant Fracture System. This major plate boundary is associated with a restraining bend in Lebanon and has been active since the Late Miocene.

Until recent days, the absence of seismic data in the central Levant Basin was an obstacle against characterizing the tectonic setting of the basin. In this area, the geometry, kinematics and the age of the tectonic structures are poorly understood. A focal question thus remains on how the Levant Basin was affected by this adjacent plate boundary. Therefore, what is the impact of the deformation along the Levant Fracture System since the Late Miocene on this basin and how can we assess it? Has the latter been affected by other tectonic regimes prior to the onset of transpression? If so, how would the existing structures influence the style of modern deformation?

In this study, high quality 2D and 3D seismic reflection data (with two 4290 m^3 3D seismic cubes and seven 830 km long 2D seismic lines) were interpreted allowing identification and timing of the structures in the Levant Basin offshore Lebanon. Several fault families, mapped along the margin, are remnants of a lasting and complex tectonic history since Mesozoic times. These include NNE-SSW striking thrust faults active during the early Tertiary and inactive since the Pliocene; NNE-SSW striking anticlines folded during the Late Miocene and overlying pre-existing structuresd; and ENE-WSW striking dextral strike-slip faults inherited from Mesozoic times and reactivated during the Late Miocene. Only the dextral strike-slip faults show evidence of current activity and are interpreted to be linked to transpression along the Levant Fracture System. They constitute the westward extension of the plate boundary, formed under a transpressif regime and a NW-SE compression. We have showed how this plate boundary has

evolved through the Neogene with a decrease in the shortening component during the Pliocene.

The identification of pre-existing structures along the eastern Levant margin shed the light on the deep structuration affecting this area, inherited from Mesozoic tectonic events. The impact of these structures was tested through analogue modeling. Results indicated a considerable impact of pre-existing structures on the development of the restraining bend, localizing deformation at the onset of transpression and responsible of segmenting the restraining bend along an ENE direction. These ENE-WSW faults are thus major and are most likely associated with the deformation affecting the Palmyra basin since the Mesozoic, which is thus extending westward to Lebanon. This study has shown the important role of a margin on a strike-slip plate boundary. Namely, the development of antithetic faults (local dextral strike-slip faults in a regional sinistral strike-slip plate boundary) known in other similar plate boundaries is associated with a deep crustal anisotropy localizing the subsequent deformation.

On the other hand, the deep Levant Basin contains a NW-SE trending dense normal fault array, in contrast with crustal structures similar to the one described along the margin. The faults are remarkably layer-bound, contained in the Oligo-Miocene units only. Quantitative and qualitative seismic analysis of these normal faults was performed, yielding important information on their growth and evolution. Results showed that they nucleated during the Early Miocene as a result of volumetric contraction of the Oligo-Miocene host rock units. This hypothesis has consequences on our understanding of the geology of the Levant Basin as it requires that the Oligo-Miocene is formed by fine-grained sediments for faults to develop. Interpretation of fault displacement profiles also indicated that a strong mechanical stratigraphy affected their growth. The detailed 3D seismic characterization of these faults has provided insights on the growth of non-tectonic faults in sedimentary basins, most likely following the isolated fault model. This array in Lebanon provided a unique case-study whereby the interpretation results served to better understand the growth and evolution of polygonal faults, linearly oriented due to an anisotropic stress field.

Résumé

Le bassin de Levant, localisé à l'extrémité la plus orientale de la Méditerranée, se situe à jonction de trois plaques tectoniques majeures (Afrique, Arabie, Eurasie ainsi que la microplaque Anatolienne). Il est bordé à l'Est par la faille du Levant (frontière Arabie/Afrique), qui représente un système transformant de 1000 km de long, reliant le rift dans la Mer Rouge au sud avec la zone de convergence le long du Taurus au nord (frontière Arabie/Eurasie). Son extrémité nord est marquée par la frontière convergente Afrique/Anatolie soulignée par l'arc de Chypre. Le bassin Levantin a enregistré l'interaction entre ces différentes plaques au cours du Cénozoïque et sa bordure Est a été en particulier déformée par la mise en place de la faille du Levant. Cette limite de plaque majeure est marquée au Liban par un relais compressif qui a été actif depuis la fin du Miocène.

Jusque récemment, l'absence de données sismiques dans la partie centrale du bassin levantin (offshore Liban) a constitué un handicap important dans la caractérisation de ce basin. Dans ce secteur, la géométrie, cinématique, l'âge des structures tectoniques ne sont pas connus. Plusieurs questions en découlent. Quel est impact de la frontière transformante du Levant sur la structure du bassin? Le bassin a-t-il enregistré d'autres déformations au cours du Cénozoïque ? Quel est l'effet de la structuration ancienne et profonde de la marge sur la déformation actuelle ?

Ce travail s'est appuyé sur l'interprétation des données sismiques 2D et 3D de haute qualité dont deux cubes 3D de 4290 m^3 et sept lignes 2D de 830 km de long. Cette étude a permis d'identifier les structures tectoniques affectant le secteur offshore Libanais et de caractériser leurs origines. Plusieurs familles de failles tout au long de la marge Est du bassin ont été identifiées et témoigne d'une histoire tectonique méso-cénozoïque longue et complexe. Les structures reconnues sont tout d'abord (1) des failles chevauchantes NNE-SSW actives depuis le début du Tertiaire jusqu'à la fin Miocène, (2) des anticlinaux NNE-SSW formés durant le Miocène supérieur et se localisant sur des structures préexistantes et (3) des failles décrochantes dextres, héritées des structures mésozoïques et réactivées durant le Miocène supérieur. Seules les failles décrochantes dextres montrent des preuves d'une activité actuelle, liée à la transpression au long de la faille du Levant. Ces structures constituent le prolongement vers l'ouest de la frontière de plaque du Levant sous un régime transpressif et une compression NW-SE. Nous mettons en évidence que cette frontière de plaque montre une évolution au

cours du Néogène avec une forte décroissance de la composante de raccourcissement à partir du Pliocène.

La mise en évidence de jeux plus anciens témoigne d'une structuration profonde E-W de la marge, vraisemblablement héritée des tectoniques mésozoïques. L'impact de cette structuration a été évalué à travers une modélisation analogique. Les résultats démontrent le rôle considérable de cet héritage sur l'évolution du relais compressif de la faille du Levant au Liban, entre autre en localisant la déformation le long de couloirs E-W et en segmentant les structures transpressives NNE-SSW. Ces résultats nous conduisent à interpréter les structures E-W comme majeures et traduisant la prolongation vers l'ouest du bassin mésozoïque des Palmyrides. Nous mettons ici en évidence le rôle majeure d'une marge sur la structure d'une frontière de plaques transformante. Le développement de failles antithétiques (failles dextres dans une frontière transformante senestre), connus dans d'autres frontières de ce type, est ici clairement associé à une anisotropie profonde forçant la localisation de la déformation.

La partie profonde du bassin du Levant est dépourvue des structures profondes comme décrites plus haut. En revanche, elle contient un réseau de failles normales NW-SE, particulièrement remarquable du fait de son caractère dense et de son confinement aux seules unités Oligo-Miocène. Ce réseau a fait l'objet d'une étude de détail, avec l'observation de séquences syn-cinématiques, la caractérisation des dimensions et profils de rejets de ces failles. Ces analyses ont montré qu'elles se sont formées au début Miocène en raison d'une contraction volumétrique des sédiments. Cette interprétation a de fortes implications sur la nature des sédiments offshore et suppose la présence de niveaux argileux et autres sédiments fins dans l'Oligo-Miocène. L'interprétation des profils de rejet a aussi conduit à souligner une stratigraphie mécanique notable qui pourra servir de base à proposer un modèle stratigraphique des unités cénozoïques de l'offshore profond. Par ailleurs, l'étude détaillée et tridimensionnelle de ces failles fournit de nouvelles contraintes sur la croissance des failles non tectoniques dans les bassins sédimentaires. Nous montrons que ces failles non tectoniques suivent un modèle de croissance à l'échelle du bassin de type faille isolée. L'étude de ce réseau de failles au Liban constitue un des grand réseau de failles non tectonique où les résultats ont conduit à une meilleure compréhension de la croissance des failles polygonales qui sont bien alignés sous l'effet d'un champ de contrainte isotropique.

Table of contents

CHAPTER I

INTRODUCTION

I. Introduction

"The memory of everything is very soon overwhelmed in time" Marcus Aurelius

The north-western part of the Arabian Plate is marked by important geologic features making this region unique for the understanding of the evolution of tectonic plate boundaries and their interactions. The break-up between Arabia and Africa during the Eocene [*McKenzie*, 1970; *Beydoun*, 1988; *Cochran and Karner*, 2007; *Fournier et al.*, 2010] and the closure of the Neo-Tethys ocean to the North are major geodynamical processes that had profound impacts on the geology and tectonics of the actual Eastern Mediterranean region. In the previous century or so, numerous studies aimed at shedding more light on the evolution of the north-western Arabian Plate in Syria and Lebanon through extensive fieldwork and geophysical techniques [e.g. *Dubertret*, 1955; *Renouard*, 1955; *Ponikarov*, 1966; *Brew*, 2001; *Wdowinski et al.*, 2004; *Le Pichon and Kreamer*, 2010]. The outcome is a wealth of data on the onshore geology and a fair amount of knowledge on the tectonics of the region. Nevertheless, an important piece of data was missing and a question remained without a clear answer for a long time: 'what is the geology of the Eastern Mediterranean Basin (offshore) and how does it relate to the evolution of north-west Arabia?'

Located in today's Eastern Mediterranean region along the north-western margin of the Arabian Plate, the Levant Basin is bordered by the Anatolian microplate and the Larnaca thrust to the North, Arabian plate to the East, African plate to the south and the Eratosthenes seamount to the west (Figure 1.1). Previous studies documented the southern part the basin (offshore Israel) [*Garfunkel*, 2004; *Gardosh and Druckman*, 2006; *Gardosh et al.*, 2010] and the most north-eastern corner (Lattakia Ridge) [*Hall et al.*, 2005a, 2005b; *Bowman*, 2011]. They demonstrated that this area was first shaped by the Early Mesozoic rifting and that several episodes of fault reactivation occurred since the Late Cretaceous time as the result of the Afro-Arabia/Eurasia convergence [e.g. *Jolivet and Faccenna*, 2000; *Stampfli and Hochard*, 2009; *Frizon de Lamotte et al.*, 2011]. These structures are known in the southern Levant as forming the curved Syrian Arc

belt running from northern Egypt to the Palmyrides in Syria and developed both onshore and offshore [*Walley*, 1998]. In the Northern Levant, the Lattakia Ridge System have switched from being compressive starting in the Maastrichtian to a strike-slip regime in the Late-Miocene as a result of regional geodynamic changes [*Hall et al.*, 2005a; *Le Pichon and Kreamer*, 2010]. The central part of the Levant Basin offshore Lebanon was never before investigated with modern scientific tools so that its geology and tectonic evolution are still not constrained. Its geological history must have been controlled by the interaction of these tectonic plates and involves rifting in the Permo-Jurassic, compression and inversion in the Late Cretaceous-Tertiary and strike-slip movement with variable degrees of transpression in Late-Miocene/Pliocene. These different tectonic events made the present day eastern Mediterranean region a geologically complex province whereby different structural styles overlap and overprint each other.

Bordering the basin to the East, the Levant margin extends from Syria, Lebanon, Israel to Northern Sinai (Figure 1.1). An important element of this margin is the Levant Fracture System (LFS) forming the north-western Arabian plate boundary with Africa. The main fault passing through Lebanon is the NE-SW Yammouneh fault, connecting the Dead Sea Transform in Israel with the Ghab segment in Syria (Figure 1.1) part of the Levant fracture system (LFS) [*Quennell*, 1958, 1984; *Dubertret*, 1972]. The complexity and variable geometry of the LFS have fostered large debates in academia around its timing, displacement variation, shortening rate and relationship with regional tectonics. All of them remain till present the most peculiar scientific problems in this region [for a review see *Beydoun*, 1999]. The uncertainty regarding the displacement and shortening along the LFS onshore has lead certain authors to propose that the missing shortening should be accommodated offshore through folding [*Gomez et al.*, 2007b; *Homberg et al.*, 2010], while others argue of an actual fold and thrust belt offshore Lebanon currently accommodating all deformation along the LFS based on shallow 2D seismic lines [*Elias et al.*, 2007; *Carton et al.*, 2009]. The unavailability of high quality seismic data during past years did not allow proving or disproving such hypothesis. Alternatively, other models were proposed to explain the problems associated with the LFS in Lebanon, such as linking the deformation to the one in the Palmyrides [*Walley*, 1998] thus necessitating a younger age for folding onshore Lebanon prior to the establishment of the LFS [*Dubertret*, 1972; *Beydoun*, 1999].

The question on the timing of folding along the Levant margin in Lebanon has been fostering debate for a long time. Several authors link the uplift and folding of Mount Lebanon to the transpressive activity along the LFS of Late Miocene time

[*Hancock and Atiya*, 1979; *Daeron*, 2005; *Gomez et al.*, 2006; *Elias et al.*, 2007; *Homberg et al.*, 2010] while others argue for an older folding time, of Early Miocene or older based [*Renouard*, 1955; *Dubertret*, 1972; *Walley*, 1998; *Beydoun*, 1999]. This question is tightly related to the nature of Levant margin. Does this margin represents a transform boundary accommodating N-S Mesozoic extension as proposed by Dewey *et al.*, [1973] and Stampfli and Borel, [2002] or is it a passive margin that underwent NW-SE extension during Mesozoic and was inactive ever since, except during Cenozoic inversion [*Garfunkel and Derin*, 1984; *Garfunkel*, 1998; *Gardosh et al.*, 2010]? It is also likely that the Levant margin is an extension of the Palmyra basin in Syria with a continental crust gradually thinning westward [*Khair et al.*, 1993; *Segev et al.*, 2006] insinuating a deformation synchronous with the Palmyrides [*Walley*, 1998]. The lack of data onshore Lebanon and in the Levant Basin is challenging when confirming the previous hypotheses, causing an absence of models explaining the Mesozoic structuration of Lebanon that is possibly affecting the style of deformation during the Cenozoic.

A likely model to explain the deformation along this major plate boundary necessitates an investigation of the central Levant Basin offshore Lebanon by means of seismic data (only recently acquired and made accessible). This PhD project thus aims to examine the effect of a large plate boundary on the evolution of adjacent basins. Similarly, in structurally complex regions with limited dataset, how can the evolution of a plate boundary, or a complex margin, be constrained by investigating the adjacent basin?

This project uses modern techniques and implements a new workflow in order to understand structurally complex basins, such as the Levant Basin. The usage of regional 2D seismic lines and 3D seismic cubes allows documenting the main tectonic elements of the basin and provides a very accurate characterisation so that timing and mechanism of deformation can be constrained in detail. Accordingly, a geologic model for the evolution of the Levant Basin offshore Lebanon is proposed serving as an analogue to other basins with similar complexities. The workflow undertaken through this project is believed to be applicable in other provinces with similar geological contexts. It consists of applying seismic interpretations and then validates resulted findings through analogue modelling. Consequently, this work aims at limiting uncertainties on the evolution and impact of the Levant Fracture System on the north-western Arabian Plate in general, and the Levant region in particular. The proposed geologic model will serve as an example on how can we relate this deformation offshore to the widely documented deformation onshore. Even though this project is not focused

on the geologic evolution of Lebanon itself, the geology of the adjacent Levant Basin, as will be presented in this thesis, is thought to be tightly affected by deformation along the margin, and hence a corollary will be to try to explain the margin by understanding the meticulous geology of the Levant Basin. Results of this PhD project presented new insights on the structural evolution of the northern Levant basin during the Cenozoic.

Recent high quality 3D seismic data set provides an unequal opportunity to study in detail the Levant Basin and its eastern margin along Lebanon. Such studies lead to better constrain and understand the stratigraphy and geodynamics of the northern Levant Basin [e.g. *Montadert et al.*, 2010; *Lie et al.*, 2011; *Hawie et al.*, 2013]. This complements the large amount of literature existing on the stratigraphy, tectonic evolution and crustal structure of the southern part of the basin based on well and seismic data [*Makris et al.*, 1983; *Mart*, 1984; *Hirsch et al.*, 1995; *Ben-Avraham et al.*, 2002; *Garfunkel*, 2004; *Gardosh and Druckman*, 2006; *Gardosh et al.*, 2006, 2011; *Netzeband et al.*, 2006; *Gvirtzman et al.*, 2008]. However these recent studies do not provide information on the tectonic structures offshore Lebanon, hence necessitating a new investigation focused on the structural elements of the basin as presented in this thesis. Nevertheless, they provide an essential framework for the sedimentary architecture of the basin that is tightly linked to tectonic events.

This manuscript is divided intro various parts based on the work performed during this project. These include three sections on the results and a final discussion chapter to integrate all findings. The methodologies adopted in the course of this project are summarised in the three results chapters because they were written in the form of an article and the methodology differs depending on the purpose of the study.

- *Chapter 1,* Introduction: this chapter presents the aims and motivations of this thesis.

- *Chapter 2,* Regional geology: this section is a dense review of literature on the structural aspect and the tectonic evolution of the region encompassing the Levant Basin and margin, north-western Arabia, north-eastern Africa and southern Anatolia.

- *Chapter 3,* The general structural setting of the basin: in this section, results of the seismic interpretation and the methodology adopted are discussed in the form of a published article: *"Impact of Cenozoic strike-slip tectonics on the evolution of the northern Levant Basin (offshore Lebanon)"* [*Ghalayini et al.*, 2014].

- *Chapter 4,* Analogue modelling: this section is focused on the modelling part of this project, whereby the methodology, results and impacts of this study are discussed. Sandbox models were constructed in order to confirm the suggested hypothesis on reactivation of pre-existing structures into a dextral strike-slip movement and test certain conceptual models on the evolution of the margin.

- *Chapter 5,* Layer-bound normal faulting in the Levant Basin: in this section, results of the 3D seismic characterisation of a NW trending layer-bound normal fault array and the methodology adopted are discussed in the form of an article currently in review: *"Growth of contractional layer-bound normal faults under a regional anisotropic stress field"*.

- *Chapter 6,* Discussion: this last section discusses the various results of this project and integrates the finding into a new 3D geologic model of the Levant Basin. The pertinence of this project regarding available literature is also discussed and focused on the importance of adopting this workflow and integrating various techniques in order to limit uncertainty in structurally complex basins worldwide. Finally, the effect of the new model on the petroleum system is discussed.

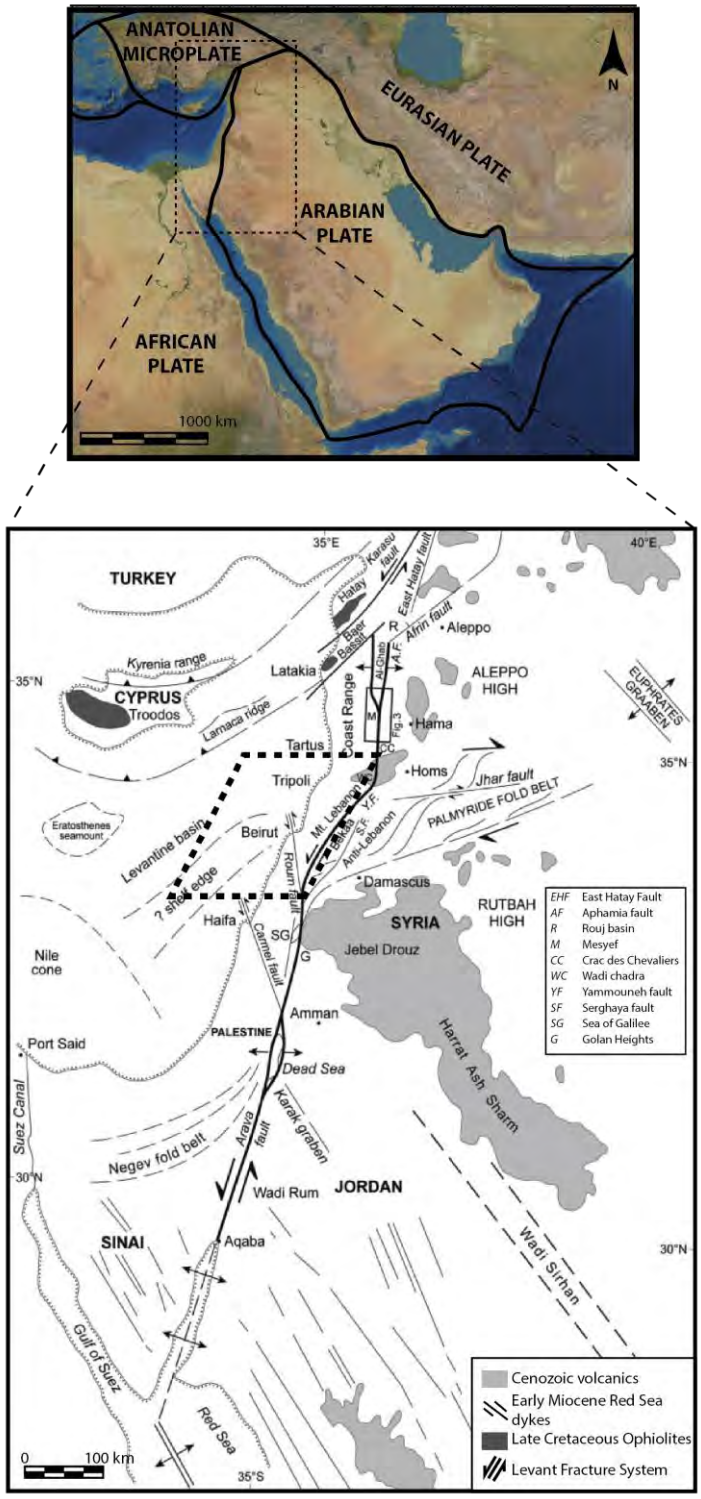

Figure 1.1: Regional tectonic map of the Arabian plate with the adjacent plates nearby and a zoom in on the Levant Region showing the existing structures. The study area offshore Lebanon is indicated in dashed lines. Modified from Searle *et al.* [2010] and Brew *et al.* [2001].

CHAPTER II

REGIONAL GEOLOGY

Table of contents

II. Regional Geology

"Stop acting so small. You are the universe in ecstatic motion" Rumi

The aim of this study is to analyse and investigate the geology of the Levant Basin. An extensive literature review is thus summarised in this chapter, mainly targetting the well documented Levant margin, and to a lesser extent discussing the little existing data on the Levant Basin. First, the current tectonic setting will be briefly described. Second, pre-Neogene tectonic history will be elucidated. The latter consists of rifting and inversion, resulting in numerous crustal structures that will influence later deformation. Third, the Neogene tectonic history follows, largely involving the evolution of the Levant Fracture System.

II. 1Current tectonic setting

The Levant Basin is found at the north-western boundary of the Arabian plate. The latter includes the Arabian Peninsula, the Fertile Crescent, the Levant countries as well as south-eastern Turkey and south-western Iran, lying to the south and south-west of the Taurus-Zagros crush zone (Figures 2.1). The tectonic framework of the region is made up of a craton occupying the greater part, consisting of the exposed crystalline basement commonly termed the Arabian shield to the west, and the Arabian sedimentary platform bordering this outward to the east and north-east (Figure 2.1). The Arabian shield was separated by a rifting process that started in Afar (Africa) and propagated eastward and northward creating the Gulf of Aden and the Red Sea, respectively [*Martinez and Cochran*, 1988]. The Levant region in the North-West is dominated by the Levant Fracture system, featuring sinistral strike-slip tectonics and transpression.

The Arabian plate thus exhibits three types of plate boundaries: (1) extensional rift-related in the west and south with Africa, (2) compressional with continent-continent collision in the north and north-east with Eurasia, and (3) strike-slip along the north-west with transtensional and transpressional tectonics with Africa. The strike-

slip plate boundary in the Levant region is the locus and the prime concern of this study, particularly in Lebanon and its immediate offshore in the Levant Basin.

Figure 2.1: Map showing the location of the Levant Basin relative to the Arabian, Anatolian, Eurasian and African plates together with major tectonic elements of the region (Modified from Alsharhan and Nairn 2003, Arsenikos *et al.* 2013 and Frizon de Lamotte *et al.* 2011).

Present day kinematics of the Arabian plate are indicated from an extensive GPS network coverage of the East Mediterranean and Middle East region [e.g. *McClusky et al.*, 2003; *Reilinger et al.*, 2006]. An important aspect of the recorded GPS velocity field is that the present-day regional kinematics is dominated by circular counterclockwise motion (Figure 2.2). Most of Arabia obeys a rigid rotation with respect to the Arabia-Eurasia following an AR-EU pole located west of Egypt (Figure 2.2). The present Arabia rotation has been going on at a steady rate since 40 Mya with relatively fast velocity of 20–30 mm.year^{-1} [*Reilinger et al.*, 2006; *Le Pichon and Kreamer*, 2010]. In contrast, the

Anatolia-Aegean rotation is much younger, as it started less than 12 Mya [*Le Pichon and Kreamer*, 2010] and is characterized by a rotation with respect to the Anatolia-Eurasia (AT-EU) pole (Figure 2.2) with an increasing rotational velocity from Anatolia to the Aegean area. Velocity increases by a factor of approximately 2 from east Anatolia to the Aegean, which implies important extension, having an important north-south component in the Aegean area [*Le Pichon and Kreamer*, 2010].

The Anatolian rotation extends south into the Levant area. Being close to AT-EU pole of rotation, the motion of the Levant area with respect to Eurasia is relatively small. The directions of the vectors are significantly different from both the Arabian and African plate motions [*Reilinger et al.*, 2006]. This indicates that westward of the Levant Fracture System, the Levant region and the Sinai block are moving independently of the Arabian plate and follow a very similar motion as the Anatolian microplate [*Le Pichon and Kreamer*, 2010]. The directions of the vectors in the Levant and Sinai fit quite well the tight curvature expected with the proximity of the AT-EU pole of rotation.

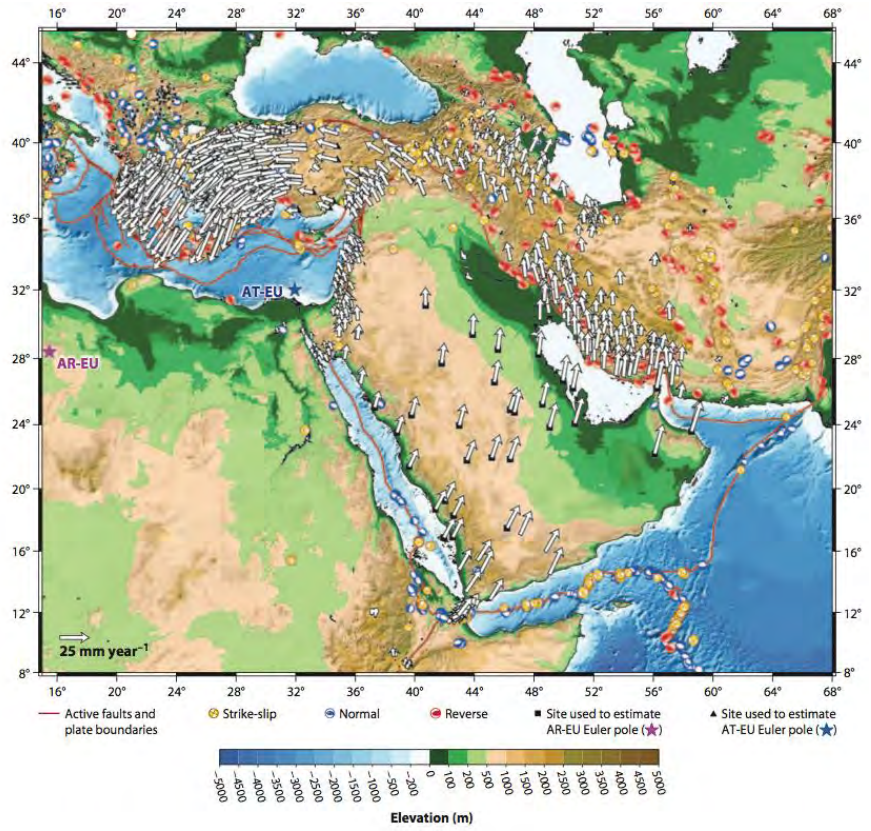

Figure 2.2: Regional GPS velocities of the Arabian and Eurasian plates relative to Eurasia. The rotation poles for Anatolia and Arabia are marked with AT-EU and AR-EU respectively. From Le Pichon & Kreamer [2010].

II. 2 Pre-Neogene geological history of the Levant

The Arabian basement was formed through cratonization by arc accretion culminated about 640 Ma [*Beydoun*, 1993]. They resulted in N-S sutures that have probably affected the deformation style in later times. The basement was consolidated in the Late Proterozoic and terminated with the convergence, collision and suturing of Arabia with Eurasia which began in the Mid-Tertiary. This continent-continent collision initiated the Zagros orogeny which commenced in the Late Eocene and culminated in the Pliocene – Holocene. It has resulted the Zagros orogen by suturing of the Arabian and Eurasian plates and overprinted the Zagros foreland basin on the outer edge of the Northeastern Arabian margin shelf [*Beydoun*, 1993].

The pre-Neogene geological history of the Levant region spans the times following the consolidation of the Arabian craton till the establishment of the Levant Fracture System. Prior to the Permian period, no significant tectonic events were recorded. Instead, the Paleozoic era was dominated by tectonic quiescence and accumulation of a sedimentary cover during several depositional cycles in Arabia and the Levant [*Alsharhan and Nairn*, 2003]. Igneous activity was sparse in this period but severe volcanic events succeeded during and after the breakup of Gondwana in the Late-Paleozoic to Early Mesozoic. The Late Cretaceous to Neogene includes several discrete, more or less widespread, tectonic events in relation with the interaction of the Arabian, African and Eurasian plates. The following sections briefly discuss the different tectonic regimes in the Eastern Mediterranean and the Levant region starting the Late Palaeozoic.

II. 2.1 Rifting and extension

The Levant basin was formed by the breakup of Gondwana and Eurasia during the Late Palaeozoic to Early Mesozoic period in different pulses [*Garfunkel and Derin*, 1984; *Robertson*, 1998a]. This was accompanied by continental breakup, rifting and drifting of various micro-continental blocks [*Robertson and Dixon*, 1984; *Garfunkel*, 1998; *Robertson*, 1998b, 2007] resulting in opening of marine basins in the present day location of the Eastern Mediterranean. The different structural events resulted in creating the Palaeotethys and Neotethys oceans (Figure 2.3).

Although the exact timing and location of rifting are still under debate [*Robertson and Mountrakis*, 2006], there is a general consensus that the most important

rifting stage took place in the Early Jurassic [*Ben-Avraham et al.*, 2002] accompanied by magmatic activity [*Gardosh et al.*, 2010] and caused variation in thicknesses of strata [*Druckman*, 1984; *Garfunkel and Derin*, 1984; *Druckman et al.*, 1995; *Alsharhan and Salah*, 1996; *Garfunkel*, 1998; *Hirsch et al.*, 1998; *Brew et al.*, 2001b; *Sawaf et al.*, 2001; *Gardosh et al.*, 2006]. This volcanic activity is recognized in the offshore Levant basin through the magnetic anomalies interpreted as volcanic intrusions [*Gardosh et al.*, 2010]. Onshore, Jurassic basalts are found in Lebanon and Syria indicating that volcanism extended along the whole Levant margin [*Brew et al.*, 2001b]. Although the original location of the detached blocks and the growth history of the basin remain incompletely understood [*Garfunkel*, 2004] we could nonetheless expect to find the remnant rift geometries characterising extensional basins. These structures associated with Tethyan rifting are preserved and documented throughout the Levant onshore from the Palmyra area in central Syria to the Egyptian western desert [*Freund*, 1965; *Druckman*, 1984; *Garfunkel and Derin*, 1984; *Guiraud and Bosworth*, 1997, 1999; *Garfunkel*, 1998; *Brew et al.*, 2001b; *Sawaf et al.*, 2001; *Gardosh et al.*, 2010].

In Israel and Sinai thicknesses and facies variation in the lower Jurassic are identified at outcrops, in wells and seismic data [*Freund*, 1965; *Druckman et al.*, 1982; *Garfunkel and Derin*, 1984; *Alsharhan and Salah*, 1996; *Hirsch et al.*, 1998; *Gardosh and Druckman*, 2006]. Thickness variations in Mesozoic strata are also documented in the Palmyrides and other parts of Syria [*Brew et al.*, 2001b; *Sawaf et al.*, 2001]. This variation in thickness of the strata indicates that repeated differential motion with different extensional pulses sometimes accompanied by magmatic activity [*Gardosh et al.*, 2010] were taking place in the Eastern Mediterranean region. This resulted in the separation of various small continental blocks from the Afro-Arabian craton like the Tauride and Eratosthenes [*Robertson and Dixon*, 1984; *Le Pichon and Gaulier*, 1988; *Robertson et al.*, 1996; *Garfunkel*, 1998]. The different rifting pulses and extensional movements documented in the Levant basin are summarized below.

Box 2.1

The Paleotethys refers to oceanic basins of Late Palaeozoic to Early Mesozoic in age (pre-Mid Jurassic oceanic crust) while the Neotethys refers to oceanic basins that rifted and then opened during Early Mesozoic time, implying a Triassic-Early Cenozoic oceanic crust [*Robertson*, 2006; *Robertson and Mountrakis*, 2006].

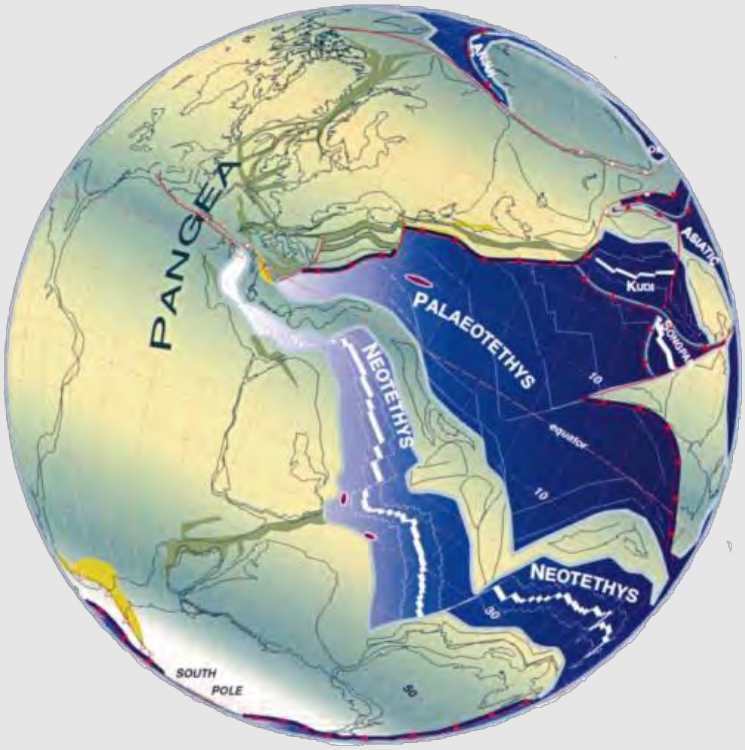

Figure 2.3: Paleogeographic map of the Permian-Triassic boundary (250Ma) showing the location of Paleotethys and Neotethys. From Stampfli and Borel [2002]

Late Palaeozoic rifting pulse

Evidence for a Late Palaeozoic continental breakup is found in the Palmyra basin in Syria and offshore Israel. In Syria, a 1 km thick Permian succession in a fault-controlled trough is is attributed to the Permian rifting event [*Garfunkel*, 1998; *Brew et al.*, 2001b; *Sawaf et al.*, 2001]. In the Mediterranean, a Permian section of several tens to a few hundred meters is found overlaying the Precambrian basement in the Gevim high imaged in seismic and well data (Figure 2.4). These stratigraphic relations would indicate the presence of two tectonic events in the Late Palaeozoic: a pre-Permian (probably carbonniferous uplift related to the Variscan orogeny) resulting in erosion of the Early Middle to Palaeozoic section and a Permian rift resulting in deposition of a thin Permian section [*Gardosh et al.*, 2010].

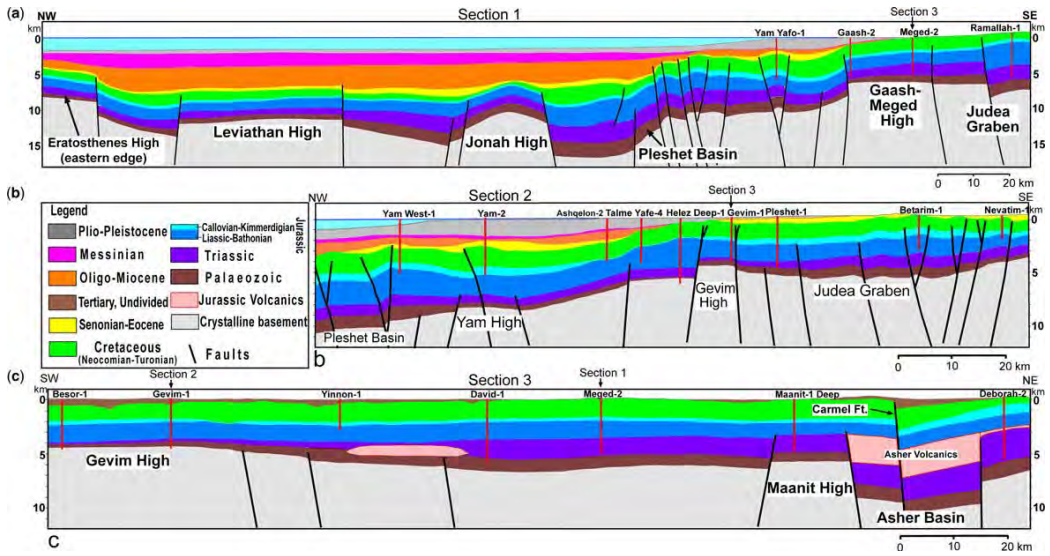

Figure 2.4: Geological cross-sections showing the main stratigraphic succession, faults and structural blocks on the Levant basin and margin. Thickness variations in the Paleaeozoic, Triassic and Lower Jurassic reflect syn-tectonic deposition, related to the development of an extensive graben and horst system during Tethyan rifting activity. The location of the sections is shown in the **Figure 2.5** (From Gardosh *et al.* 2010).

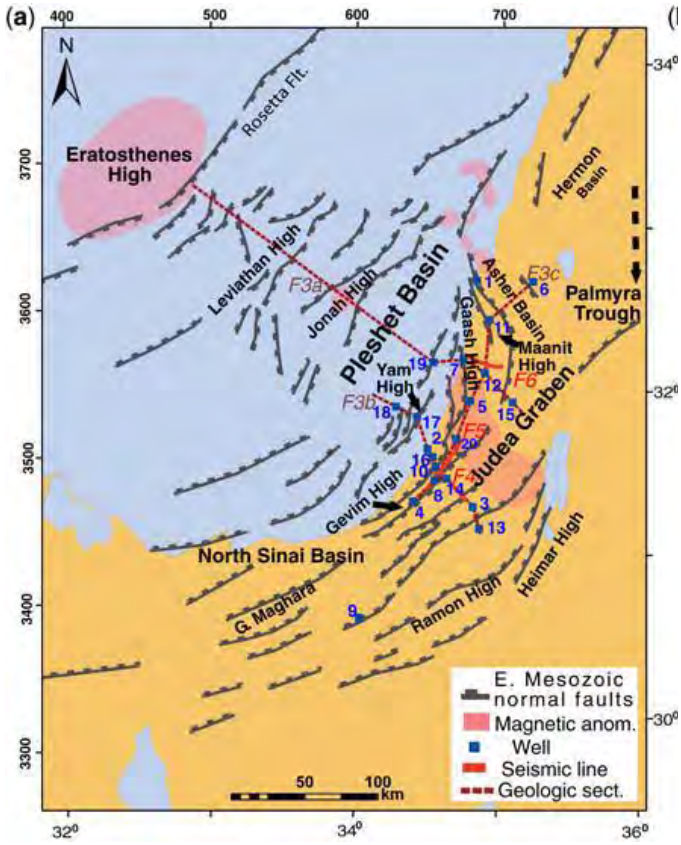

Figure 2.5: Map depicting inferred Triassic to Early Jurassic faults and structural highs and lows that were formed during Tethyan rifting activity. The geologic sections are shown in the Figure 2.4. From Gardosh *et al.* [2010].

Middle to late Triassic rifting pulse

The Early Triassic was a time of tectonic quiescence in the whole Levant Basin and the Palmyra trough [*Garfunkel*, 1998; *Brew et al.*, 2001b]. Following the Late Paleozoic pulse, faulting and extension continued during the Middle to Late Triassic, activating the inner basins, the coastal highs, and the offshore highs and lows [*Gardosh et al.*, 2010]. The ENE–WSW to NE–SW normal faults recognized in the Levant basin and along its eastern margin (onshore Israel) support a mean NW–SE extensional direction during this time.

Upper Triassic subsidence also took place within the North Sinai basin as indicated by the relatively thicker Carnian section at the bottom of wells [*Garfunkel and Derin*, 1984]. However, the Triassic subsidence and extension did not result in the development of a deep-water oceanic realm in the studied area [*Gardosh et al.*, 2010] although deep marine conditions north of the Levant are suggested [*Garfunkel*, 1998; *Robertson*, 1998a, 2007].

It is impossible to attest and quantify this deformation time in Lebanon due to the absence of Triassic outcrops and failure of onshore wells to reach deeper than Jurassic rocks (for a detailed review check Beydoun 1977, 1981).

Early to middle Jurassic rifting pulse

This appears to be the most important rifting pulse in the Eastern Mediterranean region [*Ben-Avraham et al.*, 2002] whereby severe vertical motion is documented in the Levant basin, evidenced by significant syn-sedimentary faulting [*Garfunkel*, 2004] and locally some igneous activity along the Israeli margin [*Garfunkel and Freund*, 1981]. It is unknown whether the Levant basin still shows deep marine conditions in this time. Shallow marine to fluvio-deltaic depositional environments are documented in the Lower to Middle Jurassic section throughout the Levant onshore in Israel which might indicate that Jurassic rift structures of the Levant area developed on a continental to shallow-marine platform [*Gardosh et al.*, 2010].

In Sinai, thickness variations in the Jurassic rocks are reported [*Moustafa*, 2010]. These variations are interpreted to be related to ENE-WSW oriented Jurassic basins in the North Sinai - Levant, separated by high areas containing a thinner Jurassic section. This indicate that extension and rifting in Sinai probably took place in the Early and Middle Jurassic epochs, whereas the Late Jurassic epoch was a period of gradual northward increase in thickness [*Moustafa*, 2010].

Similarly, the Palmyrides in Syria show reactivated Permian right-bounding faults during the Jurassic based on seismic profiles [*Chaimov et al.*, 1992, 1993; *Best et al.*, 1993]. This is accompanied with minor Lower Jurassic thickness changes within south-western Palmyride anticlines and the presence of two Jurassic depocenters centered around the Bilas block and the Bishri block [*Brew et al.*, 2001b; *Sawaf et al.*, 2001] (Figure 2.6). This is due to widespread faulting related to the Early to Middle Jurassic rifting pulses.

Extensional activity in the Levant Basin ceased during the Middle to Late Jurassic. The Bajocian-Oxfordian and the younger, Cretaceous section in the inner part of the Levant show minor thickness variations indicating tectonic quiescence [*Gardosh et al.*, 2010]. However, in onshore Lebanon, extensional geometries within the Kesrouan Formation are documented (Late Bathonian to Early Kimmeridgian) and are characterized by the creation of tilted fault blocks corresponding to the initiation of a

rifting phase in conjunction with intra-plate volcanism during the Kimmeridgian [*Collin et al.*, 2010].

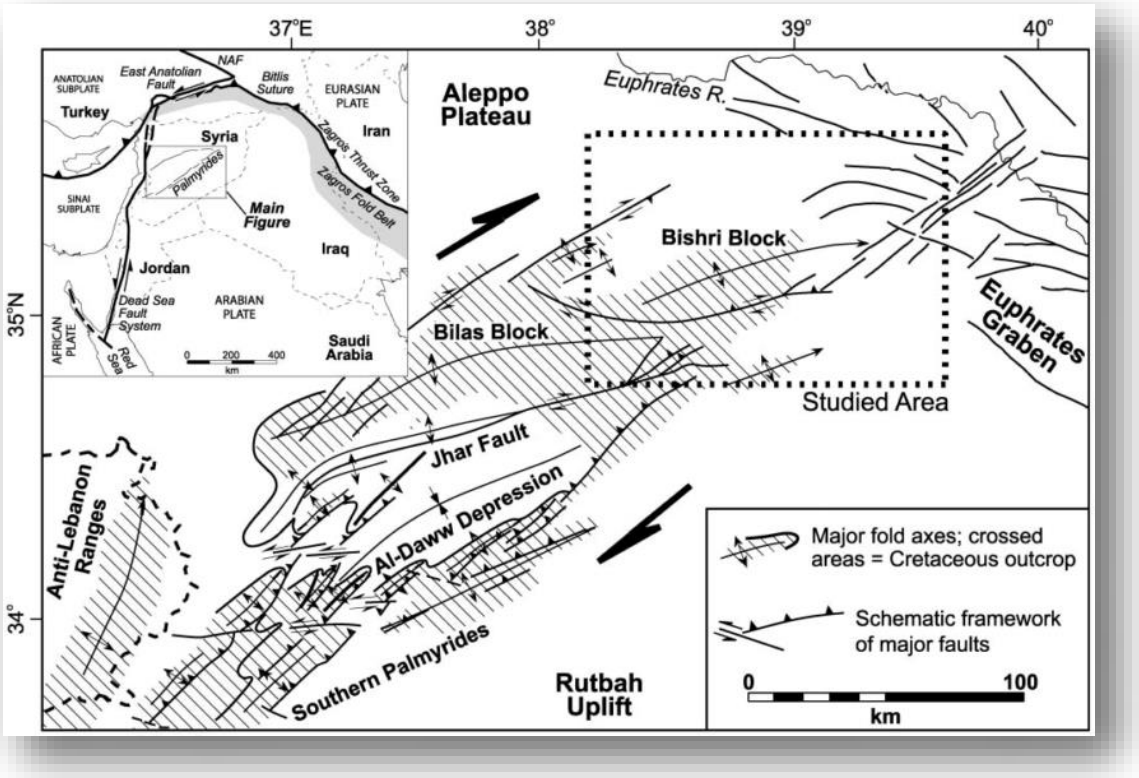

Figure 2.6: Schematic structure map of the Palmyra basin showing the location of Bilas and Bishri blocks together with major faults. From Brew *et al.* [2003].

The Early Mesozoic rifting activity was followed by subsidence and the formation of the deep marine Levant Basin in the eastern Mediterranean region [*Garfunkel and Derin*, 1984; *Garfunkel*, 1998]. Transgression in Bathonian times caused a predominantly carbonate sedimentation, extending far in to the platformal domain [*Garfunkel and Derin*, 1984] which showed some thickness variations in the Bajocian and Bathonian strata in the highs offshore Israel [*Gardosh et al.*, 2010]. Starting from the Middle Jurassic, a continental shelf and slope developed along the eastern margin of the basin. This continental margin slope, originally identified in deep wells near the present-day Israeli coastline [*Bein and Gvirtzman*, 1977; *Garfunkel*, 1998], formed a narrow transition zone, termed by Bein & Gvirtzman [1977] as the 'hinge-line'. It separated the Jurassic and Cretaceous shallow-marine shelf on the east from the deep marine basin on the west. The Mesozoic shelf-edge is identified near the modern

Mediterranean coastline from northern Egypt to western Lebanon [*Bein and Gvirtzman*, 1977; *Walley*, 2001].

Early Cretaceous extension

An Early Cretaceous extension is evidenced onshore Lebanon, and is believed to have caused large-scale thickness variations within the Lower Cretaceous sedimentary sequence [*Homberg et al.*, 2010] together with an abrupt thickening of terminal Jurassic carbonates [*Walley*, 1998]. The widespread Kimmeridgian basalts and tuffs [*Collin et al.*, 2010] attest to a volcanic event that immediately predates an intense Early Cretaceous faulting onshore Lebanon. Many normal growth faults are documented within the Early Cretaceous sequence, particularly in the Chouf sandstone formation (Neocomian-Barremian) with fault offsets ranging from several tens of meters to hundreds of meters in the southern Mount Lebanon [*Homberg et al.*, 2009]. These faults are oriented WNW–ESE to WSW–ENE and have a mean dip of 60° either to north or to south.

At the regional scale, the Chouf sandstone Fm. varies in thickness between 300 m in Chouf and Jezzine to few meters in northern Lebanon [*Nader*, 2003] accompanied by a southward thinning of the Late Jurassic to Early Cretaceous volcanic deposits [*Dubertret*, 1955]. Homberg et al. [2009] argue that this regional trend underlines the development of a roughly WNW – ESE striking basin during Early Cretaceous time in Lebanon, a direction consistent with the mean E-W trend of normal faults, and concluded that most of the WSW–ENE to WNW–ESE faults in Lebanon (except southern Lebanon faults) are Early Cretaceous in age. The depocenter of this basin was situated in the Chouf area where the Lower Cretaceous sedimentary sequence reached it maximum thickness, and then thins northwards where fluvial and shallow marine sediments diminish and are replaced by lavas flows (Figure 2.7). The northern margin of the basin was situated 50 km to the south of Tripoli while the southern margin of this basin is not visible owing to burial beneath later Palaeogene deposits in south Lebanon/North Israel. The much thinner Lower Cretaceous sequence in Israel suggests the southern margin of the Lebanese basin should be located in southern Lebanon. However, no indication for lower Cretaceous sandstone and extension are observed in the Levant Basin, suggesting that this extension is very local and restricted to onshore Lebanon only.

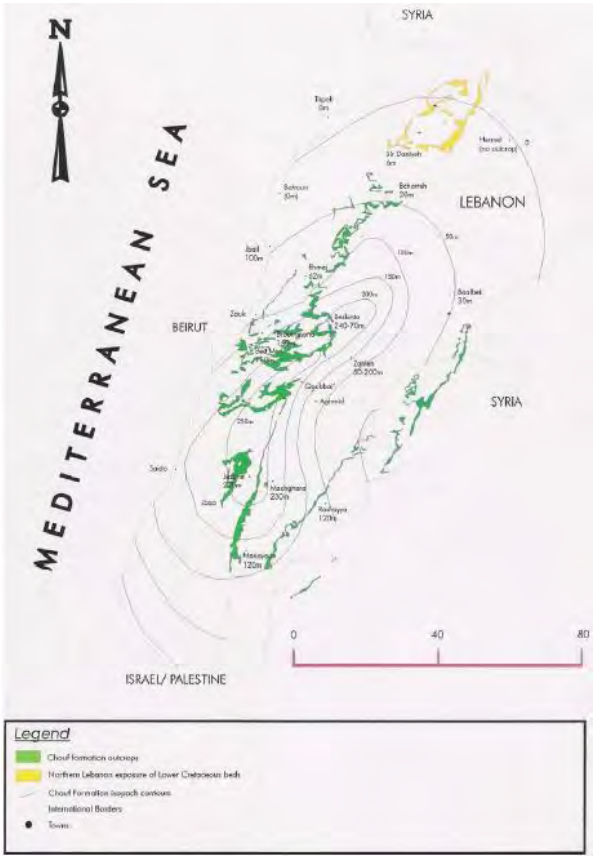

Figure 2.7: Map showing the extent of the Lower Cretaceous sandstone in Lebanon and its thickness variation across the country. From Bellos [2008].

Rifting model for the Levant Basin

The crust in this region exhibits variations in its thickness along a N-S direction from Gaza to Lebanon (Figure 2.8) and alont an E-W direction from the Arabian plate near Jordan to the Levant Basin (Figure 2.9). In the Palmyrides, the depth to Moho varies along the Palmyrides trend reaching 44 km in the southern Palmyrides and 31 km in the norther Palmyrides [Brew *et al.* 2001]. This difference in crustal thickness could indicate that the northern and southern Plamyrides are two different crustal blocks sutured along the Palmyrides trend and the Jhar fault, as a result of old Proterozoic sutures and shear zones [Brew *et al.* 2001]. Thus, it is likely that the rest of the Levant region, including Lebanon and Israel, is exhibiting an older architecture controlling the style and the location of Phanerozoic deformation, hence explaining the N-S crustal thickness variation along Judea similarly to the Palmyrides.

Refraction profiles along the Eastern Mediterranean [*Makris et al.*, 1983; *Ben-Avraham et al.*, 2002; *Netzeband et al.*, 2006] indicate an 8-10 km crustal thickness suggesting the presence of a thinned continental crust beneath the Levant basin [*Hirsch et al.*, 1995; *Vidal et al.*, 2000; *Gardosh et al.*, 2006]. This westward thinning of the crust beneath onshore Lebanon, Syria and Israel [*Beydoun*, 1977; *Makris et al.*, 1983; *Khair et al.*, 1997; *Netzeband et al.*, 2006] indicates a transition between a crust of contintental type east of the Levant margin, transitioning to a thinned continental crust beneath the Levant Basin.

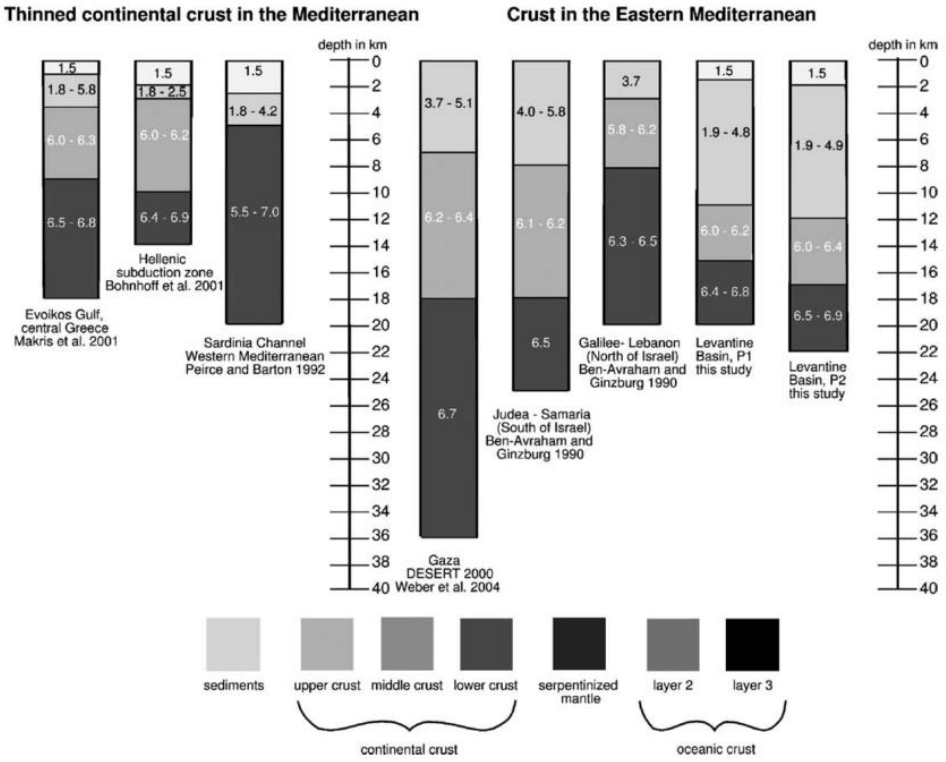

Figure 2.8: Columnar sections comparing crustal structure types in the Levant. The numbers denote p-wave velocities in kilometers per second plotted against the depth of their relative crustal units. From Netzeband *et al.* [2006].

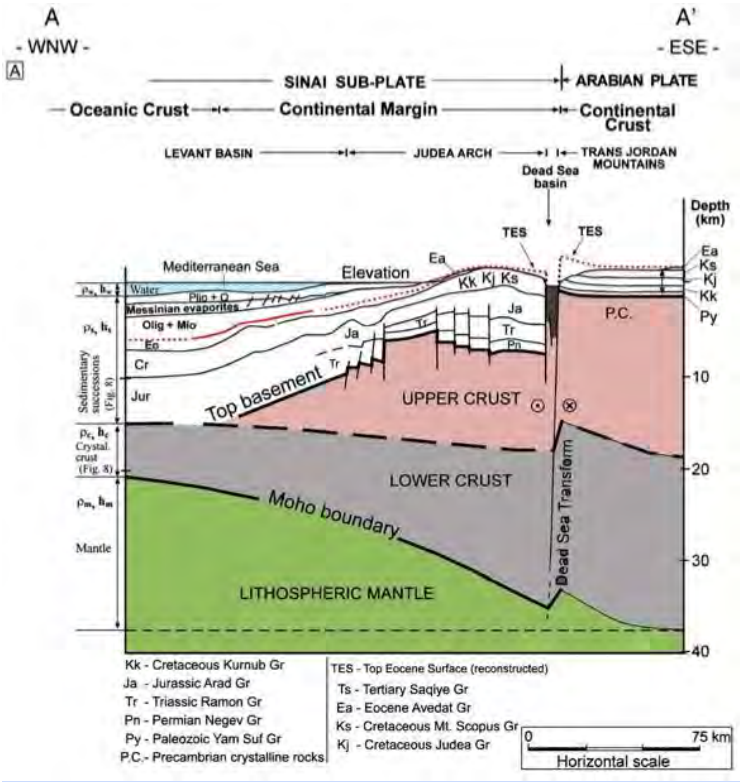

Figure 2.9: Schematic cross section across the Levant lithosphere, showing the main units and interfaces used during the isostatic calculation. Sedimentary units: Jur — Jurassic, Cr — Cretaceous, Eo — Eocene, Olig — Oligocene, Mio — Miocene, Plio +Q — Pliocene to Quaternary. Note the top Eocene reconstructed interface. From Segev *et al.* [2011].

The nature of the crust beneath the Levant basin is still debated as two models exist: the first interprets the crust as oceanic and is the result of rifting and drifting [*Makris and Stobbe*, 1984; *Garfunkel*, 1998; *Robertson*, 1998a] and the second interprets the crust as a thinned continental crust [*Hirsch et al.*, 1995; *Vidal et al.*, 2000; *Gardosh and Druckman*, 2006; *Roberts and Peace*, 2007]. The measured 20 Km depth to Moho can support both models [*Ben-Avraham et al.*, 2002] (Figure 2.9). It is suggested that rifting during the Early Mesozoic was responsible for the significant thinning of the crust in the centre of the Levantine basin. However, rifting, thinning and oceanic physical properties, as interpreted from seismic velocities by Ben-Avraham *et al.* [2002], do not necessarily imply sea-floor spreading. Furtermore, the southern Levant Basin offshore Israel exhibits numerous horst and graben structures typical of early rift episodes [*Gardosh and Druckman*, 2006; *Gardosh et al.*, 2010]. For these reasons, it is most likely that the crust of the Levant Basin is a thinned continental crust. The absence of horst and graben structures offshore Lebanon, contrary to offshore Israel (Figures 2.10 and 2.11), might be an indication that the Levant Basin also shows a N-S crustal type variation similar to the margin onshore. The absence of these rift structures might indicate a difference in the crustal properties offshore Lebanon.

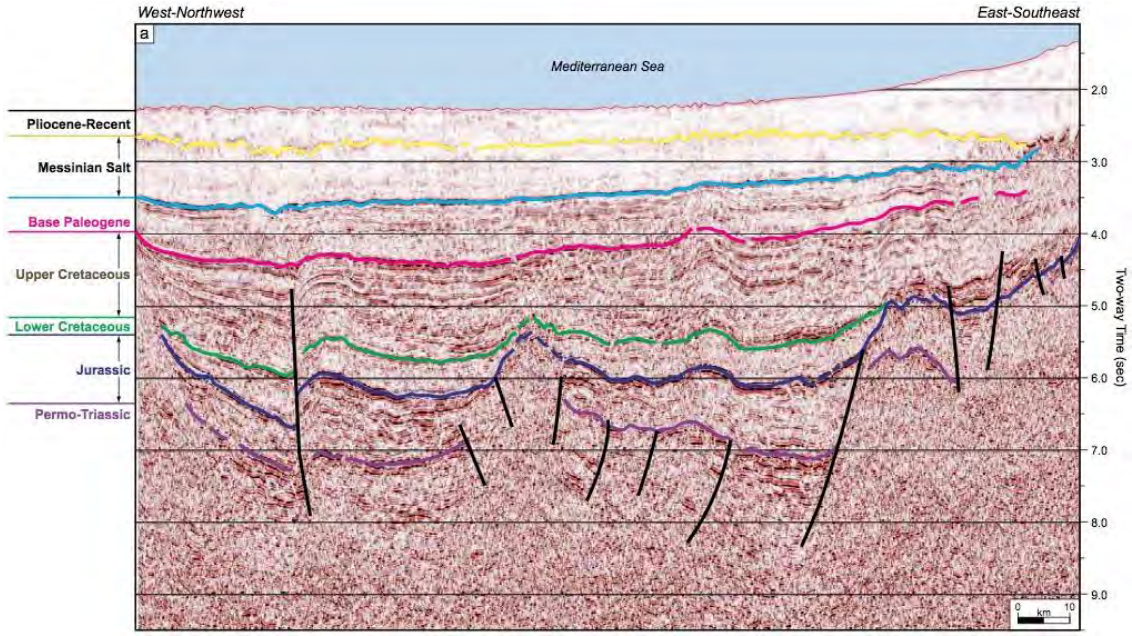

Figure 2.10: WNW-ESE seismic line over the southern part of the Levant basin showing a Jurassic rifted terrain with the presence of horsts and grabens. Note that the stratigraphy of this profile has been updated after drilling wells. From Robert & Peace 2007.

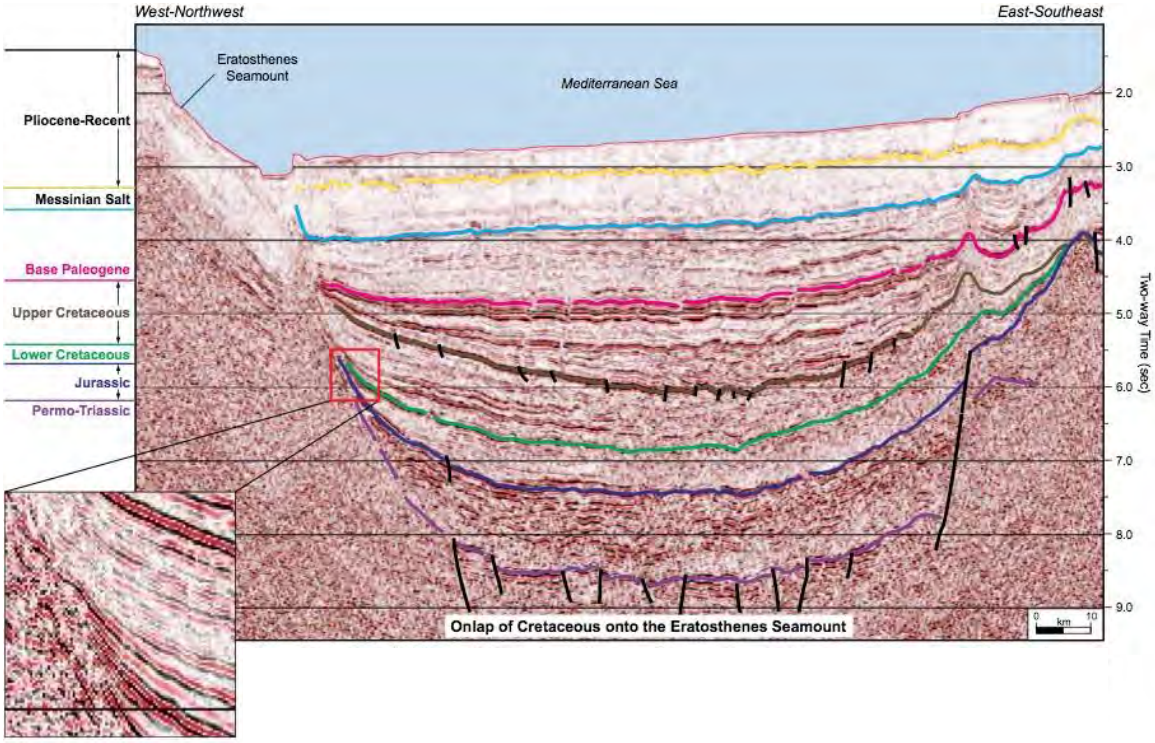

Figure 2.11: WNW-ESE seismic line over the northern Levant basin offshore Lebanon. The western portion of the line covers the eastern margin of the Eratosthenes seamount with Cretaceous onlap onto its structure. Note that in this part of the basin, horst and graben structures disappear. Section width approximately 180 km. From Roberts & Peace 2007.

As discussed above, numerous NE-SW Mesozoic normal faults in the Levant basin and margin are documented [*Gardosh et al.*, 2010; *Montadert et al.*, 2014]. They are thought to be the results of NW-SE rifting direction [*Gardosh et al.*, 2006, 2008a, 2010]. However, several models have been proposed to explain the direction of rift propagation and the different structural styles associated to it (Figure 2.12):

- NE-SW direction of opening in a N-S extension (Figure 2.12a) accommodated by a major N-S oriented transform fault along the eastern Mediterranean coast (eastern transform margins) [*Dewey et al.*, 1973; *Bein and Gvirtzman*, 1977; *Robertson and Dixon*, 1984; *Stampfli and Borel*, 2002]. This model is not consistent with the structures and fault directions that are identified within the Levant basin [*Gardosh et al.*, 2010]. It cannot explain the formation of the coastal highs and the interior basins of the Levant [*Gardosh et al.*, 2010].

- N-S direction on a Gondwanian shallow shelf with no reference to a specific fault pattern [*Hirsch et al.*, 1995]. This model is not consistent with the structures and NE-SW fault directions that are identified within the Levant basin [*Gardosh et al.*, 2010].

- NW-SE to NNW-SSE extension perpendicular to the NE-SW strike of normal faults (Figure 2.12b), resulting in the separation of the Eratosthenes and Tauride blocks from Gondwanian craton and accommodated by a transform fault along the Sinai coast (Southern transform margin) [*Garfunkel and Derin*, 1984; *Garfunkel*, 1998]. This transform fault should be located west to the Nile delta [*Bentham et al.*, 2007] and not in Sinai as this area appears to have been dominated by NW-SE extension [*Gardosh et al.*, 2010] (Figure 2.12b).

- A polyphase extension in the Levant starting with NW-SE extension in the Mid Triassic to Jurassic followed by an almost perpendicular NNE-SSW extension in the Early Cretaceous which produced WSW–ENE to WNW–ESE normal faults with offsets of several tens to several hundreds of meters (Figure 2.12c). A late extensional phase with similar driving stresses occurred during the Eocene and persisted maybe until Oligocene time [*Homberg et al.*, 2010].

Robertson [1998a] suggests that north of the present latitude of 32° 30′ (Figure 2.12b) that is north of Eratosthenes, the crust is of mid-ocean-ridge type, whereas that to the south is probably thinned continental crust, or “transitional” crust. This observation is conformable with the model presented above by Gardosh *et al.* [2010]. The

Eratosthenes Seamount is interpreted as a continental fragment, associated with mafic igneous rocks, which was rifted from the Eastern Levant continental margin in the Triassic [*Montadert et al.*, 2014]. This hypothesis is consistent with published seismic and gravity data interpretation of the Levant basin, showing a similar crustal structure beneath Eratosthenes and the Eastern Levant margin. This would also explain the difference in seafloor depth, thickness of series and tectonic style between the Northern and Southern Levant basin at the approximate latitude of 32° 30 ′.

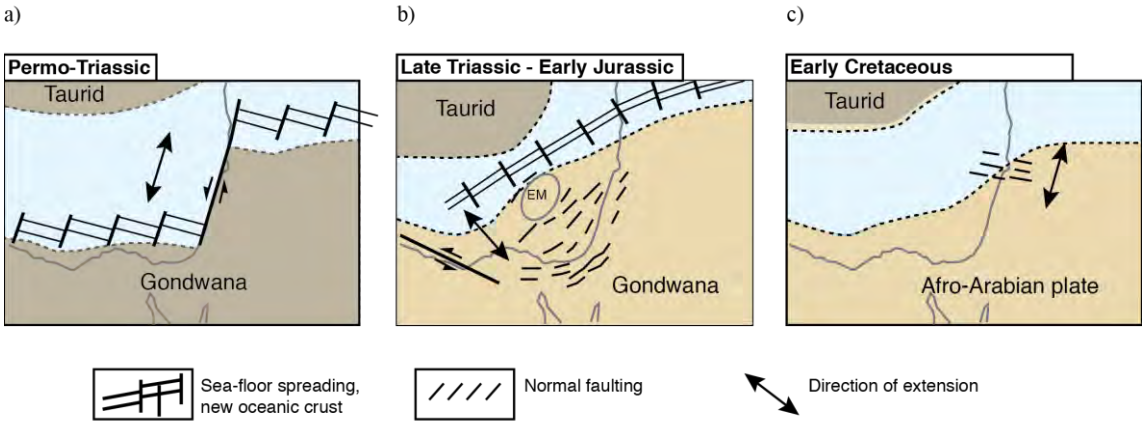

Figure 2.12: Several alternative tectonic reconstructions of Tethyan rifting in the Levant region. a) model previously proposed by Dewey *et al.* [1973] and Stampfli and Borel [2002], showing N-S extension with eastern transform margin, b) model proposed by Gardosh et al. [2010], Garfunkel & Derin [1984] and Garfunkel [1998], showing NW–SE extension with southern transform margin. c) continuation of extension as proposed by Homberg *et al.* [2010] in a NNE-SSW direction causing normal faults roughly oriented E-W. EM=Eratosthenes seamount. Modified from Gardosh *et al.* [2010].

II. 2.2Late Cretaceous / Tertiary compression

During Late-Cretaceous times, subduction and obduction led the progressive closure of the Neo-Tethys ocean [*Beydoun*, 1988; *Stampfli and Hochard*, 2009; *Frizon de Lamotte et al.*, 2011]. From late Turonian to approximately early Maastrichtian, oceanic sedimentary prisms and ophiolite masses were overthrust or glided onto the edge of the Arabian shelf to form the ophiolitic crescent [*Beydoun*, 1993]. The nappes are best observed in the Oman Mountains [*Glennie et al.*, 1973] where they extend up to 100km onto the shelf from the shelf break. Other examples are in the Eastern Mediterranean region in Cyprus and Syria. On Cyprus, to the north of the Levant Margin, the Troodos complex represents Turonian age ophiolites obducted during the Maastrichtian [*Robertson and Mountrakis*, 2006]. Other related examples are the Baer Bassit ophiolite of Syria and ophiolite-like rocks within the Bitlis Suture of Turkey, now the collisional margin of the European and Arabian plates, obducted during the Maastrichtian [*Al Abdalla et al.*, 2010]

Synchronously, this major geodynamic event caused the contraction of the Levant basin and margin and the subsequent initiation of an arcuate fold belt, the Palmyrides in Syria, folds in Israel and Sinai, collectively termed the "Syrian Arc" [*Walley*, 1998]. This results from inversion of Early Mesozoic extensional structures whereby pre-existing normal faults became reverse faults, and the Jurassic and Early Cretaceous synclines became Late Cretaceous anticlines [*Druckman*, 1981; *Chaimov et al.*, 1990, 1993; *Best et al.*, 1993; *Druckman et al.*, 1995]. Two main episodes of Syrian Arc folding are identified in literature: Early Senonian and Late Eocene/Oligocene [*Hempton*, 1987; *Moustafa and Khalil*, 1994; *Eyal*, 1996; *Garfunkel*, 1998; *Walley*, 1998, 2001]. Sawaf *et al.* [2001] argues for a third episode from the Early Miocene to present day in the Palmyrides. Convergence continues to be accommodated in the Eastern Mediterranean by a northward dipping subduction zone [*Robertson*, 1998a; *Le Pichon and Kreamer*, 2010]. At the seafloor, this zone consists of a series of ridges and thrust belts termed Lattakia Ridge System (LRS) and Larnaca thrust.

Structures of the Syrian Arc fold belt

Syrian Arc structures were documented in the Palmyra Basin in Syria, Israel, Sinai and the offshore Levant basin (Figure 2.13). More than 20 important structures form the northern Israeli part of the Syrian arc in Negev offshore and onshore [*Mart*, 1994; *Shahar*, 1994]. There is an uncertainty in the presence of such structures in Lebanon and its immediate offshore, although Walley [1998, 2001] argues about the relation of Mount Lebanon and Anti-Lebanon with the Syrian Arc. Furthermore, reconciling data describing the Syrian Arc structures in the different parts of the Levant into a common geodynamical frame is difficult as those structures span over a wide a time range. The Syrian Arc structures discussed below refer to those that have a significant shortening within the Arabian plate and that are prior to the Levant Fracture System.

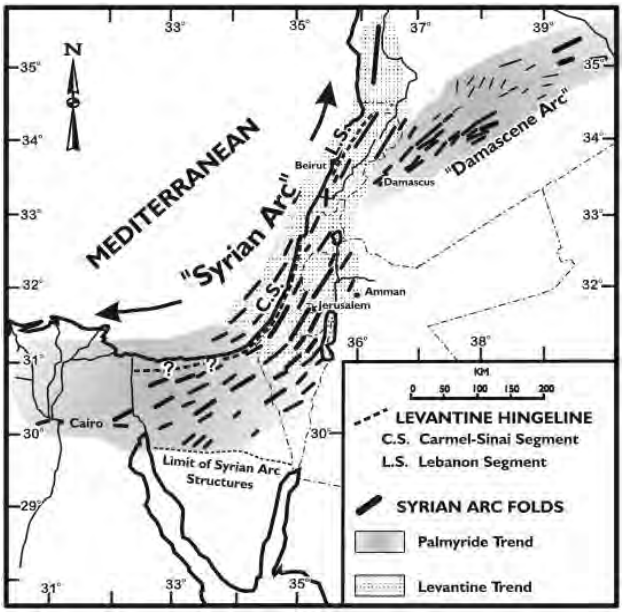

Figure 2.13 : Map of Syrian Arc structures in the Levant and Palmyride trends in the eastern Mediterranean (Levant) region. Data from various sources. The location of the 'Syrian Arc' and 'Damascene arcs' as shown here are as originally defined by Krenkel. From Walley 1998.

Syria

Syrian Arc tectonism in Syria can be divided into a North-Eastern and a south-western part. Deformation and uplift in the Palmyrides are thought to have happened in three phases: Late Cretaceous, Eocene and Early Miocene [*Chaimov et al.*, 1992; *Sawaf et al.*, 2001]. The Late Cretaceous minor episode of shortening is inferred from local onlap relations of reflections in rocks at that age seen in seismic profiles [*Chaimov et al.*, 1992]. The second phase of uplift also minor and similarly manifest by local onlap occurred in the beginning of Middle Eocene epoch (Figure 2.14). The third episode of compression from Miocene till present days is suggested [*Sawaf et al.*, 2001] while Hempton [1987] and Brew *et al.* [2001b] restrain it to the Early Miocene only and describe it as the major folding phase of the Palmyrides. The Early Miocene period corresponds to the beginning of the Arabia – Eurasia collision in this region. This collision started in northern Syria during the Late Oligocene [*Al Abdalla et al.*, 2010]. It might be that minor compressive movements took place since Upper Cretaceous [*Chaimov et al.*, 1990] in northern Syria and in Lebanon [*Walley*, 1998].

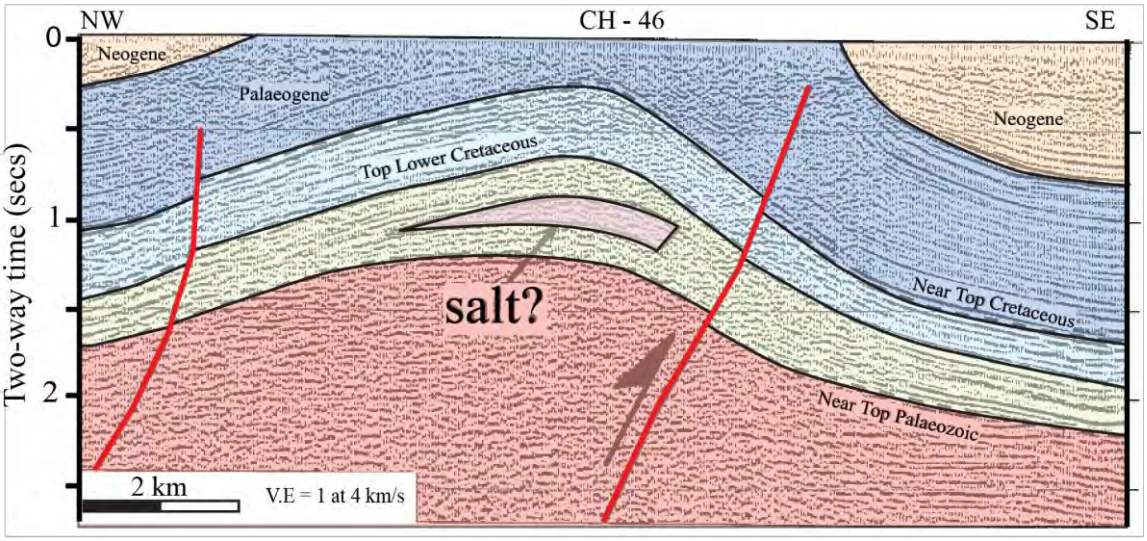

Figure 2.14: Seismic line in the south-western Palmyrides showing a normal fault that has been reactivated in a reverse sense in the Cenozoic, offsetting Triassic and younger thicketed sun-rift rocks in the hanging wall above their corresponding formations in the footwall. Coloured seismic units were added to the original interpretation from Sawaf *et al.* [2001].

The SW Palmyrides are separated from the NE Palmyrides by the Jhar fault (Figure 2.7). This fault has been traced for 200 Km in a ENE direction and shows an average of 1000m of uplift on its northern side with significant dextral strike-slip [*Al-Saad et al.*, 1992]. This fault was an active extensional fault since at least the Jurassic [*Brew et al.*, 2001b]. Below is a description of the two parts of the Palmyrides ranges, highlighting the strong along-strike structural variation with thrust faulting becoming less influential toward the northeast [*Brew et al.*, 2001b]. Furthermore, in the Palmyra basin, strong along-strike variations in gravity anomalies are seen in north-eastern and south-western parts of the Palmyrides (Figure 2.15):

- SW Palmyrides: They are dominated by a series of narrow, en echelon, short SE verging asymmetric folds controlled by reverse faults with cretaceous outcrops at their crest [*Chaimov et al.*, 1992; *Brew et al.*, 2001b]. Short wave anticlines have steeply dipping forelimbs and shallowly dipping backlimbs, steeper toward the southwest, and are the result of fault-propagation folding above inverted normal faults linked by sinistral transfer faults [*Chaimov et al.*, 1993]. This could be seen in well and outcrop data (Triassic thrust over Santonian). A locally developed Triassic detachment level can accommodate the fault-bend fold formation. It was mapped by [*Chaimov et al.*, 1992] and probably effective

in the northern part of SW Palmyrides. Another Upper-Cretaceous and lower Paleozoic detachment is also mapped by [*Chaimov et al.*, 1993].

- NE Palmyrides: In the central and northern Palmyrides, box folding dominates above an upper Triassic detachment with minor reverse faulting [*Searle*, 1994]. The Bilas and Bishri blocks (Figure 2.7) are larger-wavelength anticlinoria with Cretaceous exposure, forming the central highlands in the NE segment of the mountain belt.

In NW Syria, the Early Miocene NW-SE compression event is the major regional tectonic event associated with folding and thrusting. It has created the major NE–SW trending intra-platform Lattakia thrust as well as the regional NE–SW folding in Baer-Bassit, Afrin, and probably Palmyra regions [*Sawaf et al.*, 2001]. This tectonic phase is associated with a significant uplift and a strong erosion of the Mesozoic to Palaeogene sequence of the folded platform and inverted Palmyra Basin. In the Palmyrides, piggy-back basins developed in the main synclines, filled up with Miocene continental deposits. Because of the flexing of the platform associated with the Early Miocene thrusting, a narrow NE–SW elongated trough developed during the Middle–Late Miocene forming the Lattakia basin. Normal faults with small offsets developed in the basin and surroundings during the Middle Miocene in response to the flexure of the platform [*Al Abdalla et al.*, 2010]. In NW Syria, the Baer-Bassit platform overthrusts onto the Coastal platform along the Lattakia thrust. This major intra-Arabian platform structure constitutes the Alpine deformation front during the first stage of the Arabia–Eurasia collision [*Al Abdalla et al.*, 2010].

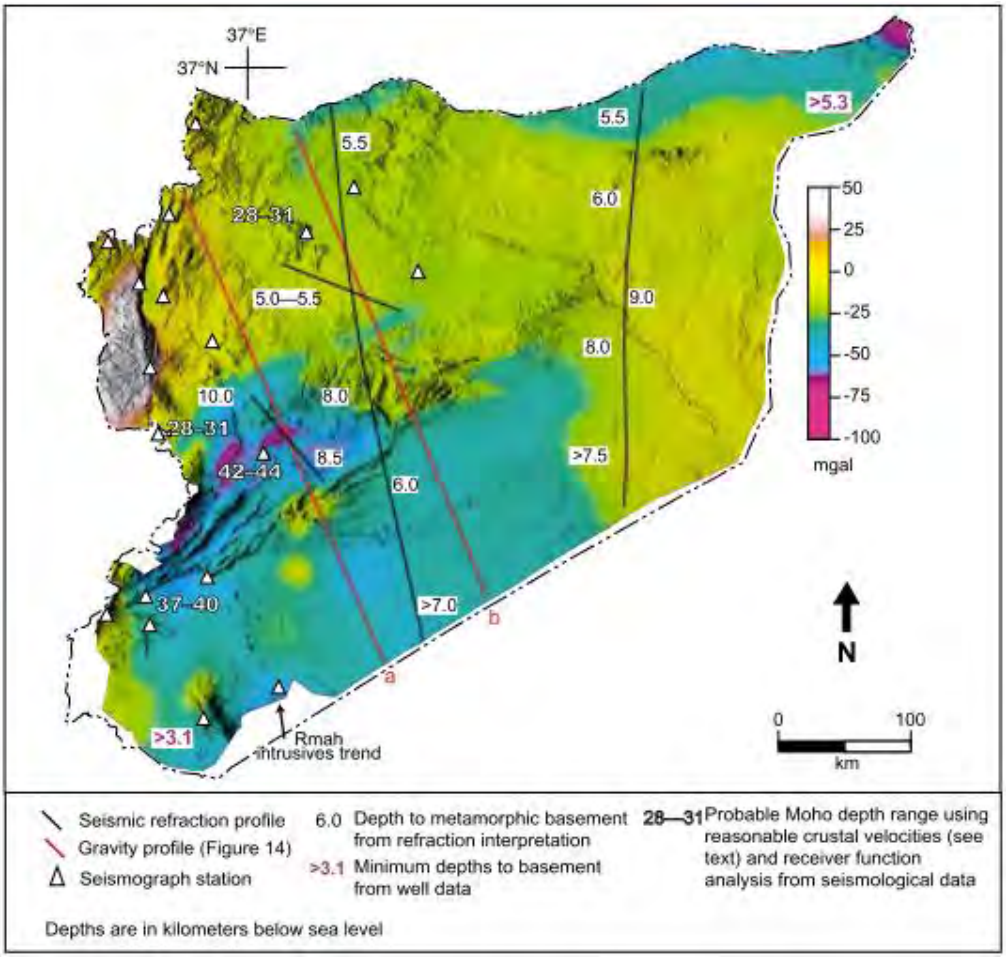

Figure 2.15: Bouguer anomaly map of Syria showing strong along-strike variation in gravity anomalies between the south-western and north-eastern Palmyrides ranges. From Brew *et al.* [2001].

Lebanon

There is currently no clear and absolute evidence for the presence of Syrian Arc structures in Lebanon. However, Walley [1998] provides logical arguments to prove that the Lebanese flexures are part of the Palmyrides in Syria and thus are affected by Syrian arc tectonism since the Late Cretaceous (Figure 2.16). Yet this has not been proven in the field due to intense erosion of Cenozoic sediments.

According to Walley [1998], the western Lebanese flexure seems to be a rejuvenation of a much older fundamental structure. He argues that the facies change across the flexure and the thickening of strata toward its west are an evidence for the presence of the Lebanese hinge line since the Mesozoic. The Lebanese hinge line is a continuation of the Israel/Sinai hinge line that marks the Mid-Jurassic to Late Cretaceous platform edge in this area [*Garfunkel and Derin*, 1984; *Walley*, 1998] with

similar Mid-Cretaceous facies development. They correspond together to a single Levant margin hinge line [*Walley*, 1998].

Searle [1994] and Searle *et al.* [2010] include Anti-Lebanon in the Palmyrides. Others prefer to separate them at the Syrian Lebanese borders. An important indication is the presence of an Early Miocene compressional phase and folding, documented by an Early Miocene 10° angular unconformity in Chekka [*Walley*, 1998; *Boudagher-fadel and Clark*, 2006; *Hawie et al.*, 2014]. This outcrop in Chekka shows Langhian strata unconformably overlying Eocene strata with the presence of gravels and boulders at the contact indicating erosion. This angular and depositional unconformity is very likely the result of block uplift and folding during late Oligocene and early Miocene. In fact, sedimentological and biostratigraphical data indicate that Mount Lebanon was already emerging at the onset of Miocene times [*Crognier*, 2013] with a more elevated position in North Lebanon compared to its south since at least the Cennomanian-Turonian also suggested by facies and thickness variations [*Hawie et al.*, 2014].

Evidences proposed by Walley [1998] to link the Lebanese deformation to the Syrian arc can be summarized as follow:

- The similar NNE-SSW trend prevalent in all the Syrian Arc in the Eastern Mediterranean region (Figure 2.13).

- The similar age of deformation of the Lebanese ranges as the one proposed for the Palmyrides: a post-Middle Eocene to Pre-Mid Miocene folding in Lebanon Widespread sedimentation gap spanning the Late Eocene and Oligocene matches the Syrian Arc II period of deformation of the Middle-Eocence/Oligocene time. Furthermore, the distribution of Eocene nummulitic facies in south Lebanon and the differentiation between the continental and lacustrine Miocene across Mount Lebanon indicates a change in depositional environments most likely related to tectonic processes. This, together with the lack of any evidence for transform movements in Lebanon related to the Levant Fracture system, and the presence of angular unconformities between the Ypresian and Late Burdigalian (later refined by Homberg *et al.* [2010] and Hawie *et al.* [2014]) at Ras Chekka all led Dubertret [1972] to suggest an Oligocene/Early Miocene deformation time in Lebanon with the main tectonic framework and initial structuration came into being in the Late Cretaceous.

- It is easier for compression to create the Lebanese flexures, whereby transpression is hardly able to fold and uplift the Lebanese mountain ranges in only 6 Ma.

- Some structures are offset by the LFS: Barouk Niha anticline and Zahle fold along the central Mount Lebanon are two parts of an anticline cross-cut by Yammouneh; and Litani river that was flowing E-W before being displaced by the LFS.

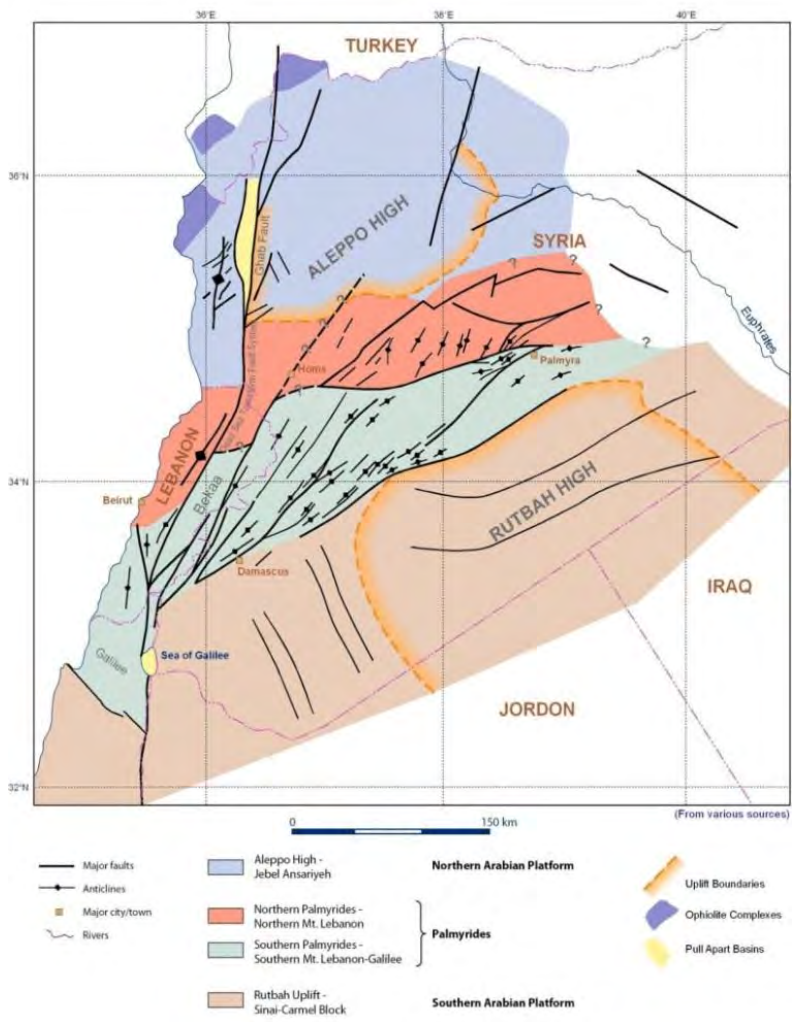

Figure 2.16: Map showing the major tectonic divisions between Syria and Lebanon and the postulated hypothesis that the Jhar Fault extends to Lebanon and separates the Northern Mount Lebanon from the Southern Mount Lebanon similarly to the Palmyrides in Syria. This would suggest that Mount Lebanon is part of the Palmyrides fold belt (modified from Walley 1998).

Israel

A number of NE-SW [*Shahar*, 1994] and NNE-SSW [*Eyal and Reches*, 1983] folds are documented in Israel in the Negev fold belt. These folds are classified as Syrian

arc structures. Similar folds are also documented in offshore Israel and are attributed to Syrian Arc tectonism [*Gardosh and Druckman*, 2006].

Two stages of folding and faulting since the Late Cretaceous related to the Syrian arc are distinguished in Israel [*Shahar*, 1994] each exhibiting a different tectonic style, but all superimposed on the same structures. The first are simple folds of Late Turonian/Middle Eocene age while the second are reverse faults of Late Eocene/Middle Miocene age [*Eyal and Reches*, 1983] (Figure 2.17).

One set of mesostructures can be found in Israel, particularly in the Negev monocline and attributed to Syrian arc structures resulting from WNW-ESE to NW-SE compression during the Senonian. This dominating maximum horizontal compression trending W to NW in the Late Cretaceous till Eocene rocks is attributed to Syrian arc tectonism [*Eyal and Reches*, 1983; *Eyal*, 1996; *Hardy et al.*, 2010; *Joseph-Hai et al.*, 2010].

Time relationships between faulting and folding in the Negev attest that the ENE–WSW to WNW– ESE compression is the oldest with folding starting in the Late Cretaceous and ceasing at Eocene times. This implies that the ENE–WSW to WNW–ESE compression was active during the Late Cretaceous, and thus drove folding in southern Israel. This compression renewed during the Cenozoic because it is documented by faults cross-cutting Eocene formations [*Hardy et al.*, 2010] (Figure 2.17).

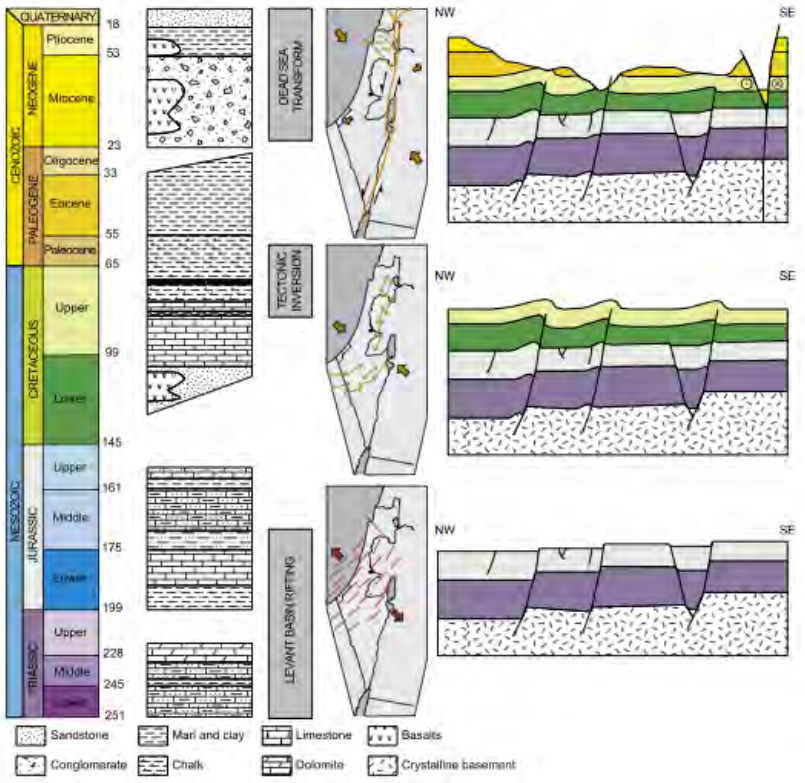

Figure 2.17: Simplified stratigraphic column and synthesis of the three main tectonic events recognized in Israel. From Hardy *et al.* 2010.

Sinai

A number of large anticlines exist in northern Sinai between the Tih plateau and the Meditarranean reaching up to 1100m height and several tens of kilometers long [*Moustafa*, 2010] (Figure 2.18). They represent a NE-SW oriented fold system belonging to the Syrian arc (Figure 2.18). In this area, compressional deformation took place in Late Cretaceous-Early Cenozoic times [*Moustafa*, 2010] coincident with timing suggested for the rest of the Levant basin and Israel in particular [*Eyal and Reches*, 1983]. This compression ended before Early Miocene time. The acme of the compressive deformation in Sinai is during the Campanian [*Moustafa*, 2010].

In Bouguer gravity maps and total magnetic intensity maps of Sinai, a boundary between North and South Sinai with distinct change in geophysical character across it is seen, similar to the Palmyrides ranges (Figure 2.15). This area, called the Sinai hinge belt (Figure 2.18), is a narrow ENE – WSW oriented structural belt forming the boundary between the North Sinai folds and the platform area lying to the south. Some of the ENE – WSW oriented faults in the Sinai hinge belt are characterized by the presence of ENE – WSW oriented anticlines. The arrangement of these folds provides evidence for

dextral simple shear deformation along the Sinai hinge belt. Horizontal and gently plunging slickenlines characterize the ENE – WSW oriented faults of the Sinai hinge belt indicating dextral slip. The eastern parts of the faults of the Sinai hinge belt were probably dragged by the LFS in response to the left-lateral slip in post-Miocene times leading to post-Miocene reactivation of the Sinai Hinge belt [*Moustafa and Khalil*, 1994].

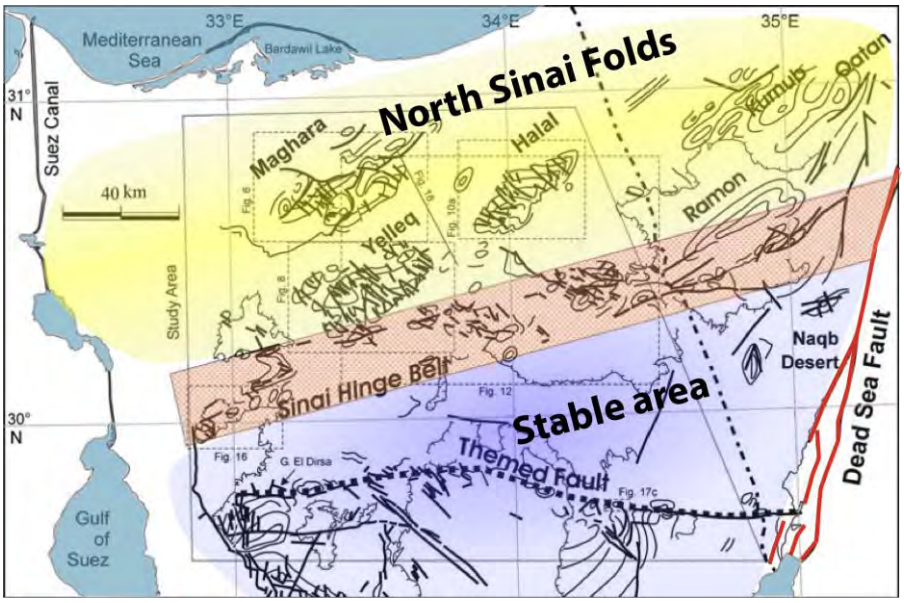

Figure 2.18 : Simplified structural map of North Sinai showing the location of some anticlines and the Sinai hinge line. Modified from Moustafa [2010].

Study of seismic data offshore northern Sinai interpreted with recently acquired gravity and magnetic data, revealed that these structural deformation, represented by large buried inversion anticlines, continue offshore [*Yousef et al.*, 2010]. Anticlinal structures offshore are all oriented NNE-SSW to ENE-WSW and represent a doubly plunging anticline with a relatively steep north-western flank. Some structures like Mango, Goliath and Ziv, represent an inverted Late Jurassic Early Cretaceous half-graben. All of these structures are controlled by major deep-seated reverse faults with thick syn-extensional strata in the core [*Yousef et al.*, 2010]. These inversion structures are characterized by fault-propagation folds with steep frontal limbs and gently dipping back limbs.

The structural deformation related to Syrian arc offshore Sinai was taking place during Post Santonian to Middle Miocene inversion phase and followed by a post Middle Miocene subsidence phase [*Yousef et al.*, 2010]. This is seen by the presence of

regional unconformities spanning the Paleocene to Pleistocene corresponding to compression and later Miocene extension, found in a set of tectonosequences mapped by [*Yousef et al.*, 2010].

Driving mechanisms

The Syrian arc results from inversion of Early Mesozoic extensional structures whereby pre-existing normal faults became reverse faults, and the Jurassic and Early Cretaceous synclines became Late Cretaceous anticlines [*Druckman*, 1981; *Best et al.*, 1993; *Chaimov et al.*, 1993; *Druckman et al.*, 1995]. This is observed in offshore Israel where all faults underlying the fold structures were subject to inversion [*Gardosh and Druckman*, 2006], in Sinai [*Moustafa*, 2010] and in Syria [*Chaimov et al.*, 1992; *Brew et al.*, 2001b] (Figures 2.19 and 2.20).

In general, the Senonian folding is caused by the initial closure of Neo-Tethys as a result of the convergence between the Eurasian and African plates causing collision of ophiolite-related units with the Arabian passive margin. This convergence created a northward dipping subduction zone in the present day of Cyprus and northern Syria [*Le Pichon and Gaulier*, 1988; *Robertson*, 1998a] leading to the contraction of the Levant basin and margin and the subsequent development of Syrian Arc fold belt as mentioned above. The implication is that initial inversion of the Syrian arc may predate ophiolite obduction onto the Arabian platform. One possibility is that the inversion dates the initiation of northward subduction within Neotethys (that gave rise to the Troodos, Hatay, Baer-Bassit ophiolites by supra-subduction zone spreading). Stress was transmitted toward the continent through dense oceanic crust and re-activated the rift-related structures on the Arabian margin. Similarly, the Eocene deformation of the Syrian arc structures in the Palmyrides, as evidenced in seismic data [*Chaimov et al.*, 1992], reflects southward stress propagation that marks convergence, and the initial stages of collision. However, this predates actual suturing of the Eurasian and Arabian plates in southeastern Turkey that was not complete until the Miocene. After the Levant Fracture system became active in the Miocene, movements along the Syrian arc largely ceased [*Robertson*, 1998a].

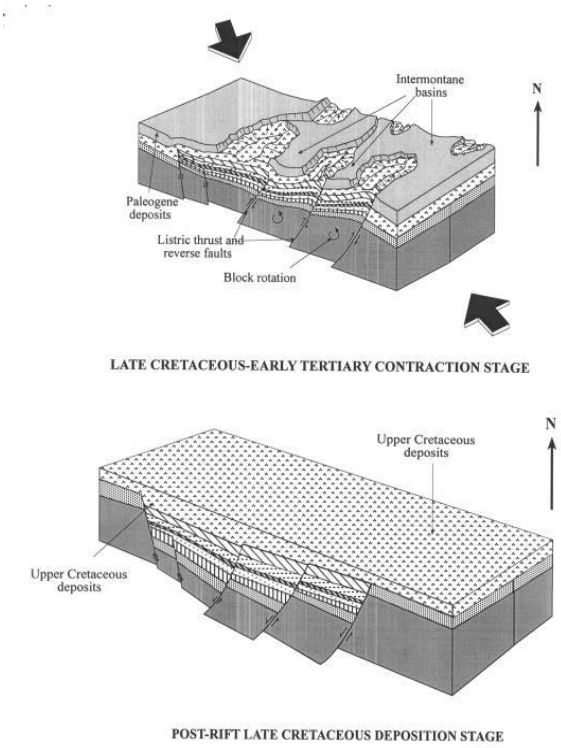

Figure 2.19: Schematic block diagrams showing the post-rift Cretaceous deposition (below) and the Late Cretaceous- Early Tertiary contractional stage (up). This contractional stage resulted in inversion of the pre-existing normal faults in Sinai and created the Syrian arc folds in Sinai both offshore and onshore. From Abed El Motaal & Kusky 2003.

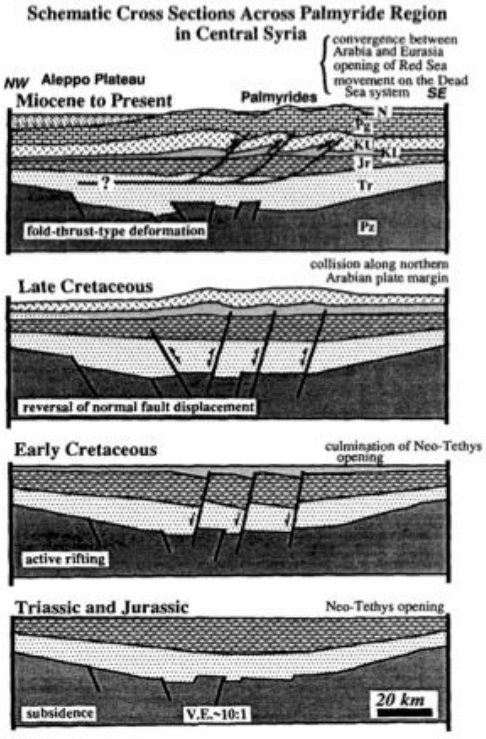

Figure 2.20 : Schematic NW-SE cross-sections showing development, chronologically from bottom to top, of the south-western intraplate Palmyrides fold belt, with a list of related major Arabian plate-boundary tectonic events. Double headed arrows indicate reversal of displacement (inversion) along normal faults. From Chaimov *et al.* [1992].

Geomorphologically, the folds are highly asymmetrical, with gentle north-western flanks, dipping at about 5°– 20°NW and steeper south-eastern flanks that are vertical or overturned in places, such as the folds seen in Sinai [*Moustafa*, 2010]. These structures show shortening in a mean NW-SE direction. Similar geometric characteristics can be seen in the folds of the SW Palmyrides [*Chaimov et al.*, 1992; *Brew et al.*, 2001b]. Broadly, Syrian arc structures range from thin-skinned open flexures and folds associated with strike slip and reverse faulting [*Salel and Seguret*, 1994; *Walley*, 1998] in the southern Palmyrides, to thick skinned deformation in northern Sinai [*Moustafa*, 2010] and the NE Palmyrides below the Bishri area [*Best et al.*, 1993; *Brew et al.*, 2001b]. In the southern Palmyrides, the faults are detached along decollement levels in the Eeocambrian and Triassic formations below the Aleppo plateau and Palmyrides zones as seen in seismic and well data together with detailed mapping and structural analyses [*Salel and Seguret*, 1994]. These broad folds and high-angle reverse faults are associated with breaks in deposition and angular unconformities [*Moustafa and Khalil*, 1994; *Salel and Seguret*, 1994; *Gardosh and Druckman*, 2006] and developed in response to regional WNW – ESE compression [*Eyal*, 1996].

II. 3 Neogene tectonic history

II. 3.1 Geodynamics of Arabia

During the Cenozoic, major geodynamic changes affected the Arabian plate and its surroundings. The Arabian/Nubian shields were separated by a rifting process that started in Afar and propagated eastward and northward creating the Gulf of Aden and the Red Sea respectively. This separation of Arabia and Africa started in the Oligocene-Early Miocene [*Le Pichon and Gaulier*, 1988] by initiation of continental rifting in the Gulf of Aden. Hempton [1987] argues that the Arabian plate started to separate from the African plate as early as Oligocene time with the initiation of rifting in the Gulf of Aden and the Red Sea, while its northern margin was already colliding with the Eurasian margin in Zagros since the Late Eocene. Syn-rift sediments, Oligo-Miocene in age, crop out in WNW-ESE trending basins along the Gulf of Aden coasts with the oldest syn-rift sediments, Rupelian in age, dating the onset of rifting in the early Oligocene [*D'Acremont et al.*, 2005].

Following rifting of the African lithosphere, seafloor spreading initiated in Early Miocene times in the eastern Gulf of Aden along the Sheba Ridge (Figure 2.2) [*Cochran*,

1983]. The spreading ridge propagated rapidly westward from the Owen fracture zone toward the Afar hot spot [*McKenzie*, 1970]. The connection of the Sheba Ridge with the Owen fracture zone and the Carlsberg Ridge formed the Aden-Owen-Carlsberg (AOC) triple junction between the Arabia, India, and Somalia plates [*Fournier et al.*, 2001]. Seafloor spreading in the Red Sea started 4–5 Mya in the southern part only [*Cochran and Karner*, 2007].

The newly formed Red Sea rift propagated northwards into the Gulf of Suez, ending during the Mid-Miocene (14 – 11 Ma), when it then switched to the Gulf of Aqaba [*Steckler and ten Brink*, 1986; *Le Pichon and Gaulier*, 1988] (Figure 2.21). Magnetic anomalies show that newly formed oceanic crust formed at 13 – 10 Ma in the Gulf of Aden, 5–2 Ma in the southern Red Sea and 2 Ma in the northern Red Sea [*Joffe and Garfunkel*, 1987] . Widespread NW–SE aligned basaltic dykes, dated at 22 – 18 Ma along both Sinai and the Saudi Arabian margins, show that rifting of the Gulf of Aqaba and initiation of the southern LFS must be younger than 18 Ma [*Lyberis*, 1988].

Continuation of rifting in Gulf of Aqaba created extensional pull-apart basins and many normal faults along the present day passage of the Levant Fracture System (LFS). These observations lead workers as [*Mart*, 1991] to extend the Red Sea rift northward into Jordan and all the way to Anatolia. He refers to this structure as the Levant rift system. Quennell [1984] however, states that the LFS is a transform fault and not a rift, and was apparently initiated as the terminating cross fault of the Red Sea spreading zone. Its northerly course was likely being influenced by (a) preferred trends in the Precambrian basement and (b) the rotation of the Arabian platform on a small circle transform. The supposed pre-existing interplate boundary between Sinai-Levant and Arabia from the Dead Sea northward was followed. However, lithospheric strength analyses done by Steckler and ten Brink [1986] reveal that the abandonment of the Sinai passage and the preference for rifting through Aqaba was because of lithospheric strength variations in the continental and oceanic crust. The presence of the Sinai hinge zone prevented the Red Sea rift from passing through Suez to the Mediterranean, so the rift preferred to bend rightward and initiate in Aqaba and Jordan since the lithosphere there was relatively weaker. This rotation in opening direction was accompanied by a decrease in subsidence rate over the Gulf of Suez until a minimum indicating that the Gulf of Aqaba had become the main northern plate-boundary. The Gulf of Suez extension continued but at a much slower rate as the northward component of separation was taken up on the transform boundary [*Steckler et al.*, 1988].

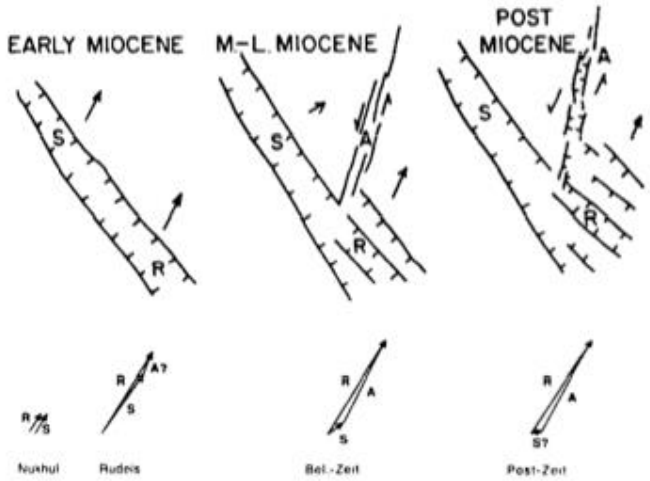

Figure 2.21 : Cartoon illustrating the geometric relationships between rifting and the directions of opening in the Sinai region. Velocity triangles are shown for the different phases in the Evolution of the rifts. From Steckler *et al.*1988.

Bordering the Arabian plate to the North is the Bitlis and Taurides block. The Taurides consist of a stack of thrust sheets; each thrust sheet generally consists of Palaeozoic to Early Tertirary sedimentary rocks, thrusted in the Late Cretaceous, Eocene and Early Miocene [*Okay*, 2008]. The Arabia-Eurasia collision started along the Bitlis suture during the Early to Middle Miocene [*Sengor and Yilmaz*, 1981] and the Bitlis ocean was completely obliterated by the latest Serravalian - Early Tortonian times around 11.8 my ago, accompanied by the beginning of widespread crustal shortening and uplift across eastern Anatolia [*Dewey et al.*, 1986]. Very shortly thereafter, terminal collision also occurred along the Zagros suture and Arabia became attached to Eurasia along the Bitlis-Zagros suture zone [*Dewey et al.*, 1973; *Sengor and Kidd*, 1979; *Sengor et al.*, 1984]. The pause or slowdown in the Red Sea rifting during the Serravallian would correlate with this collision along the Bitlis suture [*Hempton*, 1987]. In the Pliocene to present, northward convergence of the Arabian plate formed a foreland fold-thrust belt along the Bitlis-Zagros suture.

Westward of the Arabian-Anatolian boundary, the Latakia ridge forms the NW limit of the Arabian plate. Towards the southwest, the Latakia ridge system diverges into a broad zone of deformation at least 50 km wide and extends toward Cyprus. This ridge system initiated as a compressional fold-thrust belt during the Middle to Late Cretaceous contemporaneous with plate-tectonic convergence between the African and Eurasian plates which was directed NW-SE perpendicular to the overall trend of the

ridge [*Bowman*, 2011]. Compression continued throughout the Late Cretaceous as the Neo-Tethys continued to close with its initial closure during the Maastrichtian culminating in the emplacement of ophiolites in Cyprus. In the Late Miocene, a shift in the Maximum stress direction caused a change from a compressional regime to a sinistral strike-slip regime during the Pliocene to present [*Brew et al.*, 2001b; *Hall et al.*, 2005a]. This was caused by the westward escape of Anatolia as a result of the final collision between Arabia and Eurasia in the Late Miocene/Lower Pliocene [*Le Pichon and Kreamer*, 2010], and is currently evidenced by stationery GPS measurements of plate movements (Figure 2.3).

Following the previous account for the evolution of the Arabian plate, the Neogene to present tectonic setting in the eastern Mediterranean and Middle East is thus complex. In the east, subduction-collision dominates the northward convergence of the Arabian plate with Eurasia. Divergence of Arabia away from Nubia and Somalia is accommodated by sea-floor spreading in the Red Sea and Gulf of Aden, respectively, but is locally complicated by the dynamic effect of the Afar hotspot. Relative motion between Arabia and Nubia becomes strike-slip motion along the LFS farther north in the Levant. Anatolia is extruded westward and its relative motion with Eurasia to the north is accommodated along the North Anatolian Fault. Motion of Anatolia increases toward the Aegean and the Hellenic subduction zone and has resulted in widespread north-south-directed extension in the Aegean and western Anatolia.

II. 3.2 Description of LFS structures

The Levant Fracture System (LFS) comprises three segments passing through Jordan, Israel, Lebanon and Syria [*Quennell*, 1958, 1984; *Freund*, 1965; *Dubertret*, 1972]: the 400 km long southern part from the gulf of Aqaba to the Dead Sea in Jordan in a N005E trend, the 180 Km long central part in Lebanon where the transform bends to N030E and the motion becomes transpressive creating some restraining bends, and the northern 250 Km long part in Syria with a N005E trend which abuts the Taurus mountains in the Anatolian microplate (Figure 2.22). A brief overview of these segments is shown below starting from south to north.

At the southern end of the LFS, the Gulf of Aqaba is formed by a series of three deep pull-apart basins [*Ben-Avraham*, 1985]. It is surrounded by the Sinai Mountains to the west, which show large systems of faults mostly oriented parallel to the gulf [*Eyal et al.*, 1981] and Hejaz Mountains to the east showing a similar pattern (Figure 2.22).

From the Gulf of Aqaba to the Dead Sea basin, the LFS cross-cuts quaternary sediments of the Arava Valley (Wadi Araba). In Israel, the left-lateral movement along the left-stepping LFS led the development of several pull-apart basins, with the largest ones in the Gulf of Aqaba, the Dead Sea, Sea of Galilee and Hula basins along the Jordan valley [*Garfunkel*, 1981; *Garfunkel and Freund*, 1981]. The Wadi Araba-Dead Sea fault is almost purely strike–slip in this section and is composed of linear segments several tens of kilometers long connected either by compressive or extensive jogs that form, respectively, small-scale push-ups or basins [*Garfunkel and Freund*, 1981].

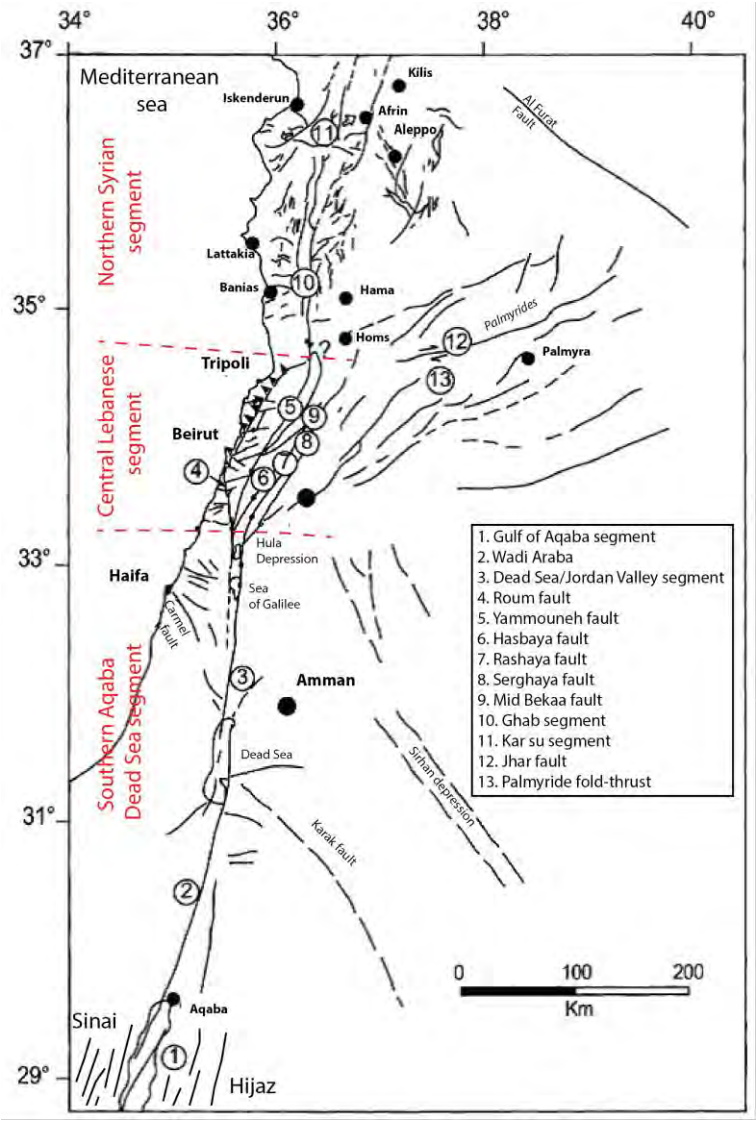

Figure 2.22: Map showing the different segments of the LFS and their associated structures. Modified from Beydoun 1999.

The Dead Sea basin connects the Wadi Araba–Dead Sea segment (Figure 2.22) that enters the basin at its southeast tip, to the Jordan segment exiting the basin at its northwest tip [*Garfunkel*, 1981] and is bounded on both sides by the continuation of the

strike–slip faults [*Ben-Avraham and ten Brink*, 1989]. The Sea of Galilee, as the Dead Sea basin, is associated with a large extensive jog, the components of which are not yet mapped in detail [*Hofstetter et al.*, 2007].

In addition to the main fault in the southern LFS, the Carmel fault, which is branching out from the Levant Fault System, is formed by a normal-like prominent fault scarp connected to the Dead Sea fault about 40 km north of the Dead Sea and runs to the Mediterranean sea toward the Cyprian arc [*Hofstetter et al.*, 2007]. Post-Pliocene vertical displacement along this structure reaches 600 m, while the strike–slip component is not very clear and well established. The Mount-Carmel belt marks an abrupt change in the landscape style of northern Israel, a northward increase of its seismicity, a considerable thinning of the crust and a change in the magnetic and gravimetric properties [*Ben-Avraham et al.*, 2002]. The carmel fault bounds Mount-Carmel, a Middle Pleistocene structural feature in Israel [*Zviely et al.*, 2009].

Linking the northern and southern portions of the LFS is the Lebanese segment of the transform (Figure 2.22). Here, there are many strike-slip faults, generally oriented NNE-SSW and N-S, together with E-W cross-faults, and folds at the kilometer and 10km scales [*Beydoun*, 1977; *Beydoun and Habib*, 1995]. Walley [1988] described the fault pattern in Lebanon as braided, whereby the deformation in the broad restraining bend has been accommodated by at least four major strike-slip faults and distributed strains in the adjacent blocks [*Beydoun and Habib*, 1995; *Khair et al.*, 1997; *Walley*, 1998, 2001; *Gomez et al.*, 2007b]. The main faults are Yammouneh, Serghaya, Roum and Rachaya (Figure 2.22).

The Yammouneh fault (Figure 2.22) is the only structural link between the southern LFS in the Jordan River Valley and the northern LFS in NW Syria. Its 160km long surface trace is sharp and clear in the topography. The southern Yammouneh Fault generally bounds the west side of the southern Bekaa Valley, and the northern part of the fault passes through the eastern flank of northern Mount Lebanon Range. Displaced landforms, such as faulted alluvial fans and wind gaps [*Dubertret*, 1955; *Daëron et al.*, 2004; *Gomez et al.*, 2007b], demonstrate that the Yammouneh Fault has experienced only strike-slip movements during the Late Quaternary [*Daëron et al.*, 2004; *Gomez et al.*, 2006], with no evidence of recent or active dip-slip along it [*Gomez et al.*, 2007b]. Evidence for strike-slip movement is described as slickenside grooves and other features [*Hancock and Atiya*, 1979]. The vertical offset, however, is variable along-strike the Yammouneh fault, reaching 2000m in the southern Mount Lebanon, and few hundred meters in norther Mount Lebanon [*Dubertret*, 1955].

The Serghaya fault (Figure 2.22) is branching from the southern LFS in the Golan Heights. It can be traced approximately 125 km through the Anti-Lebanon Mountains to the eastern edge of the Bekaa Valley. It is a sinistral strike-slip fault associated with many pull-apart basins [*Gomez et al.*, 2001, 2003]. At several locations, left-lateral striations on sub-vertical fault planes in the lake sediments at Zebedany valley depict a predominant rake of 10-15˚ implying a dip-slip component of about 20-25% [*Gomez et al.*, 2001].

The Roum fault (Figure 2.22) is visible as an array of apparently discontinuous strands on geological maps [*Dubertret*, 1955] and satellite images [*Girdler*, 1990]. It is a major zone of left-lateral displacement that has been active since Miocene [*Girdler*, 1990; *Butler et al.*, 1998]. Gorges of the Litani and Zahrani rivers which cut across the Tyre–Nabatiyé plateau show left lateral offsets across the Roum Fault strongly suggesting that this structure has accommodated displacement in the past 5 Ma [*Walley*, 1988]. Butler *et al.* [1998] recorded several river offsets along this fault ranging from 200 m to 9 km and suggested that these are presumably underestimates of the total Roum fault displacement. Griffiths et al. [2000] noted a decrease in surface expressions northward, defined the Roum fault as a "lateral domain-bounding" fault accommodating transpressive deformation at the western margin of the Lebanese restraining bend since the Pliocene, and suggested a fault tip to the south of Beirut. Khair [2001] proposed that the Roum fault lateral displacement becomes dispersed beyond its mapped trace into a complex network of faults and fractures delineated as lineaments from aerial photographs, and thus no faulted trace of the Roum fault can be seen to the north of Awali river [*Nemer*, 1999]. This contradicts with the hypothesis that the Roum fault continues offshore to make a new triple junction East of Cyprus [*Butler et al.*, 1998] or to form an offshore thrust system parallel to the Lebanese coast [*Elias et al.*, 2007; *Carton et al.*, 2009].

The Rachaya fault (Figure 2.22) has clear linear trace in the field. Field investigations [*Gomez et al.*, 2007b] found no evidence of reverse faulting along the Rachaya Fault as suggested by Daëron *et al.* [2005]. At its northern termination, the Rachaya Fault splays as it bends toward the Serghaya Fault in the Zebadani Valley [*Walley*, 1988; *Gomez et al.*, 2006]. The geometry of the Serghaya and Rachaya faults [*Ron*, 1987] suggest that they may be structurally linked as a strike-slip duplex [*Gomez et al.*, 2007b].

Recent studies suggested the presence of an offshore splay of the Levant Fracture system, some 20 km away from the coast between Beirut and Tripoli termed Mount

Lebanon thrust [*Daëron et al.*, 2004; *Carton et al.*, 2009] that accommodated all the transpression and subsequent uplift of Mount Lebanon. This is based on shallow low-quality 2D seismic data (Shalimar cruise) and uplifted terraces along the Lebanese shoreline [*Sanlaville*, 1974; *Morhange et al.*, 2006].

Many authors have reported shortening and relative displacement measurements over the Levant Fracture system structures in Lebanon. Though the values proposed might not seem to be exactly the same, they do show some similarity. Below are tables summarizing the different values presented for slip rate, transpression and shortening (table 1.1).

Table 1.1: *table showing the different uplift rates over the central LFS in Lebanon proposed by some authors.*

UPLIFT RATE

Uplift	*Time span*	*Method*	*Location*	*References*
<0.1 mm/a	-	mapping of Pliocene basalt over a paleosurface	Coastal Syria	[*Gomez et al.*, 2006]
1.2 m	6000 years	notched holocene shorelines	Lebanese coast	[*Sanlaville*, 1974]
0.28mm/a	500 ka	notched shorelines and marine terraces height	Lebanese coast	[*Gomez et al.*, 2007b]
0.75-1mm/1	-	notched shorelines	Lebanese coast	[*Pirazolli 1996*]
0.5 ± 0.1 mm/a	holocene	uplifted vermetide benches	Lebanese coast	[*Elias et al.*, 2007]

In addition to the faults mentioned above, the Levant margin along Lebanon also shows a number of ENE-WSW to ESE-WNW faults. According to Homberg *et al.* [2010], these faults were formed owing to a NNE-SSW extension in the Early Cretaceous. The argue about a consistent fault system over the entire country with a combination of WNW-ENE and WNW-ESE trends, together with the restriction of these faults to the Jurassic-Lower Cretaceous sequences only without cutting younger formations [*Homberg et al.*, 2010]. Counter clockwise rotations in Lebanon were probably responsible in reactivating the E-W faults northern of Beirut latitude as dextral

strike slip faults [*Renouard*, 1955; *Ron*, 1987; *Walley*, 1988; *Gedeon*, 1999]. The relationship of these faults to the Levant Fracture system is presented by Freund [1965] and Freund *et al.* [1970] who advocated through a combination of theoretical experimentation and field observations that several types of structures may be responsible for accommodating motion along the Levant Fracture System including sinistral and dextral faults that are synthetic and antithetic to the fault respectively. These structures apparently accommodate about 50% E-W elongation essentially forming zones of non-coaxial plane strain wherein the vertical thickness is conserved [*Butler et al.*, 1998].

Another suite of faults lies on the Tyre-Nabatiye plateau between the Roum fault and the coast of Lebanon. These faults are very poorly studied, and Hancock and Atiya [1979] interpreted them of having significant vertical slip components based on geological map. The dip slip vectors measured by Homberg *et al.* [2010] indicate a normal movement along these faults. Griffiths *et al.* [2000] also concluded that the southern latitudinal faults were normal and considered them to be part of the extensional stress regime to the west of the Roum fault. This is disputed by Butler *et al.* [1997] who considered the southern latitudinal faults to be dominantly strike-slip, though they have a peculiar planar geometry

Similar latitudinal dextral strike slip faults have also been observed along the western margins of the LFS in south-eastern Sinai [*Frei and Freund*, 1990], in Mount Hermon [*Ron et al.*, 1990] and along the margins of the LFS in Israel [*Mart and Rabinowitz*, 1986; *Ben-avraham and Charrach*, 1990]. In Israel, these neotectonic faults were observed to offset the normal faults that define the western margins of the Dead Sea basin [*Ben-avraham and Charrach*, 1990] (Figure 2.23) and are suggested to be younger than the LFS [*Mart and Rabinowitz*, 1986].

The northern segment of the LFS cuts through the eastern margin of the Syrian coastal ranges with a NS trend into the Al-Ghab basin where the fault bifurcates into a dominant eastern branch (Al Ghab fault) which has a throw down to the west of up to 1000 m and a western branch that shows a throw down to the East of about 1500-2000 m. Between these two faults, the 15 km wide, 60 km long Pliocene-recent Al-Ghab depression forms a pull-apart basin similar to the Dead Sea [*Brew et al.*, 2001a]. The coast ranges in Syria is truncated by a major regional unconformity that underlies intraplate alkali basalt flows of regional extent. These volcanic rocks are abruptly truncated by vertical left-lateral strike-slip faults that bound an impressive gouge zone up to 40 m wide.

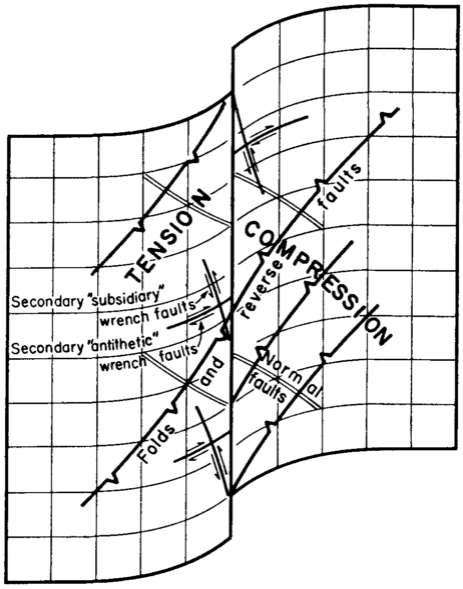

Figure 2.23: Sketch showing how secondary structures might be associated with a major strike-slip fault. From Freund [1965].

II. 3.3 Proposed models for the evolution of LFS

After reviewing all the geologic history of the Levant region, several models are proposed to explain the evolution of the Levant Fracture System. These models, discussed below, present alternative interpretations of the tectonic setting and evolution of the Levant region. Though these hypotheses seem contradictory, they are actually complementing each other and present a reliable overview over this area.

Roum fault, main active branch of the LFS in Lebanon:

Butler *et al.* [1998] propose a primary period of distributed strain, whereby the Yammouneh fault (YF) cuts through the Lebanese area to provide a hard linked through going transcurrent structure linking the Ghab fault with the southern part of the LFS. This might have occurred in Miocene times, while Arabia-Africa rotation pole was located far to the west. The position of this pole is critical in determining the amount of transpression across the YF. Transpression is manifest by coeval transcurrent displacement on the YF together with increasing uplift and amplification of the Mount Lebanon. In line folds were probably related and coeval with this upilft. These folds initiated parallel to the main faults and thus record near ideal partitioning of transpressive strain.

During the Late Miocene the Arabia-Africa rotation pole migrated closer towards the Levant Fracture system increasing the angle of convergence across the YF. Shortening and amplification rate of the inline folds increased greatly to maintain the restraining bend. However, the transform zone evolved with transcurrent displacement transferred onto the Roum fault. This has caused the migration of the triple junction from SE Turkey to NE Mediterranean. The Lebanese sector of the transform remains generally transpressive, as evidenced by uplifted shorelines and continued deformation.

Lebanon part of the Syrian Arc:

Walley [1998] provides a series of arguments to prove that the Lebanese ranges were folded as part of the Syrian arc episodes. He argues that the main structuration of Mount Lebanon took place in the Late Cretaceous Senonian times, caused by the closure of the Neo-Tethys during this time and ocean-ocean collisions [*Guiraud and Bosworth*, 1999].

The hypothesis of Walley [1998] seems to be coherent in terms of linking the Lebanese ranges with the regional deformation in Arabia. He suggested that the main mechanism for the folding of Mount Lebanon and Anti-Lebanon should involve inversion of previous extensional structures. This seems to be logical and can explain the similar trend between Mount Lebanon, Anti Lebanon, Yammouneh fault and the Bekaa syncline.

The amounts of displacement presented by Walley [1998] do not seem to have many arguments to support them. He proposes a total displacement of 47 km along the Yammouneh fault, 20 km over the Serghaya, 8 km along the Roum faults, 5km along Carmel fault and 15-20 km shortening taken up by the Palmyrides. These amounts sum up to around 100-105 km, and thus insinuate strain partitioning among the different structures onshore.

Major offshore thrusting as part of the LFS

Daëron *et al.* [2004, 2005, 2007], Carton *et al.* [2009] and Elias *et al.* [2007] argue that the uplift and folding of Mount Lebanon are accommodated by a fold and thrust belt 90 km long and 30km wide offshore the Lebanese coast between Saida and Tripoli (Figures 2.24 and 2.25). This belt is bounded to the North by Aabde fault and to the south by the Roum and Saida faults [*Elias et al.*, 2007]. According to this model, most

of the deformation is accommodated by thrusts, since motion is purely strike slip on Yammouneh and Serghaya faults. They also propose some minor shortening over onshore structures.

Carton *et al.* [2009] advocate that Early Cretaceous spreading took place along a roughly NE-SW trending axis segmented by transform fault. In the past 15 Ma, the interaction of the Levant fracture system with the ENE-WSW normal faults was responsible in creating the 160Km long restraining bend in Lebanon and subsequent inversion of Mount Lebanon. It was mechanically easier for the Levant fracture to follow the weak zone created by faulting along the margin than to slice into the more rigid oceanic lithosphere. For this reason an eastward bend along the Lebanese segment of the LFS is observed (Figures 2.24 and 2.25).

Elias *et al.* [2007] and Carton *et al.* [2009] hypothesis associates the deformation offshore with the onshore geology. It links the old inherited structural features of the Jurassic/Early Cretaceous extension with reactivation and potential inversion during the Neogene deformation. Another argument behind the formulation of the hypothesis of offshore large thrust fault system is the identification of active thrust fault in the Tripoli region (Figure 2.24) [*Elias et al.*, 2007]. The latter might not correspond to real fault scarps but rather erosional cuestaforms [*Dubertret*, 1955; *Gomez et al.*, 2007b]. Thus they're not faults and do not imply more crustal shortening and thickening than has probably occurred. Nevertheless, even though the offshore faults are affecting the overlying strata with local thrusting, they do not seem however to accommodate the whole deformation and uplift of the Lebanese ranges.

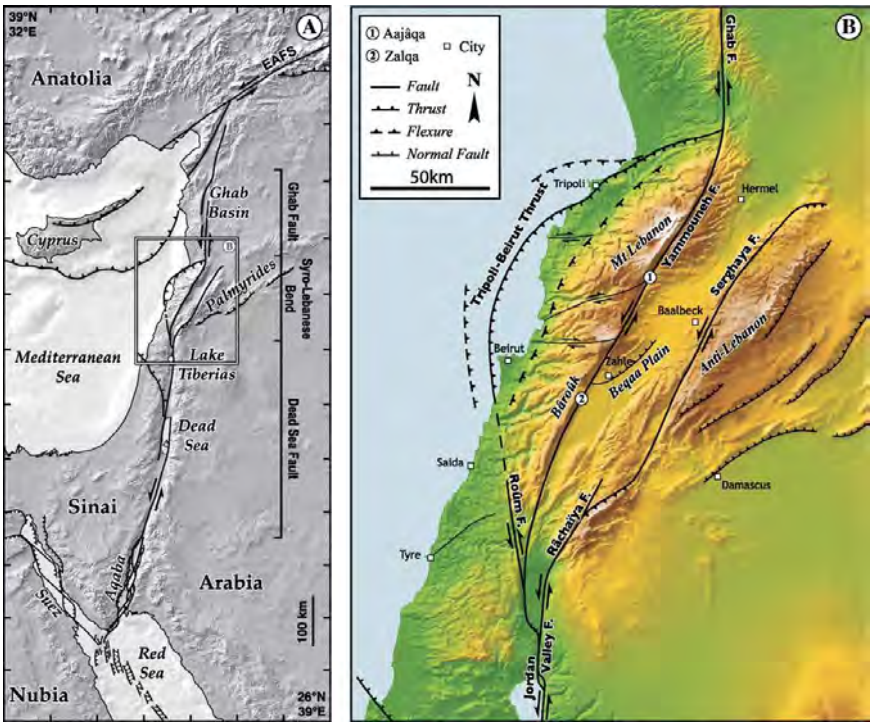

Figure 2.24: Maps showing the alternative model for the evolution of the Lebanese restraining bend. Butler *et al.* [1998] postulate about the fact that the N-S trending Roum fault accommodates all the motion on the LFS in the present days and the Yammouneh fault is no longer active. Daeron *et al.* [2004], Elias *et al.* [2007] and Carton *et al.* [2009] support this hypothesis and suggest that the Roum Fault extends offshore into the Mount Lebanon thrust) which is responsible about all the uplift of Mount Lebanon. From Daeron *et al.* [2004].

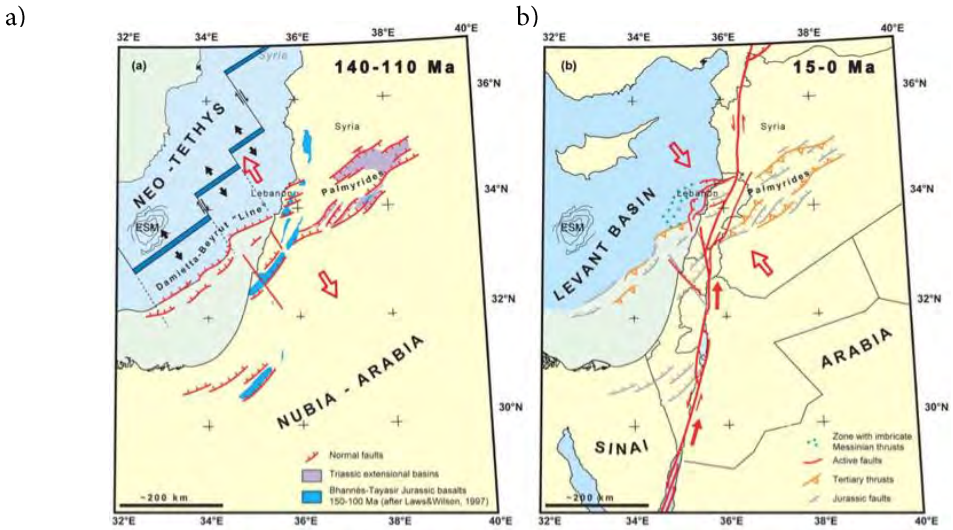

Figure 2.25: Schematic tectonic evolution of Levant margin from Mesozoic time to present-day, showing inversion along Mount Lebanon segment from Carton *et al.*, [2009]. (a) At 140–110 Ma, rifting and seafloor spreading in Late Jurassic to Early Cretaceous, (b) At 15–0 Ma, northward propagation of the LFS and formation of Lebanese restraining bend. In this model, the LFS extends offshore whereby the majority of shortening is taking place in the form of thrusting. ESM=Eratosthenes seamount.

Distributed deformation model

Gomez *et al.*, [2001, 2003, 2006, 2007b] argue that a deformation of Mount Lebanon took place during the Late Miocene and Pliocene till present days in two stages. This deformation was characterised by distribution and partitioning of strain between all the structures of the Lebanese restraining bend and the Palmyrides. Their use of recent seismogenic data, geodesy and satellite imagery reveals partitioned movement along the Yammouneh, Serghaya, Rachaya and Roum faults. The addition of their slip movements would be closer to the total suggested movement between the Arabian and African plates.

The observation that the Yammouneh fault only accommodates strike-slip displacement is taken into consideration in Gomez's model. This would need to accommodate the component of shortening perpendicular to it. This problem is solved by considering an oblique plate motion within the restraining bend partitioned into strike-slip displacements and perpendicular convergence. An important element, would be the Roum fault, oriented N010W acting as an oblique ramp structure bounding Mount Lebanon folds. Based on its geometry, this model assumes a 6km shortening across the Roum fault from geometric simulation. This corresponds to a 17% total horizontal shortening of Mount Lebanon. This is similar to what Hancock and Atiya [1979] suggested of 10-15% bulk shortening. The remaining shortening should be accommodated by the other faults in Lebanon and the Palmyrides.

The Lebanese ranges are part of the Palmyrides structures whereby the Serghaya fault and the Palmyrides may contain a structural link [*Gomez et al.*, 2007b]. The termination of the Serghaya fault suggests a possible linkage with the Jhar fault as an oblique ramp or tear fault that bounds the Palmyride fold belt, and links to the Jhar fault in the northern Palmyrides region (Figure 2.16). This would explain why the Palmyrides might be related to the Lebanese ranges and accommodation of displacement along them might be logical.

Folding followed by faulting dominated deformation

Homberg *et al.* [2010] propose that the LFS initiated south and propagated northwards into Lebanon in two stages, involving widespread mainly folding mode during the Late Miocene to a mixed folding/strike-slip mode, since the Pliocene times.

During the Late Miocene, the LFS locking in northern Israel led to the rotation or shortening of the Lebanese and Syrian blocks. The Lebanon block was affected by a counter clockwise rotation of about 11˚, while the Palmyride block underwent a northward translation. These movements were accommodated by a shortening in the two blocks through folding. Forty kilometres of plate motion were absorbed by folding in Lebanon and the Palmyrides, followed by clockwise rotation in the Palmyrides alone around the western end of the Palmyrides block and above the Palmyride trough (Figure 2.26).

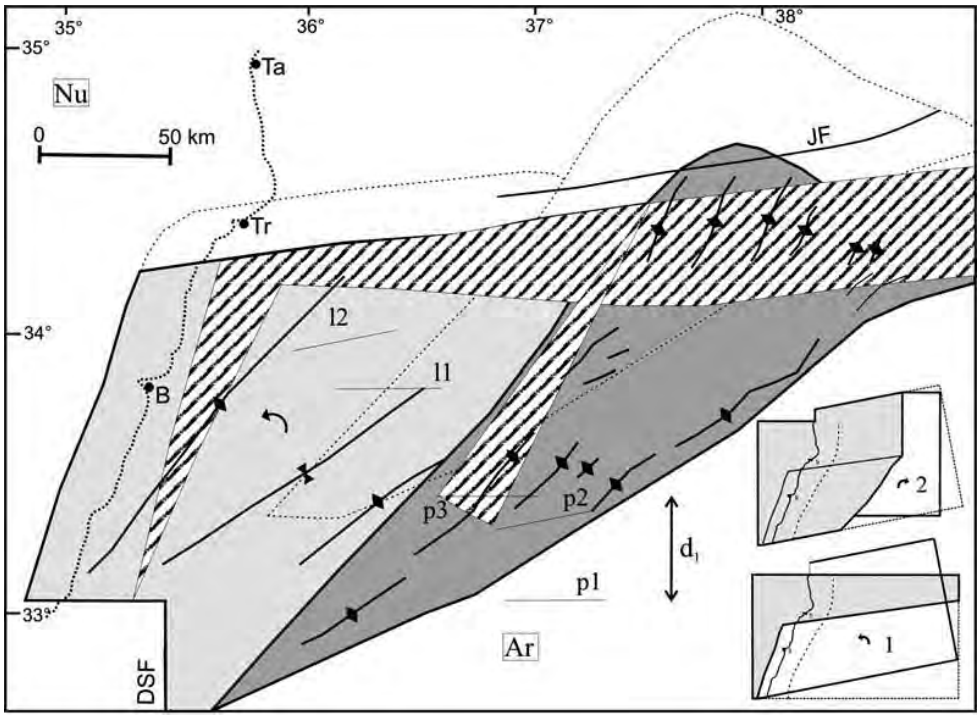

Figure 2.26: Late Miocene deformation in Lebanon and the Palmyrides. Dispalcement d1 of the northward movement of Arabia is accommodated by folding in Lebanon without strike-slip motion. 11˚ of counter clockwise rotation is measured for the Palmyrides and Lebanese blocks followed by clockwise rotation in the Palmyrides alone (right corner inset diagram). Hatched areas indicate the amount of shortening, B, D, Tr, Ta: cities of Beirut, Damas, Tripoli, Tartous. LFS, Dead Sea fault. JF, Jhar fault. From Henry *et al.* [2010].

During the Pliocene, plate movement was accommodated by strike–slip motions along the Roum and Yammouneh faults, as well as local folding and thrusting. 20 and 50 km of plate motion were absorbed by the Roum and Yammouneh faults, whereby slip on the Roum fault resulted in the thrusting and folding currently observed in the Tripoli area. Considering the offshore structures, a deficit in shortening is expected from the transpressive character of the plate boundary and the proposed 100 km of total left-lateral displacement in Lebanon is noted. Finally, due to the angle between the LFS

in Lebanon and in Syria, the left-lateral movement implied rotation of the western block and could explain the 18° counter-clockwise rotation determined in Lebanon after Henry *et al.* [2010] paleomagnetic analysis (Figure 2.27).

It is important to state that in this model, the movements onto the Serghaya and Rachaya faults are neglected. Moreover, the eastward bend of the Yammouneh fault may reflect mechanical contrasts along the western Arabia crust. A proto Yammouneh fault cannot be aligned with Arabia-Africa slip vector and cannot have rotated later to its present day NNE-SSW strike. It is thus an original bend [*Homberg et al.*, 2010].

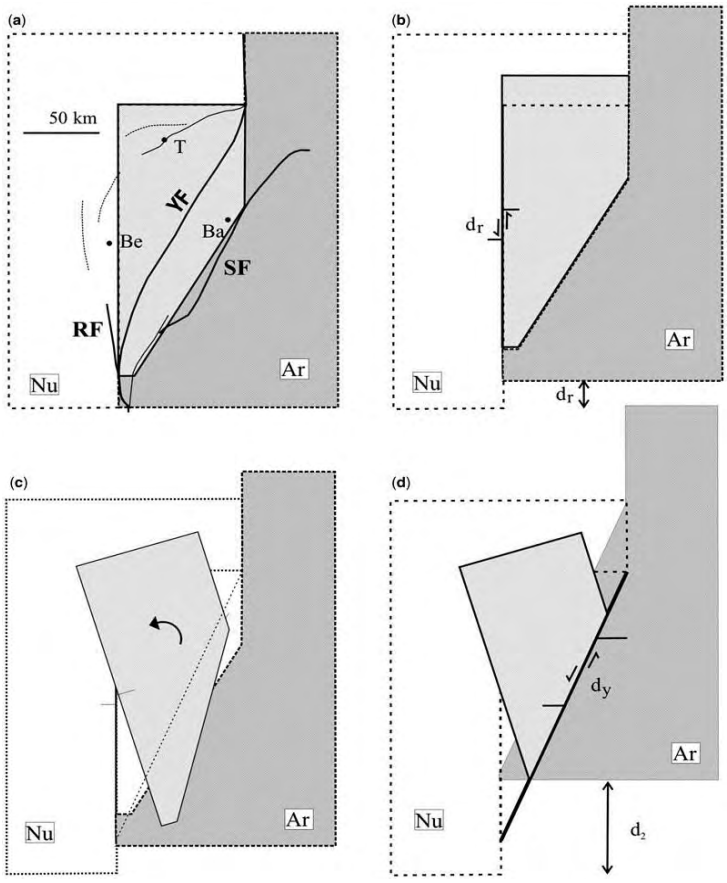

Figure 2.27: Post Miocene mechanism of deformation in Lebanon. (a) initial stage, (b) sinistral slip (dr) on the Roum fault (RF), (c) counterclockwise rotation (see Figure 2.26), (d) sinistral slip motion (dy) on the Yammouneh fault (YF). Nu, Ar, Nubian and Arabian plates. Be, Ba, T: cities of Beirut, Balbeeck, Tripoli. From Henry *et al.* [2010].

Hardy *et al.* [2010] propose a model for the development of the LFS in the Neogene whereby initiation of faulting started in Southern Israel and Northern Syria. They both propagated synchronously toward Lebanon and joined altogether along the

NE-SW deformed zone of Lebanon. Thus, the Lebanese domain might be thought as a faulted ramp structure rather than a transpressive jog.

II. 3.4 Points of convergence and similarities:

The points of similarity between the previously discussed models are considerable. Even though each group has slightly different interpretation of the available dataset. Accordingly, a successful model describing the deformation in the Levant region should involve at least:

- Characterisation of the timing and type of deformation offshore, based on seismic data
- Characterisation of the timing and type of deformation in the Palmyrides and Syria, based on subsurface and field data
- Characterisation of the timing and type of deformation along the major faults in Lebanon, based on field data. This should take into account the role of the E-W faults west and the regional evolution of the LFS in general.

Some points summarizing the agreements and disagreements in literature is presented herein:

- There is a general agreement that in the Late Miocene/Pliocene, deformation in Lebanon is affected by the transpression over central LFS segment. Disagreement is on quantifying how this deformation was accommodated through time and its amount.
- All the authors agree that the bend of the Yammouneh is original, and is not because of later rotation. Its current strike is due to either mechanical contrasts in the lithosphere or due to inherited structures. Nevertheless, some other models that were not discussed in this manuscript propose some degree of rotation over the Yammouneh fault. In any case, it is considered as a major plate boundary.
- Butler *et al.* [1998] and Homberg *et al.* [2010] suggested the presence of some potential thrust folding within Mount Lebanon. This is the core of the model of Carton *et al.* [2009] and Elias *et al.* [2007], whereby they attribute all the

deformation of Lebanon to thrusts. However, thrusting is not supposed to be solely responsible of the folding of Mount Lebanon, and geometry of thrust faults should be revised.

- Carton *et al.* [2009], Homberg *et al.* [2010] and Butler *et al.* [1999] agree that a significant amount of deformation is currently accommodated offshore and that the Levant margin has been affected by LFS activity.

- Walley [1998] suggested the presence of a major boundary fault between northern Mount Lebanon and southern Mount Lebanon, and attributed this boundary to the extension of the deep Mesozoic Jhar fault from the Palmyrides in Syria (Figure 2.16). On the other hand, Carton *et al.* [2009] argue for a large master normal fault trending NE-SW offshore Beirut (Figure 2.25), and timed it Late Jurassic / Early Cretaceous, which is the same age proposed for the Jhar fault [*Sawaf et al.*, 2001; *Brew et al.*, 2003]. It is likely then, that if an extension of the Jhar fault is found in Lebanon, it could also continue offshore and correspond to the fault mapped by Carton *et al.* [2009]. In this case, major crustal variations would extend through Lebanon

- Walley [1998] and Homberg *et al.* [2010] suggested an Early Miocene deformation in Lebanon based on unconformities. Both agree on the fact that early deformation is not related to transform tectonic or the LFS in general. The difference lies in the fact that Homberg *et al.* [2010] postulate the Early Miocene deformation minor relative to the main deformation in the Late Miocene, while Walley [1998] postulates that the Early Miocene deformation is responsible in large scale folding of Mount Lebanon.

CHAPTER III

TECTONIC STRUCTURES OFFSHORE LEBANON

Table of contents

III. Tectonic structures offshore Lebanon

"Everything we hear is an opinion, not a fact. Everything we see is a perspective, not the truth" Marcus Aurelius, Meditations

This chapter consists of two parts, one discussing the methodology adopted in seismic interpretation and the second is published article in *Tectonics* discussing the various tectonic structures mapped in the Levant Basin and their implication on the understanding of the regional geodynamics of the Levant region. The usage of high quality 3D seismic data allowed for the first time to unravel the Levant Basin offshore Lebanon and investigate it with great detail. New structures were documented and correlated with the regional geology of the region. These include NE trending anticlines, NW-SE strike-slip faults, NE trending thrust faults and an extensive NW trending normal faults array. Throughout this paper, the geodynamic setting of Arabian and Anatolian plates is noted to have a strong impact on the activity of these structures throughout geological times. This, together with the activity along the LFS, has caused the reactivation of existing structures. The interpretation of the normal faults and their effect on the basin will be discussed in detail in chapter 4. The most peculiar conclusion from the study of the basin is that no current shortening is accommodated offshore Lebanon, and the exact timing of activity of the LFS is well correlated through looking at activity of offshore structures.

III. 1 General Methodology

The study area of this PhD project covers the northern Levant basin offshore Lebanon with its corresponding eastern margin between 33°N and 35°N. Two seismic cubes are used in this study courtesy of Petroleum Geo-Services (PGS) and 830 km long seven N-S regional 2D seismic lines were also provided by PGS (Figure 3.1). This data is described in detail in in the article later in this chapter. Seismic interpretation was performed on a LINUX workstation using Paradigm's software Gocad. The interpretation workflow included a continuous integration between regional 2D seismic lines and 3D seismic cubes (Figure 3.2).

The lithostratigraphic units in the basin were adpopted from Hawie *et al.* [2013] who correlated the seismic data offshore Lebanon with wells offshore Israel. Even though this brings uncertainty in interpretation of geologic structures, it is nevertheless an essential step necessary for interpretation. The ages are thus hypothetical until wells are drilled offshore Lebanon to reduce uncertainty. Still, the Base Messinian and Base Pliocene horizons are very well constrained due to the exceptional seismic signature produced by the presence of evaporites. The seismic units include seven seismic packages corresponding to seven lithostratigraphic units believed to be: Cretaceous, Senonian/Eocene, Eocene/Oligocene, Lower Miocene, Upper Miocene, Messinian and Pliocene respectively (Table 3.1).

Table 3.1: *The different seismic units and horrizons used in this study. Naming and ages are adopted from Hawie et al. [2013].*

Depth (m)	***Hypothetical age***	***Name***	***Horizons***
2000	Pliocene	SP8	R8
3500	Messinian	SP7	R7
5000	Upper Miocene	SP6	R6
6000	Lower Miocene	SP5	R5
8000	Oligocene / Eocene	SP4	R4
10000	Eocene / Senonian	SP3	R3
-	Cretaceous	SP2	

The regional structural and stratigraphic architecture of the basin was investigated by interpreting the 2D seismic lines. This was accomplished by interpreting regional horizons and various structures in 2D lines. Construction of depth maps and dip maps for various horizons, such as the Base Messinian and the Base Miocene, allowed to locate certain regional structures controlling the basin. Isopach maps of stratigraphic units, mainly the Oligocene, Lower and Upper Miocene, were also constructed and shed the light on the geodynamic evolution of the basin by looking at regional thickness variations. Even though the seismic dataset is limited to Lebanon and does not include Cyprus and Israel, the information they convey is crucial to understand the geology of the basin.

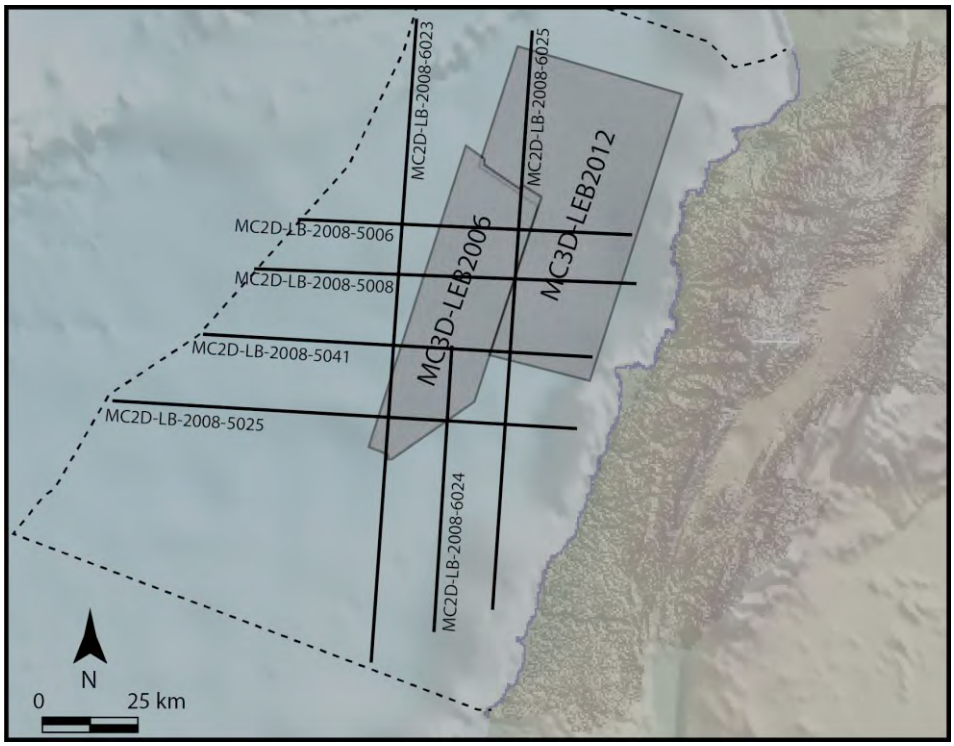

Figure 3.1: Location of the seismic data throughout this study.

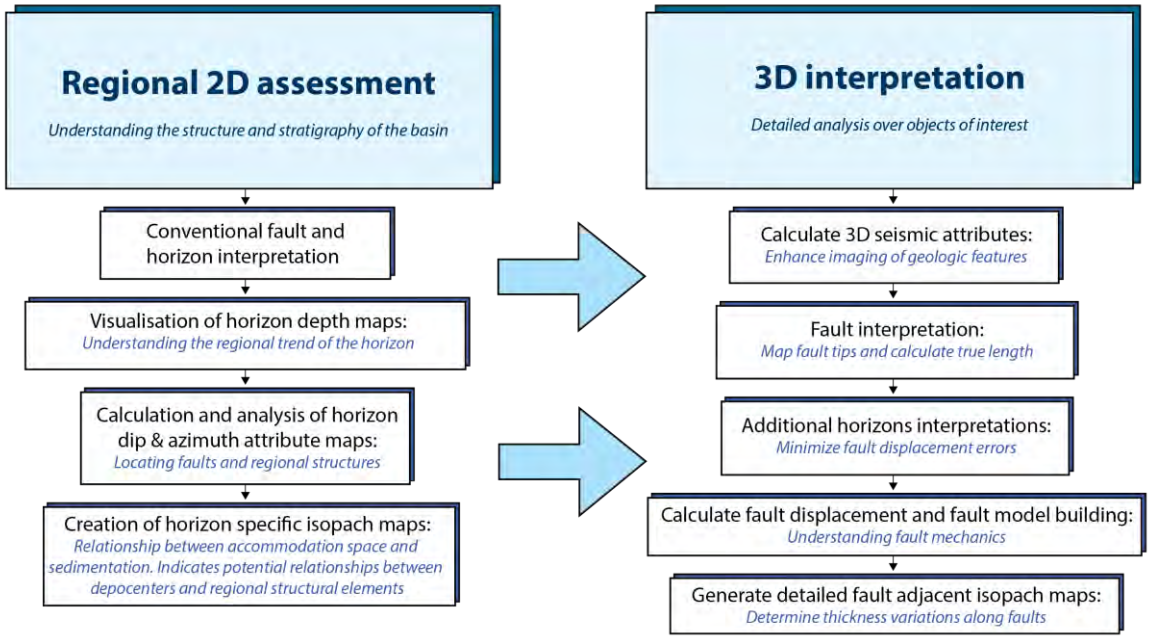

Figure 3.2: Interpretation workflow performed in this study highlighting the major steps undergone in order to perform a regional geological assessment of the basin, and a detailed structural study later on.

Once regional investigation provided enough ideas about the architecture of the basin, specific structures were analysed by interpreting the 3D seismic data. Interpretation of structures is challenging by using 2D seismic data alone given the 5 km spacing between 2D seismic lines offshore Lebanon. Orientations, linkage, displacement and extent will be hard to resolve if only 2D seismic data is used for interpretation. 3D data, however, increased accuracy of subsurface interpretation with their dense grid of traces, allowing features such as faults to be followed and mapped with much greater assurance (Figure 3.3). This, together with the ability to look at seismic sections in all directions, provided an unequal opportunity to analyse specific structures in great detail and minimum uncertainty.

Techniques used in 3D seismic interpretation in the course of this study consisted of applying specific seismic attribute to the desired cube location. Seismic attribute mapping uses variations in the amplitude and phase of the seismic wavelet and tracks these through entire data volumes. Seismic attributes thus enhance visualisation and imaging of geological features and can be applied to entire or part of 3-D post-stack seismic volumes and horizons [*Bahorich and Farmer*, 1995]. The attributes used in this study were coherence attribute to locate faults, and dip attributes to locate anticlines and structures.

The dip attributes were created by calculating for a picked horizon, or for a 3D cube extract, of the local dip and its azimuth. This attribute will highlight dip changes across the area with different colours and are thus beneficial to identify folds. A second form of attribute, coherency, was calculated by exemplifying discontinuities and disruptions in the lateral integrity of seismic reflections [*Bahorich and Farmer*, 1995]. Once calculated for the desired 3D cube, visualisation in different orientations allowed to clearly understand the structure. Sections across the faults were used to pick up and map the fault plane once it was identified in attribute or amplitude slices. Thus, every structures documented in this study was investigated through rigorous application of this workflow, by interpreting attribute cubes, depth maps mainly along the Base Messinian horizon, and seismic sections perpendicular to their strike.

3D seismic interpretation was particularly useful in this study during normal fault interpretation, discussed in chapter 5. The advantage of 3D data was to map entirely the fault extent investigate relay geometries among fault surfaces [e.g. *Kosi et al.*, 2012]. Many horizons were further interpreted to limit uncertainty in fault displacement mapping.

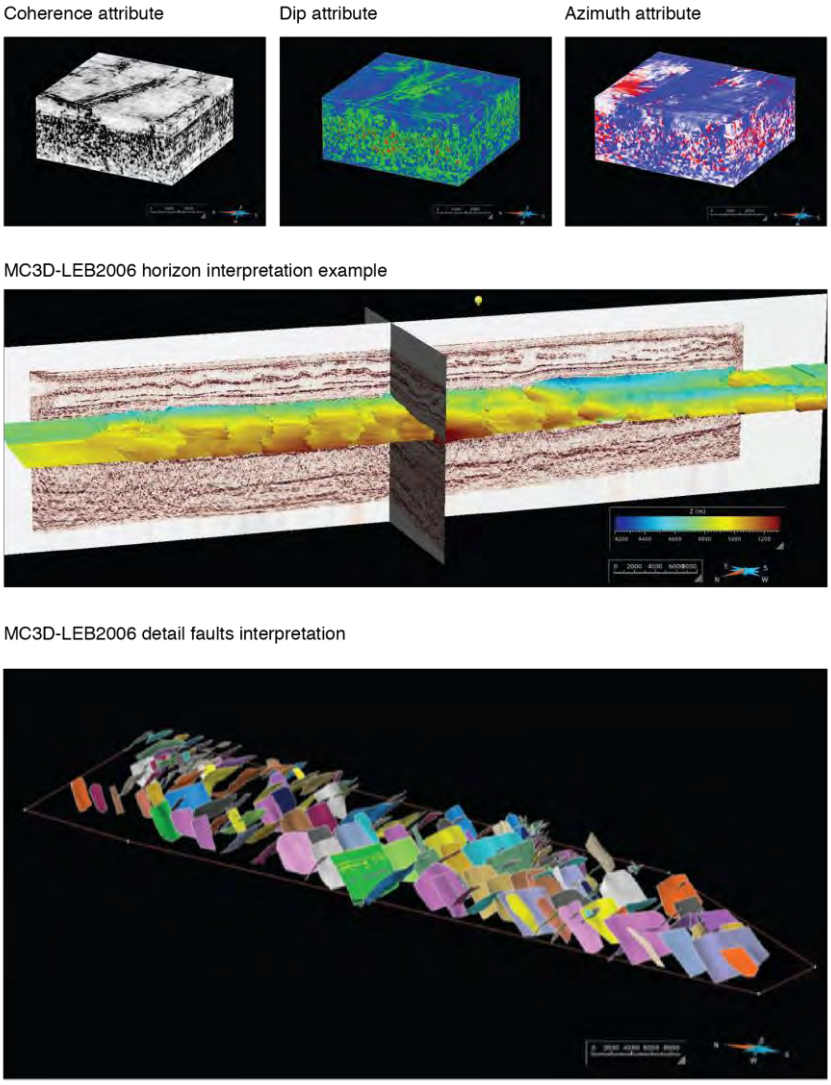

Figure 3.3: Examples of attributes applied to the seismic cube to increase imaging of geological features. An example of the Base mid-Miocene horizon and all Oligo-Miocene normal faults interpretation, shows the value of using 3D data to interpret geological structures in detail, which is very challenging to undertake by only using 2D data.

AGU PUBLICATIONS

Tectonics

RESEARCH ARTICLE

10.1002/2014TC003574

Key Points:
- The 3-D seismic data allowed tectonic characterization of the Levant Basin
- Tectonic structures in the Levant Basin are inherited and reactivated
- No active shortening is currently attested offshore Lebanon

Impact of Cenozoic strike-slip tectonics on the evolution of the northern Levant Basin (offshore Lebanon)

Ramadan Ghalayini[1,2,3], Jean-Marc Daniel[3], Catherine Homberg[1,2], Fadi H. Nader[3], and John E. Comstock[4]

[1]Sorbonne Universités, UPMC Université Paris 06, Paris, France, [2]CNRS, Paris, France, [3]IFP Energies nouvelles, Rueil-Malmaison, France, [4]Petroleum Geo-Services, Oslo, Norway

START OF ARTICLE 1

III. 2 Abstract

Sedimentary basins adjacent to plate boundaries contain key tectonic and stratigraphic elements to understand how stress is transmitted through plates. The Levant basin is a place of choice to study such elements because it flanks the Levant Fracture System and the Africa/Anatolia boundary. This paper uses new high quality 3D seismic reflection data to unravel the tectonic evolution of the margin of this basin during the Cenozoic, the period corresponding to the formation of the Levant Fracture System, part of the Africa/Arabia plate boundary. Four major groups of structures are identified in the interpreted Cenozoic units: NW-SE striking normal faults, NNE-SSW striking thrust-faults, ENE-WSW striking dextral strike-slip faults, and NNE trending anticlines. We demonstrate that all structures, apart of the NW-SE striking normal faults, are inherited from Mesozoic faults. Their reactivation and associated folding started during the Late Miocene prior to the Messinian Salinity Crisis due to a NW-SE compressional stress field. No clear evidence of shortening at present day offshore Lebanon and no large NNE-SSW strike-slip faults parallel to the restraining bend are found indicating that the Levant Fracture System is mainly contained onshore at present day. The intermittent activity of the interpreted structures correlate with the two stages of LFS movement during late Miocene and Pliocene. This paper provides a good example of the impact of the evolution of plate boundaries on adjacent basins and indicates that any changes in the stress field, as controlled by the plate boundary, will affect immediately the pre-existing structures in adjacent basins.

III. 3 Introduction

Crustal structures related to transform plate boundaries have been extensively documented worldwide [e.g., *Woodcock*, 1986; *Sylvester*, 1988; *Cunningham and Mann*, 2007]. Relative displacements at this type of plate boundary are accommodated by complex fault systems that have been classified in detail [see *Dooley and Schreurs*, 2012 for a review] and that can locally create restraining or releasing bends [e.g., *Cunningham and Mann*, 2007] forming typical strike-slip basins [*Mann et al.*, 1983] bound by sub-parallel master faults [*Sylvester*, 1988]. Considerable efforts have been concentrated on the study of the boundary itself [*Freund*, 1974; *Zoback*, 1991], while little attention has been paid on the impact of such fault systems on adjacent basins. Hence, studying such areas should provide some understanding on how stress and strain are transmitted to the plate interiors from transform plate boundaries.

The Eastern Mediterranean Levant Basin is an area where the effect of an adjacent major strike-slip fault in a complex geodynamical context can be tested. The Levant Basin is today bordered by the Levant Fracture System (LFS) to the east, a 1000 km long left lateral transform fault, linking rifting in the south with collision and suturing in the north (Figure 3.4). Extensive work over the evolution of the LFS was conducted previously, leading to a wealth of knowledge regarding its evolution. However, lack of offshore data in past years and uncertainty regarding geometry, displacement and shortening over the LFS onshore has led to major debates on the geological evolution of the Levant margin in general [see *Beydoun*, 1999 for a review], and the Lebanese restraining bend in particular [*Butler et al.*, 1998; *Walley*, 1998; *Gomez et al.*, 2007b; *Homberg et al.*, 2010]. Certain authors argue that deformation continues offshore where shortening occurred along NNE-SSW structures [*Elias et al.*, 2007; *Carton et al.*, 2009]. There are also unexpected aspects of the deformation in Lebanon like the decrease of shortening onshore since Pliocene time [*Homberg et al.*, 2010] whereas plate kinematics predict an increase in the transpressive character of the plate motion [*Le Pichon and Gaulier*, 1988]. The interpretation of the structures in the Levant Basin is also challenging due to the complex tectonic setting characterizing this basin since the Late Mesozoic.

Recent high quality 3D seismic reflection data permits a detailed study of the northern Levant Basin, offshore Lebanon. The availability of such data allowed to better constrain and understand the stratigraphy and geodynamics offshore Lebanon [*Montadert et al.*, 2010, 2014; *Hawie et al.*, 2013]. In this paper, detailed interpretation of the new 3D seismic data unveiled the structural evolution of the northern Levant

Basin during the Cenozoic, and the effects of the nearby LFS. The described structures offshore Lebanon are then correlated with regional tectonics of the Levant Basin in order to investigate causative mechanisms during their formation and growth.

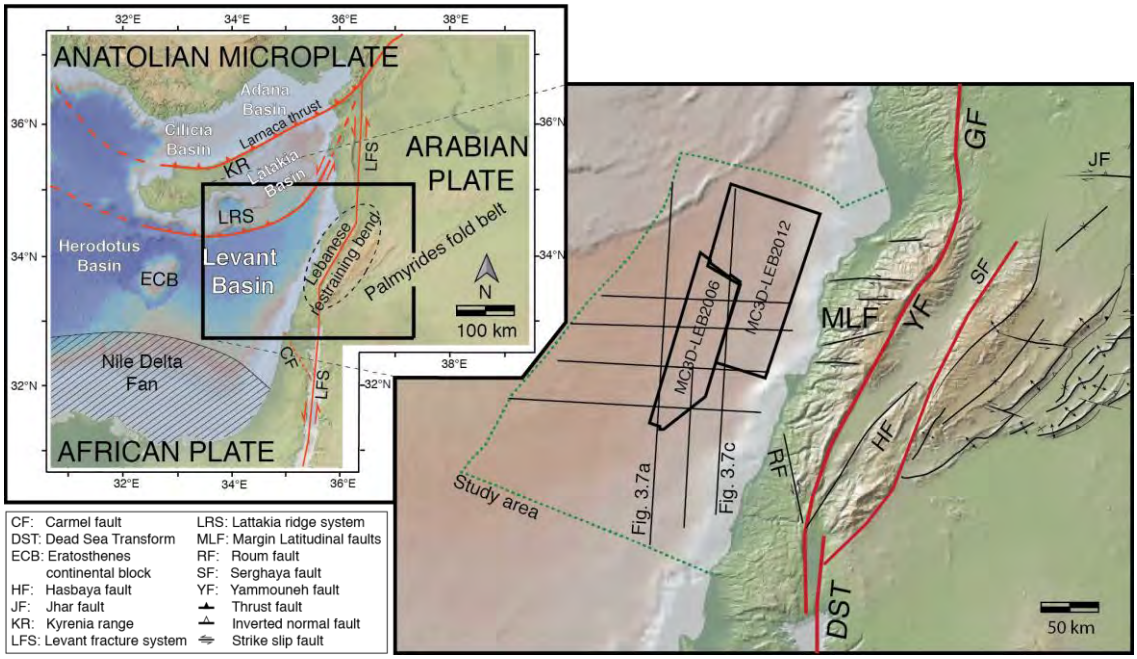

Figure 3.4: Location map of the study area showing the major structures of the Eastern Mediterranean and the dataset available for this study. Background map is from http://www.geomapapp.org.

III. 4 Regional setting

The Levant Basin (Figure 3.4) formed due to pulsed breakup of Gondwana during the Late Palaeozoic to Mesozoic [*Garfunkel and Derin*, 1984; *Robertson*, 1998a]. The strongest pulse is believed to have occurred during the Early to Middle Jurassic [*Ben-Avraham et al.*, 2002]. Numerous NE-SW striking Mesozoic normal faults were perpendicular to the rifting which occurred under a NW-SE extensional direction [*Gardosh et al.*, 2010; *Montadert et al.*, 2014]. Seismic refraction profiles in the Eastern Mediterranean [*Makris et al.*, 1983; *Ben-Avraham et al.*, 2002; *Netzeband et al.*, 2006] may indicate that the crust is only 8 km thick, and thus significantly thinned beneath the Levant Basin [*Hirsch et al.*, 1995; *Vidal et al.*, 2000; *Gardosh et al.*, 2010]. Onshore gravity data demonstrate westward thinning of the continental crust beneath Syria and Lebanon [*Beydoun*, 1977; *Khair et al.*, 1997], and seismic refraction data shows a similar trend in Israel and its offshore [*Makris et al.*, 1983; *Netzeband et al.*, 2006]. Inland, the Palmyra Basin has been an important sedimentary depocenter since the Late Permian [*Brew et al.*, 2001b] and Triassic [*Chaimov et al.*, 1992] with extension and normal

faulting in the Jurassic, and Late Cretaceous [*Best et al.*, 1993; *Chaimov et al.*, 1993; *Litak et al.*, 1998]. Lebanon and its offshore might constitute the westward continuation of the Palmyra Basin [*Walley*, 1998].

During the Late Cretaceous, subduction and obduction accommodated progressive closure of the Neo-Tethys ocean [*Stampfli and Hochard*, 2009; *Frizon de Lamotte et al.*, 2011]. This major geodynamic event also caused contraction of the Levant Basin and margin, and triggered development of an arcuate fold belt in Palmyra, Israel and Sinai termed the Syrian Arc [*Walley*, 1998]. This fold belt resulted from the inversion of Early Mesozoic extensional structures [*Druckman*, 1981; *Best et al.*, 1993; *Chaimov et al.*, 1993; *Druckman et al.*, 1995]. Two main episodes of Syrian Arc folding have been identified: Early Senonian and Late Eocene/Oligocene [*Hempton*, 1987; *Moustafa and Khalil*, 1994; *Eyal*, 1996; *Garfunkel*, 1998; *Walley*, 1998].

Collision of and suturing between Afro-Arabia and Eurasia commenced during the Oligocene to Early Miocene [*Dewey et al.*, 1973; *Sengor and Yilmaz*, 1981; *Beydoun*, 1993; *Allen et al.*, 2004; *Frizon de Lamotte et al.*, 2011]. It resulted in the formation of numerous trending NE-SW gentle folds, both onshore and offshore. Similarly, angular unconformities between the Middle Eocene and Burdigalian in Lebanon [*Dubertret*, 1955; *Walley*, 1998; *Boudagher-fadel and Clark*, 2006; *Homberg et al.*, 2010; *Hawie et al.*, 2014], NW Syria and the Palmyra basin [*Sawaf et al.*, 2001] attest together with these NE-SW anticlines to a regional folding during the Early Miocene.

The Oligocene to Early Miocene has witnessed the separation of Arabia from Africa. This has resulted in the establishment of a new plate boundary along the Red Sea and the present location of the LFS (Figure 3.4) [*Le Pichon and Gaulier*, 1988]. The LFS is a series of predominantly strike-slip faults cutting the NW Arabian margin between the Gulf of Aqaba in Jordan and the Taurus Mountains in Turkey. It forms a 1000 km long, left-lateral transform system [*Dubertret*, 1955; *Quennell*, 1958] comprising, from south to north, the N-S Dead Sea segment, the NNE-SSW striking central segment in Lebanon, and the N-S Ghab Fault (Figure 3.4)[*Quennell*, 1958; *Freund*, 1965; *Dubertret*, 1972]. The central LFS segment in Lebanon forms a restraining bend with many strike-slip faults and folds, comprising the NNE-SSW striking Yammouneh and Serghaya Faults [*Dubertret*, 1955] (Figure 3.4)Deformation within the LFS restraining bend is mainly partitioned along its different structures [*Gomez et al.*, 2007b]. Part of those structures consists of ENE-WSW to E-W faults cross-cutting the Lebanese margin, and termed the latitudinal faults [*Gedeon*, 1999]. These faults are dextral strike-slip with offsets of about 1-2 km, seismically active, and are widely recognized as reactivated

Mesozoic structures potentially extending to the offshore [*Dubertret*, 1955; *Sabbagh*, 1961; *Gedeon*, 1999]. The potential offshore expression of the LFS forms part of the focus of this paper. *Ron et al.* [1984] explain the occurrence of the dextral strike-slip faults as contemporaneous with block rotation caused by sinistral strike-slip faulting along the LFS. Synchronously with movement on the LFS, the Lattakia Ridge System (LRS) was active and accommodating during the Messinian and Pliocene sinistral strike-slip movement between Cyprus and the Eastern Levant margin. This activity was associated with westward escape of the Anatolian microplate, relative to the Eurasian plate, following an anticlockwise direction of rotation [*Sengor and Yilmaz*, 1981; *Hall et al.*, 2005a; *Reilinger et al.*, 2006; *Le Pichon and Kreamer*, 2010].

III. 5 Dataset and methodology

The study area covers the northern Levant Basin, offshore Lebanon between 33°N and 35°N (Figure 3.4). Two seismic cubes are used in this study courtesy of Petroleum Geo-Services (PGS): (i) 1516 km^2 PSTM MC3D-LEB2006 which was acquired in 2006 using six streamers and two 3,090 cubic inch air guns positioned at a depth of 6 m in water depth ranging between 1.5 and 2 km. Streamer length was 6000 m long at a spacing of 12.5 m and 25 m shot point intervals; and (ii) 2774 km^2 PSDM MC3D-LEB2012 which was acquired in 2012 using 12 streamers and two 4,135 cubic inch air guns positioned at a depth of 6 m in water depth ranging between 1.5 and 2 km. Streamer length was 7050 m long at a spacing of 12.5 m and 25 m shot point intervals. In addition, 830 km long seven N-S regional 2D seismic lines were also provided by PGS, and acquired in 2008 using a 6,180 cubic inch air gun at 8 m and 8,100 m long streamer with 9.2 seconds recording length (Figure 3.4).

The presence of a 2 km thick salt unit in the basin [*Hsu et al.*, 1973] creates significant velocity anomalies in underlying units. Furthermore, the structural complexity of the Levant Basin causes variations in lateral velocities. Thus, pre-stack depth migrated data (PSDM), where available, was of great value to this study. PSDM is an efficient way to correct image distortion caused by overburden velocities in reflections, and to reduce the effect of lateral velocity variations caused by the complex structural geometries [e.g., *Agudelo et al.*, 2009].

Interpretation of detailed structural elements was performed on depth-converted sections. This has helped to negate interpretation of artifacts related to the thick Messinian evaporites. Because no well data were available, time to depth conversion was

done using a velocity model built from stacking velocities. Frequency ranges are between 40 and 80 Hz yielding a tuning thickness of about 6 m in the Pliocene and 15-25 m in the Miocene. The interpretation workflow included a continuous integration between regional 2D seismic lines and 3D seismic cubes. Interpretation of horizons and faults, and creation of isopach maps were performed on 2D data by using several depth structure maps at different levels, which allowed understanding the geometry of the basin and the distribution of key stratigraphic units (Figure 3.5). Following this step, detailed interpretation of structural elements was performed using amplitude cubes, structural seismic attributes and depth structure maps (Figure 3.8). The attributes used included coherence attributes to image discontinuities and faults [e.g., *Bahorich and Farmer*, 1995], and dip attributes to enhance visualization of anticlines and folds.

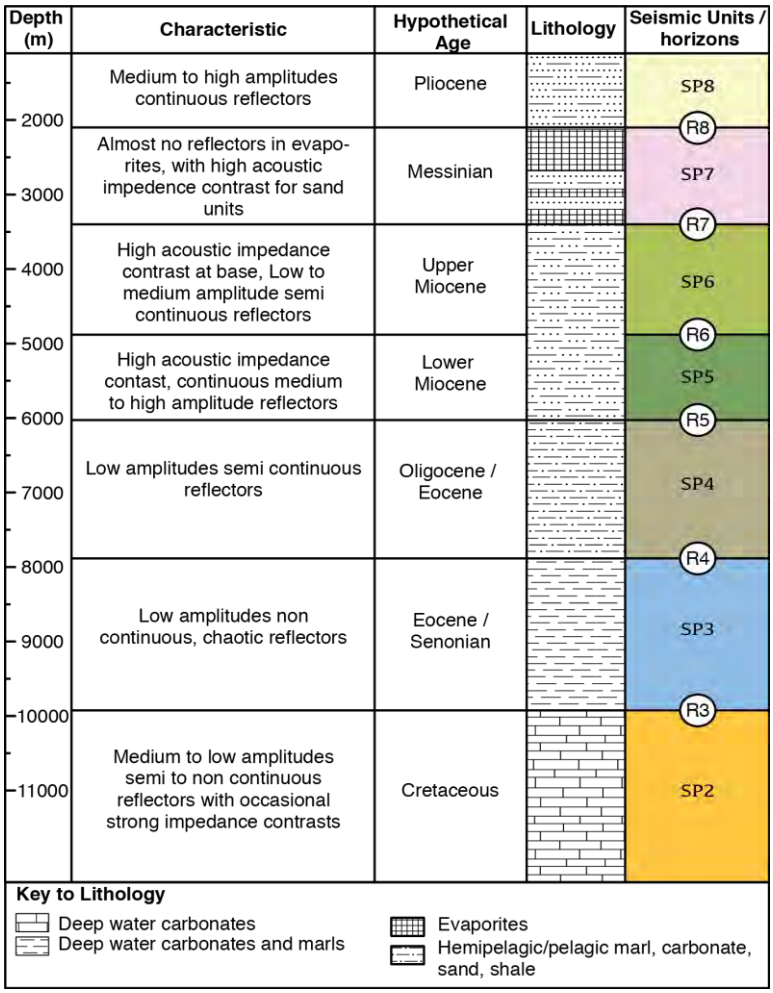

Figure 3.5: Regional stratigraphic column of the Levant Basin. Seven seismic units are interpreted in this data set consisting of deep water carbonates and marls SP2 unit, hemipelagic/pelagic sediments SP3 unit, stacked deep-water clastic and hemipelagic deposits SP4-5-6, evaporite SP7 unit and intercalated turbidites/hemipelagic SP8 unit. These seismic sequences are mapped based on the interpretation of seismic packages and their bounding surfaces. Due to lack of drilling activities and well data offshore Lebanon, dating of these packages is based on wells offshore Israel [*Gardosh et al.* 2006], and thus remains speculative. Nomenclature of units is adopted from Hawie *et al.* [2013].

III. 6 Structural style of the northern Levant Basin

The interpretation of seismic data was used to build the structural scheme illustrated in figure 3.6. The main structural elements in the basin can be divided into Pre-Cenozoic and Cenozoic structures. The former will not be investigated in detail in this paper due to large uncertainties in the Pre-Cenozoic units and the relatively poorer seismic resolution at greater depths.

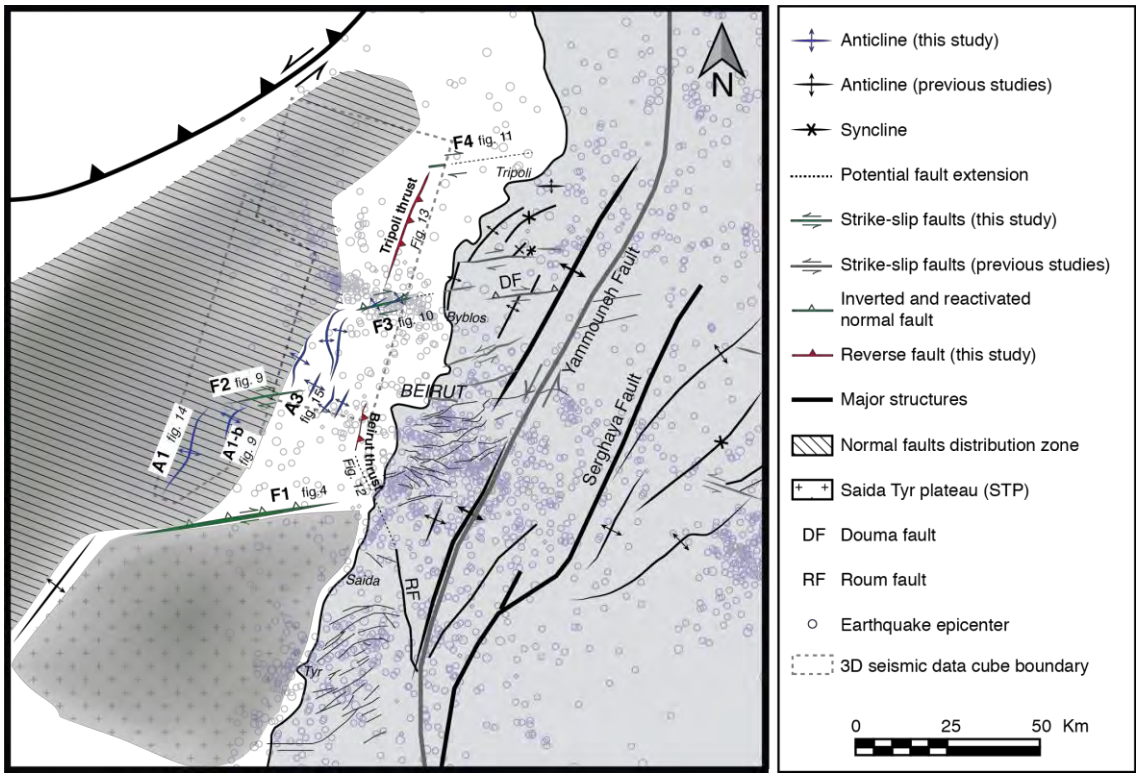

Figure 3.6: Structural map of the Levant Basin offshore Lebanon showing the structures of the basin, together with the structures onshore in Lebanon and part of Syria. The structures mapped in the course of this study are based on 3D seismic interpretation and consist of four predominant fault sets: (i) NE-SW trending thrust faults (in red), (ii) ENE-WSW striking dextral strike-slip faults (in green), (iii) NNE trending anticlines (in blue), and (iv) NW-SE striking normal faults (in hachure). Onshore structures are from Brew *et al.* [2001] and Dubertret [1955].

III. 6.1 Pre-Cenozoic structures

Description

Regional 2D seismic lines show the overall geometry of the basin (Figure 3.7). An important structure named the Saida-Tyr plateau (STP) is found to the south of the study area (Figure 3.7). It is bounded to its north by a deep crustal fault (F1) separating it from the distal part of the Levant Basin. To its west, it is separated from the thick Cenozoic units by NNE-SSW striking strike-slip faults [*Hawie et al.*, 2013]. Magnetic maps of the Levant Basin show the presence of an irregular body below the STP, evidenced by relatively stronger magnetic anomalies than its surrounding [e.g., *Segev and Rybakov*, 2010]. The Levant Basin north of STP is characterized by a 9 km thick succession of Cenozoic sediments. SP3 and SP4 units (interpreted as Senonian/Eocene and Oligocene) thicken to the north whereas units SP5 and SP6 (interpreted as Lower and Upper Miocene) thicken towards the basin center (Figure 3.7).

In the NW part of the study area, the LRS marks the northern boundary of the Levant Basin (Figure 3.7). LRS forms a fold and thrust belt, with a vertical cumulated displacement of Tertiary strata of about 3 km, and comprises many deep thrust faults, ramp anticlines, hanging wall cutoffs and growth strata architecture. It affects all the units in the basin, from the Cretaceous till Pliocene and marks a prominent topography at the seafloor.

Interpretation

The relatively thinner Miocene units on top of STP indicate that the latter was in place during the Cenozoic when the Miocene sediments were deposited. Furthermore, the geophysical and structural observations over STP indicate that this structure might be an old fragment of a thick continental crust bordered by faults. The crustal thickness below STP is larger than the rest of the basin and hence it might resemble the Eratosthenes seamount [e.g., *Makris et al.*, 1983].

Variations of thicknesses of Tertiary units in the basin indicate a certain geodynamic control prior to and during the Cenozoic, shaping the current architecture of the basin. Thickening of SP3 (Senonian/Eocene) and SP4 (Eocene/Oligocene) is observed close to the LRS [*Hawie et al.*, 2013] and indicates active subduction in the Upper Cretaceous [*Hall et al.*, 2005a] (Figure 3.7). The thickening of the Miocene units (SP5 & SP6) suggests a geodynamic change during the Miocene responsible in shifting

the sedimentary depocenter toward the center of the basin, after being closer to LRS in the Senonian and Eocene.

III. 6.2 Cenozoic structures

A depth-structure map of the mid-Miocene horizon (R6) and a depth slice in the dip attribute cube near the base-Messinian horizon (R7) show the presence of several anticlines and faults (Figure 3.8). The geometry, age and relationship between these structures, can be studied in detail with the available 3D seismic data (Figures 3.6 and 3.8). Overall, four different groups of structures are identified (Figure 3.6) and these are described below.

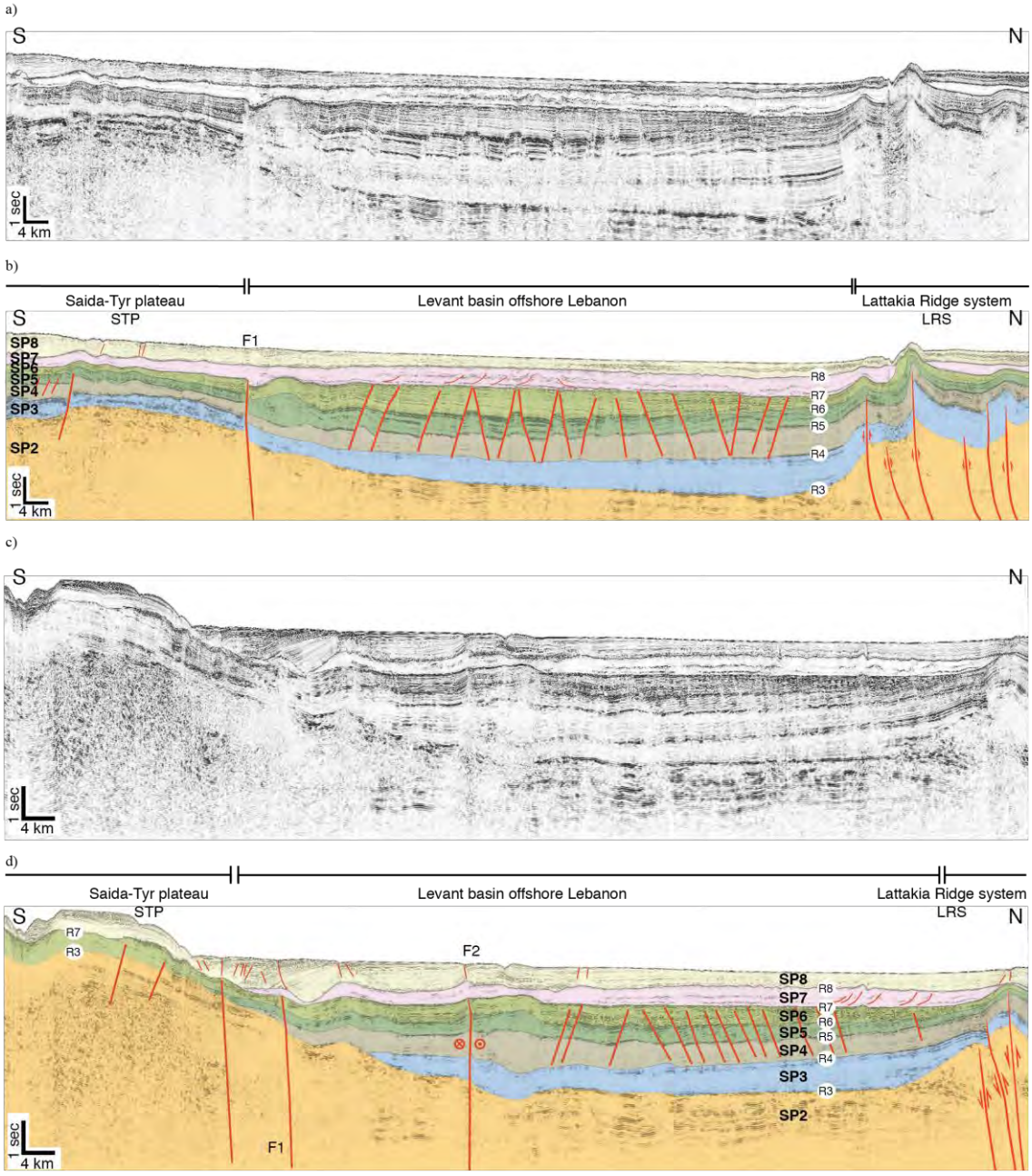

Figure 3.7: regional N-S 2D seismic sections across the Levant Basin offshore Lebanon showing the different structural and stratigraphic elements of the basin, delimited by the Lattakia Ridge System to the north and by the Saida-Tyr Plateau to the south. For location, see Figure 3.4.

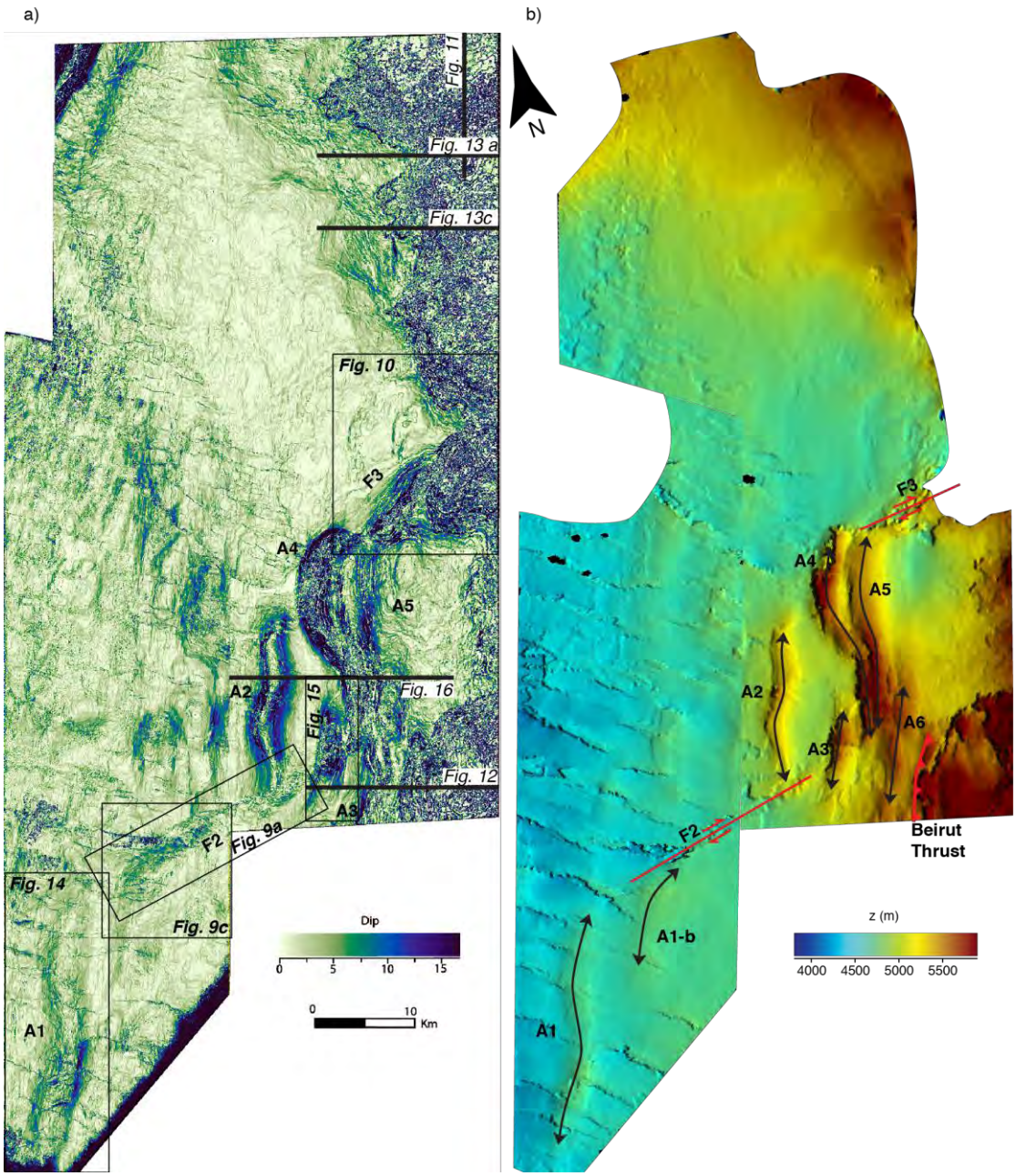

Figure 3.8: a) Depth slice in the dip attribute cube taken below R7 horizon along the MC3D-LEB2006 and MC3D-LEB2012 seismic cubes; and b) depth structure map of R6 (base mid-Miocene horizon). These maps show the multitude of folds and faults in the Levant Basin offshore Lebanon and their distribution. The boundary and location of the 3D blocks is shown in Figure 3.4.

Normal faults

Description

A dense array of normal faults is found in the central, deepest part of the Levant Basin (Figures 3.6, 3.8 and 3.9). These faults are regularly spaced and typically strike NW-SE. They dip 60° either to the NE or SW. Furthermore, they are layer bound, being developed only in the Oligo-Miocene units (SP4, 5 and 6), and bounded above and below by the interpreted Base Messinian (R7) and Eocene unconformity (R4) (Figures 3.7 and 3.9). The maximum documented displacement along these faults is 415 m. Superposition of a basin-wide fault mapping [*Dupin et al.*, 2012] and a Miocene isopach revealed that these faults are tallest and have highest displacement where the Miocene sequence is relatively thick (Figure 3.10). They are almost absent along the margin of the basin and on the STP, and are less well-developed in the southern Levant Basin where the Miocene unit is thinner [e.g., *Gardosh and Druckman*, 2006]. Sediment thickness calculations for units belonging to Lower and Upper Miocene (SP5 and SP6 respectively) along fault planes revealed expansion index ratio as defined by [*Cartwright et al.*, 1998] between 1.02 and 1.2 (Figure 3.11).

Interpretation

The thickening of units in the hanging wall blocks indicates that these faults have nucleated in the Early Miocene. They were syn-sedimentary during the Miocene, with uncertainty on their current activity. The presence of NW trending normal faults in the basin is not coeval with any documented NE-SW extension during the Miocene in the Levant Basin. It is hence difficult to relate these faults with a tectonic origin. Knowing the strong correlation between sediment thickness and the distribution of these faults, it is very likely that their distribution might be associated with the thickness of the Miocene units. It is out of the scope of this paper to perform detailed analysis of displacement distribution and variation along the fault planes in order to constrain the temporal and spatial evolution of these faults [*Walsh and Watterson*, 1988].

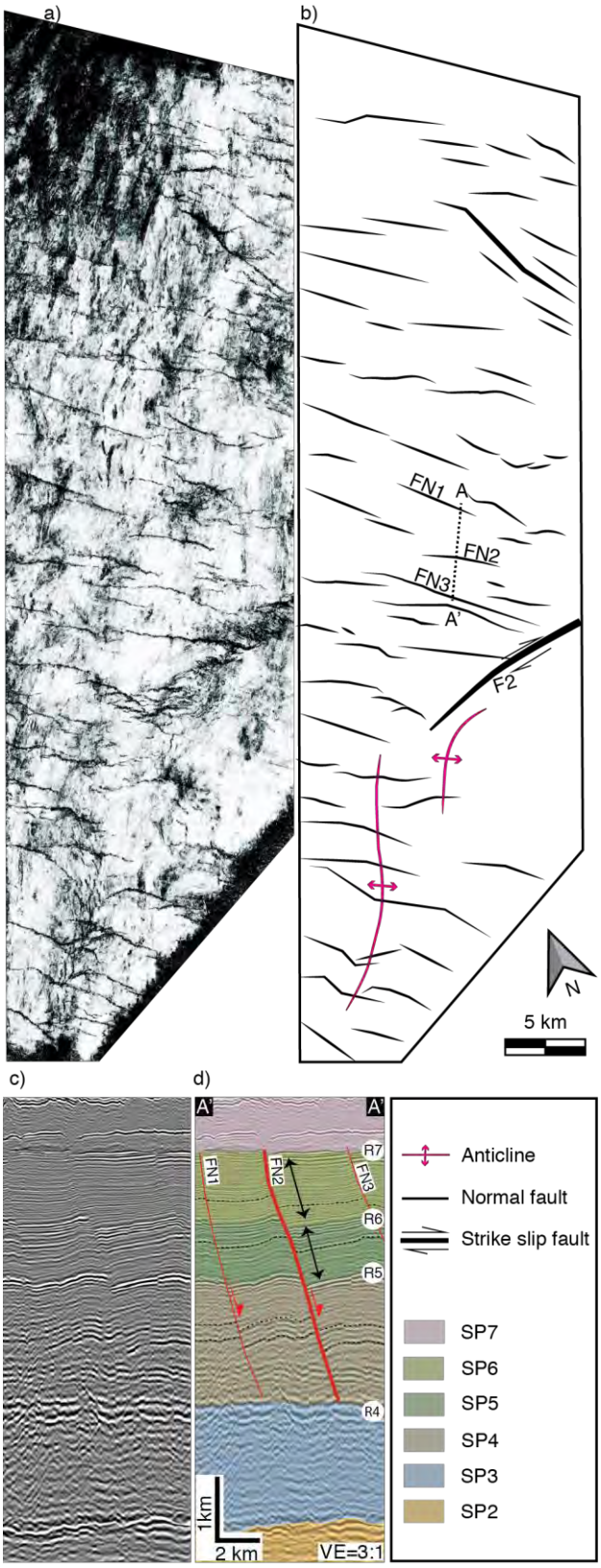

Figure 3.9: a) Coherence attribute slice below R7 horizon from MC3D-LEB2006 PSTM seismic cube. b) Interpretation of the coherence map showing the distribution and orientation of the normal fault array. c) – d) Seismic section across three normal faults showing thickening of units in the hanging wall block in SP5 and SP6 units along FN2. The arrows in d) indicate the units on which EI>1 have been recorded. For location of the seismic block, see Figure 3.4.

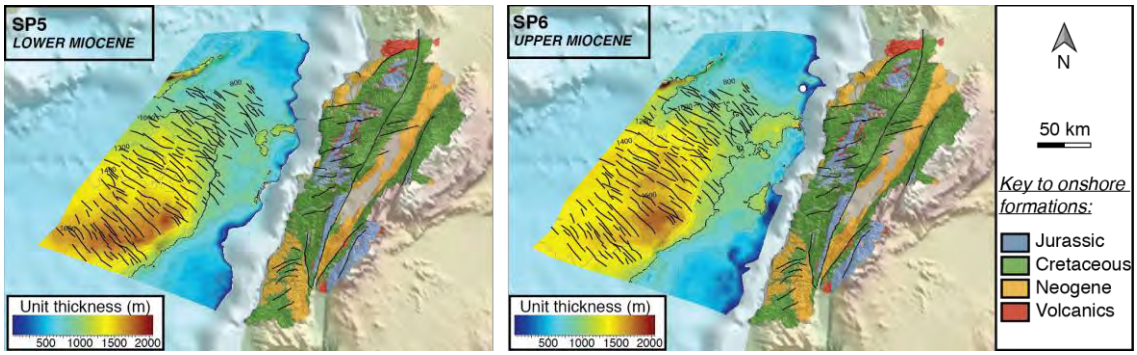

Figure 3.10: Isopach maps of the Lower and Upper Miocene with superposed normal fault distribution map in the Levant Basin offshore Lebanon. Basin-wide mapping of the normal fault is taken from *Dupin et al.* [2012].

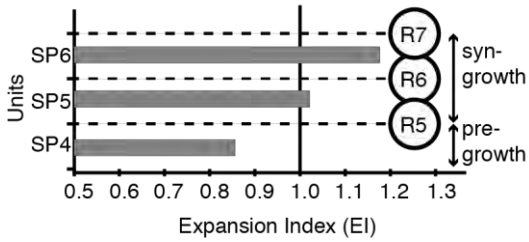

Figure 3.11: Expansion index plot for one Oligo-Miocene normal fault. The black vertical line indicates EI values of 1. Values <1 or >1 imply stratigraphic thinning or thickening of units in the hangingwall respectively. In the Levant Basin offshore Lebanon, all normal faults show thickening of SP5 and SP6 (Lower and Upper Miocene) in the hangingwall, indicating synsedimentary faulting during the Miocene.

ENE-WSW striking strike-slip faults

Description

Four parallel ENE-WSW striking faults are observed in 2D (fault F1) and 3D data (faults F2, F3 and F4) (Figures 3.6, 3.7 and 3.8). These faults are nearly vertical and affect all the units from the Cretaceous (SP2) till Messinian (SP7). At seabed, they are associated with localized deformation and faulting (Figures 3.13 & 3.14). Fault F1 has a variable throw along its strike, reaching 750 m in places (Figure 3.7). It is bordering the STP described in previous sections and is only observed in 2D data in this study, which limits observation and interpretation.

Fault F2 is a 25 km long steep fault that appears locally as a negative flower structure toward the westward tip of the fault (Figure 3.12e). The vertical throw associated with this fault is variable along its length. In section AA' and BB' (Figure

3.12), R3 (Senonian unconformity horizon) is 500 m displaced downward NW of the fault plane while the remaining horizons show no displacement. In section BB' R5, R6 and R7 are 300 m displaced downward SE of the fault (Figure 3.12). An erosive surface along the base Messinian horizon (R7) is observed in section AA' above the structure (Figure 3.12e). In map view (Figure 3.12b-d), small-scale closely spaced faults oriented at 60° to and cross-cut by F2 are observed. These structures consist of small normal faults of 200 m throw that displace the Miocene units (SP5-6) and which branch off on the vertical master fault. The absence of displaced markers does not allow verifying if any strike-slip movement occurred along these faults. An anticline (A1-b) with a 10 km long axis and 200 m fold amplitude is observed adjacent to F2. It is bending 30° clockwise when it approaches the westward tip of F2 (Figure 3.12d).

Fault F3 is 15 km long and is located closer to the Levant eastern margin than F2 (Figure 3.6). It consists of a vertical or NW dipping steep fault cross-cutting SP2, SP3, SP4, SP5 & SP6 (Cretaceous to Upper Miocene units). R3 (Senonian unconformity) and R4 (Eocene unconformity) are displaced downward of 1 km (Figure 3.13). Reverse drag is observed along R6 (base mid-Miocene horizon) in both the footwall and the hangingwall. In the footwall, the Oligocene/Eocene unit (SP4) is significantly reduced or absent, overlying a clear erosional surface along R4 (Eocene unconformity), and the top of the Upper Miocene unit (SP6) is eroded and truncated (Figure 3.13d). In SP6, two parallel 6 km long anticlines are crosscut by F3, and oriented 60° from the F3 fault plane (Figure 3.13b). On top of F3, the Messinian is folded, and gentle uplift and deformation are observed in SP8 (Pliocene).

Fault F4 can only be seen in a small area in the north-eastern side of the MC3D-LEB2012 seismic survey (Figure 3.6). It consists of a nearly vertical fault, with a displacement of 750 m of Cretaceous horizons (within SP2) (Figure 3.14). SP8 (Pliocene unit) is severely deformed by this fault and the seabed is vertically displaced for about 500 m. Erosion and truncation of R2 (Senonian unconformity horizon) are recorded in the hanging wall. A significant hiatus is observed along this fault and includes the Eocene, Oligocene, Miocene and Messinian units (SP3 to SP7) (Figure 3.14).

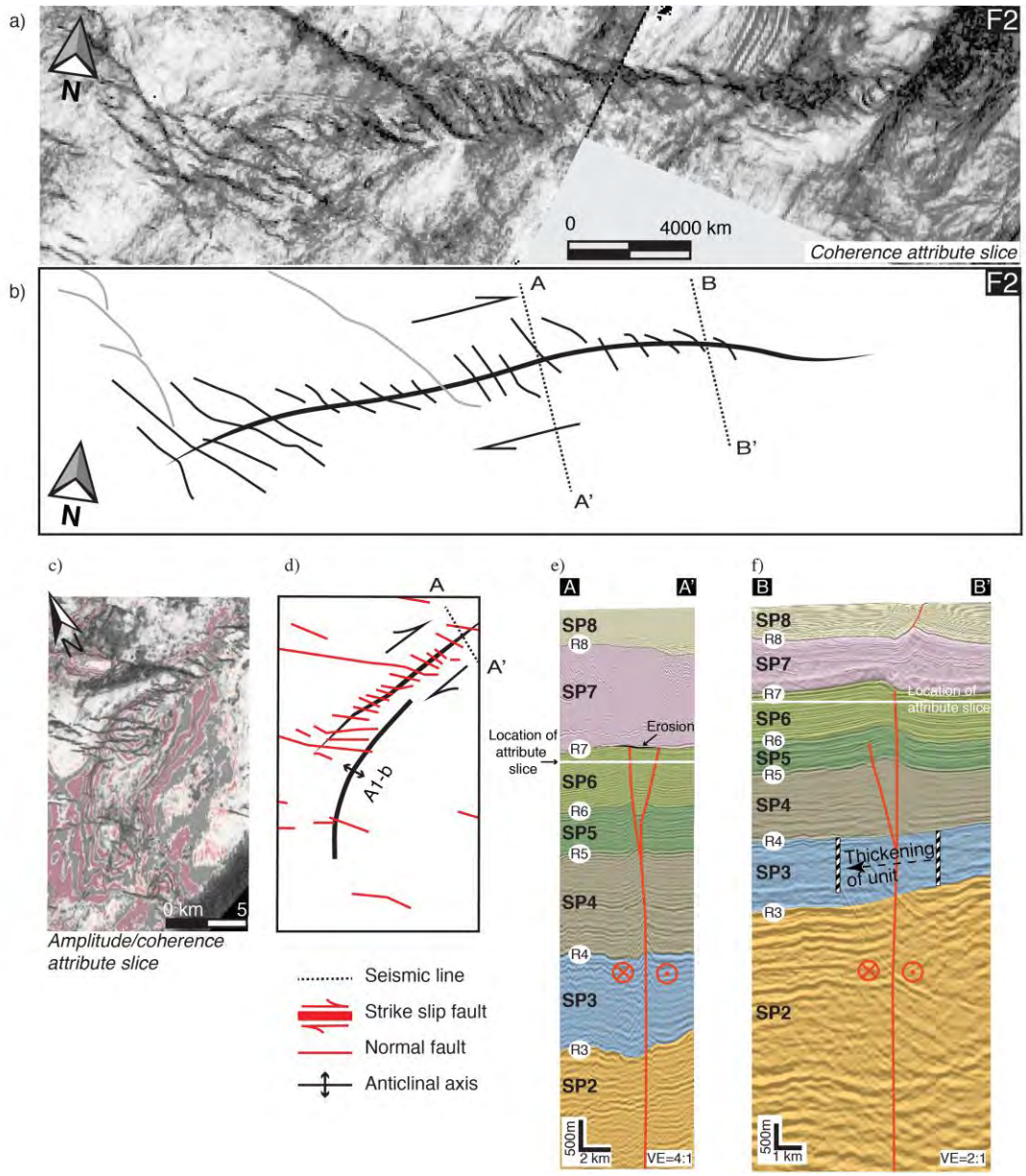

Figure 3.12 : a) – b) coherence slice below R7 horizon (base Messinian) showing fault F2 along MC3D-LEB2006 and MC3D-LEB2012 seismic cubes, together with the numerous normal faults along the plane of fault F2, c) – d) merged amplitude and coherence attribute slice below R7 horizon in MC3D-LEB2006 seismic cube, showing the location of an anticline bending to the east, e) – f) interpreted seismic sections along the strike-slip fault. For location, see Figure 3.6 and 3.8.

Interpretation

The ENE-WSW striking structures are believed to be dextral strike-slip faults, based on the following arguments: (i) the faults are narrow, nearly vertical and thoroughgoing; (ii) abrupt thickness changes in correlative stratigraphic units across fault planes (Figures 3.12, 3.13 and 3.14); (iii) passive eastward bending of anticlinal axis

close to F2 (Figure 3.12), (iv) shallow splay faults resembling Riedel-like structures at 60° from F2 and converging at depth into a steep fault zone (Figure 3.12); (v) en echelon alignment of two anticlines in the Upper Miocene oriented at 60° from the F3 fault plane (Figure 3.13); and (vi) presence of dextral strike-slip faults onshore with same strike (Figure 3.6) [*Dubertret*, 1955; *Gedeon*, 1999].

The timing of activity of these faults is not straightforward. In F2, no onlap or growth strata in the pre-Messinian packages can be observed to date this fault. The erosion of parts of the base Messinian horizon (R7) along F2 suggests that the latter was active prior to the Messinian event. In contrast, F3 shows evidence for an even older activity during the Oligocene. The Oligocene hiatus observed in the hangingwall is an indication that the Oligocene unit (SP4) is syn-kinematic and that F3 was active during this time, probably as a normal fault. As presented above, the F1 Fault borders the northern part of STP which is a crustal element with different crustal properties. Hence the faults bounding it might also consist of deep crustal faults. We thus suggest that F1 is an inherited crustal fault nucleated during Mesozoic extension. Superposition of earthquake data (www.cnrs.edu.lb) reveals significant seismicity in the area adjacent to F3, attesting to its current ongoing activity (Figure 3.6). Similarly, F4 displaces the seabed for about 500 m and hence is considered as currently active.

The presence of dextral strike-slip faults on the margin, termed latitudinal faults, with a similar trend suggests that the structures both onshore and offshore are genetically related. It is widely accepted that the margin's latitudinal faults are old structures inherited from previous extensional activities [*Dubertret*, 1955; *Sabbagh*, 1961; *Hancock and Atiya*, 1979; *Gedeon*, 1999]. Thus, by analogy, we can advocate that if several structures offshore (F2 and F3) show similar history, trend, and mechanism as the latitudinal faults onshore, then the rest of the structures offshore (F1 and F4) that show the same trend and inheritance history might also be dextral strike-slip. They belong, as such, to the same system of wrench faults prevalent on the Levant margin. We thus advocate that all ENE-WSW strike-slip faults offshore are old inherited structures and still active today, in a similar fashion to onshore strike-slip ENE-WSW latitudinal faults.

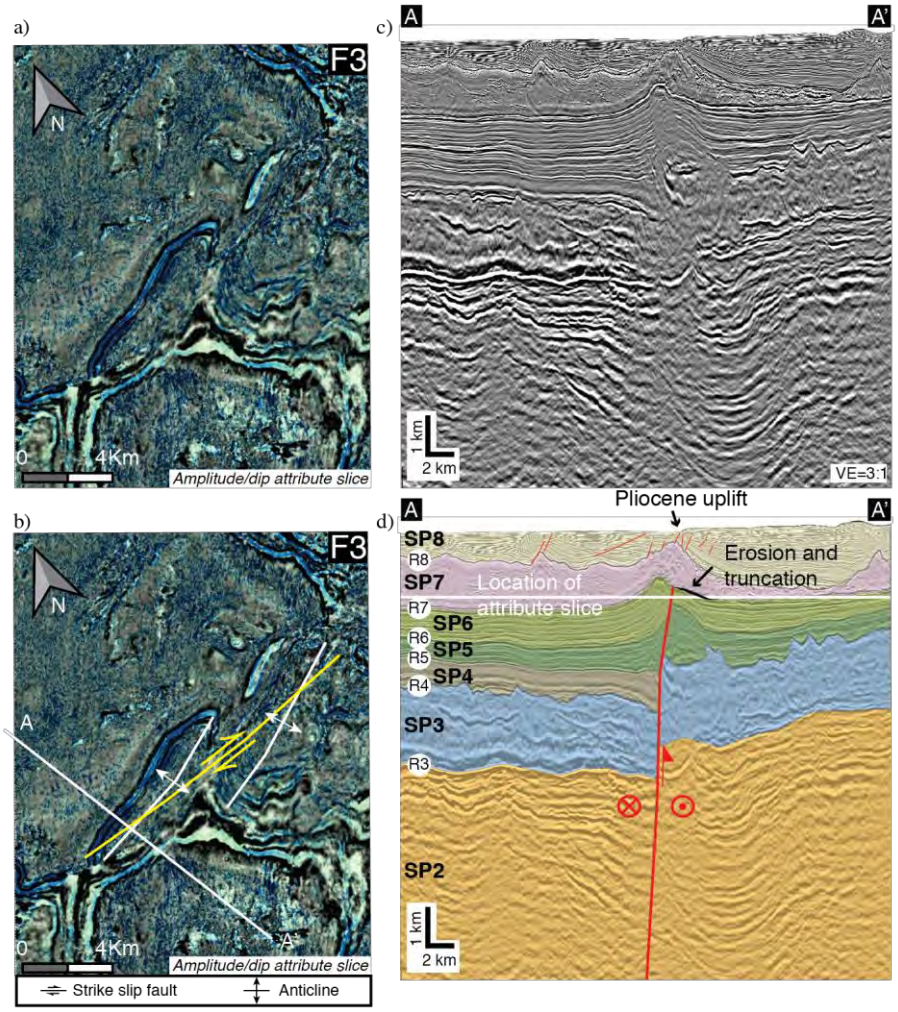

Figure 3.13: a) – b) merged amplitude and dip attributes slice of fault F3 from MC3D-LEB2012 PSDM seismic cube, showing the orientation of two anticlines along the strike-slip fault, c) – d) seismic profile across the fault, showing inversion and deformation of seabed. For location, see Figure 3.6 and 3.8.

Thrust faults

Description

Two thrust faults are mapped in the Levant Basin offshore Lebanon: Beirut thrust and Tripoli thrust (Figures 3.6, 3.15 and 3.16).

Beirut thrust is located at the latitude of the city of Beirut. It is dipping 50° to the east, strikes NNE-SSW and is crosscutting SP2, SP3, SP4, SP5 & SP6 (Cretaceous to Upper Miocene units) (Figure 3.15). R3 and R4 (Senonian and Eocene unconformity horizons) show 2 km vertical displacement along this fault, while R5 (base Miocene) shows only 1 km of vertical displacement. Strong thickness variations are observed along Beirut thrust in the Oligocene (SP4) and the Eocene (SP3) whereby these units are

thinner in the hanginwall (Figure 3.15). Horizons R6 and R7 (Base Mid-Miocene and Base Messinian horizons) are truncated at the hangingwall of the fault, and part of the Upper Miocene (SP6) is absent and eroded (Figure 3.15c). The fault does not breach the Messinian (SP7); the latter instead is pinching out onto the uplifted hangingwall. The Messinian is observed again toward the East in the hangingwall but is significantly thinner (Figure 3.15).

Toward the north, another thrust fault is found at the latitude of Tripoli [*Elias et al.*, 2007; *Carton et al.*, 2009]; this is referred to as the Tripoli Thrust (Figure 3.16). It is dipping 50° SE and strikes NNE-SSW. It is crosscutting SP2, SP6 and SP7 (Cretaceous, Upper Miocene and Messinian). The Cenozoic units are onlapping on R3 (Senonian unconformity) and hence SP4 and SP5 are never cross-cut by this fault. It is not possible to know the total displacement of R3 (Senonian unconformity) because of erosion and truncation of the top of SP2 (Cretaceous) in the hangingwall. However, reflectors within SP2 show displacement of around 3 km which might be considered as the total displacement in the Cretaceous unit. In contrast, reflectors within the Upper Miocene (SP6) are displaced for a maximum of 200 m, while R7 (base Messinian) is only displaced for 100m in some profiles (Figure 3.16d). In other profiles, the Messinian is pinching out on Cretaceous units (SP2) (Figure 3.16b). The overlying Pliocene (SP8) does not seem to be very heavily disturbed and shows minor amount of normal faulting (Figure 3.16b-d).

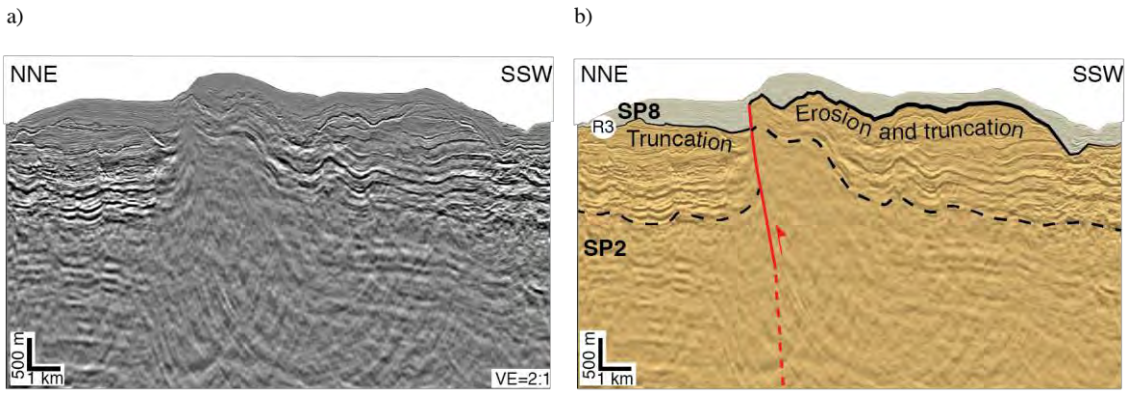

Figure 3.14: a) – b) Seismic profile across F4 showing a vertical fault affecting units SP2 (Cretaceous) and SP8 (Pliocene), with a vertical displacement up to 750 m. Significant hiatus of the Eocene, Oligocene, Miocene and Messinian is observed, together with erosion and truncation of the Upper Cretaceous. The seabed and Pliocene are uplifted for about 500 m.

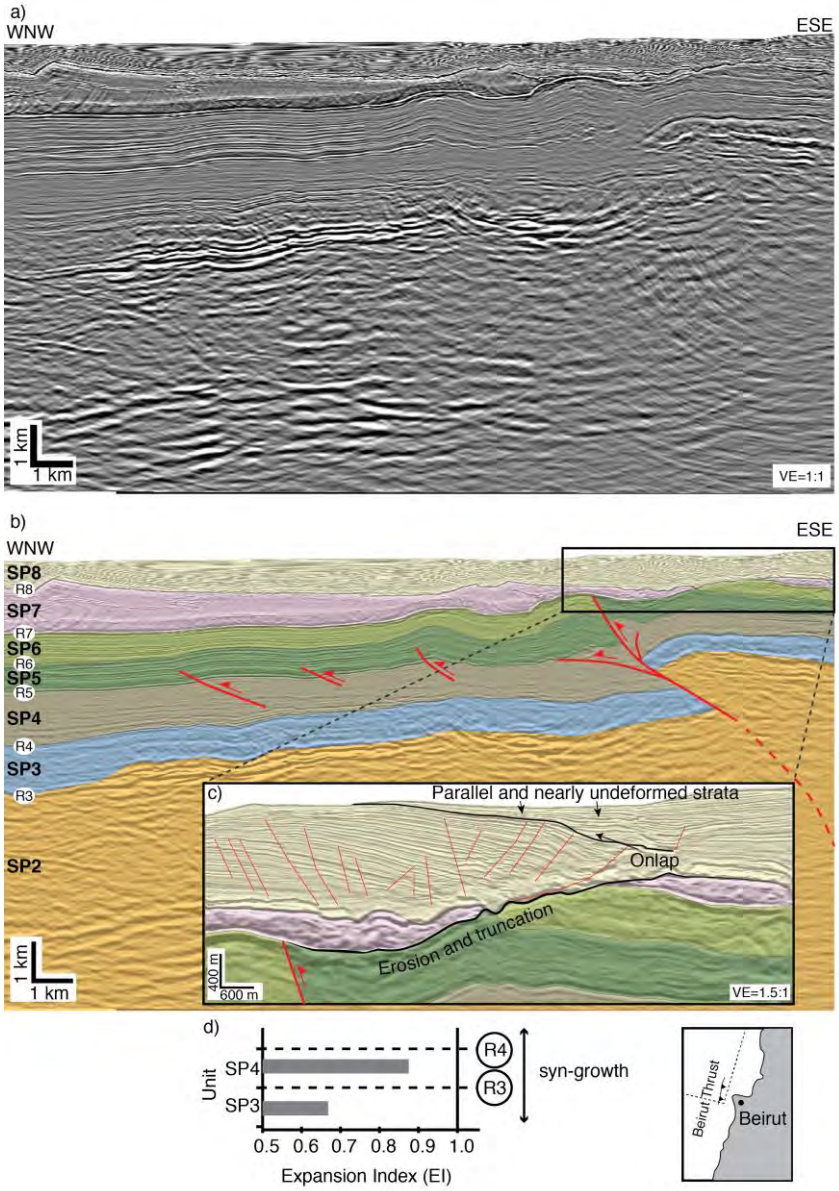

Figure 3.15: a) – b) seismic profile across the Beirut thrust from MC3D-LEB2012 PSDM seismic cube, showing thrusting and uplift, c) zoomed section on the top of the hanging wall of the thrust showing potentially a cessation of movement in the Messinian and Pliocene, d) Expansion Index (EI) plot for units SP3 and SP4. The black vertical line indicates EI values of 1. Values <1 imply stratigraphic thinning of units in the hangingwall. Because of erosion of SP5 and SP6 in the hangingwall, no EI plots could be constructed for those units. For location, see Figure 3.6 and 3.8.

Interpretation

Thickness variation of units along Beirut thrust indicates that the Eocene and Oligocene are syn-kinematic (Figure 3.15d). The erosion of some parts of the Miocene unit does not allow checking whether the fault was active during this time or not by comparing the thickness of units. It is possible to argue that the thickening in units in the footwall of the thrust might be related to global thickening of the Eocene and

Oligocene units toward the basin. Though a global thickening toward the basin is generally attested, the thickness change is so abrupt and large along the fault plane that it cannot be related to general thickening of the unit toward the basin. The truncation and erosion of parts of the Lower and Upper Miocene units indicates that thrusting is pre-Messinian. In the overlying Pliocene unit, small deformation and faulting is related to salt tectonics. A Pliocene sequence is pinching out on a deformed unit, indicating a cessation of Pliocene faulting (Figure 3.15c). This is explained by the removal of the underlying evaporitic decollement layer, allowing the fault blocks to be welded on the pre-salt layers and becoming stable as proposed by *Lundin* [1992]. Hence, Pliocene sediments are being deposited today without significant deformation in the hanging wall, which is an evidence for no activity observed along this fault during the Pliocene. The Messinian and Pliocene are hence post-kinematic units.

Tripoli thrust shows similarity with Beirut thrust. The truncation and erosion of a large part of the top Cretaceous, together with the larger displacement recorded over horizons in the Cretaceous unit compared with the Miocene one (Figure 3.16), may indicate that this fault was active prior to the deposition of the Miocene unit. It is not possible to determine when faulting started exactly since the Eocene and Oligocene units are not cross-cut by the fault, but it is very likely that the major part of deformation took place prior to the Miocene and continued with lesser magnitude during the Late Miocene. By analogy to Beirut thrust, we can advocate that deformation took place in the Late Cretaceous or Early Tertiary. The fact that the Messinian is pinching out on the hangingwall and the lack of major deformation and uplift in the Pliocene (Figure 3.16) indicate that the thrust was inactive during the Messinian and Pliocene. Indeed, it's hard to consider that large amount of vertical displacement took place during the Messinian or Pliocene without affecting the Pliocene units, even if the deformation is accommodated by the Messinian salt. The normal faulting observed in the Pliocene is related to salt tectonics similarly to the rest of the margin.

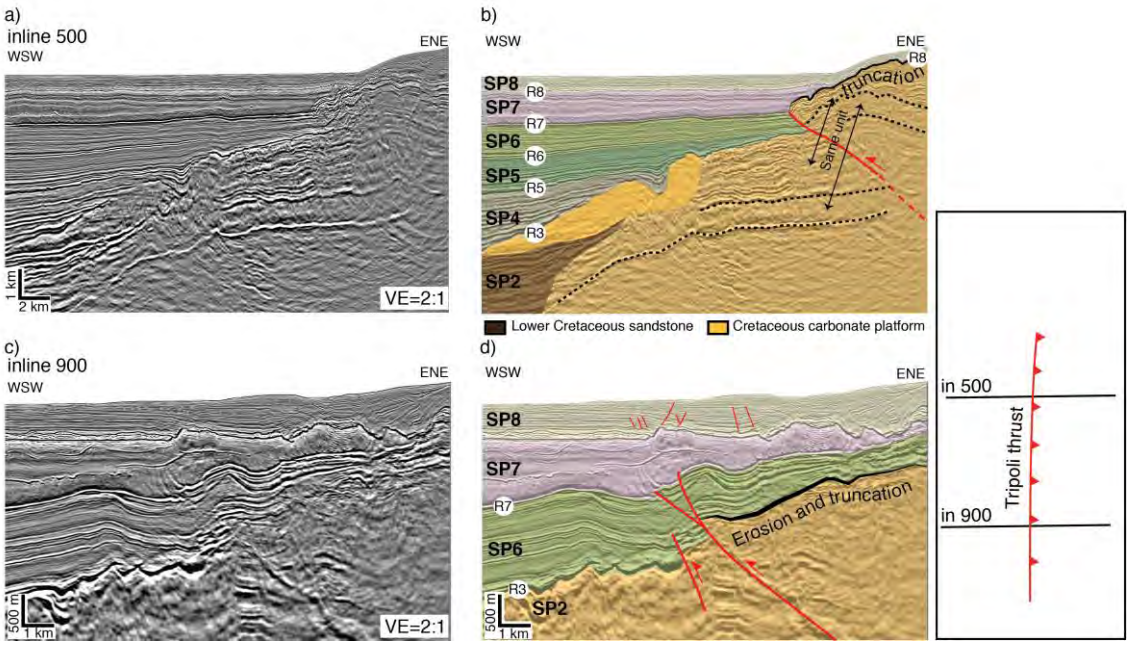

Figure 3.16: a) – b) – c) – d) seismic profiles across the Tripoli thrust offshore northern Lebanon from MC3D-LEB2012 PSDM seismic cube. For location, see Figure 3.6 and 3.8.

NNE trending anticlines

Description

Seven anticlines are mapped in the Levant Basin offshore Lebanon using the available dataset. For the purpose of this study, only one anticline "A1" will be described in detail. A1 is located 50 km to the west of Beirut (Figure 3.6) and is a symmetric fold in map view (Figure 3.17a). The anticlinal axis is 12 km long trending N28E and is slightly sinuous. The fold amplitude is 350 m. The units affected by this fold are SP4, SP5, and SP6. One continuous seismic horizon with strong impedance contrast in SP7 (Messinian) close to R7 (base Messinian horizon) is folded and deformed by the anticline (Figure 3.17e). In contrast, R3 and R4 (Eocene and Senonian unconformity horizons) are sagging below A1. No thickness variations, onlap or erosional surfaces can be observed on the flanks of the anticline in the deformed units. However, erosion and truncation along R7 (base Messinian horizon) are documented and the SP3 (Senonian/Eocene unit) is thickening abruptly west of A1 (Figure 3.17).

Offshore Beirut, between faults F2 and F3, five other anticlines that detach on R4 are outlined in depth structure and dip attribute maps (Figure 3.8). All these anticlines are capped by an erosional surface and truncation along the base of the Messinian (R7)

(Figure 3.18) and show no onlap or growth folding along their flanks. In a similar way, all these anticlines are associated with thickness variations of Senonian and Eocene units (SP3 and SP4) toward their western flanks.

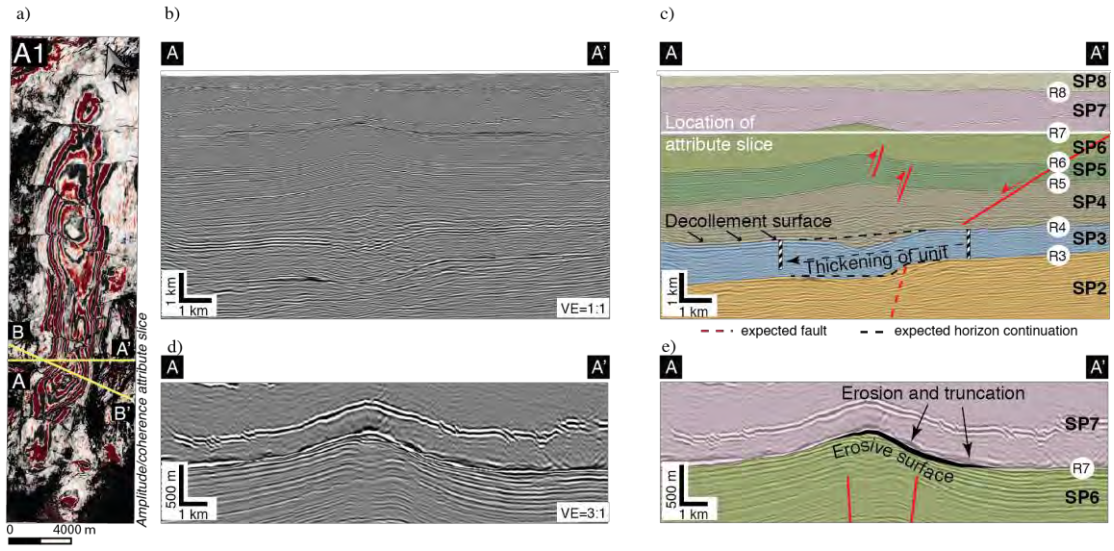

Figure 3.17: a) Merged coherence and dip attribute slice from MC3D-LEB2006 PSTM seismic cube showing the geometry of the NNE-SSW anticline, b) – c) – d) – e) seismic profiles across the anticline showing thickening along SP3 unit and an erosive surface at the anticlinal crest. For location, see Figure 3.6 and 3.8.

Interpretation

The sagging of the horizons below anticline A1 constrains the ability to understand the folding mechanisms and geometries. It is possible that this sagging is caused by unexpected velocity anisotropies during seismic imaging and is hence a seismic artifact. We believe that if R3 and R4 had the same fold amplitude as the anticline, then a very strong velocity variation is needed to displace these horizons up to 1 km downward. For this reason, we advocate that R3 and R4 should be flat below the anticline. This would make A1 a detachment fold formed over the Eocene unconformity horizon, which is the decollement surface in this situation.

Erosion and truncation of the crest at the base-Messinian horizon (R7) indicate that this anticline started to grow shortly before Messinian times (Figures 3.17 and 3.18). Thickening of the Senonian/Eocene (SP3) and Miocene units (SP5, SP6) is noticed at the western limb of anticline A1. It denotes the presence of a pre-Eocene palaeo-structure, possibly active in the Late Cretaceous/Early Tertiary. This structure appears to have caused vertical displacement along the Senonian unconformity horizon (R3) responsible for thickening of the overlying Tertiary units. Hence, it is likely that

during deposition of the Senonian/Eocene units (SP3), a topographic morphology was already in place, which explains the thickening geometries west of the anticline. The corresponding fault trace cannot be mapped accurately due to velocity problems below the anticline A1. Though it is possible to argue that this thickening is related to bulk westward thickening of the units toward the basin, we believe that the strong and abrupt thickness increase west of the anticline is caused by a pre-existing topographic high, or structure, rather than general thickening of units toward the basin. The description of A1 is applicable to the remaining anticlines offshore Beirut as they show the same geometric relationships. We hence advocate that all the anticlines (Figures 3.6 and 3.8) were formed by a similar mechanism and during the same time.

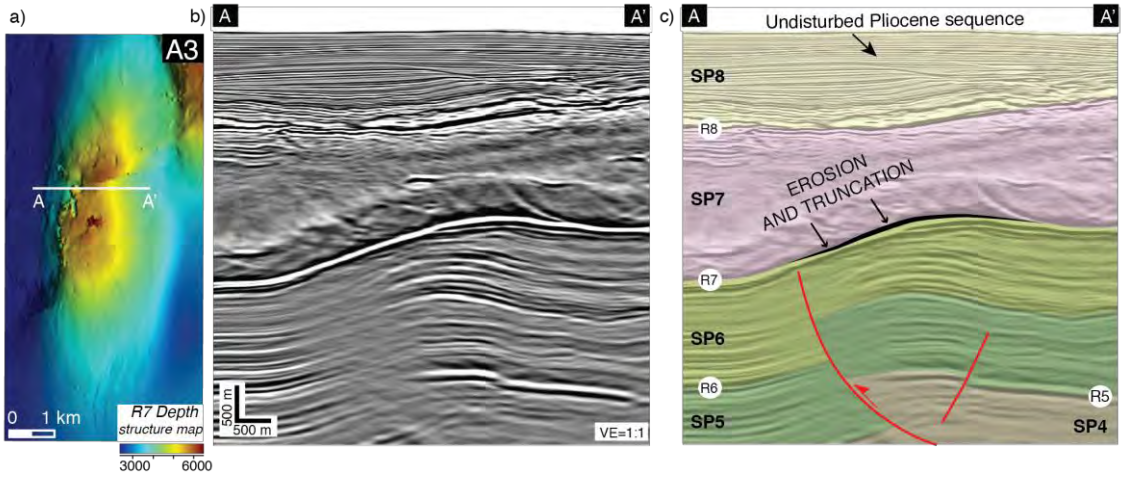

Figure 3.18: a) Depth structure map of R7 (Base Messinian horizon) from MC3D-LEB2012 PSDM seismic cube showing the geometry of anticline A3, b) –c) seismic profile across A3 showing erosion and truncation of R7 horizon. For location see Figure 3.6 and 3.8.

III. 7 Discussion

III. 7.1 Influence of pre-Cenozoic structures

Mapping of structures in the Levant Basin offshore Lebanon reveals a number of predominant fault sets: (i) NE-SW trending thrust faults, (ii) ENE-WSW striking dextral strike-slip faults, (iii) NNE trending anticlines, and (iv) NW-SE striking normal faults. With the exception of the NW-SE striking normal faults, all of the structures appear to be inherited and reactivated during the Miocene. Structures such as the ENE-WSW oriented strike-slip faults show reactivation and inversion evidence, and most probably are linked to crustal origins. Along the Levant eastern margin in Lebanon,

dextral strike-slip faults are aligned with the offshore strike-slip structures documented in this study (Figure 3.6). It is widely recognized that the onshore latitudinal strike-slip faults are reactivated Mesozoic structures [*Sabbagh*, 1961; *Hancock and Atiya*, 1979; *Ron and Eyal*, 1985; *Nemer*, 1999]. We hence postulate that both of these structures are genetically linked and were initially caused by Mesozoic extension [e.g., *Garfunkel*, 2004; *Gardosh et al.*, 2010; *Homberg et al.*, 2010].

Similarly, NNE-SSW anticlines seem to overly deeper faults or structures in the pre-Tertiary strata (Figure 3.17). Though such faults cannot be observed accurately in the seismic data due to lower resolution at depth, the thinning and the thickening within the Eocene units suggest a Late Cretaceous structuration (Figure 3.17). Such thickness variation cannot be attributed to global thickening toward the basin [e.g., *Hawie et al.*, 2013b] because the Eocene units thicken abruptly below the anticlines which insinuates that existing structuration was affecting sedimentation.

The variability of structural styles in the Levant Basin can be explained in terms of pre-existing structuration influencing the style of current brittle deformation. It is widely acknowledged that fault reactivation is controlled by (i) optimal orientation for frictional slip in the stress field; (ii) size of the fault; (iii) overpressure; and (iv) frictional resistance along the fault plane [*Wiprut and Zoback*, 2002; *Bonini et al.*, 2012]. Hence, a fault is likely to follow a complex history when submitted to several successive states of stress. In the case of the Levant Basin, the various regional geodynamic events, such as the pulsed Mesozoic rifting [*Druckman*, 1984; *Robertson*, 1998a; *Barrier and Vrielynck*, 2008; *Gardosh et al.*, 2010], were probably responsible in creating crustal structures. With the subsequent Late Cretaceous to Tertiary subduction, inversion, collision, Anatolian extrusion and LFS transpression [*Frizon de Lamotte et al.*, 2011], concurrent reorientations of the regional stress field may have caused the reactivation of the pre-existing structures into a variety of structural styles. In fact, inversion of Mesozoic extensional structures has been documented offshore Israel, in the Sinai and the Palmyrides [*Best et al.*, 1993; *Chaimov et al.*, 1993; *Druckman et al.*, 1995; *Brew et al.*, 2001b; *Gardosh and Druckman*, 2006; *Moustafa*, 2010] *and is believed to have taken place during the Late Cretaceous, and Eocene to Early Miocene* [*Hempton*, 1987; *Moustafa and Khalil*, 1994; *Eyal*, 1996; *Garfunkel*, 1998; *Walley*, 1998; *Sawaf et al.*, 2001].

III. 7.2 Origin of the NW-SE normal fault system

All the structures discussed so far are rooted in pre-Oligocene layers. In contrast, the NW-SE normal faults are Oligo-Miocene layer bound, and die out at the Eocene unconformity horizon (Figures 3.7 and 3.9). In order to tectonically create normal faults in the basin, the maximum principal stress must be vertical. This would be in contrast with the NW trending maximum horizontal stress field prevalent since the Late Cretaceous [*Barrier and Vrielynck*, 2008] that is causing regional shortening and thick-skinned deformation. Since such normal faults are restricted to the Oligo-Miocene unit, while no NE-SW extension is documented in the Levant Basin at that time, we might speculate that these faults are non tectonic and probably related to the nature of sediments in the host-rock unit. The detailed study of the geometry of this fault network and its mechanical origin deserves a specific paper but it is worth mentioning here that they share many characteristics of polygonal faults systems [e.g., *Cartwright*, 2011] such as: (i) layer-bound geometries, (ii) fine grained sediments in the host unit [*Hawie et al.*, 2013], (iii) regional extent, and (iv) correlation between their distribution and thickness of the host-rock unit.

III. 7.3 Late Cretaceous to Early Tertiary deformations

The closure of the Neo-Tethys ocean at the onset of the Late Cretaceous has caused inversion, thrusting and folding throughout the Levant region (e.g Syrian Arc folds, Palmyrides fold and thrust belt; cf. Figure 3.4) [*Hempton*, 1987; *Moustafa and Khalil*, 1994; *Eyal*, 1996; *Garfunkel*, 1998; *Walley*, 1998; *Frizon de Lamotte et al.*, 2011]. The presence of thrust faults offshore Lebanon could fit in this regional geodynamic framework whereby inversion, thrusting, and shortening were dominant. Though there is no indication that Beirut and Tripoli Thrusts (Figures 3.15 and 3.16) are inverted, we believe they are likely crustal structures linked to the evolution of Mount Lebanon. The timing of Beirut Thrust is Lower Tertiary, based on thickness variation of Eocene units along the fault plane (Figure 3.15). Beirut thrust could be the offshore continuation of the Roum fault which shows a similar timing and evolution [*Dubertret*, 1955; *Butler et al.*, 1998; *Nemer and Meghraoui*, 2006]

Determination of the accurate timing of activity of Tripoli Thrust has proved to be challenging. The large vertical displacement recorded in the pre-Tertiary units and the erosion of a large part of the Upper Cretaceous (Figure 3.16) insinuate that the

Tripoli fault was an already existing structure prior to the Tertiary, and it continued to grow during the Miocene.

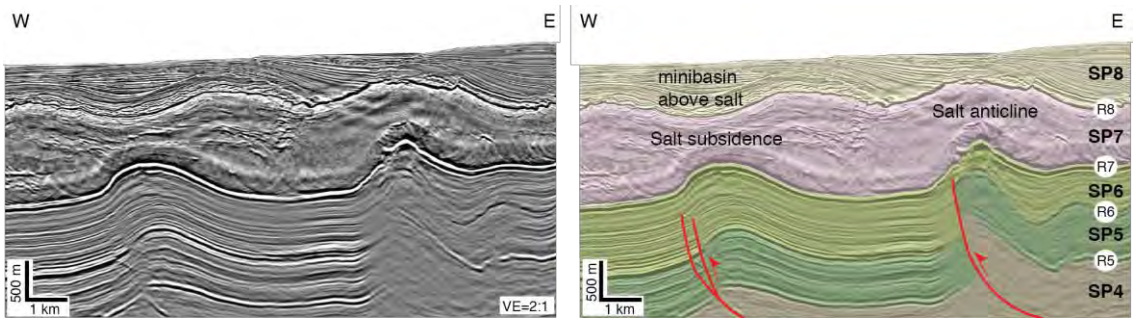

Figure 3.19: Seismic profile offshore central Lebanon from MC3D-LEB2012 PSDM seismic cube showing the occurrence of salt anticline and subsidence above two adjacent Miocene anticlinal structures. The occurrence of the Messinian evaporites, decoupling sub- and supra salt deformation, is challenging to determine continuous activity of structures. For location see Figure 3.8.

III. 7.4 Late Miocene Pre-Messinian deformation

The material presented in this paper suggests that offshore anticlines and strike-slip faults have been deformed immediately prior to the Messinian. This is demonstrated by: (i) absence of growth strata and angular unconformities in the Miocene units of these structures (Figures 3.12 and 3.17) and (ii) local erosion and truncation at the overlying base Messinian horizon (Figures 3.13, 3.17 and 3.18). If the anticlines were folded in large part during the Early or Late Miocene, then we would expect to find growth folding or drape sequences in these units. The fact that top of the anticlines is capped by an erosive surface signifies that deformation is immediately pre-Messinian.

At the onset of the Messinian, major geodynamic changes occurred in the Eastern Mediterranean region. The northward propagation, development and first phase of movement along the LFS took place in the Mid-Miocene [*Freund et al.*, 1970; *Garfunkel*, 1981; *Quennell*, 1984] with the transpressive activity along the Lebanese restraining bend initiating in the Late Miocene [*Butler et al.*, 1998; *Walley*, 1998; *Gomez et al.*, 2007b; *Homberg et al.*, 2010]. The northward propagation of the LFS during the Mid to Late Miocene was a direct response to rifting and sea-floor spreading along the newly formed Red Sea [*Cochran*, 1983; *D'Acremont et al.*, 2005; *Fournier et al.*, 2010]. In

the Levant basin, the deformation, documented in this paper along anticlines and strike-slip faults starting immediately before the Messinian (Figure 3.20), correlates well this major reorganization.

III. 7.5 Post-Messinian tectonics

It is difficult to determine if many of the interpreted Oligo-Miocene structures are currently active using seismic data alone. Yet, 3D seismic data interpretation allowed providing evidence for local Pliocene uplift –i.e. current activity– along ENE-WSW faults (e.g., F1, F3 and F4; Figures 3.7, 3.13 and 3.14). One of these faults (F3) is associated with a cluster of earthquake epicenters (www.cnrs.edu.lb), confirming ongoing deformation. This fault is believed to be an offshore extension of the Douma ENE-WSW striking fault (Figure 3.6), which is also known for being seismically active [*Gedeon*, 1999]. Consequently, most of the observed ENE-WSW striking strike-slip faults are believed to be currently active. Due to the decoupling effect of the thick Messinian salt (Figure 3.19), it is hard to determine whether the other investigated structures are also still active.

The structural map presented in figure 3.6 together with the age constraints provided by the seismic-stratigraphic and earthquakes records, can be used to propose two tectonic scenarios for the northern Levant Basin offshore Lebanon (Figure 3.20): (i) all structures are still active today, having their activity masked by the decoupling effect of Messinian salt; or (ii) only the ENE-WSW striking strike-slip faults are active, with the rest of the structures becoming dormant since the Messinian or Pliocene. We favor the second scenario, due to the lack of evidence to prove current activity for the remaining structures.

At regional scale, the asthenospheric flow below Anatolia and accelerated rollback of the subduction zone along the Hellenic-Cyprus arc during the Tortonian [*Le Pichon and Kreamer*, 2010] caused a westward extrusion of Anatolia during the Messinian and Pliocene. The propagation of the North Anatolian Fault toward the Aegean facilitated the westward escape of Anatolia which was followed by a decrease in the onshore LFS slip rate during its second phase of movement in the Pliocene [*Freund et al.*, 1970; *Quennell*, 1984; *Le Pichon and Gaulier*, 1988]. In the Levant Basin, the Lattakia Ridge System (Figure 3.4) was reactivated into a sinistral strike-slip regime during the Pliocene after a long period of thrusting and subduction [*Hall et al.*, 2005a]. These regional events are coeval with the cessation of folding demonstrated offshore in

this paper (Figure 3.20).

The continuous activity of the ENE-WSW striking dextral strike-slip faults might be related to the sinistral shear along the LFS, causing counter-clockwise block rotations along latitudinal faults [*Ron et al.*, 1984; *Ron*, 1987]. In strike-slip restraining bends, progressive deformation causes rotation of the rock volume within the bend, as it is commonly observed in scaled analogue models [*Mcclay and Bonora*, 2001; *Mitra and Paul*, 2011]. This has also been observed in the complex restraining stepover systems of the San Andreas fault in southern California [*Dickinson*, 1996]. In general, where the basement is already faulted prior to such rotations, it is not surprising that these faults will be reactivated into strike-slip faults [*McKenzie and Jackson*, 1986]. We have shown that ENE-WSW striking faults active from the onset of Messinian, reactivate pre-existing structures located primarily along the Levant margin onshore and offshore (Figure 3.20). This extends the Ron *et. al* [1984] hypothesis to the offshore domain. In the Levant Basin offshore Lebanon, this deformation mode corresponds to the second phase of deformation along the LFS.

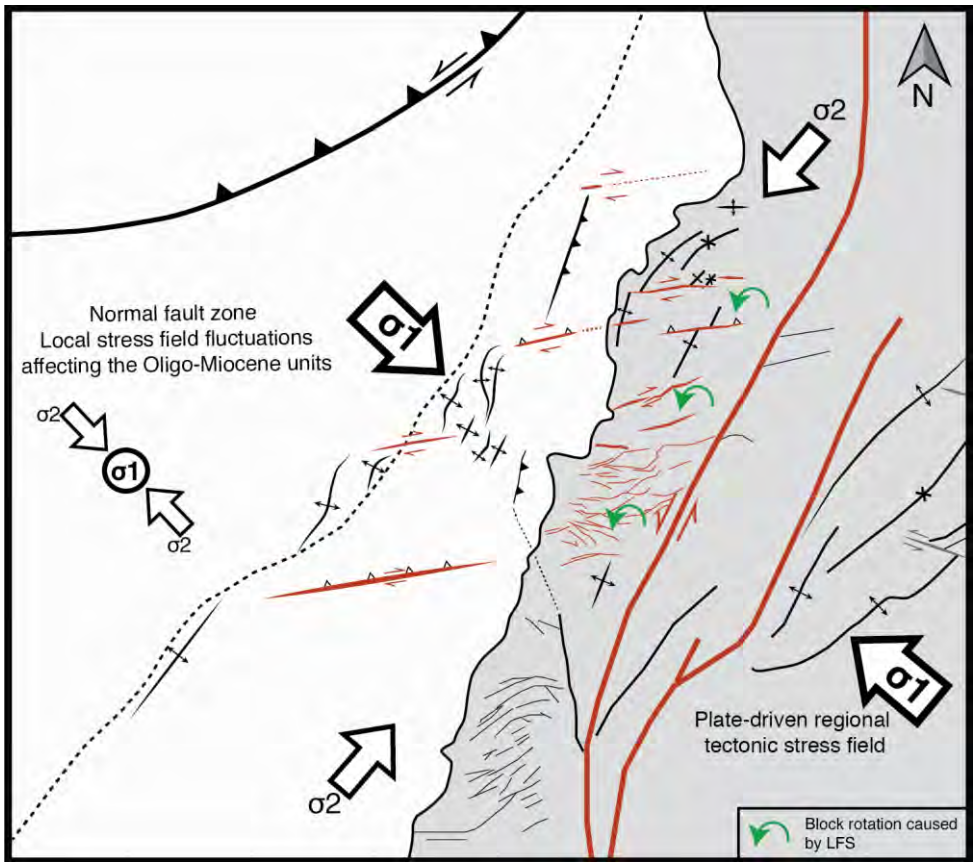

Figure 3.20: Sketch summarizing the results of this study in the Levant Basin offshore Lebanon. The faults in red are the structures that show evidence of current activity, including: offshore ENE-WSW dextral strike-slip faults (this study), onshore ENE-WSW latitudinal dextral strike-slip faults (referenced herein) and NE-SW sinistral strike-slip faults (referenced herein). In the first phase of LFS movement, all structures in this map were active. During the second phase of LFS in the Pliocene to present day, only the ENE-WSW dextral strike-slip faults were active, and might be linked to block rotations caused by the continuous sinistral movement of the LFS in Lebanon. The occurrence of the NW-SE normal faults in the deep basin might not be caused by these regional geodynamics, but rather to a local stress-field fluctuation affecting only the Oligo-Miocene units.

III. 7.6 Strain partitioning along the LFS and current shortening

The southern and middle segments of the LFS have slipped by different amounts [*Beydoun*, 1999]. The total recorded horizontal displacement in Lebanon amounts to 20-25 km [*Dubertret*, 1972] in contrast with the total displacement of ≈ 100 km along the Dead Sea Transform in Israel [*Freund et al.*, 1970; *Quennell*, 1984]. From GPS measurements, the movement of Arabia relative to Africa amounts to 4-6 mm/a [*Wdowinski et al.*, 2004; *Mahmoud et al.*, 2005; *Reilinger et al.*, 2006]. The Yammouneh Fault zone accommodates 3-4 mm/a slip rate [*Walley*, 1988; *Westaway*, 2004; *Gomez et al.*, 2006], leaving 1-2 mm/a of the motion along the LFS to be accommodated by

different structures [*Gomez et al.*, 2007a].

Gomez *et al.* [2007] argued that the Yammouneh Fault only accommodates strike-slip displacement, while the shortening component accommodated through oblique plate motion within the restraining bend partitioned into strike-slip displacement and perpendicular convergence. They postulated, through geometric calculations on different structures of the restraining bend, a 17% horizontal shortening of Mount Lebanon, close to the 10-15% bulk shortening suggested by Hancock & Attiya [1979]. Hence the remaining shortening should be accommodated by other faults or structures, and the larger horizontal motion measurable south of Lebanon should be transmitted northward through Lebanon in another way. A suggestion was that the Palmyrides, or the offshore domain, were good candidates to accommodate parts of the missing displacement.

Carton *et al.* [2009] argue that an active fold and thrust belt exists along the Levant margin, incipient of a future subduction zone in the Levant Basin offshore Lebanon, which might accommodate all the shortening onshore. On the other hand, Homberg et al. [2010] pointed to the absence of regional significant post-Miocene shortening onshore, questioning the magnitude of transpression during this time.

We have proved in this paper that the Levant Basin offshore Lebanon does not contain large strike-slip faults parallel to the restraining bend that could accommodate part of the LFS displacement. In addition, we find no evidence for current folding and deformation, since most of the structures are currently inactive. We therefore believe that the Levant Basin offshore Lebanon does not accommodate part of the shortening of the Lebanese restraining bend, and other models should be developed to solve this controversial geologic question. Based on our observations, only the ENE-WSW striking dextral strike-slip faults provide evidence of current activity, as they accommodate the counter-clockwise block rotations in Lebanon caused by the transpressive deformation of the LFS.

III. 7 Conclusions

Based on the analysis of 3D seismic reflection data in the Levant basin offshore Lebanon, a variety of structures were investigated in detail consisting of:

- Thick-skinned Late Cretaceous or Early Tertiary NNE-SSW striking thrust faults found offshore Tripoli and Beirut. They do not show any evidence of present-day activity.

- Thin-skinned NW-SE striking Early Miocene normal faults found in the deeper part of the basin in the Oligo-Miocene unit only. Their timing, orientation and localization indicate a non-tectonic control on their origin.

- Thick-skinned ENE-WSW striking dextral strike-slip faults. These structures are inherited from Mesozoic extension and reactivated during the Late-Miocene immediately prior to the Messinian event. They are the only structures in the basin that provide evidence for continuous present-day activity, and might be caused by the counter-clockwise block rotation onshore triggered by the LFS movement.

- NNE trending anticlines folded immediately prior to the Messinian event, and overlying existing Late Cretaceous to Early Tertiary structuration in the basin. These anticlines do not provide evidence for present-day deformation and are inactive currently.

This paper provides a good example of the impact of the evolution of plate boundaries on adjacent basins. The first stage of LFS propagation during late Miocene is associated with the onset of folding and ENE-WSW strike slip faulting in the basin, while the second in the Pliocene corresponds to the cessation of folding and dominance of ENE-WSW strike-slip faulting only.

In the absence of evidence for current shortening in the Levant Basin offshore Lebanon and the non-existing large sinistral strike-slip faults in the basin parallel to the LFS trend, we advocate that the Lebanese restraining bend is mainly contained along the margin. Hence, the missing shortening and displacement of LFS cannot be found offshore.

END OF ARTICLE 1

CHAPTER IV

EFFECT OF THE PALMYRA GRABEN ON THE LEBANESE RESTRAINING BEND

Table of contents

IV. Effect of the Palmyra graben on the Lebanese restraining bend: insights from analogue modelling

"How much truth can a spirit bear, how much truth can a spirit dare? That became to me the real measure of value" Friedrich Nietzsche

In chapter III, seismic interpretation revealed the presence of inherited structures offshore Lebanon that are remnant of the Mesozoic rifting event. Of particular importance, are ENE-WSW striking strike-slip faults currently active due to transpression along the adjacent Levant Fracture System. This chapter discusses the evolution of the Levant margin through analogue modelling by testing of several scenarios, namely the ones involving reactivation of pre-existing structures in a sinistral strike-slip setting. On a first hand, the first section includes review of the theory behind analogue modelling. The various laws are listed and the commonly used materials are reviewed. The results of other experiments published in literature are discussed, particularly those involving strike-slip tectonics and transpression. On the other hand, the second section targets to describe the modelling parameters used in this work, and discusses the results of several key experiments undertaken throughout this project.

The complexities of geological phenomena and the difficulties associated with understanding past events that happened in Earth's history, urges us to pursue and develop new tools to reduce uncertainties in interpretation and reconstruct the geology of any region. Thus, the development of analogue and physical modelling during the past century was aimed to reach such ends and is considered as an important tool to understand the architecture of sedimentary basins [*Hubbert*, 1937]. As the lithology and facies distribution in nature are extremely complex and variable, both vertically and horizontally, their representation in analogue models is thus unfeasible. Sedimentological events require a combination of chemical and depositional processes that are very challenging to be reproduced under laboratory conditions and in small physical models. Thus, models are primarily targeted to recreate and reproduce structural features at basin scales.

IV. 1 Modelling parameters

Analogue models have been long used to study the development of tectonic structures. In order to successfully model structures in a laboratory condition, it is essential to downscale the natural example by a certain factor. This is referred to as scaling, and it controls the choice of materials to be used during the experiments. Hubbert [1937] and Ramberg [1967] derived scaling laws to be fulfilled in order to link analogue models to natural systems. Thus, in analogue experiments, geometries, stresses, timing and rheologies should be scaled down properly. Laws and equations, discussed below, govern such scaling.

IV. 1.1 Scaling

Scaling is based on the similarities between the natural example and the model. Thus, they both need to have similar rheologies, densities, gravitational forces and stress, all scaled down appropriately, in order to draw comparisons [*Hubbert*, 1937; *Ramberg*, 1967; *Davy*, 1986]. Three important scaling aspects should be respected in this sense: Geometric similarity, dynamic similarity and kinematic similarity.

The geometric similarity consists of having a fixed length/wide ration in both the experimental and natural systems. Thus, the equation governing this will be of the form:

$$\mathrm{Sg} = \frac{L_a}{L_n} \tag{4.1}$$

with Sg being the geometric similarity ratio, L_a the length of the system in the model and L_n the length of the natural example in question. In this sense, the resulting geometries of the model will be scaled to the geometries in nature by the ratio Sg.

The dynamic similarity consists of having a fixed ratio between the external forces acting on the model and the material properties. In this sense, the equation of rheology and of dynamics must be respected in the model. The equation of dynamic governs the equilibrium between the tectonic and gravitational forces [*Richard*, 1990] and is written:

$$\frac{\partial \sigma_{ij}}{\partial X_i} + \rho\, g_i = 0 \tag{4.2}$$

whereby σ_{ij} is the deviatoric stress tensor in the system, X_i being its coordinates, ρ being the density and g the gravitational acceleration. Thus, stresses should be scaled down as the product of density, gravity and length vectors. This equation can be rewritten for non-dimensional variables in the natural example:

$$\sigma^n = \rho^n \,.g^n \,.l^n \tag{4.3}$$

and in the analogue model:

$$\sigma^a = \rho^a \,.g^a \,.l^a \tag{4.4}$$

whereby ρ is the density, *g* the gravitational acceleration and *l* the length. The ratio for these two equations becomes:

$$\frac{\sigma^a}{\sigma^n} = \frac{\rho^a}{\rho^n} \cdot \frac{g^a}{g^n} \cdot \frac{l^a}{l^n} \tag{4.5}$$

As we will run the experiments under natural gravity with material characterised by density close to natural system equation 4.5 can be simplify as:

$$\frac{\sigma^a}{\sigma^n} = \frac{l^a}{l^n} \tag{4.6}$$

Concerning rheology, as far as crustal rocks are concerned, both brittle and viscous rocks must be considered. Brittle geological systems are described by the mohr-coulomb law:

$$\tau = \mu_i . \sigma + S_0 \tag{4.7}$$

with τ being the shear stress, σ the normal stress, μ the coefficient of internal friction and S_0 the cohesion.

BOX 4.1

Cohesion of rocks represents the interception of the Mohr failure line (with a slope of μ_i) with the shear stress axis (Figure 4.1). As cohesion is hardly measurable, it is more common to express rock strength in terms of C_0 or the uniaxial compressive strength (UCS) [*Zoback*, 2010]. The relationship between S_0 and C_0 is:

$$C_0 = 2S_0 \left[(\mu_i^2 + 1)^{1/2} + \mu_i\right] \quad (4.8)$$

Coefficient of internal friction is the slope of the failure line in the Mohr-Coulomb failure envelope (Figure 4.1). Allowable stress states are those that do not intersect this failure envelope. Stress states corresponding to Mohr circles which exceed the failure line are not allowed because failure of the rock would have occurred prior to the rock having achieved such a stress state.

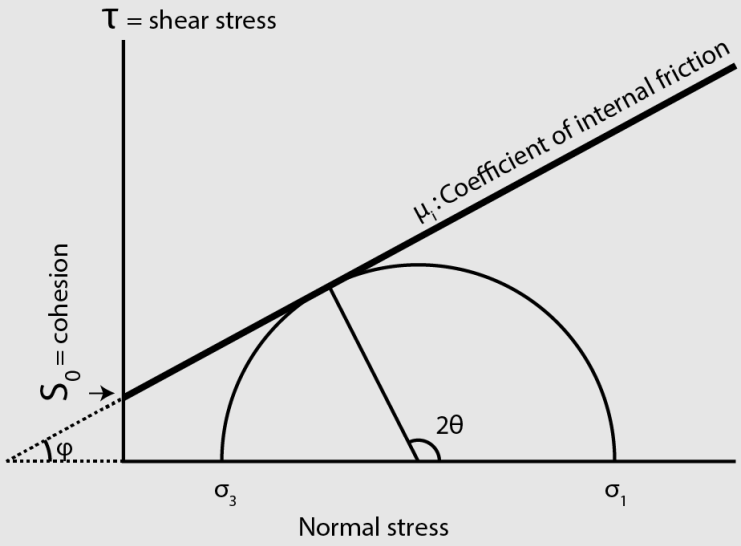

Figure 4.1: Mohr-Coulomb failure envelope is graphically represented by the Cohesion S_0, the normal stress axis and the shear stress axis. The slope of the envelope is referred to as μ_i or the coefficient of internal friction, $\mu = \tan \varphi$ and the angle of internal friction θ is the angle of this line with the normal stress axis. $\varphi = 90 - 2\theta$, with θ being the angle between the fault plane and $\sigma 1$.

Following equation [4.6], σ is principally equal to the length ratio of the system since the density and the gravity are chosen and considered to be the same in both the experiment and the natural example. Following [4.7], we see that granular material that are characterized by friction angle similar to rocks and negligible cohesion will be good candidates for scaled experiments of brittle rocks.

BOX 4.2

A newtonian fluid is a fluid in which the viscous stresses arising from is flow at every point are linearly proportional to the local strain rate – the rate of change of its deformation over time.

In many scaled experiments, a Newtonian fluid is used to simulate ductile behaviour with the crust. Such behaviour corresponds to specific rocks such as evaporites or rocks at temperature corresponding to the lower crust. The chosen velocity must satisfy an equation linking stress and deformation rate and the equation of rheology becomes:

$$\sigma = \mu . \dot{\varepsilon} \tag{4.9}$$

with σ being the stress, μ viscosity and $\dot{\varepsilon}$ the deformation rate in s^{-1}. $\dot{\varepsilon}$ is equal to V/L with V being a characteristic velocity and L a characteristic length. For dimensionless variables, the stress σ can be written following equation (3) or (4) and rewriting equation (9) will give:

$$\mu = \frac{L . g . \rho}{\dot{\varepsilon}} \tag{4.10}$$

If we choose an invariable gravitational acceleration g and density ρ in the model, the viscosity will be thus be a function of velocity by the equation:

$$\mu = \frac{L^2}{V} \tag{4.11}$$

Thus, the chosen velocity must satisfy the viscosity of the chosen Newtonian material when undertaking analogue models. The kinematic similarity thus consists of fixing the time ratio between the model and the natural example by following the equation of rheology. In analogue models, the deformation is regulated by computer-controlled stepper motors. This allows choosing the proper velocity of deformation, which could range from few minutes to several days. Thus, a temporal scale, or kinematic similarity with natural examples, could be set up. Accordingly, one hour of deformation in the lab for example could correspond to 1 My in geologic times.

IV. 1.2 Analogue material

Similarity and scaling rules discussed above will govern the choice of materials. In physical models, dry granular materials, such as sand, are usually used to represent brittle deformation of upper crustal rocks. In some experiments [*Miller and Mitra*, 2011; *Mitra and Paul*, 2011] wet clay is preferred over sand for reasons discussed in the following paragraphs. Viscous material, such as silicone, is used to simulate the lower crust or a weak detachment layer in the upper crust. In some experiments, honey is deposited below the silicone to simulate the asthenosphere. Below is a small description of these materials

Sand

The sand is by far the mostly used material to simulate sediments in basins [*Horsfield*, 1977; *McClay*, 1990]. It represents the upper crust and behaves as a brittle material deforming according to the Coulomb failure [*Davy*, 1986]. In theory, to represent the bulk sediments of the upper crust, the sand used in experiments must have a low (or negligible) cohesion and a coefficient of internal friction close to that in nature. For this reason, the Fontainbleau sand is commonly used in analogue physical modelling. This sand is well sorted with a grain size of around 120 µm. The density of sand is between 1.53 and 1.78 depending on the physical handling technique, with

usually sifting and sprinkling producing greater densities than just pouring sand [*Krantz*, 1991]. Fontainbleau sand has a negligible cohesion ranging between 300 and 520 Pa and a coefficient of internal friction between 0.58 and 1.00 [*Krantz*, 1991]. The difference in these values is again due to the physical handling technique, with low values being for poured sand and high values for sprinkled sand [*Krantz*, 1991]. Thus, a positive correlation exists between the coefficient of internal friction and sand density with higher μ values for densely packed (sifted or sprinkled) sand. As revealed by shear testing, friction coefficients for reactivation are essentially the same as for fault initiation [*Krantz*, 1991]. The addition of clay or cement does not significantly change the internal friction compared with that of pure sand. However, most publications on models made with sand quote a value for μ of around 0.58 [e.g. *Hubbert*, 1937; *Vendeville et al.*, 1987] even where the models are built with sifted sand [*Mcclay and Ellis*, 1987]. Measurements performed by Schellart [2000] yielded a coefficient of internal friction value of 0.88 (with angle of internal friction of 41°) and a cohesion around 240 Pa. Table 4.1 shows values for cohesion and coefficient of internal friction for intact sedimentary and igneous rocks in nature.

Table 4.1: *Values of μ (coefficient of internal friction), Φ (angle of internal friction) and C (cohesion) for different rock types. From Schellart [2000].*

Rock type	***μ***	***Φ***	***C (MPa)***	***Reference***
Granite	0.64	32.6	31	[*Jeager and Cook*, 1976]
Gabbro	0.66	33.4	28	[*Jeager and Cook*, 1976]
Trachyte	0.68	34.2	41	[*Jeager and Cook*, 1976]
Serpentinized olivine	0.65	33.0	90	[*Raleigh and Paterson*, 1965]
Sandstone	0.51	26.6	28	[*Jeager and Cook*, 1976]
Berea sandstone	0.49	26.1	24	[*Twiss and Moore*, 1992]
Weber sandstone	0.60	31.0	70	[*Twiss and Moore*, 1992]
Tennessee Sandstone	0.84	40.0	50	[*Handin*, 1969]
Lueders sandstone	0.53	27.9	15	[*Handin*, 1969]
Solnhofen sandstone	0.53	27.9	105	[*Handin*, 1969]
Marble	0.75	36.9	110	[*Jeager and Cook*, 1976]
Blair dolomite	1.00	45.0	45	[*Handin*, 1969]

Equation (4.5) governs the scaling for the stresses in both the natural system and the analogue. By considering the scaling laws discussed above, sand is the material that resembles most the natural sediments of the upper crust in analogue models. The angle of friction ϕ is supposed to be the same in both the natural system and the model [*Horsfield*, 1977] depending on our material choice. Thus, the cohesive strength of the

natural system should be scaled down by the same factor as stresses and lengths [*Horsfield*, 1977; *Schellart*, 2000]:

$$\frac{C^a}{C^n} = \frac{\sigma^a}{\sigma^n} = \frac{\rho^a}{\rho^n} \cdot \frac{l^a}{l^n} \quad (4.12)$$

where C is the cohesion. Thus, a stress scaling ratio of 10^{-7} will lead to a cohesion value of few hundreds of Pa in analogue models, which is in the range of the cohesion of sand.

Wet clay

Wet clay has been documented to be an appropriate modeling material because the fractures and faults formed in clay as a response to applied stress are similar to that in natural rocks [*Oertel*, 1965; *Reches*, 1988], because the strain fields associated with faulting in clay are similar to those predicted by dislocation calculations [*Hildebrand-Mittlefehldt*, 1979], and because the faults are developed as discrete surfaces whose geometry and evolution can be easily studied [*Cloos*, 1968]. Miller and Mitra [2011] favour wet clay in their experiments because clay allows a much better definition of fault geometries and evolution and also enables the deformation to be studied for mature structures involving steep surfaces. The coefficient of internal friction of clay is 0.6 and its cohesion is 330 Pa [*Krantz*, 1991].

In some experiments, basement is represented with stiff clay of 1.85 g/cc density [*Miller and Mitra*, 2011]. The overlying sedimentary cover is represented with clay of 1.6 to 1.65 b/cc density. The density of clay is usually adjusted by varying the water content.

Silicone

The silicone in analogue models represent ductile layers, such as the lower crust [*Davy*, 1986], salt [*Vendeville and Jackson*, 1992a, 1992b] or detachment surfaces [*Mattioni et al.*, 2007]. The silicone used in experiments is polydimethylsiloxane (PDMS SGM-36) of Dow Corning and Gomme G.S.1R manufactured by Rhône-Poulenc. These two materials have densities of 0.965 and 1.3, respectively, and display an almost perfectly Newtonian viscous behaviour [*Weijermars*, 1986]. Their viscosity is (5×10^4 Pa·s) for both [*Weijermars*, 1986], although a viscosity range between 2×10^4 Pa·s and 3.5×10^4 Pa·s was measured for the PDMS SGM-36. This low viscosity is not representative of the natural system or the lower crust in general but it is imposed due

to scaling of the models. A large silicone viscosity will not be compatible with scaling properties of the models [*Davy*, 1986].

Honey

In models whereby it is necessary to incorporate the mantle, honey is used. Its density of 1.45 and relatively low viscosity of 10 Pa.s could well represent the upper ductile mantle. The Hungarian Acacia honey is used in some experiments [*Davy*, 1986; *Schueller*, 2004] and is favoured due to its slow crystallization. Such experiments are referred to as 4 layers analogue experiments.

IV. 2 Previous work

Analogue experiments have significantly contributed to the theoretical understanding of tectonic structures. Despite their limitations and simplifications, they have proved especially useful in developing kinematic models, providing the opportunity to study the evolution of complex 3D fault geometries in detail. Of particular importance, are regions where limited geophysical and subsurface data are available and where the current structural geometry is only a snapshot of the evolutionary history of the fault system. In such case, analogue modelling proved to be of great importance to reproduce current geometries in laboratory conditions, validate or reject current interpretations, and predict the subsurface geometries with great accuracy. Published modelling studies are discussed in the following paragraphs. Such studies had a big impact on our understanding of structural geology processes.

IV. 2.1 Analogue modelling of strike-slip systems

The first experimental studies investigating strike-slip tectonics were performed by Cloos [1928] and Riedel [1929] and consisted of two plates with a straight and vertical basement fault and overlain by undeformed overburden. No bends in the basement faults were simulated so deformation was purely strike-slip. This experiment was later known as the "Riedel experiment" [*Tchalenko*, 1970]. The results showed the classical R shears striking approximately 12° to the main basement fault (Figure 4.2). Faults in the overburden are, in fact, secondary structures generally directly rooting down to the pre-existing basement fault and restricted to its immediate vicinity.

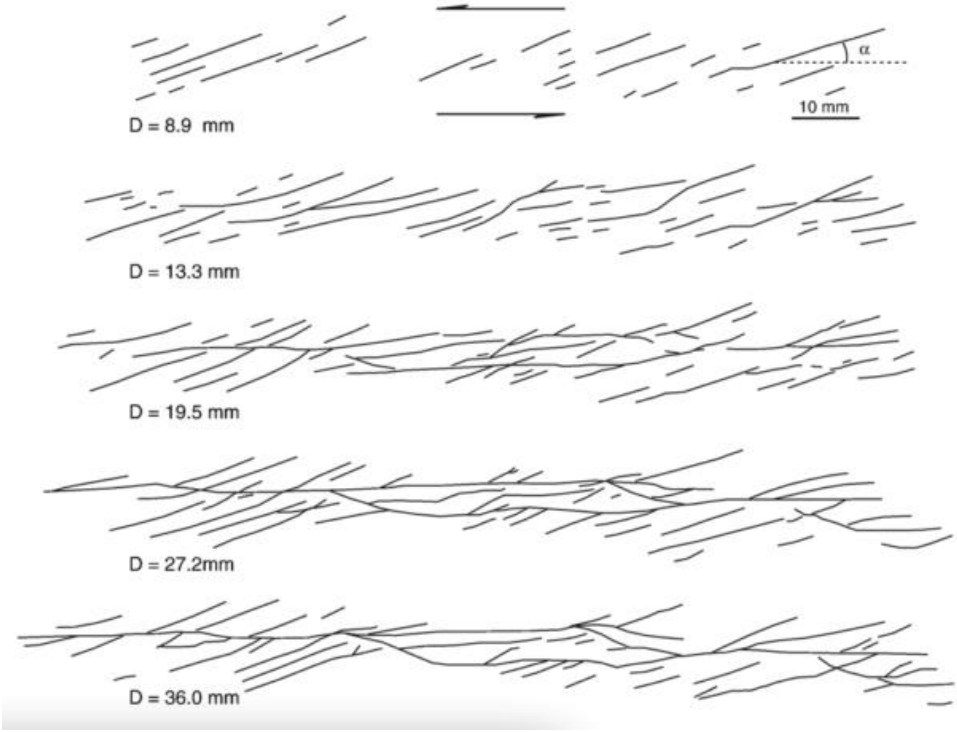

Figure 4.2: Surface results of the Riedel experiment displaying classical R shears. From Dooley *et al.* [2012] and redrawn from Tchalenko [1970].

Dooley and Schreurs [2012] contributed to the understanding of strike-slip fault systems by revising the existing knowledge on the evolution of intraplate strike-slip tectonics through series of analogue experiments. In addition to some classical experiments they reproduced, they provided results of two new experimental setups that investigated the effect of weak crustal zones on the segmentation of strike-slip faults, and strike-slip and transpressional reactivation of extensional basins. In their model, they demonstrate that the presence of a weak body along a developing strike-slip fault zone has a profound influence on segmentation. It will produce fault segments that diverged from the surface trace of the basement fault to form a left-stepping restraining stepover centred on the weak body (Figure 4.3). This model converges with the one of Mann [2007] targeting the influence of crustal heterogeneity on paired-bends in strike-slip faults and with the models of Dooley *et al.* [1999] who had similar results in strike-slip fault segmentation. In their second experiments, Dooley and Schreurs [2012] tested the effect of initial extension followed by strike-slip deformation. Results showed that the orientations of strike-slip faults was not affected much by the existence of initial extensional structures and were similar to the one observed in distributed strike-slip and transpression experiments [*Schreurs and Colletta*, 1998]. The results are different from experiments of Mattioni *et al.* [2007] who undertook a very similar approach and

showed that initial extensional structures were reactivated and affected the geometry of a succeeding strike-slip system (Figure 4.4). This difference is likely related to the model design of each experiment.

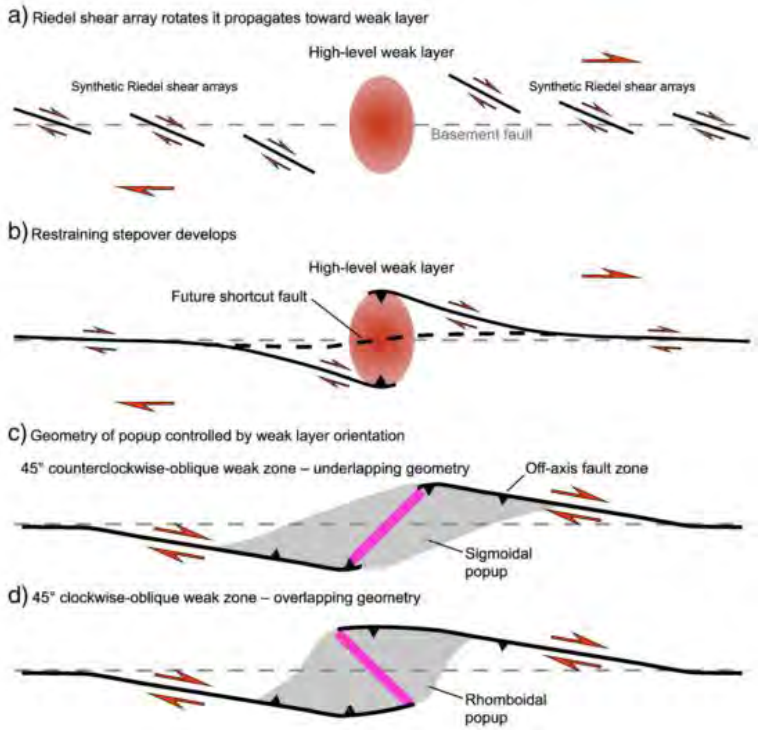

Figure 4.3 : Diagram illustrating typical restraining stepover geometry formed across weak bodies. (a) Riedel shears propagate toward the weak body and gradually diverge from the trace of the basement fault. (b) Linked faults form restraining stepover centred on the weak body. (c) Weak bodies oriented 45° counterclockwise-oblique to the basement fault approximate popups formed above underlapping master-fault geometries. (d) Weak bodies oriented 45° clockwise-oblique to the basement fault approximate popups formed above overlapping master-fault geometries. From Dooley & Schreurs [2012].

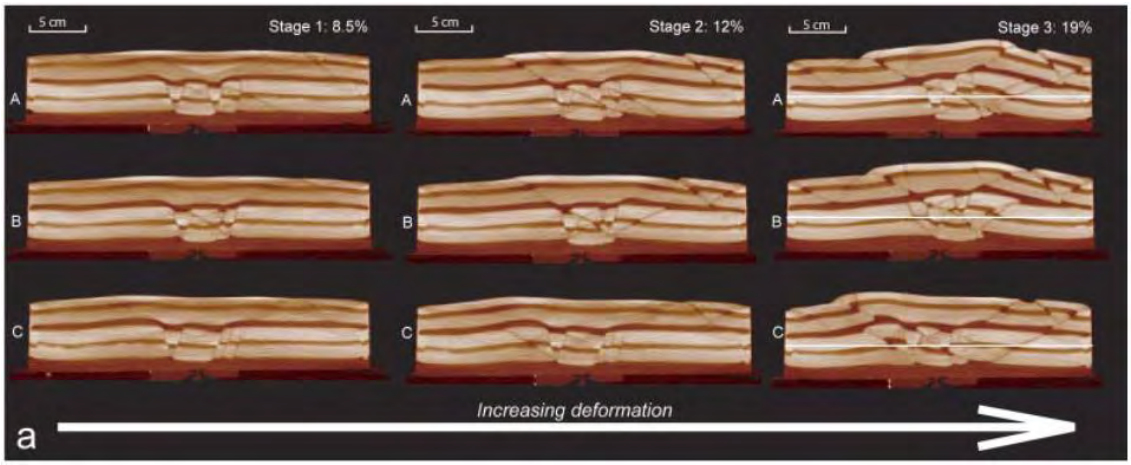

Figure 4.4: Vertical sections (A, B, and C) showing faults at three consecutive stages of transpression following extension to create pre-existing normal faults. The pre-existing faults were parallel to the main strike-slip faults in their experiment. Pre-existing faults were inverted and reactivated upon transpression. From Mattioni *et al.* [2012].

Few studies were targeted to understand transpressive tectonics using analogue models. Brittle-ductile analogue systems were studied by Richard *et al.* [1991] who analysed the deformation above low-angle and high-angle basement faults below a sand-silicone model under pure thrusting and pure wrenching conditions. The results obtained consisted of steeply dipping faults within the sand layer, with partitioning of the deformation between strike-slip faults and thrusts. The structures induced by transpression, and the geometric and kinematic evolution of faulting in zones of transpression at basin and crustal scale were investigated by Casas *et al.* [2001] and Schreurs and Colletta [1998]. The surface geometry of releasing and restraining bends was investigated by Mitra and Paul [2011] who introduced fault bends or offsets in the main basement faults with different orientations (Figure 4.5). Results show a great variability of surface geometries in strike-slip systems suggesting a strong link between the geometries of the structures and that of the connecting basement faults. The orientation and geometry of the basement faults is found to control the shape of the major uplift. A similar study was conducted by Mcclay and Bonora [2001] with a difference in that they adopted a different technique which investigated the cross-sectional geometries of restraining bends without referral to releasing bends as shown in Mitra and Paul [2011]. Mcclay and Bonora [2001] looked at the 4D evolution of restraining stepovers by taking into account syntectonic sedimentation. Their models illustrate the progressive evolution of the pop-ups together with the geometries of the growth sequences deposited at the same time as the uplift developed. The effect of synsedimentation and erosion on the evolution of strike-slip faults was also described by Le Guerroué and Cobbold [2006] whereby they noted that it changes the geometry of the faults and controls the activity of some structures.

In summary, strike-slip and transpressive systems exhibit a large variability in their geometry. Existing analogue models are not sufficient to explain a number of hypothesis on strike-slip structures, such as the role of pre-existing faults and weak bodies on the evolution of these structures.

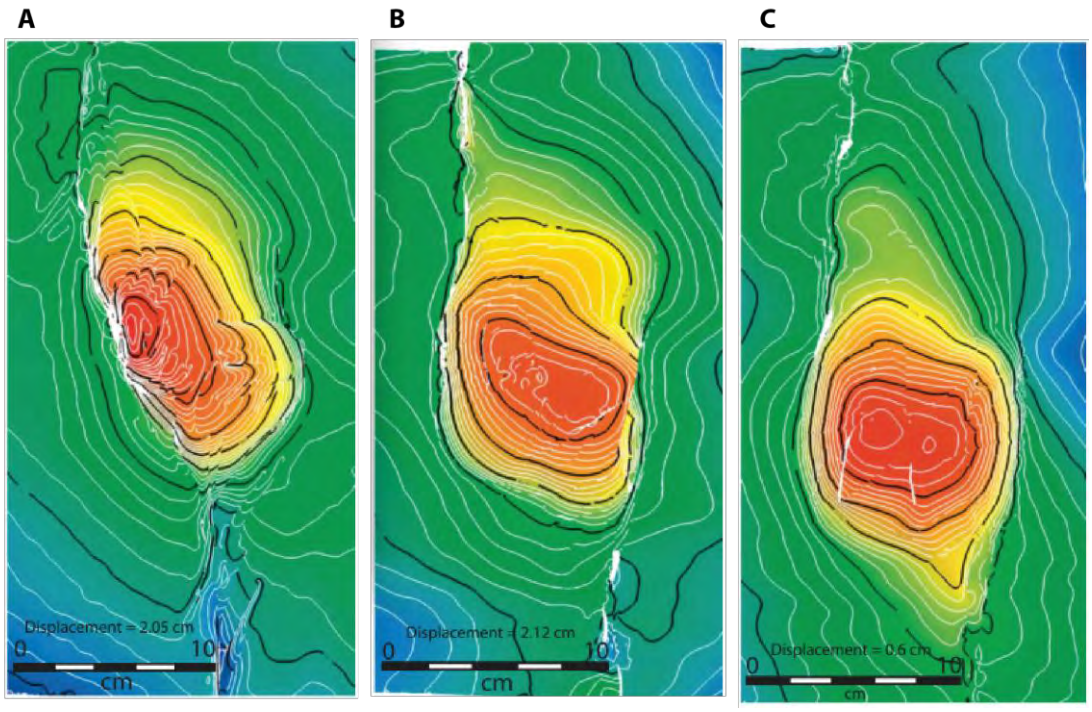

Figure 4.5 : 3D geometry of the top of the sedimentary cover for a restraining bend with variable oblique bend connecting two strike-slip fault segments in the basement. In (A), the bend is 45°, in (B) the bend is 90°, and in (C) the bend is 135°. The different bend orientations have an important effect on the resulting geometry of the restraining bend. White contours represent topographic relief. From Mitra & Paul [2011].

IV. 3 Modelling of the Levant margin

Results presented in Chapter 3 show that the margin offshore Lebanon is affected by ENE-WSW dextral strike-slip faults synchronous with the activity on the restraining bend (Figure 4.6). These faults are inherited from the Mesozoic rifting phase and are reactivated under the effect of the adjacent Levant Fracture System (LFS) starting the Late Miocene. They are still active today and likely accommodate a bookshelf rotation of the margin.

In this section, the workflow adopted in analogue modelling and the documented results are described. The observations of several experiments are then put into context by correlating them to regional tectonics.

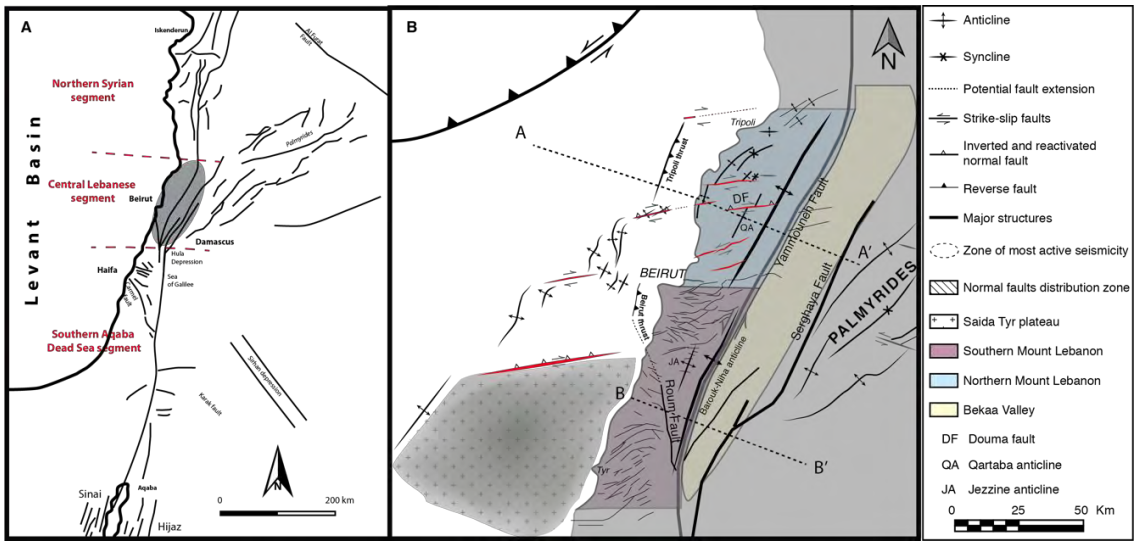

Figure 4.6 : Structural sketch of the Levant Fault System in (A) showing the different segments along its path. The Levant restraining bend in grey is shown in detail in (B) whereby the major structures are highlighted together with the ENE-WSW dextral strike-slip faults (in red) accommodating count erclockwise block rotations caused by the LFS activity.

IV. 3.1 Natural example

The Levant margin offshore Lebanon is marked by a series of ENE-WSW dextral strike-slip faults [*Ghalayini et al.*, 2014]. Similar dextral strike-slip deformation is also evidenced onshore Lebanon [*Dubertret*, 1955; *Sabbagh*, 1961; *Gedeon*, 1999] which makes these structures a striking feature of the eastern margin of the Levant basin. These faults are inherited from Mesozoic extensional regimes and are currently active as evidenced by seafloor deformation and earthquake seismicity [*Gedeon*, 1999; *Ghalayini et al.*, 2014].

The activity of the ENE-WSW striking dextral strike-slip faults is associated with the activity along the main sinistral NNE-SSW Levant Fracture System. The latter is major plate boundary separating the Arabian from the African plate and active since the mid-Miocene, with transpressive activity in Lebanon initiating in the Late Miocene. The dextral movement of the ENE strike-slip faults recorded today could be due to counter-clockwise rotations caused by the restraining bend in Lebanon [*Ron et al.*, 1984]. It is likely that the presence of a fractured basement has facilitated block rotations in Lebanon whereby the existing extensional structures acted as weak planes and were reactivated as dextral strike-slip faults.

Strike-slip faults with the same orientation are also found in the Palmyra Basin in Syria [*Brew et al.*, 2001b]. The latter is a Mesozoic basin inverted starting the Late Cretaceous times [*Searle*, 1994]. Lebanon and its offshore might constitute the continuation of the Palmyra Basin [*Walley*, 1998] which could explain the presence of extensional structures of the same age and trend.

To test this hypothesis, a series of analogue models were performed with ductile-brittle materials. In these models, the Palmyra Basin is considered to extend westward to Lebanon and its immediate offshore (Figure 4.7). This is in order to simulate basement structuration, which is likely related to Mesozoic rifting, causing thickness variations in the crust.

The aim of this study is: (1) to investigate the effect of oblique structuration on the development of strike-slip fault systems in general and the Levant restraining bend in particular, (2) test if pre-existing structures are reactivated only in transpression or a through a transition from a compressional regime first followed later by a transpressive one, (3) to test a geological scenario in which the adjacent Palmyra Basin extends to Lebanon and check its reproducibility in laboratory models, (4) Confirm that E-W structures observed in seismic data are reactivated faults, and what conditions govern this reactivation.

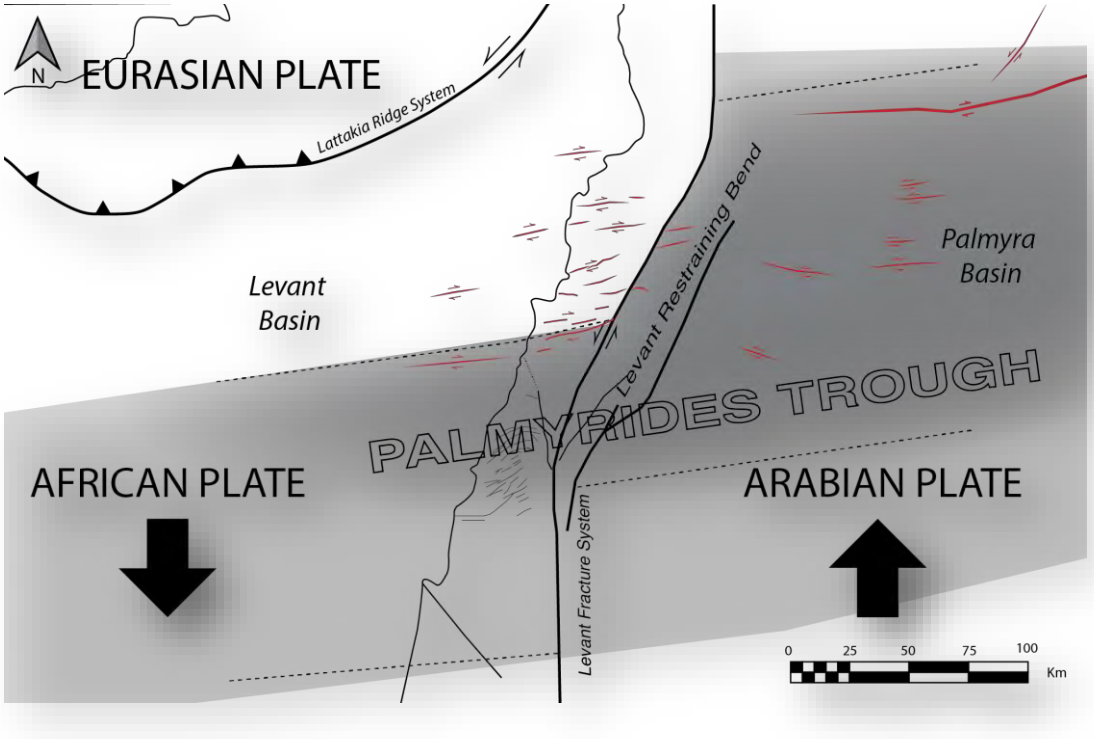

Figure 4.7 : Regional map of the Levant area showing the presence of ENE-WSW strike-slip faults along the Levant margin and in the Palmyra Basin. The Palmyrides trough is likely to extend to Lebanon which was represented in the analogue experimental model by pre-existing faults bordering a graben in the silicone. The ~100 km displacement along the LFS is taken into account when extending the Palmyra graben westward to Lebanon.

IV. 3.2 Experimental setup and procedure

Testing of variable parameters

A total of 44 experiments were undertaken in this project in order to study the interplay between pre-existing structures, compression and transpression along a major strike slip zone affected by a restraining bent. These are included in appendix 2 for reference. Only 12 will be described and discussed in details in this chapter. The variable material properties for these experiments are summarised in table 4.2:

Table 4.2: *Experiments discussed in this chapter with the main parameters used during their construction*

Name	*Exp nb in Appendix*	*Sand thickness*	*Silicone thickness*	*Velocity Compression*	*Velocity strike-slip*	*Important parameters*
A	2	3 cm	-	-	20 cm/h	
B	3	3 cm	-	5 cm/h	20 cm/h	Testing of bend geometry
C	5	3 cm	-	5 cm/h	20 cm/h	
D	6	3 cm	-	5 cm/h	20 cm/h	
E	16	2 cm	1 cm	50 cm/h	-	Pre-existing Faults in sand
F	18	2 cm	1 cm	-	50 cm/h	
G	19	2 cm	1 cm	12.5 cm/h	50 cm/h	
H	27	2 cm	1 cm	12.5 cm/h	50 cm/h	Discontinuities below silicone
I	12	2 cm	1 cm	12.5 cm/h	50 cm/h	No pre-existing faults
J	39	2 cm	1 cm	6.25 cm/h	50 cm/h	Graben in silicone
K	44	2 cm	0.5 cm	5 cm/h	5 cm/h	Reducing velocities

Initial setup

The performed experiments investigates strike-slip tectonics by deformation from a reactivated, straight, and vertical basement fault into an overdunden. The experimental setup consisted of a 70x41 cm wooden box with two overlapping plates (Figure 4.8). One of these plates is movable, driven by computer-controlled stepper motor, whereas the other is fixed (Figure 4.8). The overlapping plates simulate basement master faults in which two parallel strike-slip faults are connected by a 45° oblique bend (Figure 4.9). This is in order to simulate a restraining bend similarly to the one observed at the modern Levant margin. The stepover size is 9x4.5cm in experiment C while it is 9x1.9cm experiments A & B and 9x3cm in the rest of the experiments.

The wooden box is bordered by two mobile longitudinal confinement walls (Figures 4.8 and 4.9), which are also controlled by computer-controlled stepper motors. The movable confinement walls simulate lateral compression in these experiments. Thus, transpression (or oblique shortening) could be achieved by combining the basal strike-slip shear component of the overlapping plates and the transverse shortening by the longitudinal confinement walls.

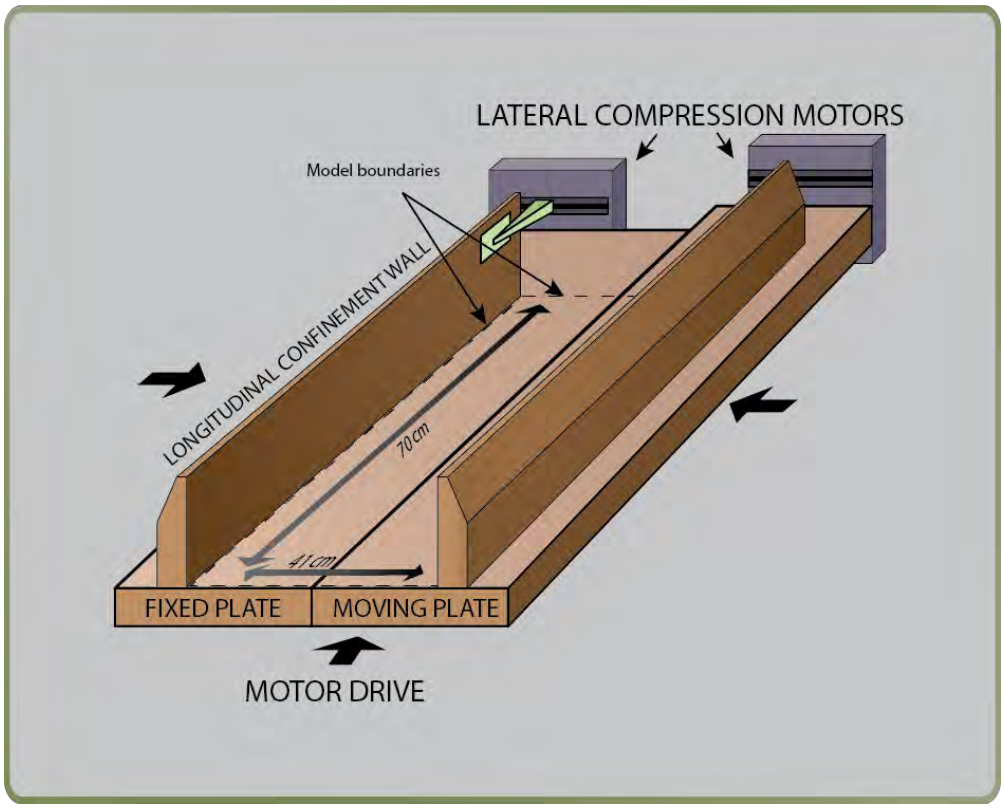

Figure 4.8 : Experimental setup consisted of a 70x41 cm wooden box bordered by two latitudinal confinement walls. The different parts of the box are moved by computer stepper motors.

All models were gridded by 5x5 cm grid at the surface in order to measure and quantify surface deformation using a camera. Only experiment J was scanned by X-ray computerized tomography using a General Electric CT-scanner. This technique is non-destructive and generates 3D cross-sectional images through the models [*Hounsfield*, 1973; *Colletta et al.*, 1991]. The model was scanned before and during deformation. The scanner was run every 1 cm of strike-slip movement while simultaneously taking surface pictures using a camera. The end result is a 4D model of the strike-slip system allowing us to investigate its evolution in time.

Pre-existing structures

Oblique inherited structures were simulated in experiments E, F and G by cutting vertically through the undeformed sand with a small 7 cm large cardboard (Figure 4.9). In experiment H, square foam bars 0.8 mm thick were attached to the plastic board below the silicone to simulate discontinuities in the ductile material (Figure 4.9). In experiment I, inherited structures were taken into consideration by creating two parallel faults at about 70° to the main strike-slip faults (Figure 4.10). They were cut through the silicone and filled with micro-balls to decrease friction along fault planes and prohibit the silicone to amalgamate. Between the two faults, the silicone thickness was reduced to 0.5 cm (Figure 4.10). The end result setup represented an oblique graben structure (with respect to the strike slip system) bordered by faults. The thickness of the silicone varied across the mimicked graben. In the natural example, this is associated with a trough below Mount Lebanon with crustal thickness changes. Once the faults were cut, the sand was sifted uniformly on top of the silicone and was thus considered as undeformed.

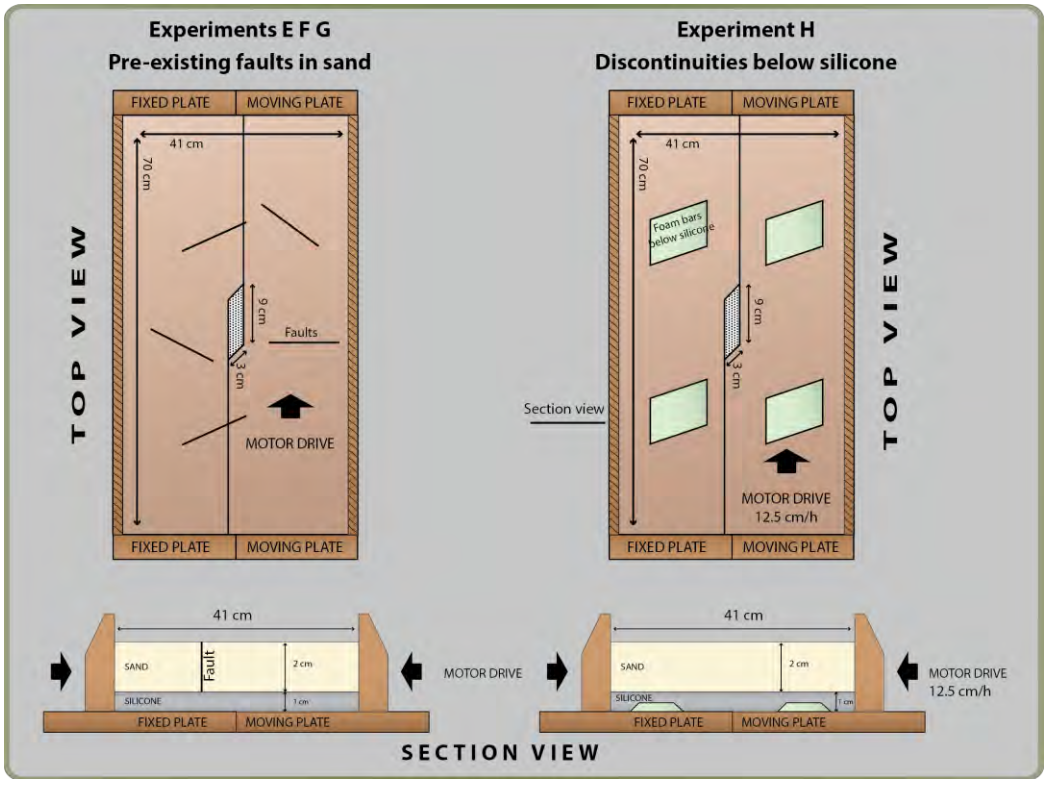

Figure 4.9 : Experiments with pre-existing faults in sand (experiments E, F & G) and with discontinuities below the silicone (experiment H). Experimental materials consisted of a 1 cm thick silicone base overlain by 2 cm pack of sand. In experiments E, F and G, several faults were created in the sand at different directions. The faults did not penetrate the silicone. In experiment H, discontinuities consisting of 0.8 cm thick foam bars were deposited below the silicone to change its thickness and test their role in localising deformation during transpression.

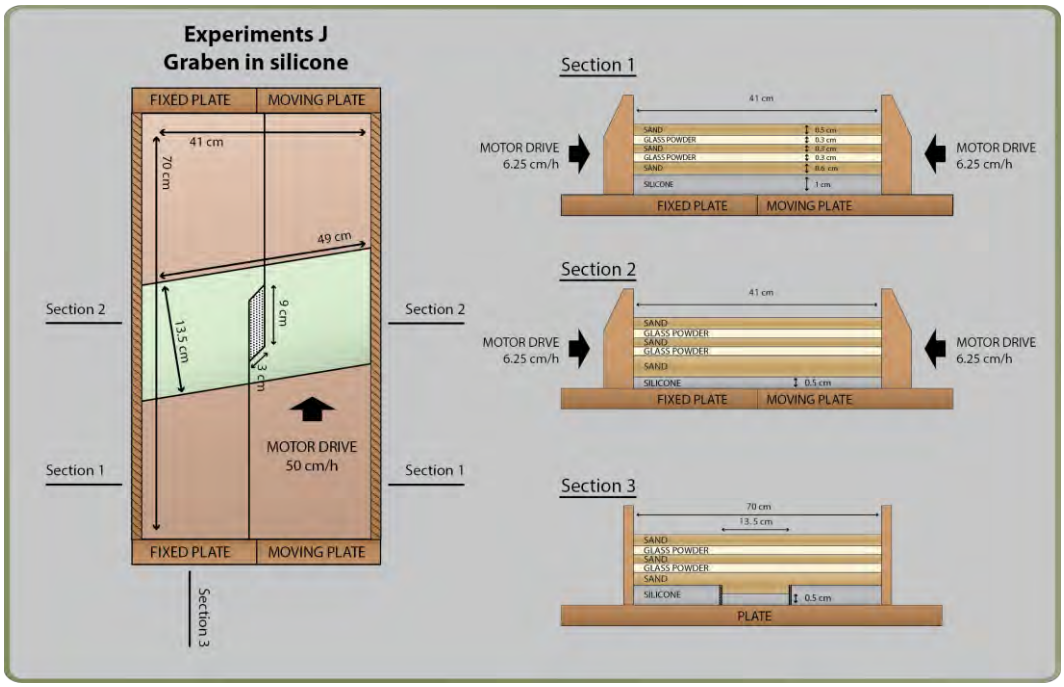

Figure 4.10: Experiment with an oblique graben within the silicone below the sand. Experimental materials consisted of a 1 cm thick silicone base overlain by 2 cm pack of intercalated sand and glass powder. A graben was simulated oblique from the bend in the basement faults whereby the thickness of the silicone was reduced to 0.5 cm. Bordering the graben, two faults were created in the silicone and their planes filled with micro-balls.

Materials and scaling

The sedimentary sequence was simulated by quartz sand (Figures 4.9 and 4.10). This unit represents the upper crust and the sedimentary cover in the Levant region, which amounts to ~20 km in thickness. In experiments A, B, C & D, this layer equals 3 cm and consists entirely of quartz sand. In experiments E, F, G, H, I, & K, this layer is 2 cm thick consisting entirely of quartz sand while in experiment J it is 2 cm thick layer of alternating quartz sand and glass-powder (pyrex). Both materials are well sorted and have a mean grain size of 115 μm. The sand has a low/negligible cohesion, an angle of internal friction of 30°, and a density ranging from 1400 to 1600 $kg.m^{-3}$. The glass powder acted as a stratigraphic marker due to its higher densities of 2230 $kg.m^{-3}$, thus allowing the identification of structures on cross-sections due to contrasting densities during scanning. In order to be able to tune how deformation applied at the bottom impact the sedimentary sequence, the base of the model was made of a 1 cm thick silicone layer (PDMS SGM-36 of Dow Corning) in experiments E, F, G, H, I, & J and 0.5 cm thick silicone layer in experiment K. Experiments A, B, C & D did not contain any silicone. The latter behaves nearly as a Newtonian fluid, with a density of 0.965 g cm^{-3}, a viscosity of 2.5x 10^4 Pa s at room temperatures [*Weijermars*, 1986] and strain rates

below $3x10^{-3}$ s^{-1}. The silicone allows diffusing the deformation in the model. The silicone was deposited directly on top of the overlapping plates. This layer can be seen as lower crustal material in the experiments. This is discussed further in the following section.

The models were scaled for length and time following the basic principles of Hubbert (1937) and Ramberg (1967). The length ratio, or geometric sale, between the natural example and the model is in the order of 10^{-6}, i.e. every 1 cm in the model equals 10 km in nature. The chosen time scaling factor depended on the deformation velocity chosen (table 4.2) and is thus around 5 x 10^{-11} (every 1 min of deformation in the model represents 1 My of in the natural example) in experiments E, F, G, H & I, 5 x 10^{-10} in experiments J & K and 2 x 10^{-11} (every 1 min of deformation in the model represents 0.5 My of in the natural example) in experiments A, B, C & D. It is important to keep in mind that some geological parameters such as temperature evolution through time and effects of pore pressure on sediment rheology could not be taken into account as in most analogue modelling studies due to the related technical difficulties.

IV. 3.3 Results

The results of the experiments are discussed below based on their geometry as observed when several parameters are varied. Thus, three important aspects will be described: (1) size of the popup, (2) effect of the ductile material, and (3) reactivation of faults.

Popup size

Experiments A, B, C & D investigate the effect of varying the size of the stepover on the final geometry of the popup. They were undertaken with brittle material only, such as sand, without the usage of silicone.

In these four experiments, deformation outside the popup is accommodated by a set of nearly parallel sinistral strike-slip faults (Figure 4.11). The popup itself is bounded by two thrust faults. In experiment A & B, the width of the popup is 6 cm while it is 10 cm in experiment C and 8 cm in experiment D. Counterclockwise block rotation is 20° in experiments A & B, and ~30° in experiments C & D. Secondary structures are found within the popup and are particularly observed in experiment C (Figure 4.11). These consist of a set of 5 cm long ESE-WNW dextral strike-slip faults having ~1 mm

horizontal displacement. These faults are concentrated in a small area in the popup and are ~1 cm spaced. Another set of 5 cm long NNE sinistral strike-slip faults is also found having 1mm or less horizontal displacement. The other experiments do not show similar secondary structures, but the popup is deformed by a set of large NNE-SSW sinistral strike-slip faults accommodating the major sinistral displacement.

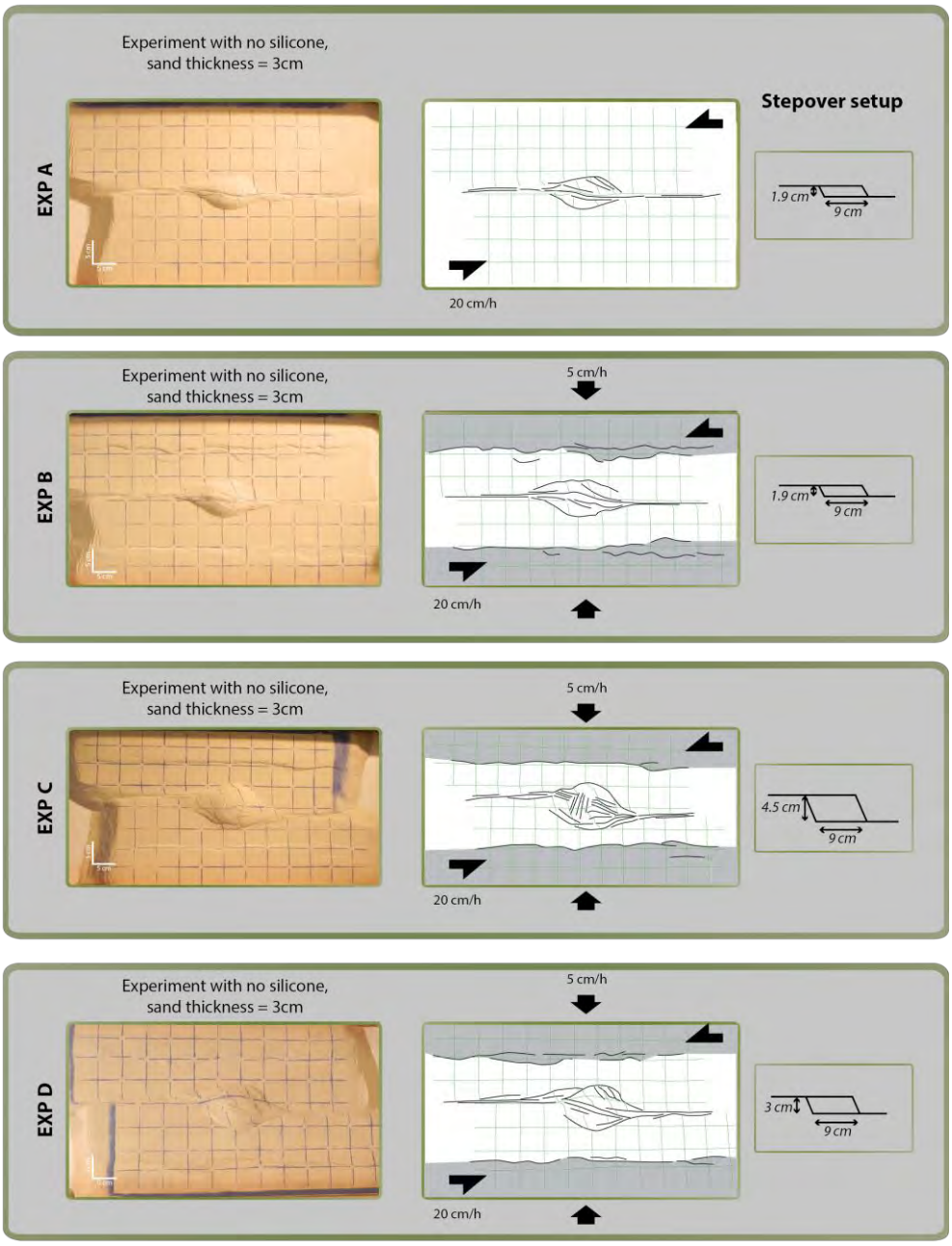

Figure 4.11 : Experiments with varying stepover bend geometry. Surface pictures of experiments A, B, C & D performed with only sand. In experiments B, C & D compression was added to the models to test its effect. Total strike-slip movement in all experiments was 9 cm while compression was 4.5 cm (2.25 cm on every side).

Experiments with silicone

Following the previous experiments with brittle materials only, a 1 cm unit of silicone was added below the sand in order to test the effect of ductile materials on deformation of strike-slip fault systems. In experiments F & I, the main difference with the models without silicone is that away from the restraining bend, overlapping en echelon R shears striking at around 17° to 20° to the trace of the basement fault are observed. These R shears are accommodating all the strike-slip displacement. In experiment K however (Figure 4.12), the silicone thickness was further reduced to 0.5 cm resulting in less pronounced en echelon R shears outside the popup and a strike-slip deformation resembling experiments made with sand only.

In experiment I, strike-slip deformation is applied simultaneously with compression. A restraining bend was observed on the surface of the model resembling the classical ones described by previous studies [*Mitra and Paul*, 2011] and also in the previous experiments. It consists of 15 cm long and 10 cm large symmetric popup (Figure 4.14a). It is bordered by two thrust faults roughly parallel to the main trace length of the basement strike-slip fault. The popup uplift amounts to 1.3 cm. Outside the popup, the strike-slip segment that are accommodated by en echelon R shears show a small uplift and folding, due to compression. Such folding is not visible in experiment F because only strike-slip deformation was applied with no compression. In experiment K, compressional deformation amounts to 2.25 cm, equalling half of the compression applied in experiment I. Smaller folding outside the popup is thus observed, with amplitudes significantly less than the ones recorded in experiment I.

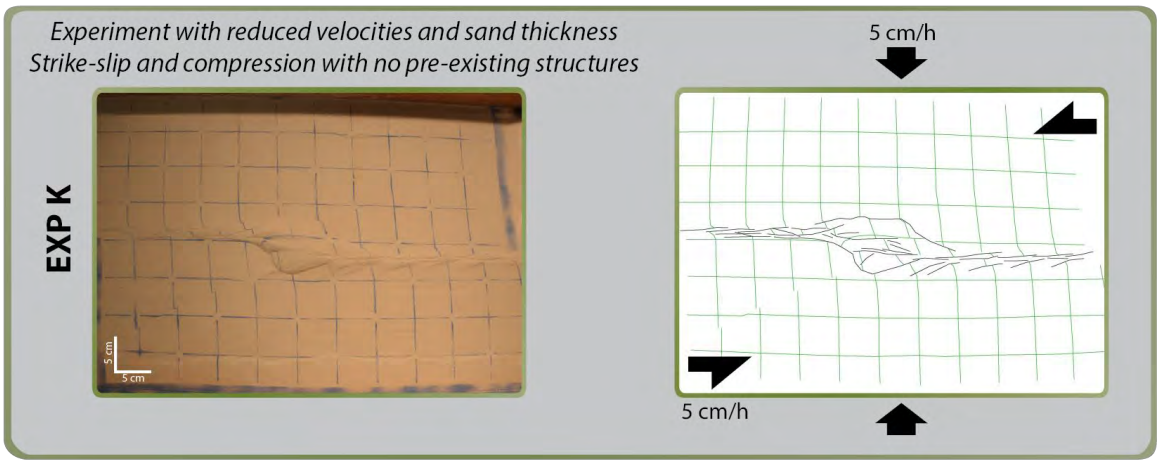

Figure 4.12 : Experiment with reduced silicone thickness. Surface picture of the experiment K undertaken with 0.5 cm thick silicone overlain by 2 cm thick sand. Results are slightly similar to experiment I with less pronounced Riedel structures. Total strike-slip movement was 9 cm while total compression was 2.25 cm (1.125 cm on every side).

Reactivation of pre-existing structures

Several experiments were designed to test the reactivation of pre-existing faults in a transpressional system. Initially, faults were created in the sand while keeping the silicone undeformed. The faults were created at different angles in order to optimise the orientation of the fault plane relative to the direction of compression. Experiments E, F & G show the results of these faults under different configurations (Figure 4.13). These configurations involved deformation of the sandbox under pure compression, pure strike-slip and strike-slip with simultaneous compression. In these three experiments, no indication of reactivation was observed at the surface of the model stating that faults were not reactivated regardless of the adopted configuration (Figure 4.13).

Discontinuities below the silicone were created in order to test their role in localising structures during transpressive deformation in experiment H. For this purpose, four square foam bars were deposited below the silicone (Figure 4.9) while the silicone surface remained flat. Deformation under a strike-slip movement of the plates coupled with compression did not result in any localised deformation above the foam bars. The results were very similar to experiment I discussed below.

As the reactivation of pre-existing structures failed in previous experiments, a new configuration consisted of creating a graben in the silicone, thus creating discontinuities in the ductile unit below the sand (Figure 4.10). Experiments I & J are compared in order to test the effect of this graben on the resulting restraining bend (Figure 4.14).

Figures 4.14 show the results of experiment J run with the oblique graben (in silicone), bordered by faults. Here, the resulting popup is asymmetric and segmented. It is composed of primarily three compartments. The middle one 15 cm long and 20 cm large while the lateral ones are 13 cm long and 10 cm wide. They are all bordered by thrust faults. Similarly to the previous experiment, en echelon R shears striking at around 17° to 20° to the trace of the basement fault are observed away from the popup. 20° to 35° counterclockwise rotation is also observed within the popup. The striking observation in this experiment is the presence of dextral strike-slip faults oriented 55° to 65° to the trace of the main basement sinistral strike-slip. These structures are aligned with the faults created in the silicone. The displacement along these faults ranges between 0.2 mm and 1 cm. Segmentation of the popup is controlled by these oblique strike-slip faults as the fault location coincides well with the different boundaries of the popup compartments.

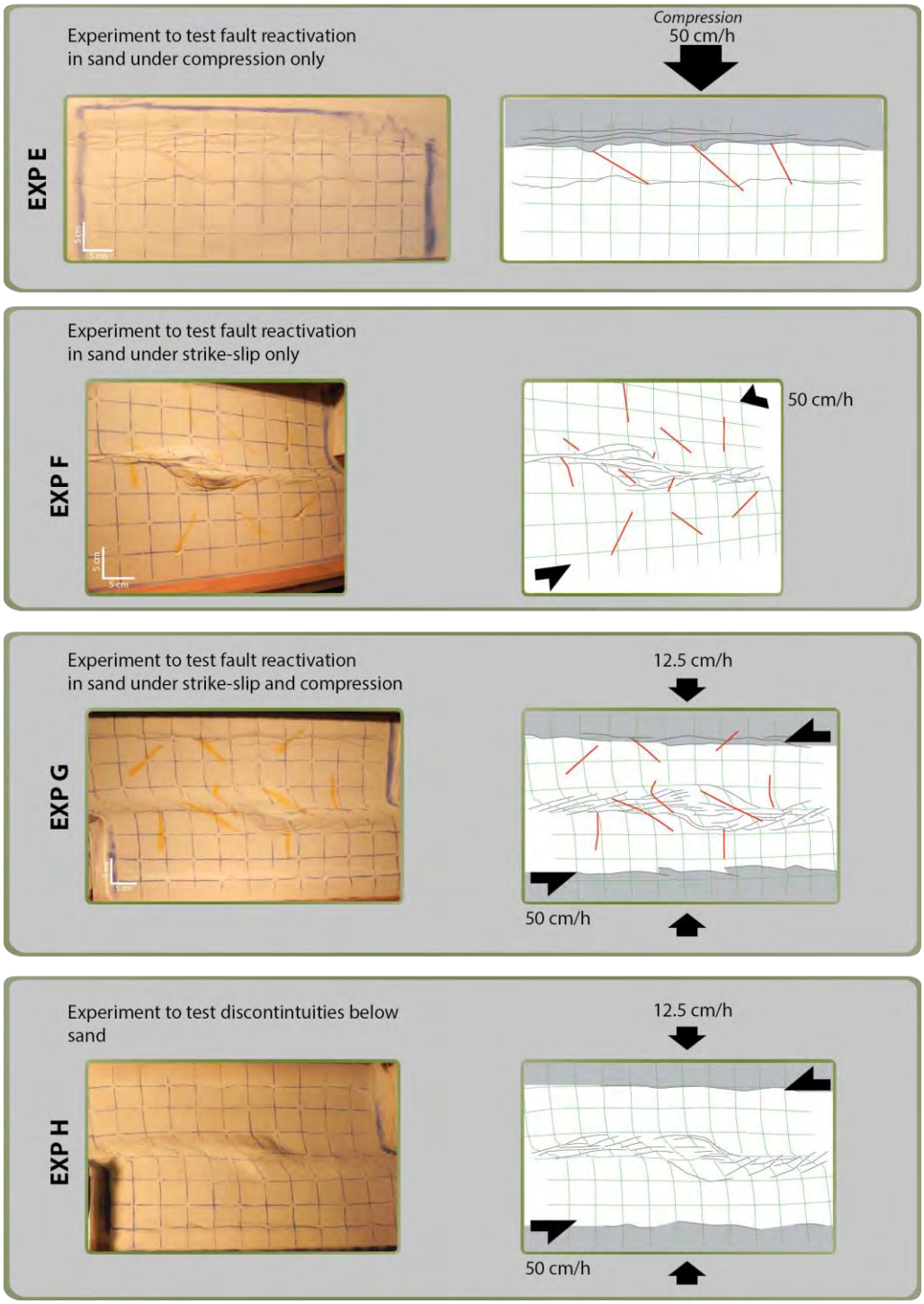

Figure 4.13: Experiments testing the reactivation of pre-existing faults in sand (E, F & G) and discontinuities below the silicone (experiment H). In these experiments, several configuration for pre-existing structures were tested (see Figure 4.9 for details). The faults were not reactivated in these configurations. Total strike-slip movement was 9 cm in experiments F, G & H, while total compression was 2.25 cm (1.125 cm on every side) in experiments G & H and 10 cm in experiment E.

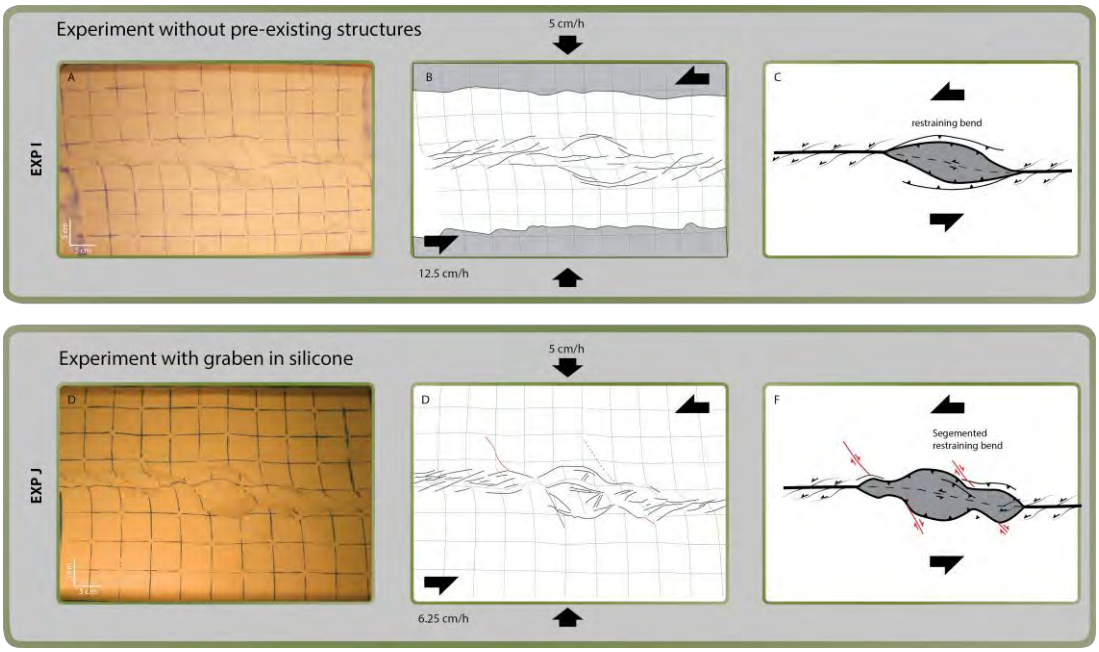

Figure 4.14 : Comparison between experiments without pre-exsiting structures (experiment I) and those with a graben in silicone (experiment J). When pre-existing structures are introduced in the silicone, the overlying sand package was cross-cut by dextral strike-slip faults parallel and aligned with the faults in the silicone. The resulting popup was also segmented into at least two compartments. In contrast, the experiment without inherited deformation results in a classical restraining bend showing symmetry in its geometry. Total strike-slip movement was 9 cm in both experiments and total compression was 4.5 cm (2.25 cm on every side) in ecperiment I and 2.25 cm (1.125 cm on every side) in experiment J.

Experiment J was scanned in order to investigate its sectional geometries. The geometry of the central restraining bend (section AA', Figure 4.15) has the shape of a classical popup structure [e.g. *Mcclay and Bonora*, 2001] with a symmetric box-shaped uplift bounded by reverse faults with moderate dips of 30°. The centre of the popup is crosscut by near-vertical faults. All faults are dying out at the silicone level and cannot be mapped all the way down to the presumed basement fault as ductile shear zones. They have a maximum vertical displacement of 5 mm.

Vertical sections of the popup reveal the changing geometry along strike. Section BB' intersects the passage of the oblique dextral strike-slip fault with the trace of the basement fault. The popup in this location is different than the one in AA' and has an asymmetric geometry. It consists of an overturned fold trending 22° from the main basement fault. It exhibit a major reverse fault rooted in the silicone with a dip of 30° and a displacement of 5 mm, and smaller antithetic reverse faults with 2 mm maximum displacement.

These two differing geometries characterise the segmented popup discussed in the previous paragraph. The central popup thus consists of a symmetric box-fold, and at the contact with the pre-existing basement faults the popup changes its structural character to appear as an asymmetric overturned fold. 19% total shortening is attested in the central popup while 23% shortening is observed in the lateral popups at the intersection with the pre-existing faults in silicone.

Section CC' (Figure 4.15) is orthogonal to the graben created in the silicone. It shows the deformation associated with the pre-existing structures implemented at the boundaries of this graben in the silicone. This section shows that the faults were not reactivated into a single vertical strike-slip fault. Instead, localised reverse faulting is observed in the sand package, with 4 mm of vertical displacement. Antithetic reverse faults are also seen in some instances, resulting in double dextral strike-slip faults in the surface (Figure 4.15). This indicates that the pre-existing normal faults have localised faults not purely dextral strike-slip at surface, but containing a significant amount of associated reverse movement. It is likely that this reverse movement is intensified at the intersection with the main basement sinistral strike-slip fault, resulting an asymmetric fold in the popup (Figure 4.15).

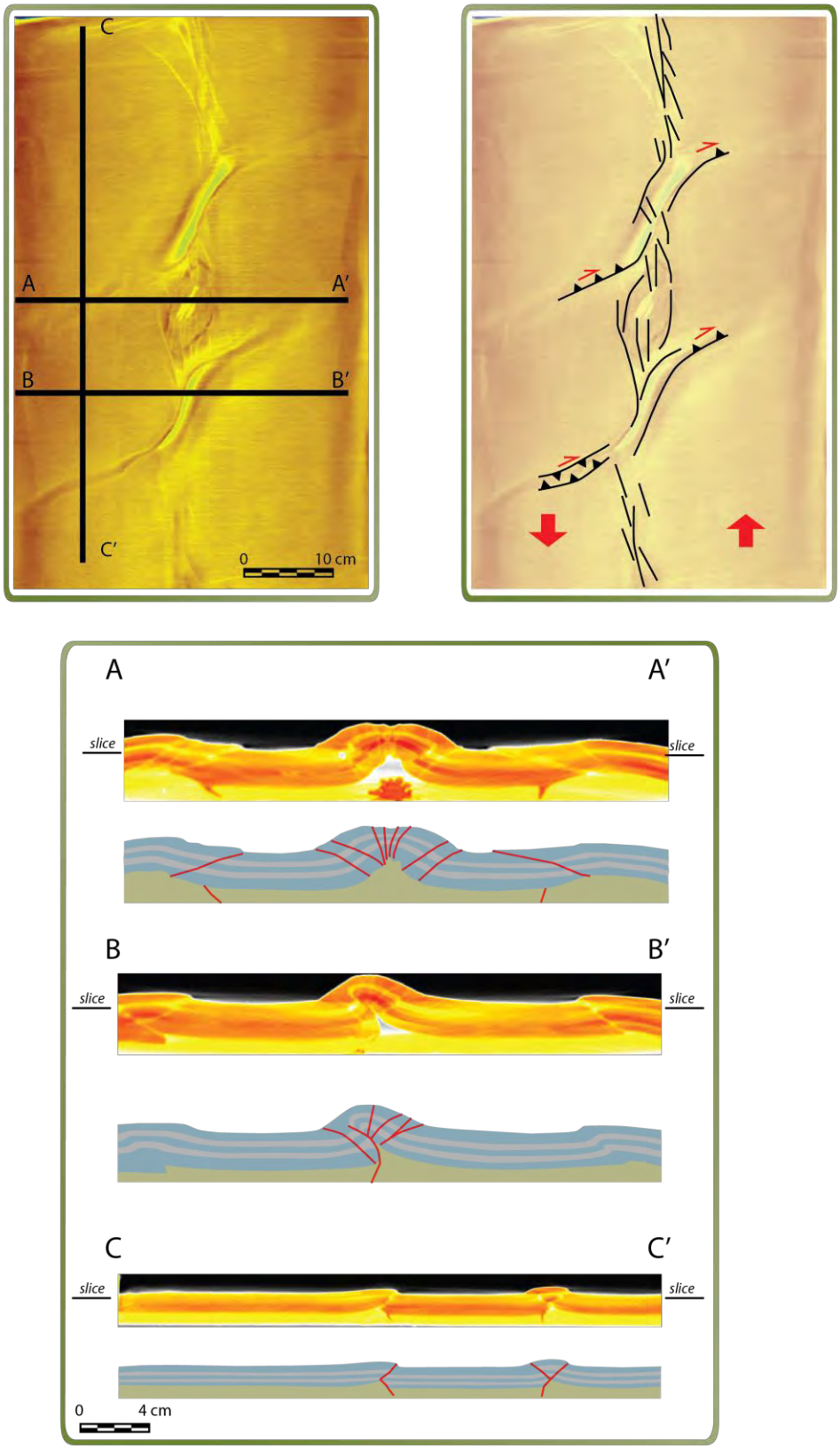

Figure 4.15 : Sections along the analogue experiment with a graben in the silicone. Section AA' is along the central popup showing a symmetric box-fold anticline, while section BB' shows an asymmetric fold at the intersection with the dextral strike-slip fault. Section CC' shows the geometry of the reactivated pre-existing faults. The topview is a horizontal slice taken near the surface of the model. The location is shown next to the sections

IV. 3.4 Discussion

The experimental results provide insights into the evolution of strike-slip systems in general and the Levant restraining bend in particular. As the model is geometrically scaled, it is hence possible to extrapolate from experimental observations to kilometre scale systems and compare the results with the natural example.

Effect of pre-existing structuration

The role and effect of pre-existing structuration on the development of strike-slip fault systems were investigated in available literature. Mattioni *et al.* [2007] examined the inversion of structures during transpression after they exerted extension to an undeformed silicone/sand model followed by oblique shortening. The resulting model showed that the orientation of existing extensional structures had affected the resulting stress field with respect to the applied simple shear component of the transpression, and hence strongly affected the geometry of a succeeding strike-slip system. In contrast to their experiment, we tested the effect of a graben in an undeformed silicone/sand model lying obliquely to the direction of simple shear, while they tested the effect of grabens in a deformed silicone/sand model lying parallel to the direction of simple shear.

Several experiments were targeted to understand the inversion of extensional fault patterns by using analogue modelling, such as reactivation of a simple listric normal fault or tilted fault blocks [e.g. *McClay*, 1989, 1996; *Mitra*, 1993; *Sassi and Colletta*, 1993; *Eisenstadt and Withjack*, 1995; *Viola et al.*, 2004]. These studies indicate how the orientation of old faults relative to the stress field strongly affects the rate and degree of reactivation. Brun and Nalpas [1996] indicate that the angle between compression and faults trend should be less than 45° in their experiments where an extensional phase was followed by compression. Moreover, fault reactivation is also controlled by the sand thickness whereas reactivation is easier if the overburden is thin [*Nalpas et al.*, 1995; *Dubois et al.*, 2002]. In our experiments, none of the faults in the brittle material were reactivated even when their orientation relative to the stress field was varied. This indicates that frictional reactivation of faults planes either necessitated a different model configuration, or something was missing in these models that might facilitate fault reactivation, such as representing the role of the mantle for example.

The experiments described in this work differ slightly from the experiments discussed in previous studies. We have placed a pre-existing graben in the silicon prior to deformation to simulate existing crustal faults as no other configuration was successful. This graben has created lateral velocity discontinuities between the sand and the silicone. The graben, which lies obliquely to the direction of simple shear, has localised deformation by having thrust faults nucleating directly above the boundaries of the graben and propagating upward as seen in section view with a dextral strike-slip component as observed at the surface of the model. Their 2 mm maximum displacement in the model amounts to 2 km in nature if scaling rules apply.

The natural example along the Levant margin contains a set of dextral strike-slip faults oriented ENE-WSW obliquely to the main transpressive jog of the LFS. They are associated with a relatively small lateral displacement amounting to ~ 2 km, as they cross-cut anticlines in northern Lebanon (Figure 4.16). In some locations, these faults are associated with thickness changes of Jurassic strata [*Collin et al.*, 2010] and Jurassic basalt is occasionally found at their fault plane [*Dubertret*, 1955]. Such observations indicate that these faults have nucleated very likely during the Jurassic and consisted primarily of normal extensional faults [*Sabbagh*, 1961; *Gedeon*, 1999]. Dextral strike-slip faults with the same trend are mapped in the Levant Basin offshore Lebanon and consist of old reactivated structures [*Ghalayini et al.*, 2014]. These offshore structures exhibit a dextral displacement of about 500 m (Figure 4.17) and are believed to be still active today. They constitute the offshore continuation of the ENE-WSW dextral strike-slip faults along the Levant margin in Lebanon.

The activity of the ENE-WSW dextral strike-slip faults in Lebanon is controlled by the motion along the LFS and the evolution of the restraining bend. These faults were reactivated during the Late Miocene at the onset of transpression in Lebanon [*Ghalayini et al.*, 2014]. They thus serve as weak planes to localise compression and to help counter-clockwise rotation of the Levant margin [*Ron et al.*, 1984; *Ghalayini et al.*, 2014] in later stages of transpression following the model of Jackson [1987]. This rotation amounts to 18° in Pliocene times and 28° in total since Late Cretaceous [*Henry et al.*, 2010]. A larger value of 20° to 30° is observed in the analogue model described in this work and in previous experiments [*Mitra and Paul*, 2011] making block rotation a primary feature of restraining bends. The amount of block rotation was observed to be in relation to the geometry of the initial stepover. In smaller stepover dimensions, rotation was measured to be around 20°, while with increasing dimensions, rotation increased to 30°.

The existing structures in the model were bounding a graben in the silicon prior to transpression. In the natural example, the graben might correspond to the Palmyra trough extending to Lebanon and responsible of establishing a pre-existing fabric. This is not surprising since the Palmyra Basin is bordering the LFS and the Palmyrides ranges are considered to extend to Lebanon encompassing the Anti-Lebanon ranges [*Searle*, 1994; *Brew*, 2001]. Thus, it is very likely that Lebanon constitutes the western margin of the Palmyra Basin, given that the modelled graben in the analogue experiment yielded results very similar to observations along the Levant restraining bend upon its deformation and inversion.

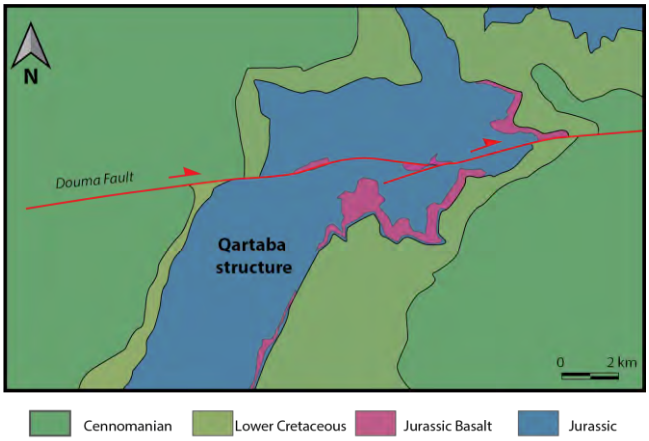

Figure 4.16 : Simplified geologic map showing the passage of the Douma fault, a ENE-WSW dextral strike slip fault, displacing the Qartaba structure 1-2 km to the east. Modified from 1/50000 map of Qartaba.

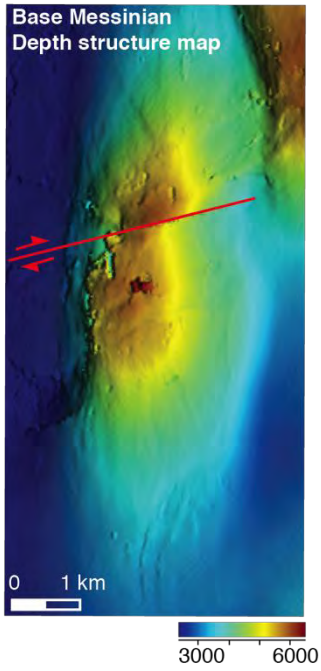

Figure 4.17 : Base Messinian depth structure map of NNE trending anticline in the Levant Basin offshore Lebanon. Its anticlinal axis is displaced by one dextral strike-slip fault for about 500 m. Modified from Ghalayini *et al.* (2014).

Growth of restraining bends

Pre-existing structures

The analogue models described were not aimed to describe the evolution of restraining bends in general. However, some observations can be drawn from these experiments regarding the growth of segmented restraining bends caused by oblique structuration.

The presence of pre-existing structures in the analogue model has affected the final geometry of the restraining bend. The latter was compartmentalised at the intersection between the main sinistral strike-slip fault and the reactivated dextral strike-slip faults having a reverse component in section view. The different compartments in the restraining bend exhibited different structural styles, consisting of a symmetric box-fold anticline in the central popup and asymmetric folds in the outwards compartments. The asymmetric folds are the result of the applied horizontal shear on the oblique reverse faults, causing the development of large thrusts. The horizontal shear has rotated these faults as soon as oblique shortening initiated, and the faults exhibited a strong vertical movement along the intersection with the sinistral basement fault (Figure 4.18).

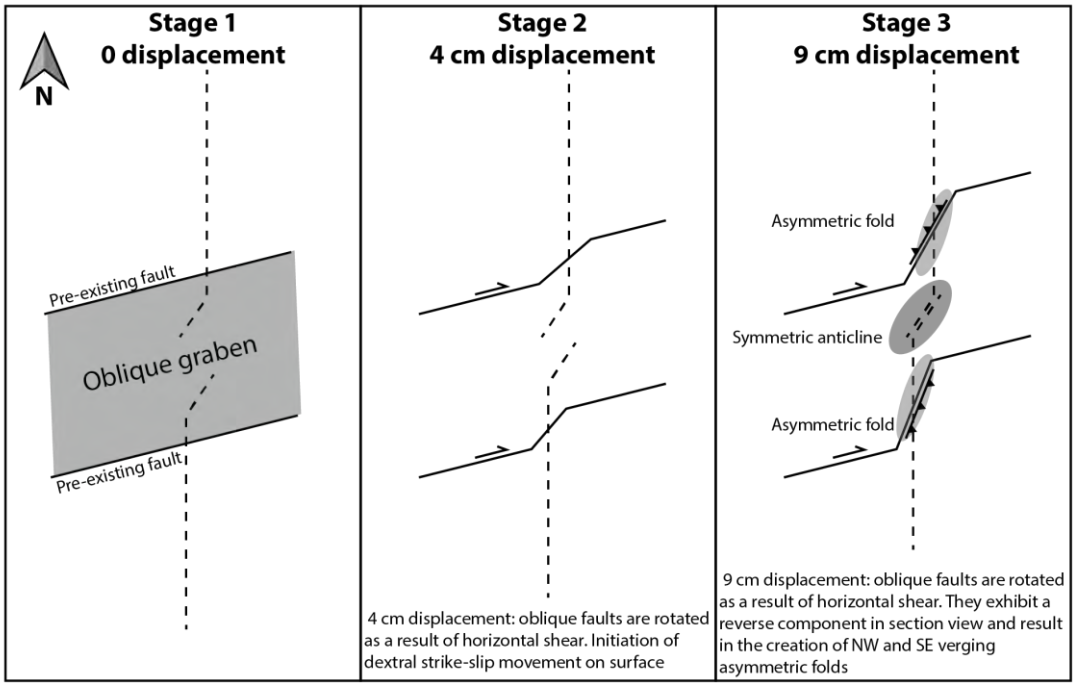

Figure 4.18 : Sketch showing the evolution of the restraining bend. The reactivation and rotation of the pre-existing oblique structures created asymmetric folds. The initial deformation consisted of sinistral strike-slip movement along the master N-S basement fault, followed by initiation of activity along the ENE-WSE striking pre-existing structures at almost halfway through the experiment

In the natural example, the Levant restraining bend has been long considered as complex with significant structural variations along strike. Northern Mount Lebanon consists of a broad and symmetric box-fold anticline (Figures 4.19 and 4.20) while southern Mount Lebanon is topographically lower and the deformation zone includes several shorter wavelength folds including a tight overfold termed the Niha-Barouk anticline (Figure 4.21) [*Dubertret*, 1955; *Walley*, 1998]. Mount Lebanon is thus divided into two compartments separated by narrow zones of ENE-WSW trending nearly vertical dextral strike-slip faults [*Hancock and Atiya*, 1979].

The different structural styles of Mount Lebanon were rarely explained in literature. Walley [1998] does not propose a mechanical model to explain the variability of styles along the Lebanese restraining bend but instead makes an analogy between the different compartments along Mount Lebanon with the southern and northern Palmyrides. He attributes the structural styles along the Levant restraining bend to be an extension of the Palmyrides fold belt into Lebanon, making northern Mount Lebanon part of the northern Palmyrides, while southern Mount Lebanon part of the southern Palmyrides. A corollary of this assumption is that the deformation pattern in northern and southern Mount Lebanon will be the same as the northern and southern Palmyrides respectively [e.g. *Searle*, 1994; *Brew*, 2001; *Brew et al.*, 2003]. The difference in structural styles along the Palmyrides fold belt has been attributed to strong along-strike structural variations. The SW Palmyrides is a series of narrow, en echelon, asymmetric folds with a SE vergence, cored by reverse faults with Cretaceous outcrops at their crest [*Ponikarov*, 1966; *Chaimov et al.*, 1992]. In contrast, in the NE Palmyrides Searle [1994] mapped complex folding often in the form of box folds above an Upper Triassic detachment. This had induced a total shortening decreasing from around 20 km in the SW Palmyrides to almost zero in the far northeast [*Chaimov et al.*, 1990].

In addition to the hypothesis that the deformation along Mount Lebanon is likely related to the deformation along the Palmyrides, we propose that the compartmentalisation, or segmentation of the Levant restraining bend with variable structural styles in northern and southern Mount Lebanon is also attributed to the reactivation of oblique inherited faults. It is thus likely that the origin of such ENE-WSW faults was due to a Mesozoic trough below modern day Levant margin, causing crustal heterogeneity. Moving southward from Lebanon to Israel and Sinai, the crust gradually thickens [*Segev et al.*, 2011]. Similarly, the crust thins from the Palmyra Basin in the East to the Levant Basin in the west. Thus, the Levant margin in Lebanon constitutes a crustal transition zone separating the northern margin of Neotethys from its southern margin in modern day Israel, and the western margin of the Palmyra basin

from the Levant Basin. The difference with the models performed in this work is that there is no gradual variation of ductile material thickness in these models since the modelled trough, or graben, was considered to be uniform in its dimension.

Evolution and ongoing activity

Plate movement along restraining bends is usually accommodated by all the structures in the transpressive system whereby oblique plate motion within the restraining bend is partitioned into strike-slip displacements and perpendicular convergence in a process referred to as strain partitioning [*Gomez et al.*, 2007b]. This partitioning marks an important aspect of restraining bends in general. In the analogue experiment described in this study, the different structures making the restraining bend were each accommodating a small amount of the plate movement. When summed, their movement amounted to the total slip imposed on the plates (i.e. 9 cm).

Hatem et al. (2015) argue that within a restraining bend, evolving mechanical efficiency controls the activity and the slip rate along faults based on claybox models. Such observations were not recorded in the sandbox models, described during this project, whereby all structures evolved with time and accumulated displacement with increased transpression. This indicates that the structures were active throughout the entire experiment and evolved through time.

In the natural example, the variable displacement over time recorded along the LFS in general and the Levant restraining bend in particular can be explained in terms of regional geodynamics controlling the intermittent activity of structures. The folding of anticlines and reactivation of faults in the Levant Basin were affected by subtle regional variation of plate motion which directly controlled the deformation rate along the LFS [*Ghalayini et al.*, 2014]. It is probably this regional aspect that resulted in the variability of slip and shortening along the different structures of the Levant restraining bend throughout its history, and which resulted today in structures that are active while others are believed inactive. The efficiency of restraining bends does not only comes from their aspect ratios and bends angles [*Hatem et al.*, 2015] but also from the orientation of the structures relative to the evolving regional stress field, which affects the activity of structures [*Wiprut and Zoback*, 2002; *Bonini et al.*, 2012]. In the experimental models, the stress fields are static and not dynamic, as they are uniform through time. This does not allow to test whether some structures are inactive due to

evolving stress fields or not. Instead, we postulate that all structures were active since their inception.

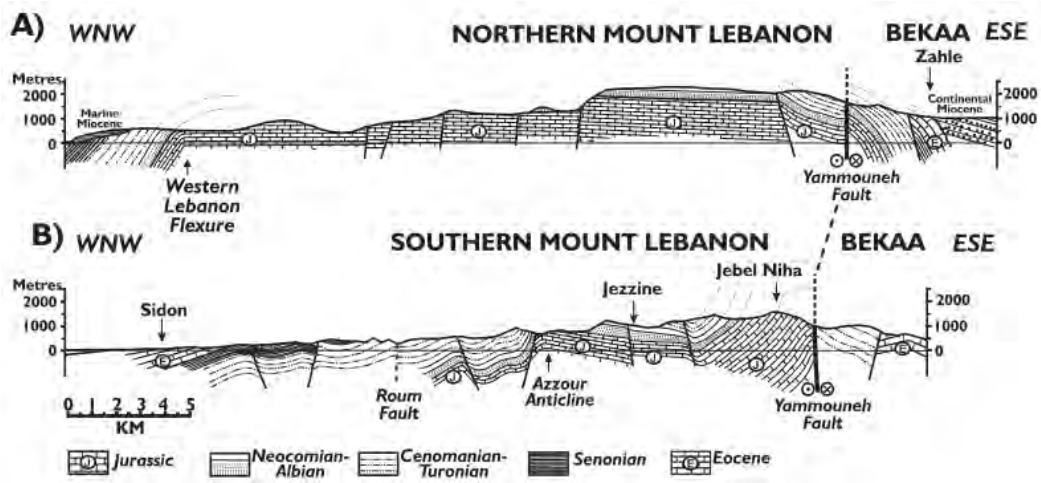

Figure 4.19 : Structural cross-sections across (A) northern and (B) southern Mount Lebanon showing differing structural style, namely box folding in the north. From Waley [1998].

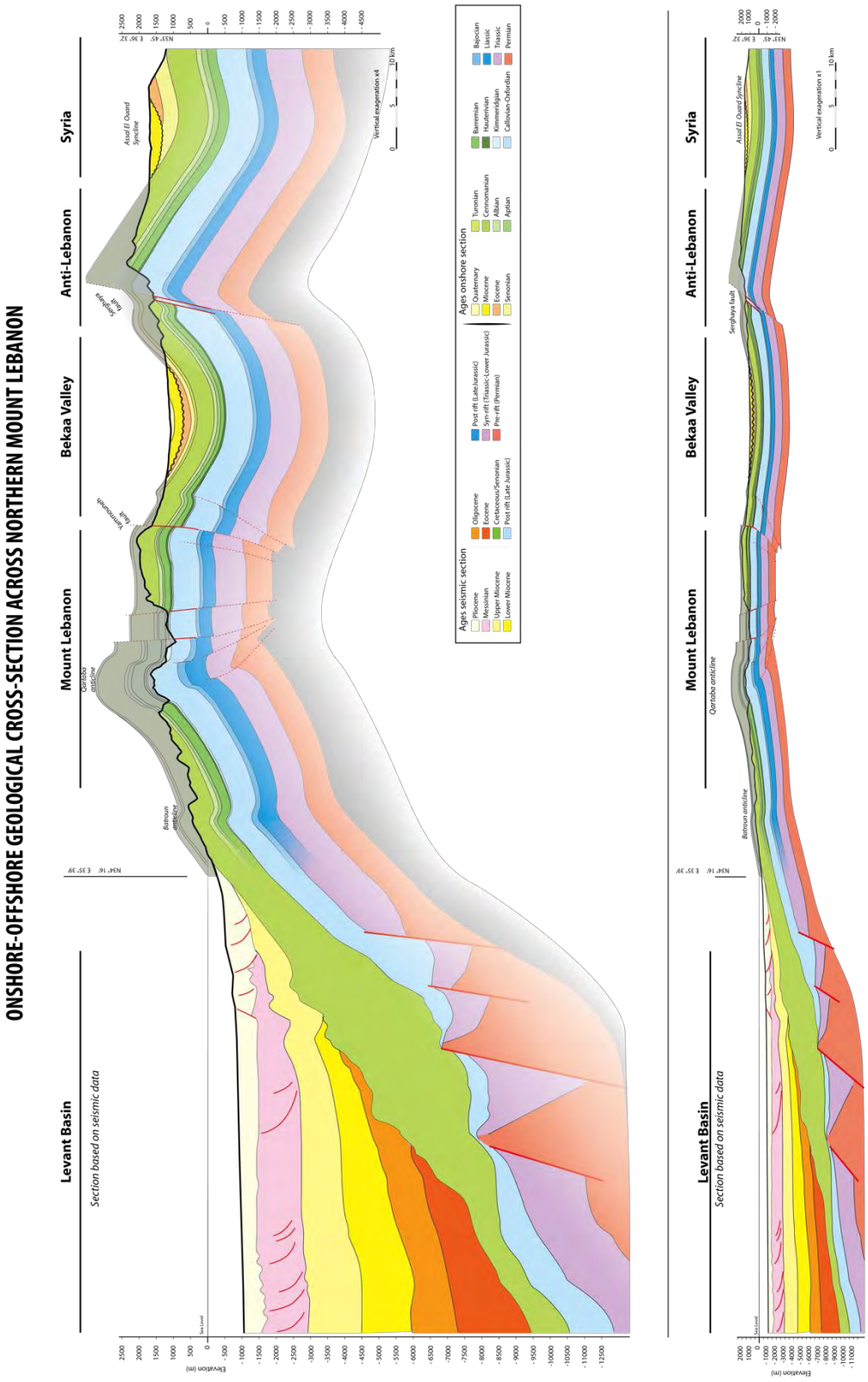

Figure 4.20: Cross section along the northern Mount Lebanon showing the box-fold symmetric geometry of the anticline. The offshore continuation of the section is interpreted from the 3D seismic data offshore Lebanon. Unit thicknesses are taken from published literature. Units are shaded with depth to highlight uncertainty. Modified from Sabbagh [1962]. For location see figure 4.6.

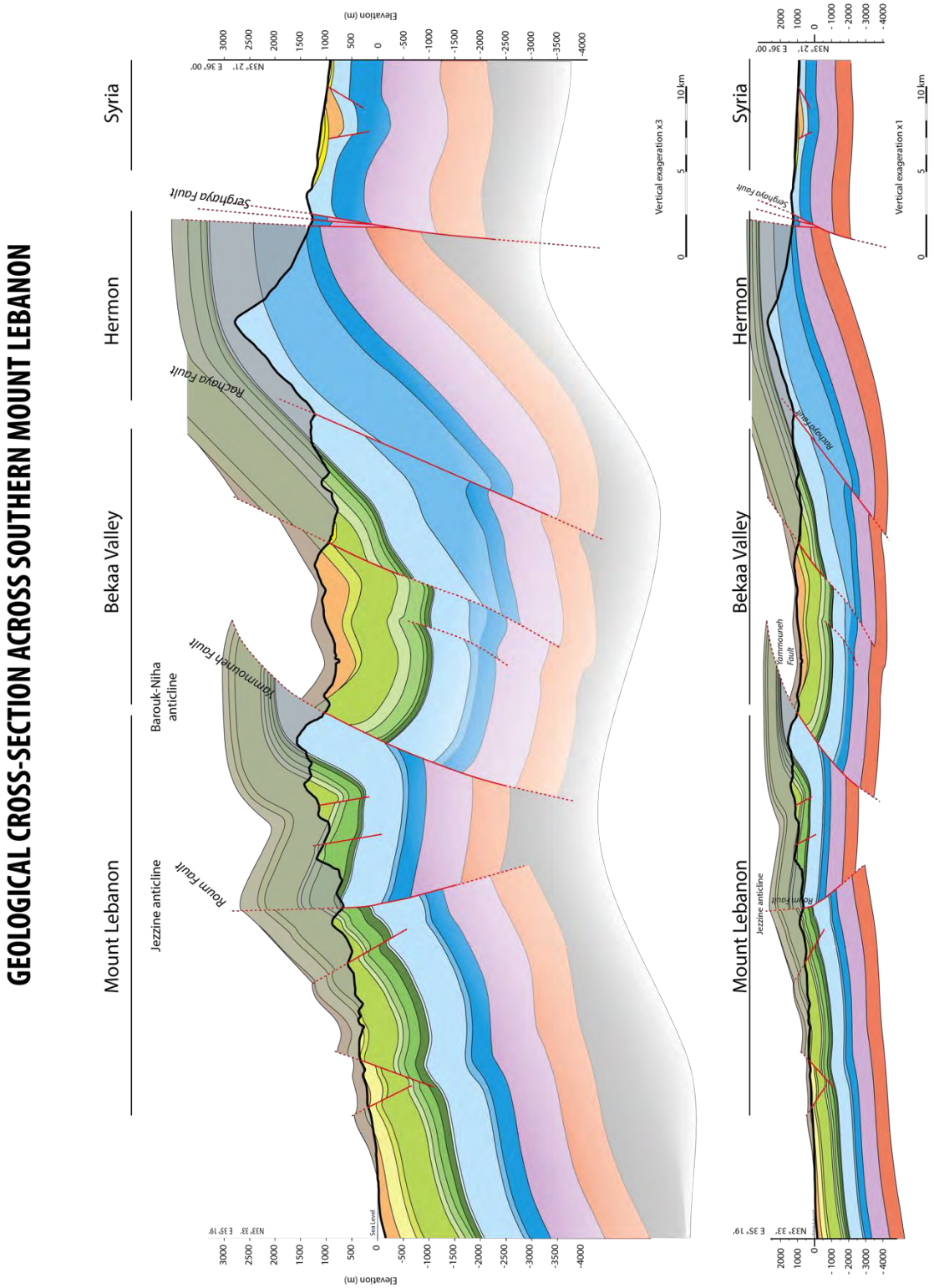

Figure 4.21 : Cross section along the southern Mount Lebanon showing the asymmetric geometry of the Barouk-Niha anticline. Unit thicknesses are taken from published literature. Units are shaded with depth to highlight uncertainty. Modified from Sabbagh [1962]. For location see figure. 4.6.

IV. 3.5 Conclusion

The Levant margin in Lebanon contains a structurally complex restraining bend with variable along-strike structural style. The Northern Mount Lebanon is characterised by a broad box fold anticline while the Southern Mount Lebanon is topographically lower with tight folds. The restraining bend is crosscut by a series of ENE-WSW dextral strike-slip faults extending toward the basin. These faults are believed to be inherited from the Mesozoic rifting event and reactivated due to transpression along the LFS.

Analogue modelling of the Levant margin has provided insights into the evolution and growth of the Levant restraining bend in Lebanon and confirmed the hypothesis that the inherited ENE-WSW faults were reactivated due to transpression. In the experimental setup, a graben was deposited in the silicone whereby the thickness of the silicone was reduced to the half. This graben was also bordered by two normal faults to simulate pre-existing structures. This experiment was compared with another experiment whereby no graben and no pre-existing structures were deposited in the silicone. Results show pre-existing normal faults were reactivated into dextral strike-slip faults at the surface while having a strong reverse component in section view. When these faults intersected the popup, they strongly affected its final geometry and made it segmented into different compartments with a different structural style each. One compartment exhibited symmetrical box folding while the second exhibited an asymmetric overturned fold

The Levant margin in Lebanon is thus very much affected by the pre-existing oblique structural fabric which has affected the final geometry of the restraining bend. It is very likely that the along-strike structural style variation of Mount Lebanon is caused by the presence of pre-existing normal faults. Similarly, the counter-clockwise block-rotation in Lebanon might be facilitated by these ENE-WSW dextral strike-slip faults, even though rotations can happen without the need of such faults. Further experiments are needed to understand the double restraining bend in Lebanon and by taking into account the anti-Lebanon ranges.

The faults bordering this graben were not truly reactivated as the silicone was not free to move laterally at its base. This is caused by a strong velocity discontinuity between the silicone and the wooden base of the model. A solution.

CHAPTER V

THE NORMAL FAULT ARRAY OF THE LEVANT BASIN

Table of contents

V. The normal fault array of the Levant Basin

"Let yourself be silently drawn by the strange pull of what you really love. It will not lead you astray" Rumi

In chapter 3, an extensive normal fault array was documented and mapped in the Levant Basin. Its nature, timing and implication are not clear and necessitate an investigation. Generally, the growth and evolution of normal faults is still not perfectly understood and several points are yet to be clarified. Particularly, the growth of faults at basin scale and the effect of mechanical stratigraphy are still under debate and several models exist to explain these concepts. The normal fault array of the Levant Basin, imaged by high quality seismic data, is a very good case study to explain the growth of normal faults. In order to proceed with the description of the this array in the Levant Basin, a literature review of the latest research efforts on fault nucleation, fault propagation, growth models and mechanical stratigraphy are summarised below. This review also includes a description of the techniques widely used in normal fault interpretation such as displacement analysis that we applied in order to understand the normal faults in the Levant Basin. It is followed by an article in review, whereby the growth of these faults is investigated and compared with published studies in other basins. The geometry and interaction of the Levant Basin faults provide great details to understand their nature and evolution, and answer some pending questions on normal faults in general.

V. 1 Literature review of normal fault systems

V. 1.1 Definition of a fault

Disturbances in layered rock sequences produce faults or "defects" to the primary stratigraphic framework. Faults are thin zones accommodating discontinuous displacement by offset of stratigrahic markers. They form what is referred to as "fault

zone" [*Mcgrath and Davison*, 1995] consisting of a multitude of structures, such as smaller syntethic and antithetic faults, fractures and joints. In fault zones, displacement is usually partitioned between the fault segments [*Walsh and Watterson*, 1989; *Peacock and Sanderson*, 1991; *Dawers and Anders*, 1995; *Walsh et al.*, 2003], and complex geometries related to interaction and linkage are created.

Simplistic representation of faults usually portray them as single lines of even thickness. However, faults rarely consist of simple surfaces in detail but are considered as complex structures containing a number of structural elements that may be hard to predict (Figure 5.1). These are the fault core (or slip surface), fault damage zone (the surrounding volume of brittely deformed wallrock) and fault rock (the rocks found in the fault core and are hence differentiated from the rocks in the damage zone that is wider).

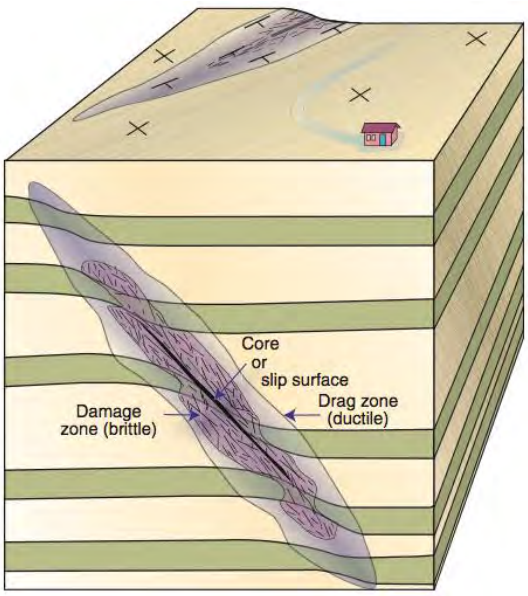

Figure 5.1: Simplified anatomy of a fault. From Fossen [2010]

V. 1.2 Mechanics of faulting

The style and type of faulting in the crust is directly induced by a given stress state. Stress magnitudes depend on depth, pore pressure and active geologic processes that act at a variety of different spatial and temporal scales. The simplest, and yet the powerful explanation of *in situ* stresses is described by [*Anderson*, 2012], and referred to

herein as the Anderson stress scheme. This scheme leads naturally to some general constraints on stress magnitudes as a function of depth and pore pressure.

In simplest terms, stress is defined as force acting over a given surface. In general, to fully describe the state of stress at depth, knowledge of the stress is requested to describe forces acting on all surfaces passing through a given point. The stress tensor is defined by three stress magnitudes characterised by a specific orientation with respect to a reference coordinate system, the principal coordinate system. These are referred to in terms of magnitudes of the greatest, intermediate and least principal stress at depth (σ1, σ2 and σ3 respectively) and in terms of S_v, S_{Hmax} and S_{Hmin} (Figure 5.2). For what concerns this manuscript, the Anderson scheme classifies an area as being characterised by normal faulting when $S_v > S_{Hmax} > S_{hmin}$ (Figure 5.2).

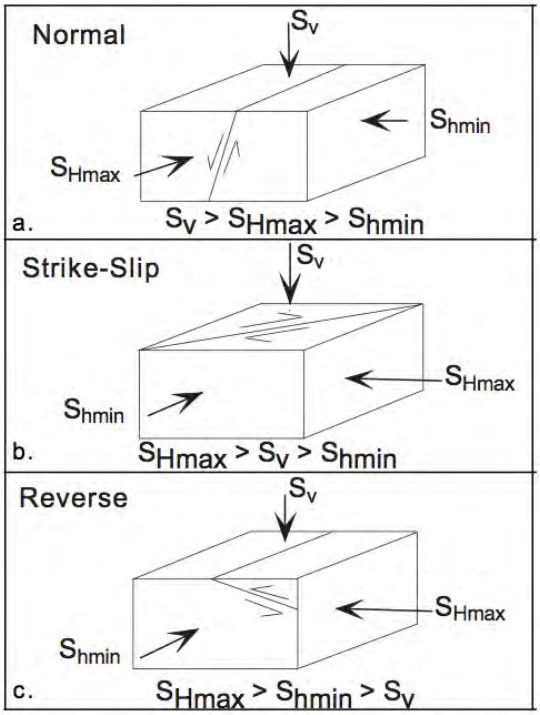

Figure 5.2 : The three orientations of stress magnitudes leading to the creation of three fault types: normal, strike-slip and reverse according to the Anderson scheme. From Zoback [2010]

The failure of rocks under different confining pressures is represented by the empirical Mohr-Coulomb failure envelope (Figure 5.3). Allowable stress states are those that do not intersect the Mohr-Coulomb failure envelope. When a rock is faulted, it is referred to as "failure" and the stress state intersects the failure envelope (Figure 5.3).

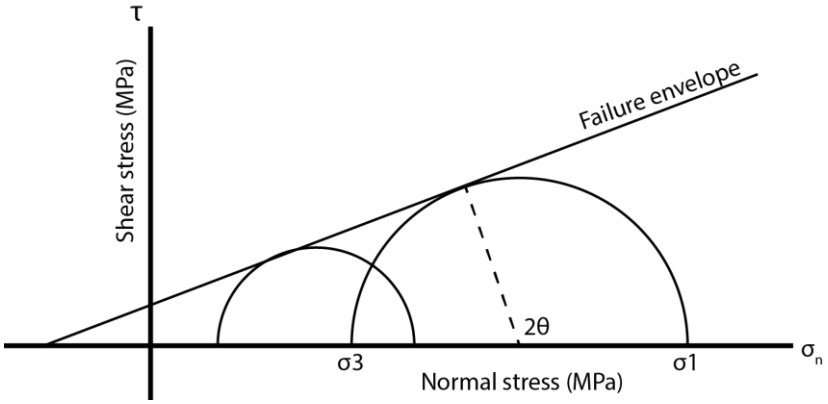

Figure 5.3 : A linear simplification of the Mohr failure envelope (or Mohr-Coulomb failure). The maximum stress σ1 is plotted toward the right (since it is the largest by definition), while the least stress σ3 is plotted always to the left. The failure of rocks happens when the semi-circle of differential stress σ1-σ3 touches the failure envelope. The last one is defined by the coefficient of internal friction together with the rock cohesion. A fault is thus created with an angle θ. See figure 4.1 for more details.

V. 1.3 Fault displacement

The temporal and spatial evolution of normal fault systems in 3D seismic reflection data is typically studied using displacement mapping (or displacement profiles) [e.g. *Rippon*, 1984; *Barnett et al.*, 1987; *Childs et al.*, 1995; *Walsh et al.*, 2002, 2003; *Baudon and Cartwright*, 2008a, 2008b, 2008c; *Jackson and Rotevatn*, 2013; *Tvedt et al.*, 2013]. To fully constrain the growth history of a normal fault system, these techniques require that sedimentation rates are high relative to fault slip rate (i.e. balanced or overfilled basin conditions).

Displacement profiles represent the distribution of displacement along the fault plane. Such profiles, sometimes referred to as "strike projections", are constructed by projecting displacement values at points on a fault surface onto a surface parallel to the fault strike and later on contoured [*Rippon*, 1984; *Barnett et al.*, 1987; *Walsh and Watterson*, 1991] (Figure 5.4).

In the ideal case, displacement decreases from a maximum located at the centre of the fault plane to a tip line of zero displacement (Figure 5.4). In the absence of significant mechanical heterogeneity and if displacement accrued over the entire fault plane at each slip event, the tip line is elliptical. Ideal faults grow by radial propagation with no migration of the point of maximum displacement, which is also the nucleation site of the fault [*Watterson*, 1986; *Barnett et al.*, 1987]. Such faults are usually identified

as “blind” which is a post-sedimentary fault that does not interact with the free surface at any time during evolution [*Watterson*, 1986; *Baudon and Cartwright*, 2008a].

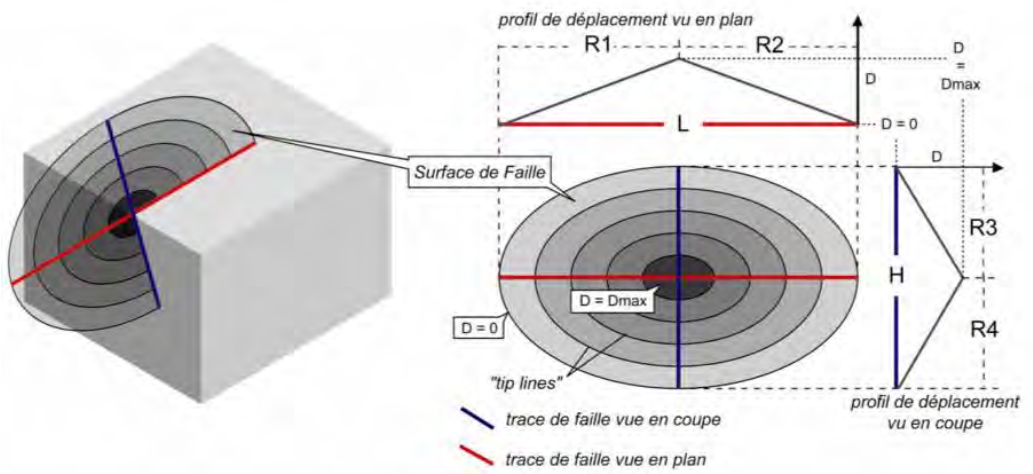

Figure 5.4 : The displacement profile of an ideal normal fault with the Dmax located at the center of the fault. The displacement profile is projected on the fault surface and contoured. The different terminologies used in normal faults interpretation, such as the length L, height H and radius R are listed. From Roche [2011].

Displacement contours projected on fault surfaces can be analysed by constructing D/L or D/H profiles (Figures 5.4 and 5.5), where the displacement variation is visualised relative to the length or to the height of the fault respectively. These are characterised by their general form which could be “C-shape” or “M-shape” [*Muraoka and Kamata*, 1983]. C-shape is characterised by a nearly symmetrical shape with a gentle change of displacement (Figures 5.4, 5.5a and b) while M-shape consists of a broad central section with no significant change of slope and flanking portions with an abrupt change of displacement shown by the steep slopes of the graphs (Figure 5.5 c and d). The Dmax/L ratio of M-type faults is approximately twice that of C-type [*Muraoka and Kamata*, 1983].

C-type faults are considered to be a characteristic of homogeneous units [*Muraoka and Kamata*, 1983]. M-type faults are those which cut through a rigid unit or a competent layer and they display a flat central section to the curve. Their steep slopes in the flanking sections indicate that the faulting of a rigid unit usually terminates in a strain absorber, an incompetent unit or that the fault interacts with another fault or barriers to its propagation.

Simple blind normal faults, in the absence of barriers and strong interaction with other faults are expected to exhibit a linear lateral displacement profiles or C-shape [*Muraoka and Kamata*, 1983; *Peacock and Sanderson*, 1991; *Nicol et al.*, 1996], though a hybrid and M-type patterns can also exist [e.g. *Baudon and Cartwright*, 2008a; *Jackson and Rotevatn*, 2013].

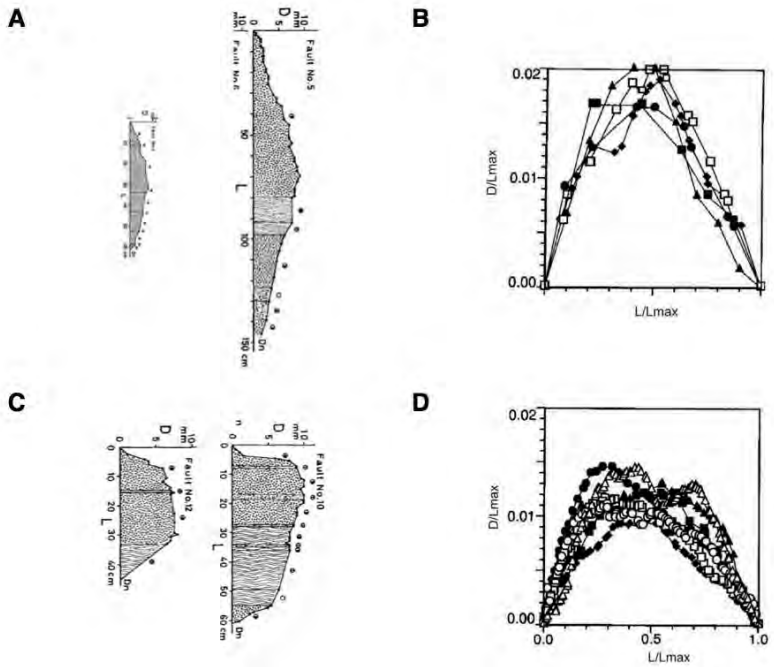

Figure 5.5 Displacement profiles along normal faults showing the typical C-shape distribution in A-C and M-shape distribution in C-D. A and C are from Muraoka and Kamata [1983] while C and D is from Dawers and Anders [1995].

Apart of the Dmax and the general shape that characterise the displacement profiles, the displacement gradients are extremely important to understand the evolution of the fault. These are usually measured at the tip of the profiles or along a specific length of the fault. It expresses the ability of the fault to propagate, laterally or vertically, by looking at displacement accumulation [*Walsh and Watterson*, 1989; *Cowie and Shipton*, 1998; *Ferrill and Morris*, 2001; *Soliva et al.*, 2006]. High tip-gradients near the upper tips in displacement/depth profiles may indicate syn-sedimentary activity because the faults have reached the free surface and are unable to propagate [*Nicol et al.*, 1996; *Childs et al.*, 2003; *Baudon and Cartwright*, 2008b; *Tvedt et al.*, 2013]. The displacement hence accumulates without propagation, which explains the high displacement gradients near the tips. Similar observation can be made in displacement/length profiles showing high lateral tip gradients, indicating lateral

barriers to fault propagation. Those could consist of other nearby faults causing interaction among fault surfaces [*Peacock and Sanderson*, 1991; *Walsh et al.*, 2002].

An important aspect documented by [*Walsh and Watterson*, 1987] from their observations of faulting in sedimentary rocks, is that a proportion of the total stratigraphic offset across a fault may be accommodated by drag folding of the adjacent strata. This phenomenon might affect the absolute value of slip across a fault surface.

V. 1.4 General aspects of fault growth

As noted in paragraph I.I.II, when the increased stress over a rock volume attains critical values, failure of rocks is produced instantaneously and a fault is formed. Once a fault nucleates, it will grow in 3D as long as the stress field is suitable. An important characteristic of a fault, which distinguishes it from fractures, is that it shows intrinsic displacement along its fault plane.

Faults growth is generally attributed to the superposition of many earthquake slip events on a fault surface [*Cowie and Scholz*, 1992b] (Figure 5.6), creating a relationship between the slip scale and the fault-rupture length [*Scholz*, 1982; *Wells and Coppersmith*, 1994]. Hence, the maximum displacement on a fault (Dmax) should be directly related to the length of the fault (L) following the expression:

$$D = c \cdot L^n \qquad 5.1)$$

where c is constant and n between 1 and 1.5 [*Walsh and Watterson*, 1988; *Cowie and Scholz*, 1992a; *Schlische et al.*, 1996]. The representation of Dmax and L for a large number of faults in different localities would indicate a relationship between the displacement and the length of a fault.

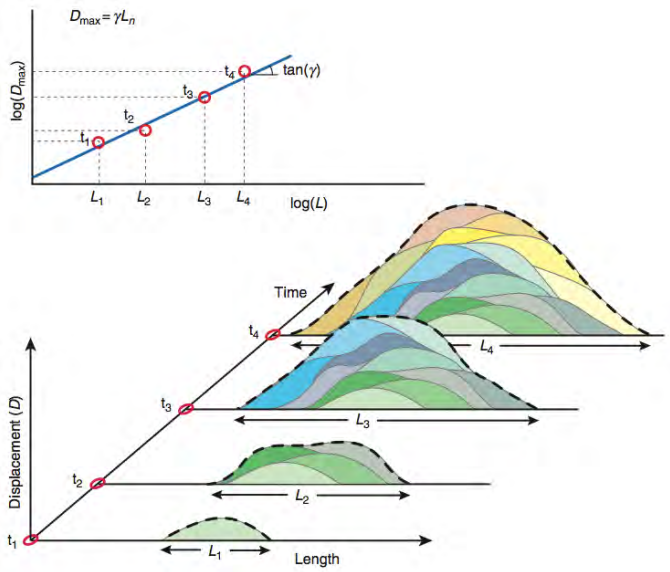

Figure 5.6 **:** Schematic illustration of displacement accumulation by repeated earthquake events. Each event results in up to a few meters of vertical displacement. The end result would be a bell-shaped cumulative displacement of the whole fault. This model produces a straight line in a logarithmic D-L diagram. γ represents the slope of the line in the logarithmic plot and is thus equal to c in equation 1. From Fossen [2010].

This indicates that faults grow by lateral and vertical propagation from a central nucleation point, which is the point of maximum displacement. The faults, growing radially and having an elliptical fault shape, will thus have their length increase when displacement accrues [*Walsh and Watterson*, 1988; *Cowie and Scholz*, 1992a] (Figures 5.7 and 5.8).

However, in many instances, two or more displacement maxima are found on a fault plane. It has been argued that faults growing essentially in isolation are in general only slightly elliptical, with axial ratios of approximately 2 [*Walsh and Watterson*, 1989]. Therefore, a fault formed by coalescence of precursor segments, by linkage, with only moderate ellipticities could be expected to exhibit an arrangement of anomalies that define the segment boundaries by combinations of oblique, sub-vertical and sub-horizontal zones of throw minima (Figure 5.9). Dip-linkage sites might also be expected to arrest or impede slip, such that the continued partitioning of slip between relict fault segments after linkage will accentuate the displacement minima at linkage points, producing irregular displacement distributions. Consequently, whilst seismic data may be unable to resolve the structure, the mechanical influence of these structures on the local accommodation of slip will leave a strong signature in the displacement field,

which can be imaged by detailed mapping of the fault displacement distribution [*Mansfield and Cartwright*, 1996].

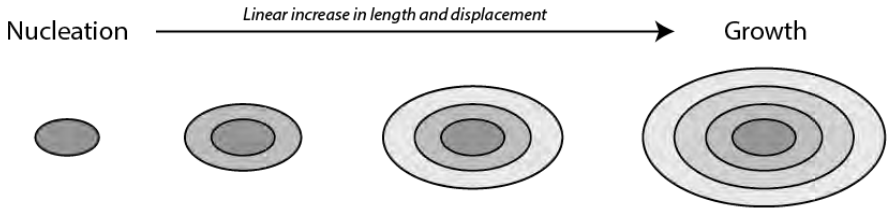

Figure 5.7 : Fault growth through time has a linear relationship between length and displacement. As displacement accrues, faults propagate laterally and vertically.

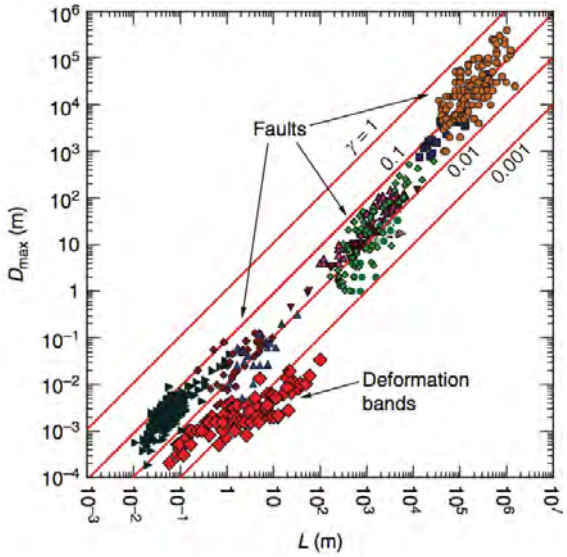

Figure 5.8 : Displacement-length diagram for faults showing the linear relationship between the maximum displacement (Dmax) and the length (L) of a fault. The data was gathered from several fault systems in different localities. γ represents the slope of the red line in the logarithmic plot and is thus equal to c in equation 1. From Schultz and Fossen [2002] and Fossen [2010].

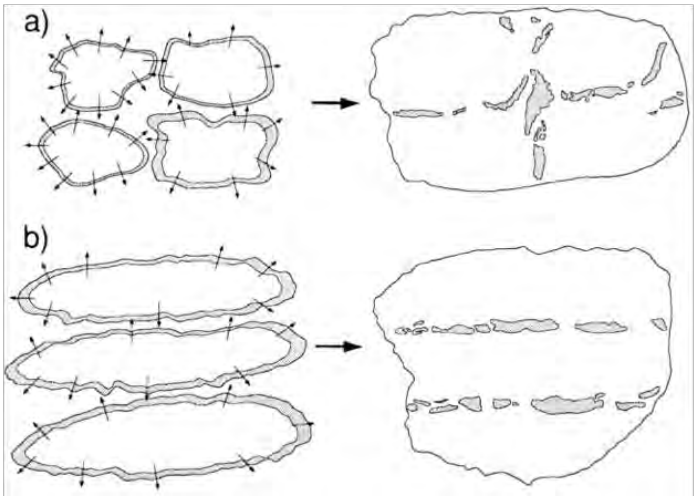

Figure 5.9 : Illustration showing the contrasting patterns of displacement minima expected from linkage between faults with different axial ratios. Initially isolated faults are normally expected to be only slightly elliptical (a) and linkage should therefore produce patterns of displacement minima at the relict segment boundaries that reflect this. However, the identification of predominantly sub-horizontal displacement anomalies (b) implies that the linking faults are highly elliptical, with large axial ratios sub-parallel to fault strike.

Vertical mechanical anisotropies caused by lithological changes will affect the growth and vertical propagation of faults. This will result in a staircase growth as seen in Dmax/L plots [*Cartwright et al.*, 1995; *Schultz and Fossen*, 2002; *Roche*, 2011] (Figure 5.10). It is suggested that when geological restrictors halt fault propagation, the vertical fault growth will be prohibited and the faults propagate horizontally while interacting and joining with nearby structures through segment linkage without accumulating much displacement. Thus, faults will be characterised by nonproportional growth with increasing fault surface until the fault breaks through bedding cutting up and/or down sction to increase displacement [*Cartwright et al.*, 1995; *Roche et al.*, 2012b].

Fault growth is separated in general into two groups: the isolated fault model and the coherent fault model. These two models are discussed below.

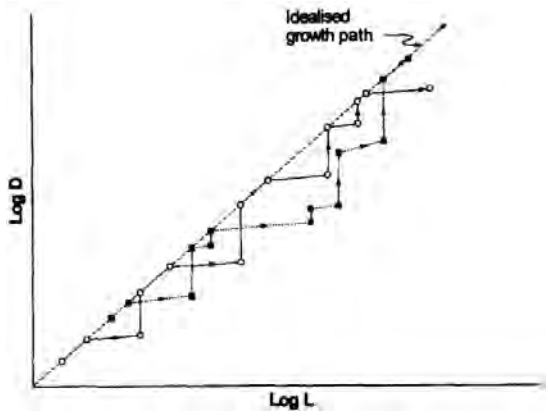

Figure 5.10 : Hypothetical pathway of fault displacement on a log/log plot of displacement vs. length of two faults growing by segment linkage. When faults reach a geological restrictor, they stop propagating vertically, interact and link with nearby segments laterally. The linkage will result that the fault will acquire displacement and become underdisplaced for its new length, exhibiting the staircase geometry seen in log/log plots. From Cartwright *et al.* [1995].

Isolated fault model

Fault growing radially from a central displacement maxima, follow the "isolated fault model" [*Walsh et al.*, 2003] whereby single faults will interact at a later stage with other nearby faults and join as they grow. In reality, the growth of "non isolated" faults, or faults network, is complicated due to the interaction between fault segments. Faults are unlikely to grow as individual structures over long periods of time. As they grow, they are likely to interact with nearby faults. In this way, two faults can join to form a single and much longer fault. This is also referred to as "fault growth by segment linkage" [*Cartwright et al.*, 1995; *Mansfield and Cartwright*, 2001] whereby the original isolated faults join to become a larger master fault.

In fact, segmented fault arrays containing two or more fault segments (Figure 5.11) are a common feature of faults on all scales [*Walsh and Watterson*, 1989, 1991; *Peacock and Sanderson*, 1994; *Cartwright et al.*, 1995; *Dawers and Anders*, 1995]. Segmented arrays may show aggregate displacement variations that are similar to those of a single isolated fault (Figure 5.12) [e.g. *Walsh and Watterson*, 1989; *Peacock and Sanderson*, 1991; *Dawers and Anders*, 1995] suggesting that they are elements of a single coherent structure. Their growth is marked by early-stage nucleation and propagation of kinematically independent segments, followed by incidental overlap, interaction and the formation of fault relay zones (Figure 5.11) [e.g. *Cartwright et al.*, 1995; *Dawers and Anders*, 1995].

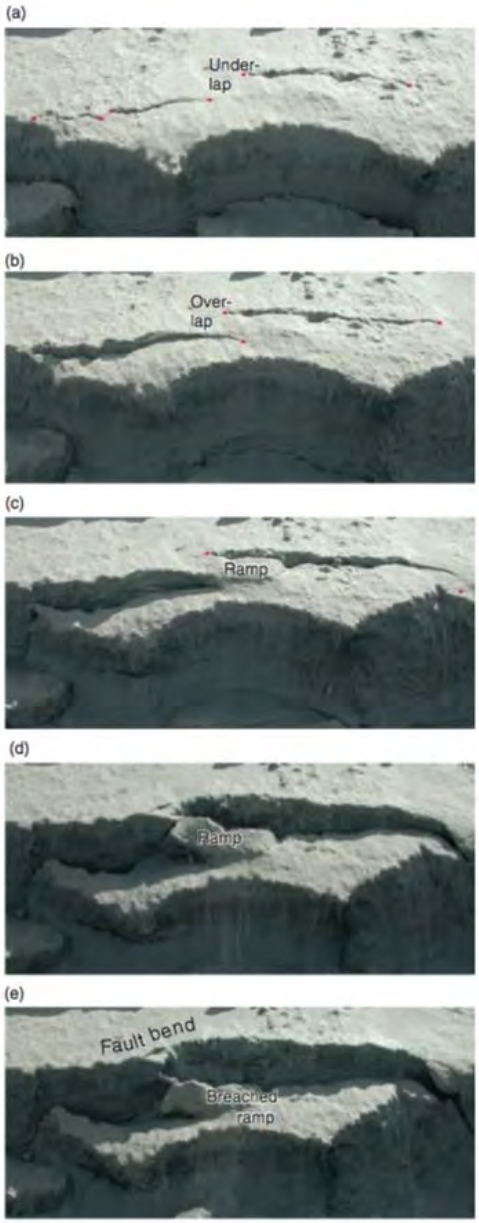

Figure 5.11 : The development of curved fault systems in unconsolidated sand. Two isolated fractures (a) overlap (b and c) to form a relay ramp that eventually becomes breached (d and e). Faults were initiated by splashing water on the beach sand of Colorado Lake. The width of sand in each picture is c. 50-60m. From Fossen [2010].

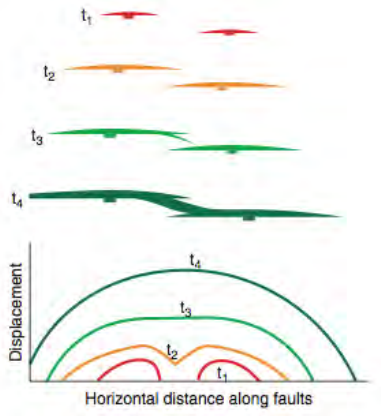

Figure 5.12 : illustration of the change in displacement along two faults that overlap and coalesce. The upper part shows the two segments in map view at four different stages of growth (t1-t4). The lower part shows the displacement profile at four different stages. From Fossen [2010].

Coherent fault model

In reality, individual data sets showing the linear relationship between Dmax and L have a large scatter, making their interpretation less conclusive (for review see Cowie and Scholz 1992a; Kim and Sanderson 2005). Thus, it is suggested that no linear relationship exists between Dmax and L [*Walsh et al.*, 2002]. This is at odds with the belief that fault-growth trends define lines of constant displacement to length ratios. Hence, an alternative model for the growth of faults is suggested, in which fault lengths are established rapidly at the beginning and faults grow principally by increases in displacement with minimal fault propagation [*Walsh et al.*, 2002]. This model is referred to as the "coherent fault model" whereby growth of fault surfaces that in map-view appear isolated, but in three dimensions are, from their inception, components of a single, geometrically- and kinematically-coherent structure [*Childs et al.*, 1995; *Walsh et al.*, 2002, 2003; *Schöpfer et al.*, 2007].

In this model, fault segmentation may occur by fault surface bifurcation, i.e. splaying, resulting in fault segments that are hard-linked to a single fault out of the plane of inspection (Figure 5.13c). Alternatively, fault segmentation may occur by stepping during propagation or localisation of an individual fault, giving rise to fault segments, which are, at least initially, unconnected in three dimensions (Figure 5.13d). Relay zone formation in the coherent fault model is not incidental but is a product of bifurcation or 3-D segmentation processes.

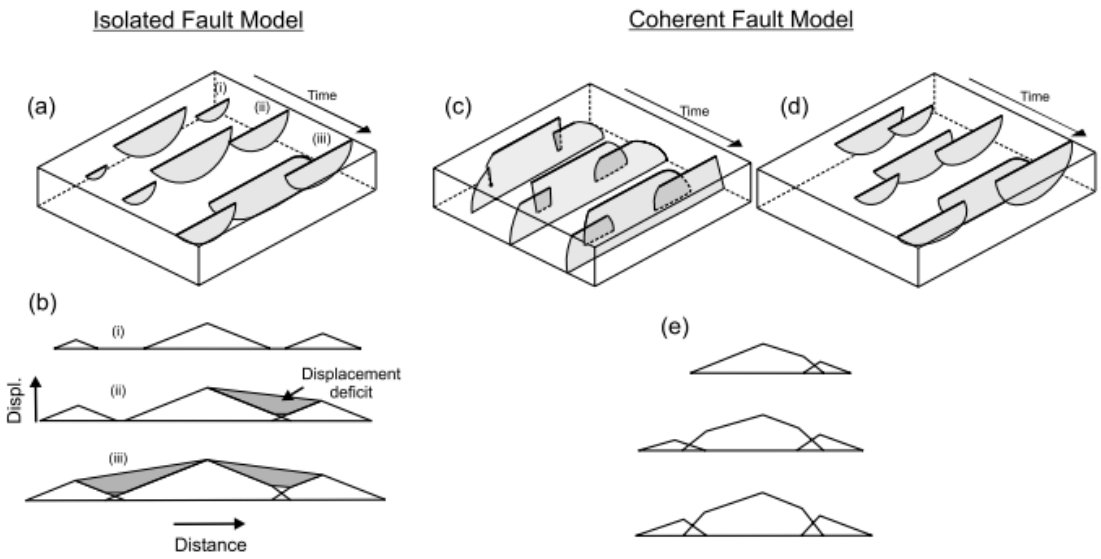

Figure 5.13 : Schematic illustrations of the two end-member models of formation of segmented fault arrays. The block diagrams (a, c and d) each show three stages in the growth of a segmented fault array (i–iii). The displacement-distance plots (b and e) are for the fault traces on the upper surfaces of the block diagrams (bold lines). The bold dashed lines in (c) indicate branch-lines. The coherent fault model is illustrated for segmented fault traces that are (c) hard-linked and formed by fault surface bifurcation and (d) soft-linked and formed by 3-D segmentation. The shaded areas in (b) indicate deficits in displacement between the adjacent fault segments, which are not due to continuous deformation within relay zones (see text). The aggregate displacement profiles (not shown) for the two models differ in that the points of maximum displacement are preserved where the faults were initially isolated (b–iii) but a simple aggregate profile occurs at all stages of development in the coherent fault model. From Walsh *et al.* [2003].

A crucial requirement of this model is that a wide range of fault lengths is established at an early stage of deformation. One means of departing from conventional models involving initial sizes that are small and cover a narrow size range would be to reactivate pre-existing faults (Figure 5.14). Size distributions of later faults could be the same as those of the underlying established fault system. It is unclear whether this alternative model is applicable to the growth, or some stages in the growth, of faults systems that are not reactivated.

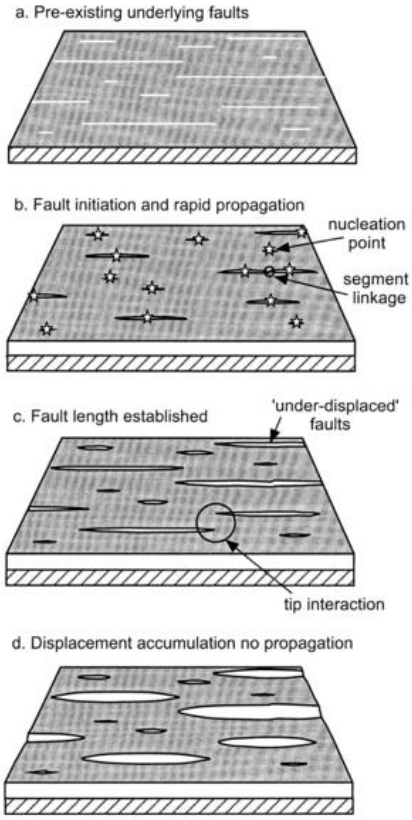

Figure 5.14: Schematic block diagram illustrating the coherent fault growth model. Pre-existing faults (a) play an important role in localising deformation, whereby faulting initiates on the horizon above the pre-existing fault system with nucleation close to the centre of each fault. In the early stages, fault length increase rapidly while displacements accrue relatively slowly. From Walsh *et al.* [2002]

Most studies have either explicitly or implicitly supported the isolated fault model, although some studies [*Walsh et al.*, 2002, 2003] have argued that the growth scheme outlined by the coherent fault model may be the dominant mode of normal fault growth in many extensional settings. There are, however, very few studies [*Jackson and Rotevatn*, 2013] that have examined the geometric and kinematic evolution of normal fault systems with these alternative models in mind. Analogue modelling testing the applicability of these models show that faults will primarily reach their length early on and accumulate displacement at a later stage, thus confirming the coherent fault model [*Schlagenhauf et al.*, 2008]. The widespread endorsement of the isolated fault model derives largely from the 2-D nature of most fault data.

In summary, the isolated fault model has achieved a certain degree of acceptance that might not be always proved by observation [*Walsh et al.*, 2003]. The coherent fault is a likely interpretation of the displacement distributions of most segmented fault

arrays. However, there are still uncertainties on how normal faults grow, their initial size distributions and what is the extent of interaction between faults during their growth.

V. 1.5 Faults in multilayer systems

Having discussed the lateral evolution of normal faults, being either through the isolated or through the coherent model, their vertical evolution also follows different models. A forward, or continuous, propagation model is proposed and consists of faults propagating vertically from their nucleation point while affecting successively layered units without connections of initially vertically isolated segments [*Schöpfer et al.*, 2006; *Roche et al.*, 2012a, 2012b]. Thus, no vertical relay zones are observed in faults nucleating following this model, even though small refraction of the fault plane can be noted and discussed in following paragraphs.

In contrast, faults nucleating in a multilayer system can grow by vertical segmentation and relays of initially isolated segments. In multilayer systems, i.e. in superposed units of variable lithologies, faults show different architectures and geometries, as discussed below. A particular example is the case of confined faults, or faults restricted to one sedimentary unit only. This phenomenon, mainly dependant on variable mechanical properties of host rocks, is observable in many areas around the globe, and represents the extreme case of faulting in strong boundary conditions.

Boundary conditions thus arise from the mechanical strength of rock units, which is controlled by the lithology forming these units. This is referred to as mechanical stratigraphy. In the following paragraphs, the effect of mechanical stratigraphy on nucleation and propagation of normal faults will be discussed.

The relationship between nature of host rocks and faults

The nature of the sedimentary units and the host rock lithology have great impacts on faults, in both outcrop and basin scales. On the outcrop scale, lithological changes can lead to particular geometries as stated earlier. On the basin scale, however, studies were targeted to mainly investigate how a particular type of faulting is affected by specific sedimentary facies. Such faults are referred to as “polygonal faults” discussed in detail below.

Mechanical stratigraphy

As stated earlier, lithological contrasts among rock units result is what is commonly referred to as "mechanical stratigraphy". Mechanical stratigraphy is defined as discontinuities between superposed rock units or layers of contrasting lithologies, with each having a different mechanical property. Such discontinuities can represent barriers to vertical fault propagation producing vertically restricted normal fault surfaces [*Nicol et al.*, 1996; *Wilkins and Gross*, 2002] as stated previously. A mechanical unit does not necessarily correspond to a lithologic unit because: (1) several lithologic units may deform as a single mechanical unit, (2) a single lithologic unit may be comprised of several mechanical units, (3) mechanical units may be defined by structural contacts rather than lithologic contacts and (4) mechanical units may be defined at different scales within the outcrop [*Wilkins and Gross*, 2002].

The importance of mechanical stratigraphy, and the development of segmented fault systems, are emphasised in different studies discussing lithological boundaries acting as barriers to fault propagation [*Rippon*, 1984; *Childs et al.*, 1996; *Nicol et al.*, 1996; *Wilkins and Gross*, 2002; *Ferrill and Morris*, 2003, 2008; *Soliva et al.*, 2006; *Schöpfer et al.*, 2007]. These studies however, are based on outcrop observations, and limited studies have targeted the mechanical stratigraphy from seismic data on a basin scale.

Forced nucleation

Faults are found in rock units, having not necessarily a uniform lithology. Hence, a large number of faults in strata with variable lithologies are observed worldwide. Their fault tip geometries, preferred localisation of fault segments and geometric dimensions suggest that lithologies might control the nucleation and propagation of fault systems. This phenomenon can be explained by the Mohr-Coulomb fracture envelope discussed earlier. In this sense, lithological units can sustain different shear stresses and hence the failure envelope is different for contrasting lithologies.

Discrete Element Models [*Schöpfer et al.*, 2007] indicate that, during the initial stages of fault growth in mechanically-layered sequences, Mode I fracturing and then normal faulting (Mode II failure) typically occur in 'strong' layers, whereas 'weak' layers deform by ductile flow (see also Peacock and Zhang [1993]; Childs *et al.* [1996]; Ferrill and Morris [2003]). During this stage, fractures and faults forming at shallower structural depths are offset into the proto-footwall of underlying structures. Increasing

strain results in growth of faults in strong layers, failure of intervening weak layers, and eventual linkage of faults to form a through-going fault. Because fault dip is relatively gentle in 'weak' layers and relatively steep in 'strong' layers, the through-going fault may have a 'staircase' geometry, characterised by refraction of the fault plane at strong-weak lithological contacts [*Schöpfer et al.*, 2007] (Figure 5.15).

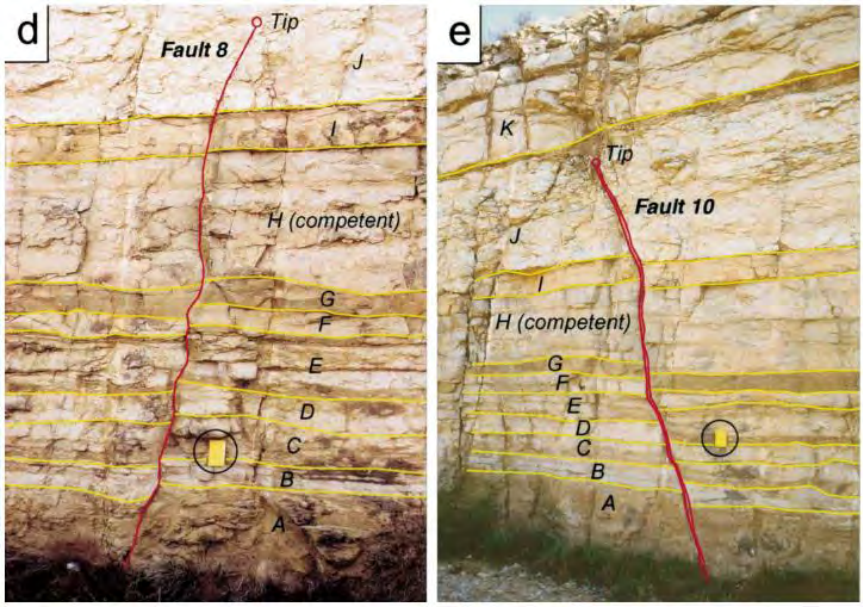

Figure 5.15: Photographs showing normal faults cutting limestone layers in the Buda Limestone, along I-10 East near Balmorhea, Texas. d) Northeast-dipping fault (8) has 7 cm displacement near the base of the exposure, and loses displacement upward to a tip in layer J. (e) Southwest-dipping fault (10) has 15 cm displacement near the base of the exposure, and loses displacement upward to a tip in layer J. Note the fault dip changes in the competent units becoming steeper. From [*Ferrill and Morris*, 2003].

The variation in fault dip, or the "staircase geometry" is the result of variations in the mechanical strength of rock layers coupled with the co-existence of different failure in relation with variation of the mean stress [*Ferrill and Morris*, 2003] (Figure 5.16). These conditions can cause different layers to fail in different modes, hence generating markedly different fracture orientations from bed to bed. Beds exhibiting steeper fault dips are more competent under the conditions during faulting than those with shallower fault dips (Figure 5.16).

Two broad possibilities exist with respect to relative timing of failure in a mechanical multilayer. Failure may nucleate first in either the stronger [e.g. *Peacock and Zhang*, 1993] or weaker layers [*Wilkins and Gross*, 2002] depending on the strength and

relative proportions of the mechanical layers and the effective stresses (especially differential stress) experienced by the mechanical layers. The parametric numerical modelling of Roche *et al.* [2013] showed that both situations may occur because the change in the σ3 magnitude and the strength properties of rocks have opposite effect, so that the net effect depends on the lithology and thickness of the layers. To this respect, the contrast in the Young modulus and the strength of each unit are fundamental parameters and account well for the situation observed over the range of sedimentary rocks.

In the normal faulting regime, maximum principal compressive stress (σ_1) is vertical [*Anderson*, 2012]. The vertical effective stress increases downward primarily as a function of depth. Therefore σ_1 in both strong and weak layers at a point on a mechanical layer interface would be essentially the same. Horizontal σ_3 magnitude may fluctuate with depth, as a function of the ability of different mechanical layers to support the differential stress. These changes in σ_3 imply that the maximum differential stress differs from one layer to another. It has a higher value in the stiff layers than in the compliant layers. Similarly, the Coulomb failure criterion increases in the stiff layers and decreases in the compliant layers. The fault will therefore likely nucleate preferentially in the stiff layer (Figure 5.16a). Roche *et al.* [2013] argue that if the stiffness is constant in all the blocks and the strength properties vary throughout the layering, then the faulting is inhibited in the more cohesive layers (Figure 5.16b) or is promoted in the low internal friction layer (Figure 5.16 c). Thus, nucleation on faults in multilayer systems depends on the characteristics of the system and the values of differential stress in competent and incompetent rocks [*Ferrill and Morris*, 2003; *Roche et al.*, 2013].

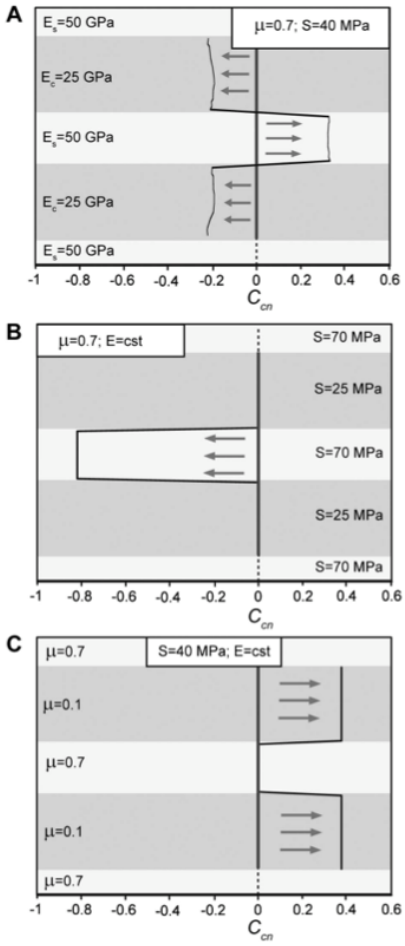

Figure 5.16: Figures showing the effect of contrast between the stiffness and the strength properties in multilayers plotted on normalised Coulomb failure criterion (Ccn). The mechanical layers are indicated in light gray and gray. Figures 4b and 4c show the Ccn variation in layered system with a constant Young's modulus (E) and either variable cohesion (a) and constant internal friction or variable internal friction and constant cohesion (c). From Roche *et al.* [2013].

Propagation and refraction

When a fault propagates through a rock volume it rarely does so as a single planar surface but as an irregular and, to a greater or lesser extent, segmented array of faults. Segmentation is due to local retardation or acceleration of propagation of the fault tip-line, controlled by the heterogeneous nature of the rock volume [e.g. *Jackson*, 1987]; heterogeneities occur on a range of scales, from grain-scale to crustal scale.

Heterogeneities in a multilayer system cause variation in the mechanical properties of the rock units, or layers, as stated in the previous paragraph. A consequence of failure occurring under different conditions in the two mechanical layers is that the failure angle in each layer is different. Specifically, the failure angle in the stronger layer is smaller than that in the weaker layer, which produces steep fault

segments in the stronger layer and more gentle fault dips in the weaker layer [*Ferrill and Morris*, 2003] (Figure 5.15). This phenomenon is called "refraction" of the fault trajectory [*Peacock and Sanderson*, 1992; *Ferrill and Morris*, 2003, 2008; *Schöpfer et al.*, 2007] as the fracture propagates through the rock mass. The direction of propagation (from strong layers to weak layers, or from weak layers to strong layers; vertically or horizontally) does not affect these failure angles. In general, the optimal (that requiring least energy to generate) fracture trajectory will be shorter in stronger layers than in weaker layers, and that explains why competent units have steeper fault dips [*Ferrill and Morris*, 2003; *Schöpfer et al.*, 2007]. Faults propagating in several units of the same lithology will have a similar dip in these units [*Roche*, 2011]. Table 5.1 shows that specific fault gradients are found depending on the lithology of the unit.

Table 5.1: *Summary of fault gradients in multilayer systems. The value of gradients corresponds to the mean average value of gradients of faults cross-cutting a multilayer system, taken in every lithology. Competent units are limestone, except for some where the competent units are sand* [*Muraoka and Kamata*, 1983; *Wilkins and Gross*, 2002; *Soliva and Benedicto*, 2004]. *From* [*Roche*, 2011].

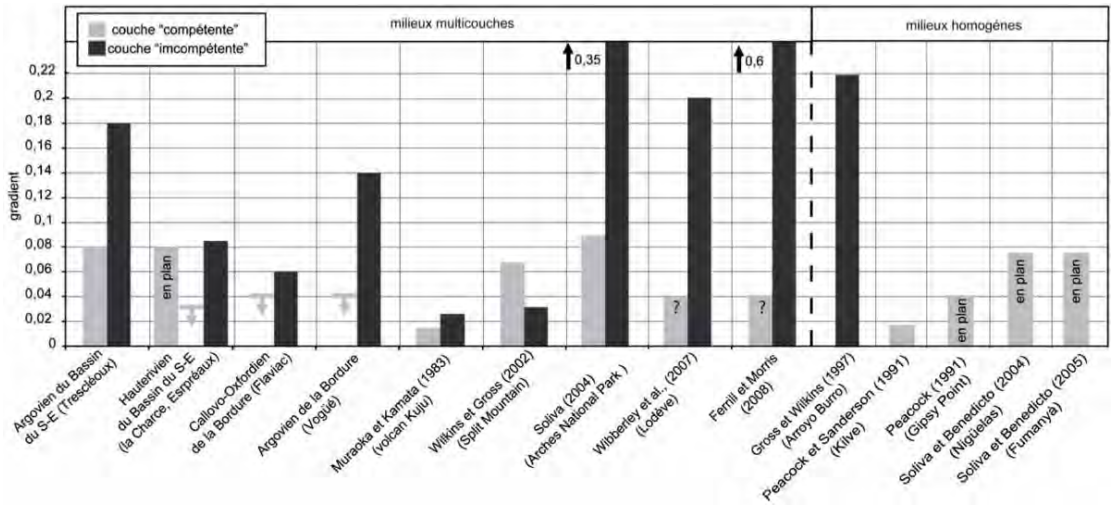

Vertical restriction and segment linkage

The vertical propagation of normal faults in multilayer systems is greatly affected by the mechanical properties of the superposed rock units as stated earlier. Certain lithologies, such as salt and mudstone, can accommodate strain and displacement by ductile flow, and hence they can inhibit the vertical propagation of faults [*Pascoe et al.*, 1999; *Withjack and Callaway*, 2000; *Ford et al.*, 2007; *Kane et al.*, 2010], or cause full or partial geometric and kinematic decoupling by sub- and supra-detachment deformation [*Withjack and Callaway*, 2000; *Ford et al.*, 2007]. Faults that are vertically restricted are

forced to accumulate displacement by growing horizontally. For this reason, it is important to understand restriction in order to infer the growth and geometry of faults through time.

However, the continuous growth of the fault systems reduces the decoupling effects and allows the faults to join and interact [*Pascoe et al.*, 1999; *Withjack and Callaway*, 2000; *Tvedt et al.*, 2013]. In this sense, many models were suggested to explain the vertical propagation of normal faults, including the vertical linkage of initially decoupled segments [*Baudon and Cartwright*, 2008c; *Jackson and Rotevatn*, 2013]. In this model, degree of coupling increases as slip on a normal fault also increases [*Pascoe et al.*, 1999; *Withjack and Callaway*, 2000] or with a lower thickness of the decoupling incompetent unit [*Withjack and Callaway*, 2000].

Restriction to lateral fault propagation in homogenous units is also documented and is believed to be caused by a low stress zone. This might be related to the presence of a relay zone at the lateral tip of the fault [*Gupta and Scholz*, 2000], transferring the displacement to adjacent fault segments. In any case, fault restriction is accompanied by an increase in fault tip displacement gradients [*Gupta and Scholz*, 2000; *Welch et al.*, 2009; *Roche*, 2011]. Thus, faults restriction is typically identified in fault displacement profiles.

Restricted faults are distinguished primarily by locally higher displacement gradients adjacent to tip-lines [*Nicol et al.*, 1996; *Wilkins and Gross*, 2002] (Figure 5.17) and also by significant departures from elliptical tip-line geometries (Figure 5.18). Therefore, they are characterised by "M-shape" displacement profile [*Muraoka and Kamata*, 1983; *Schultz and Fossen*, 2002; *Soliva and Benedicto*, 2005; *Soliva et al.*, 2006] with the exceptionally high gradients toward the tip (Figure 5.17). A high displacement gradient is also attested in clay units [*Roche et al.*, 2014].

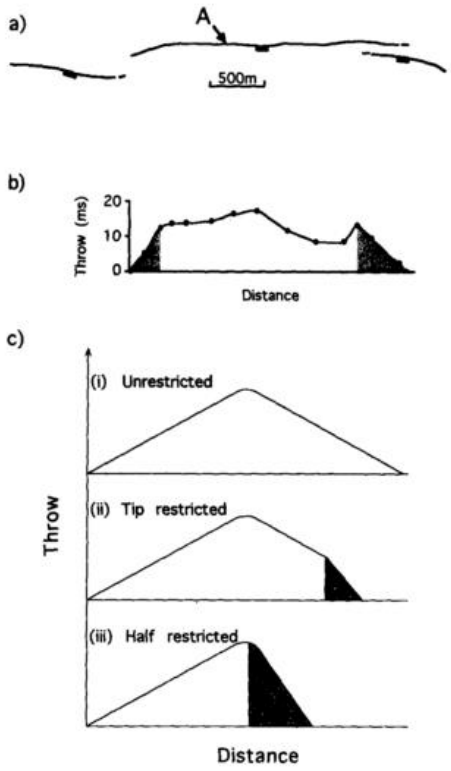

Figure 5.17: (a) Fault map showing a normal fault trace, labelled A, restricted at both lateral tip-points by adjacent faults. (b) Horizontal throw profile for the restricted fault in (a), the restricted parts of the fault trace (stippled) have throw gradients significantly higher than elsewhere. The horizontal scales in (a) and (b) are the same. (c) Schematic diagram illustrating the three main types of fault displacement profile for: (i) unrestricted faults; (ii) faults restricted only towards a tip-point; and (iii) faults which are 50% restricted, i.e. between the point of maximum throw and the tip-point. Restricted parts of the throw profiles are stippled. Each profile type may occur along any orientation on a fault surface. From Nicol *et al.* [1996]

Similarly restricted faults have locally more closely spaced throw contours (Figure 5.18), lower overall symmetries and a wider range of aspect ratios than unrestricted faults (table 5.2). The shapes of laterally and vertically restricted faults are clearly differentiated on a plot of dip dimension vs strike dimension (Figure 5.19). Restricted faults generally plot outside the data field for unrestricted faults with aspect ratios <1.3 generally associated with laterally restricted faults, and values of >2.5 with vertically restricted faults [*Nicol et al.*, 1996]. The aspect ratio is simply L/H or strike dimension/dip dimension [*Nicol et al.*, 1996]. The different aspect ratios documented in literature for restricted faults is shown in table 5.2. The high values of aspect ratios observed along restricted faults is due to the fact that vertical propagation is inhibited by a restrictor and faults will propagate only horizontally [*Nicol et al.*, 1996; *Schultz and Fossen*, 2002; *Soliva et al.*, 2006].

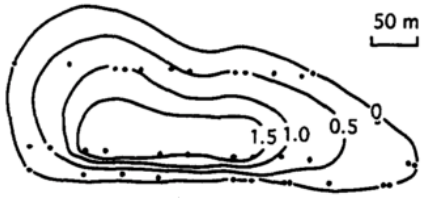

Figure 5.18 : Throw contour (m) diagram for a normal fault from the North Derbyshire Coal-field. The view is normal to the fault surface which has an aspect ratio of ca 2.7. Propagation of the lower tip-line of this fault is interpreted to have been retarded by a thick sandstone bed. Vertical and horizontal scales are approximately equal. From Nicol *et al.* 1996.

Table 5.2: *Aspect ratio values reported for isolated and restricted faults in literature.*

Isolated faults	*Vertical restriction*	*Lateral restriction*	*References*
1	-	-	[*Walsh and Watterson*, 1987; *Peacock and Sanderson*, 1991; *Nicol et al.*, 1996; *Schultz and Fossen*, 2002; *Soliva et al.*, 2006]
1.0 to 3.4	1.8 to 8.4	0.5 to 1.8	[*Nicol et al.*, 1996]
2	2 to 8	-	[*Soliva et al.*, 2006]
	1 to 11	-	[*Schultz and Fossen*, 2002]
	≈ 10	-	[*Cartwright et al.*, 1995; *Soliva and Benedicto*, 2005]

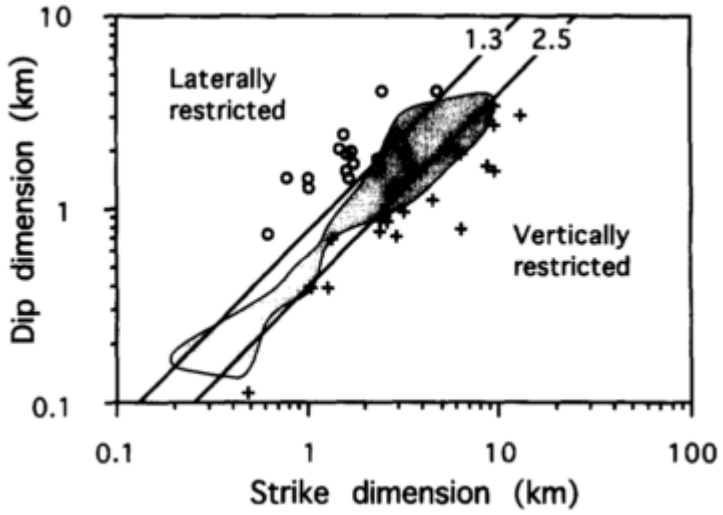

Figure 5.19 : Dip dimension vs strike dimension for 39 laterally (open circles) and vertically (crosses) restricted faults. Straight lines show aspect ratios of 1.3 and 2.5. Faults with aspect ratios of < 1.3 are commonly laterally restricted and those with aspect ratios of >2.5 are frequently vertically restricted. From Nicol *et al.* [1996].

In summary, ductile layers may significantly affect the geometry and evolution of extensional fault arrays, resulting in marked temporal and spatial variations in structural style, fault-related folding and displacement distribution.

V. 1.6 Polygonal fault systems

Definition

Polygonal Fault Systems (PFS) are a types of dip-slip normal faults defined as laterally extensive arrays of extensional faults that are characterised by a polygonal planform geometry and are confined to a specific stratigraphic interval i.e. they are layer-bound [*Cartwright*, 2011] (Figure 5.20).

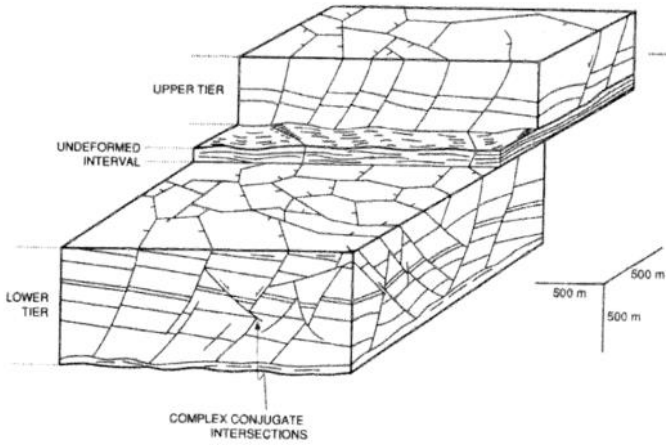

Figure 5.20: Schematic representation of polygonal faults arranged in two supperposed tiers. In cross section, these faults dip in either direction, while in planform they exhibit what a polygonal geometry. From Cartwright [2013].

PFS are recognised in over 100 basins worldwide (Figure 5.21). In the past few years, extensive research was performed on PFS mainly based on seismic reflection data alone. There are many geometrical observations that are so far common with PFS worldwide and are summarised in the following paragraphs. However, the mechanism behind PFS is still largely debated as many models to explain their genesis are proposed [e.g. *Cartwright*, 2011].

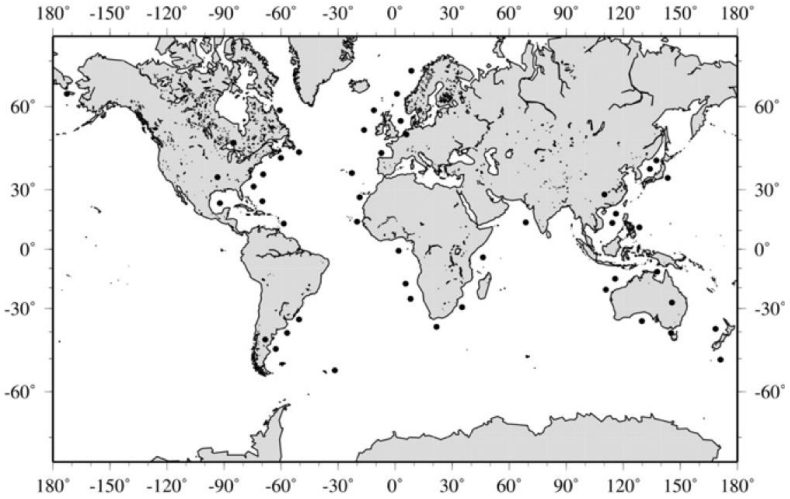

Figure 5.21: Map showing the occurrence of PFS worldwide. From Cartwright [2011].

Characteristics

The fundamental characteristics of PFS can only be seen by using 3D seismic reflection data. Their understanding in the past few years was linked to technological development in 3D data acquisition and processing [*Cartwright*, 1994]. Hence, PFS have the following features:

- The polygonal planform pattern is the most critical characteristic of PFS. There is a huge variation in the polygonal planform, both laterally within a single PFS and for different PFS (Figure 5.22).
- They become aligned toward at the end of the system if the lower detachment surface is slightly bending, or when an anisotropic stress field is present (Figures 5.23 and 5.24).
- They are exclusively normal and appear to be dominantly dip-slip in their kinematics.
- Individual faults are typically planar in tiers of modest thickness (<200-300 m) but tend to be more gently listric in thicker tiers [*Stuevold et al.*, 2003].
- Have dips in the range of 50-80° where observed close to the modern seabed, whereas deeper buried tiers have much flatter dips, of the order to 20-50° [*Lonergan et al.*, 1998].
- They are located along "tiers" [*Cartwright*, 1994] ranging in thickness from a few tens of metres to over 2 km.

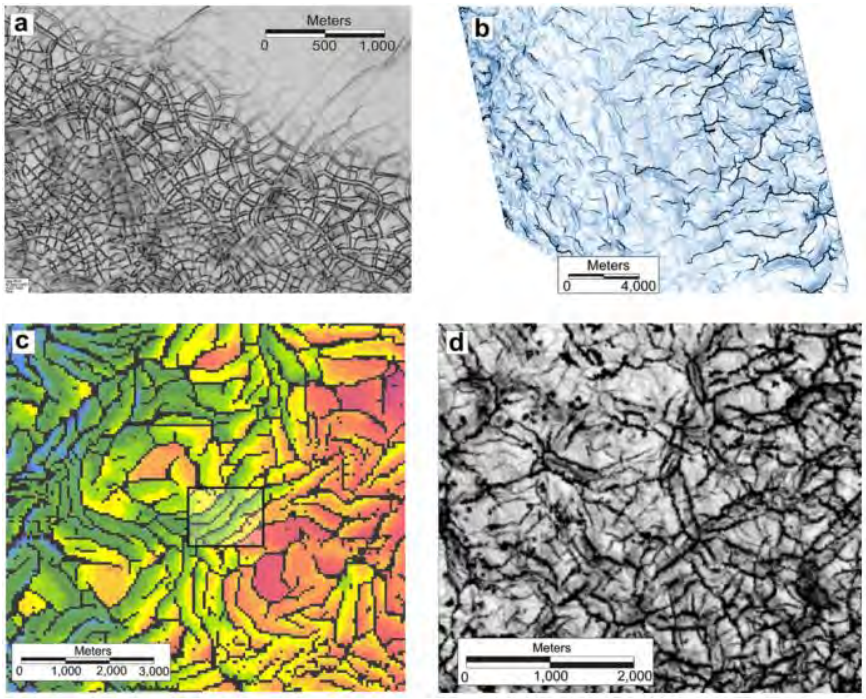

Figure 5.22: Dip attribute (a-b-c) and time-structure maps (c) showing the variability in the polygonal geometry in PFS. Some are densely packed with no free lateral tips (a) while others are relatively open network (b). From Cartwright [2013].

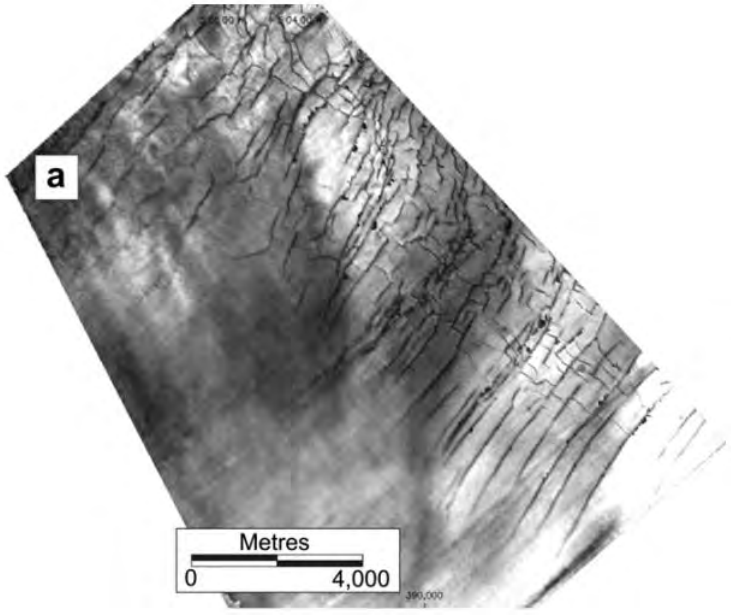

Figure 5.23: An amplitude slice showing a transition from fully polygonal to linear faults toward the edge of the system. From Cartwright [2013].

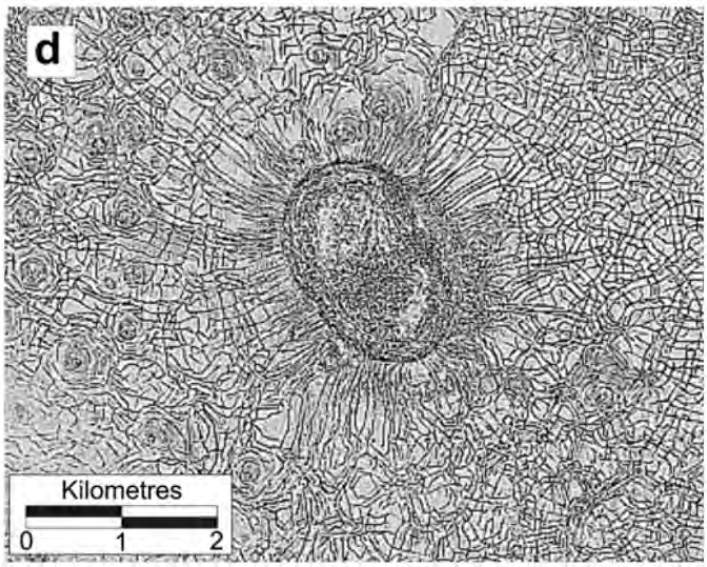

Figure 5.24: Coherence attribute slice showing polygonal faults becoming radially oriented close to the salt intrusion because of local stress field variations caused by the intrusion. From Cartwright [2013].

- Tiers are generally dominantly composed of very fine grain size particles (clay grade), and commonly comprise smectite-rich claystones or biogenic mudstones (both carbonate and biosiliceous compositions) [*Cartwright and Dewhurst*, 1998; *Dewhurst et al.*, 1999]. The edges of many PFS occur either where the tier thins beneath some critical limit of a few tens of metres [*Cartwright*, 1994] or where there is a pronounced bulk facies change within the tier, e.g. from a dominantly clay-rich interval (PFS present) to a sand rich interval (PFS absent). Where thin sandstone units are interbedded with much thicker intervals of fine-grained strata, the sandstones are offset by the polygonal faults which propagate from the adjoining clay-rich layers [*Stuevold et al.*, 2003].

- Fault have throws ranging up to a maximum of c. 100 m , and spacing of 100–1000 m.

- PFS develop over very large areas, with no other type of faults or fracture network as uniformly developed on such a vast areal scale [*Cartwright*, 2011].

- They are developed in many abyssal basins, and some foreland and intracratonic basins [*Cartwright and Dewhurst*, 1998]. Over 90% of these occurrences are in divergent continental margin basins, and are generally hosted in slope depositional systems consisting mainly of hemipelagites where the successions are dominated by high proportions of clay-sized grains. They are generally absent from convergent margin and foreland basins.

Mechanism

One of the factors contributing to the uncertainty in the origin of PFSs is the Lack of field analogues, and the almost total reliance on seismic and well data for basic lithologic and structural information, creating large uncertainties in the origin and the mechanism of polygonal faulting. More than any other single observation, the enormous lateral extent of many PFS is a powerful argument by itself that the genetic mechanism must be constitutive rather than externally imposed [*Cartwright*, 2011].The main candidates that have been proposed as the underlying mechanism responsible for the development of polygonal fault systems are generally considered to be density inversion, gravitational loading and Syneresis [e.g. *Cartwright et al.*, 2003] briefly discussed in the paragraphs below.

The earliest models for the genesis of PFS have been based entirely on studies of the lower Tertiary interval of the North Sea Basin. The first genetic model to account for these structures was proposed by [*Henriet et al.*, 1991], and was based on their field and seismic-based studies of faulting in lower Tertiary sequences that were deposited on the southern margin of the North Sea Basin. Their model involved periodic build-up and release of high pore-fluid pressures in the fine-grained successions, and the faulting was linked to movements induced by density inversion between undercompacted and normally compacted shale layers. Cartwright [1994] mapped the extent of the intensely faulted lower Tertiary interval over a large part of the central North Sea, and adapted the Henriet *et al.* [1991] model to take account of this large areal extent of the deformed interval, suggesting that episodic collapse of basin-scale overpressured shale compartments was responsible for the distribution of the fault system. Some form of overpressure-related mechanism could certainly be compatible with the large areal extent of the deformed lower Tertiary interval and with its development in the fine-grained depositional system of the slope and basin floor. However, this type of mechanism does not easily explain the important geometrical result obtained from three-dimensional seismic mapping, i.e., that the faults are organized in polygonal networks. It also does not explain how significant apparent extensional strains could develop at the depositional surface, as observed by Cartwright [1994].

Watterson *et al.* [2000] took the main elements of the density inversion model and modified it to explain the specific features of the Lake Hope 3D survey in the Eromanga Basin, in Australia. In their case study area, Watterson *et al.* [2000] found that a large proportion of the polygonal faults appeared to form conjugate intersections near the base of a tier and from this argued that the faults must have propagated

upwards from a basal mobile layer, which originally formed the lower, less dense layer of a reverse density stratification.

Cartwright and Lonergan [1996] focused on more detailed three-dimensional seismic mapping of the polygonal fault networks, and by measuring the extensional strain using standard line-balancing techniques, they proposed that the faulting in the lower Tertiary interval was related to shrinkage (volumetric contraction) during early burial and compaction. The most important result of this strain analysis was that apparent extension on any given polygonally faulted horizon was approximately uniform in all directions, and they concluded from this that the fault system could not be tectonic in origin. The only explanation for the observed extensional strain in the layer-bound fault system is that it is merely an apparent extensional strain that results from lateral contraction of stratal surface area during faulting. This lateral contraction was considered to be a component of a general volumetric contraction of the sedimentary succession as it was buried and as pore fluid was expelled. An essential component of the model is that as pore fluid is expelled, the sedimentary particles contract inward as well as compact vertically, and this lateral contraction would create space problems due to the lateral basin constraints, unless continuity is maintained by some form of deformation. The volumetric contraction model of Cartwright and Lonergan [1996] thus provides a simple explanation for the almost paradoxical occurrence of large numbers of normal faults in a basinal sequence deposited during a period of postrift thermal subsidence.

In the gravity/sliding model, polygonal faults are regarded as the result of sliding down a slope, with a basal detachment at the boundary separating the intraformational faults from undeformed, deeper sedimentary units [e.g. *Higgs and Mcclay*, 1993; *Clausen et al.*, 1999]. The downslope gravitational stress provides the necessary conditions for failure, but this would be expected to produce a strong alignment of fault strikes parallel with the slope contours and the extension should also be balanced by down slope contractional strain of a similar amount. Since this bias of strikes is obviously not the case for most polygonal fault systems, gravity sliding is not considered a viable mechanism, although down slope gravitational stresses can provide a modifying influence on the type of polygonal pattern that evolves wherever a strong slope is present. Whilst many polygonal fault systems are known from passive continental margin settings where such a slope would have been a factor [*Cartwright and Dewhurst*, 1998], they are also widely developed on basin floors, with no discernible slope on any part of the deformed sequence, and this slope-induced mechanism cannot be viable as a primary controlling process

Syneresis is by definition a spontaneous contraction (shrinkage) without evaporation, but is a process that is specifically restricted to gels [*Brinker and Scherer*, 1990]. To invoke syneresis for the development of polygonal faults thus requires that the deforming interval be in a gel state at the time of deformation. Gels are a framework of colloidal particles [*Cartwright and Dewhurst*, 1998; *Dewhurst et al.*, 1999], and the primary condition for gel formation is the very fine size range of the constituent particles (clay size range). The host sediments of PFS fall into the range of colloidal materials and this means they had the potential for gel formation on deposition, although it is not possible to be sure they were actually gels when deposited. [*Cartwright and Dewhurst*, 1998] and Dewhurst *et al.* [1999] offered some possible physical mechanisms for syneresis that might have occurred in the specific lithological and geochemical contexts of polygonal fault development. Syneresis, by definition, is volumetric contraction and thus offers a possible physical explanation for the volumetric strains of polygonally faulted intervals measured from reduction in bed lengths on seismic data. For a clay layer undergoing syneresis it is envisaged that the particles in the porous gel framework move closer together under the influence of a net increase in inter-particle attractive forces, and hence induce faulting.

A more recent model involves diagenetic reactions in host sediments leading to polygonal faulting. It is argued that some diagenetic reactions can lead to major and abrupt changes in physical properties of the bulk sediment with complementary porosity changes as a result [*Cartwright*, 2011]. These porosity changes can be dramatic in magnitude and occur very rapidly over depth thresholds of a few metres. Although far from proven, such changes match the predictions from laboratory experiments [*Shin et al.*, 2008] that diagenesis can trigger shear failure, which raises the possibility that this new mode of shear failure may be much more prevalent in the geological record than currently appreciated.

In simple terms, the polygonal planform geometry could be explained by the Anderson stress classification scheme. On a regional and local scale, the large range of orientations in a typical polygonal fault array implies a causative state of stress in which intermediate and least principal stresses are almost equal ($\sigma2=\sigma3$), which for horizontal layering would equate to a horizontally isotropic state of stress (Shmax=Shmin) (Figure 5.25). A typical normal fault would have $\sigma1>\sigma2>\sigma3$, with a strike parallel to the direction of $\sigma2$. This generalisation fails wherever a significant horizontal stress anisotropy occurs either due to local changes of slope gradient, to the presence of active tectonic structures, or to the imposition of regional or local tectonic stresses. Polygonal faults are

sensitive to quite subtle stress anisotropy, and can thus be useful as palaeostress indicators.

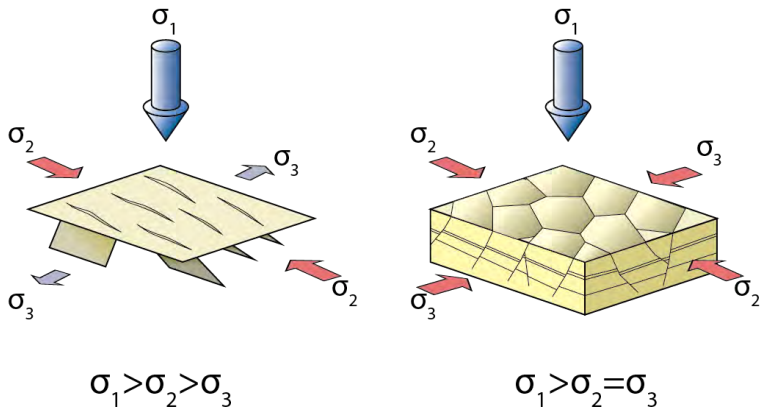

Figure 5.25: Schematic representation of normal faulting under isotropic and anisotropic stress fields. If σ2= σ3, then normal faults with a polygonal planform geometry will develop.

V. 1.7 Literature review conclusion

A large amount of literature exists on the normal faults systems from a vast amount of outcrop data, analogue and numerical models. Important landmarks have been achieved to understand the evolution of normal fault systems, their nucleation, propagation and interaction. Even though we possess a fair amount of knowledge on how faulting occurs, there is still a number of uncertainties and open questions that are yet to be answered:

- How do faults evolve? Is the coherent or the isolated fault models the most representative of fault populations worldwide? This aspect of fault growth is of great importance as it constrains our understanding of faults and provides an insight on faulting mechanisms in immature stages.

- Is mechanical stratigraphy important and has a strong impact on the development of large faults at the basin scale? So far, all studies targeted to understand mechanical stratigraphy and faults in multilayer units are primarily based on outcrop data. Few and limited studies attempted to look at the mechanical stratigraphy from seismic data, which is probably related to the lower resolution of seismic compared to outcrop. It is important, however, to check if mechanical stratigraphy affects faulting at a basin scale or not.

- What is the mechanism of polygonal fault systems? Many models exist, with uncertainty on the true nature of these faults.

V. 2 Growth of layer-bound normal faults under a regional anisotropic stress field

The tectonic structures documented in the Levant Basin contain a conspicuous array of NW trending normal faults, as stated in chapter 3. The faults are found over the entire basin and are restricted to the Oligo-Miocene unit only. How did they nucleate, grow and evolve is of great importance, as it will help us to understand the structural and geologic setting of the Levant Basin during the Oligo-Miocene, and allow us to better understand the growth of faults at a regional scale in general. Furthermore, these faults might have an important effect on the petroleum system in the basin. They might constitute conduits to fluid flow as well as impermeable barriers to petroleum reservoirs. In order to quantify this effect, it is essential to examine these faults in detail. Thus, understanding their history and evolution will provide valuable information for both academia and industry.

The tools described in the literature review discussed previously will serve as a basis to understand the evolution of the normal fault system of the Levant Basin. Particularly, fault displacement profiles were constructed in order to understand how these faults nucleated and interacted with each other during their growth. They showed that the normal faults were formed in the Early Micoene and grew following the isolated fault growth model, accumulating displacement with increased length. The following analysis of this normal fault array is presented in the form of an article currently in review.

START OF ARTICLE 2

V. 2.1 Abstract

Contractional layer-bound normal faults, commonly called polygonal faults, are structures formed in fine-grained sediments early in their burial history. When subject to relative stress anisotropies, these faults will be preferentially re-oriented. How do they grow, evolve and interact with each other is important in order to increase our understanding of compaction-related deformation since well-oriented faults were never documented on a regional scale previously. This paper aims to understand their geometry and growth by applying qualitative and quantitative fault analysis techniques to a 3D seismic reflection dataset from the Levant Basin, an area containing a unique

contractional layer-bound normal fault array. This analysis indicates that the faults were affected by mechanical stratigraphy, causing preferential nucleation sites of fault segments, which later linked. Our interpretation suggested that growth of contractional faults on a basin-scale generally follows the isolated model, accumulating length proportionally with displacement and when subject to an anisotropic regional stress field they will grow very similarly to normal tectonic faults.

V. 2.2 Introduction

Layer-bound normal faults are extensional structures confined to a particular sedimentary unit without propagating to the underlying and overlying layers, hence their name layer-bound. Such confinement to discrete stratigraphic units has been well documented in the field and in literature [*Gross*, 1995; *Gross et al.*, 1997; *Wilkins and Gross*, 2002] and can occur when the stress or lithological conditions in adjacent stratigraphic units are unfavourable for vertical fault propagation into those units. A particular type of layer-bound faults is the polygonal fault system (PFS). Different mechanisms may explain their nucleation, including volumetric contraction, compaction, diagenetic shear failure and pressure variations [*Henriet et al.*, 1991; *Cartwright and Lonergan*, 1996; *Cartwright and Dewhurst*, 1998; *Dewhurst et al.*, 1999; *Shin et al.*, 2008; *Cartwright*, 2011]. In this paper, such faults are referred to as contractional layer-bound normal faults. Developed primarily in fine-grained sediments early in their burial history [*Cartwright and Lonergan*, 1996; *Cartwright and Dewhurst*, 1998; *Dewhurst et al.*, 1999; *Davies and Ireland*, 2011], this type of normal faults is mainly characterised by its distinctive polygonal planform geometry [*Cartwright et al.*, 2003; *Cartwright*, 2011]. However, local re-orientation of the faults has been observed, especially in proximity to other structures or toward the end of the system over a slope [*Rank-Friend and Elders*, 2004; *Stewart*, 2006; *Carruthers et al.*, 2013]. Hence PFS do not always have the perfect polygonal planform geometry and might be linear, at least on a restricted scale.

The distinctive planform geometry of PFS is interpreted as the result of isotropic horizontal stress field, and for this reason, when polygonal faults are close to other structures, such as salt domes, local stress-field variation becomes responsible for re-orienting these faults and making them linear [*Cartwright*, 2011; *Carruthers et al.*, 2013]. Thus, there is a strong relationship between the relative stress magnitude in any area and the geometry of the faults. What would be the final geometry of PFS faults where a regional anisotropic horizontal stress field is imposed? Would these faults become

perfectly linear and well-oriented? Moreover, how would they grow through time and what are the factors affecting their evolution? These are important questions never answered before since no PFS were ever documented to be well oriented on a regional scale. In order to answer these questions and understand how contractional faults grow, displacement/length and displacement/depth analysis should be performed on normal faults. Few studies, however, were targeted to understand the growth of contractional layer-bound normal faults with polygonal planform geometry [*Nicol et al.*, 2003; *Stuevold et al.*, 2003; *Nelson*, 2006].

The aim of this study is to investigate the evolution and growth of a unique layer-bound normal fault system, found in the Levant Basin over an area of 70,000 km^2 [*Kosi et al.*, 2012] (Figure 5.26). This NW trending normal fault array is present in a region where NW-SE compression is attested during the Oligo-Miocene [*Ghalayini et al.*, 2014; *Montadert et al.*, 2014]. The presence of such exceptionally preserved layer-bound normal faults makes this study area unique in terms of testing the displacement patterns, growth and interaction of faults. In particular it can also be used to test the applicability of the isolated and coherent fault models [e.g. *Mansfield and Cartwright*, 2001; *Walsh et al.*, 2002] to the growth of contractional faults, and the effect of mechanical stratigraphy on the evolution of a regional normal fault array. For this study, we used recently acquired high quality 3D seismic reflection data from the Levant Basin offshore Lebanon. We applied qualitative and quantitative fault analysis techniques, such as displacement distribution analysis on fault planes, to understand the growth of a contractional layer-bound normal fault system exhibiting classical polygonal planform geometry in a small region in the basin; and well-oriented and linear planform geometry in the major part of the Levant Basin. The evolution of these faults is important to complete our understanding of the structural setting of the Levant basin. It has also a strong industrial impact since these structures very likely have an effect on the petroleum systems of the Levant Basin.

After an introduction to the regional context of the Levant basin and a definition of the applied methodology, we describe the normal fault array by looking at the geometry, displacement profiles and the thickness variations along fault planes. Based on this description we then propose a model for the fault timing and growth in the Levant basin. Finally the implications for normal faults growth in general, and contractional faults in particular are discussed.

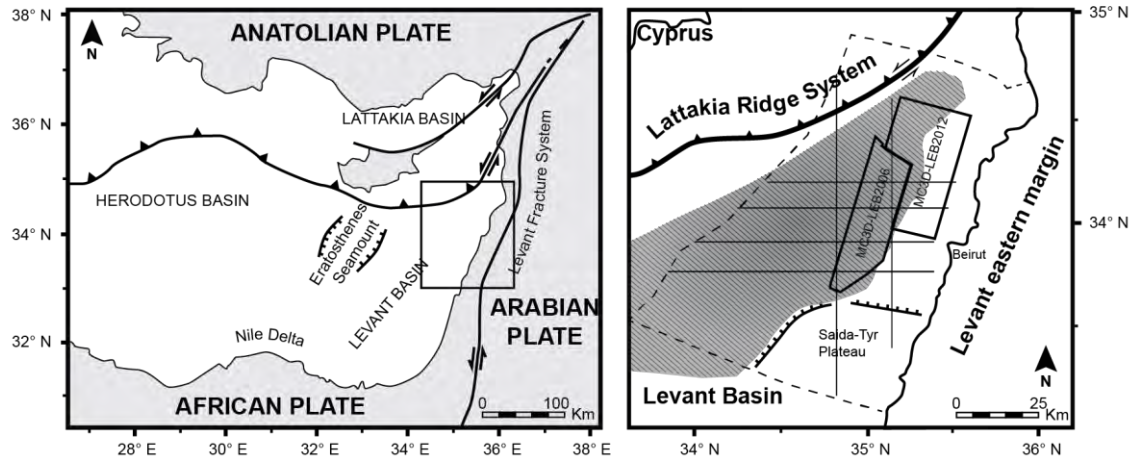

Figure 5.26: Simplified structural map showing the location of the Levant Basin in the Eastern Mediterranean and the extent of the normal fault array. The study area is located offshore Lebanon and benefits of two seismic cubes and six 2D seismic lines, courtesy of PGS and the Lebanese Petroleum Administration.

V. 2.3 Regional framework

The Levant basin is located in the easternmost part of the Mediterranean Sea (Figure 5.26). It is bordered to the East by the Arabian plate, to the North by the Lattakia ridge system, to the West by Eratosthenes seamount and to the South by the Nile Delta and the African plate. The basin was formed through polyphase rifting in the Permo-Jurassic [e.g. *Garfunkel*, 2004; *Homberg et al.*, 2009; *Gardosh et al.*, 2010]. Its geological setting is marked by the evolution of Neotethys and the interaction of the Arabian plate with the Anatolian plate. In the Late Cretaceous, convergence tectonics have caused the inversion of previous extensional structures and contraction of the Levant basin. In the Neogene, collision of Arabia with Anatolia has established a NW-SE contractional stress field in the basin and uplift along the margins [*Barrier and Vrielynck*, 2008]. Extensive erosion of Upper Eocene and Oligocene units in Lebanon [*Dubertret*, 1955; *Hawie et al.*, 2014] together with angular unconformities between Lutetian and Burdigalian [*Dubertret*, 1955; *Boudagher-fadel and Clark*, 2006; *Hawie et al.*, 2013] attest to a regional event with NE-SW initiation of folding due to this NW-SE compressional stress field [*Homberg et al.*, 2010].

During the Messinian, dessication of the Mediterranean sea resulted in deposition of a 2 km thick evaporite unit, commonly known as the Messinian evaporite sequence [*Bowman*, 2011; *Lie et al.*, 2011; *Hawie et al.*, 2013]. The Miocene times were coeval with the formation of the Levant Fracture System (LFS), a sinistral transform fault system forming the plate limits between the Arabian and African plates. The

central part of the LFS in Lebanon consists of a restraining bend formed of a multitude of folds and faults [*Gomez et al.*, 2007b]. Recent investigation of the Levant basin showed that the margin offshore Lebanon is affected by E-W dextral strike-slip faults synchronous with the activity on the restraining bend. These faults are still active today, whereas the NE-SW anticlines were folded in the Late Miocene prior to the Messinian event [*Ghalayini et al.*, 2014].

V. 2.4 Dataset and methodology

This study is based on two high quality 3D seismic surveys, MC3D-LEB2006 covering 1700 km^2 and MC3D-LEB2012 covering 2600 km^2, located offshore Lebanon, and seven 2D seismic lines, courtesy of Petroleum Geo-Services (PGS) (Figure 5.26). MC3D-LEB2006 survey is time-migrated and was acquired in 2006 using six streamers and two 3,090 cubic inch air guns positioned at a depth of 6m in water depth ranging between 1.5 and 2 km. Streamer length is 6000 m long at a spacing of 12.5m and 25m shot point intervals. Frequency ranges are between 40 and 80 Hz giving a tuning thickness of about 5m in the Pliocene and 15m within the Miocene. Time to depth conversion is done using stack-velocities due to the absence of well data offshore Lebanon to date.

MC3D-LEB2012 survey is depth-migrated and was acquired in 2012 using 12 streamers and two 4,135 cubic inch air guns positioned at a depth of 6m in water depth ranging between 1.5 and 2 km. Streamer length is 7050 m long at a spacing of 12.5m and 25m shot point intervals. Frequency ranges are between 40 and 80 Hz giving a tuning thickness of about 5m in the Pliocene and 15m within the Miocene. Time to depth conversion is done using stack-velocities due to the absence of well data offshore Lebanon to date.

Fault and horizon interpretation were conducted on a Linux workstation using Paradigm's Gocad and Skua software. The following nine horizons were mapped in the seismic surveys (Figure 5.27): (i) H1 (Senonian unconformity); (ii) H2 (Eocene unconformity); (iii) H3; (iv) H4; (v) H5 (base Miocene); (vi) H6 (base mid-Miocene); (vii) H7; (viii) H8 (Base Messinian) and (ix) H9 (Base Pliocene). Assigning ages can only be done for H1, H2, H5, H6, H8 and H9 by regional correlations with wells from Israel [*Hawie et al.*, 2013; *Ghalayini et al.*, 2014] (Figure 5.27). The remaining horizons were essential to constrain timing and displacement along the normal faults. They were

chosen based on their strong impedance contrast and the possibility to track them through the whole seismic surveys.

More than 200 faults were mapped in the course of this study, but only 20 were subject to quantitative analysis of displacement. These faults were chosen based on the following criteria: (i) excellent continuity and mapping of the fault plane, (ii) ability to correlate clear and strong reflectors across the fault plane, (iii) isolation with respect to nearby structures such as strike-slip faults, (iv) ability to map fault plane entirely by avoiding, when possible, faults cut by the data bounding box. Among the 20 selected faults, 13 were considered as isolated faults with no horizontal relay with other faults and three segmented faults consisting of a coherent system containing two or three soft-linked segments.

Geometrical and temporal evolution of faults was studied through displacement analysis along fault planes. In order for displacement to be fully recorded and growth history properly constrained, sediment deposition rate should be higher than faulting rate. In the case of the Levant Basin, the Oligo-Miocene were times when an increased amount of sediments was eroded from the uplifted Levant margin and deposited in the basin [*Hawie et al.*, 2013]. This has resulted in an excellent preservation of the growth history of the Oligo-Miocene normal fault array and allowed full recording of the growth history of the faults. In this study, the techniques used to investigate and constrain the temporal and spatial evolution of these faults consist of: (i) displacement/length analysis; (ii) displacement/depth analysis; (iii) expansion index (EI) and growth index (GI) analysis.

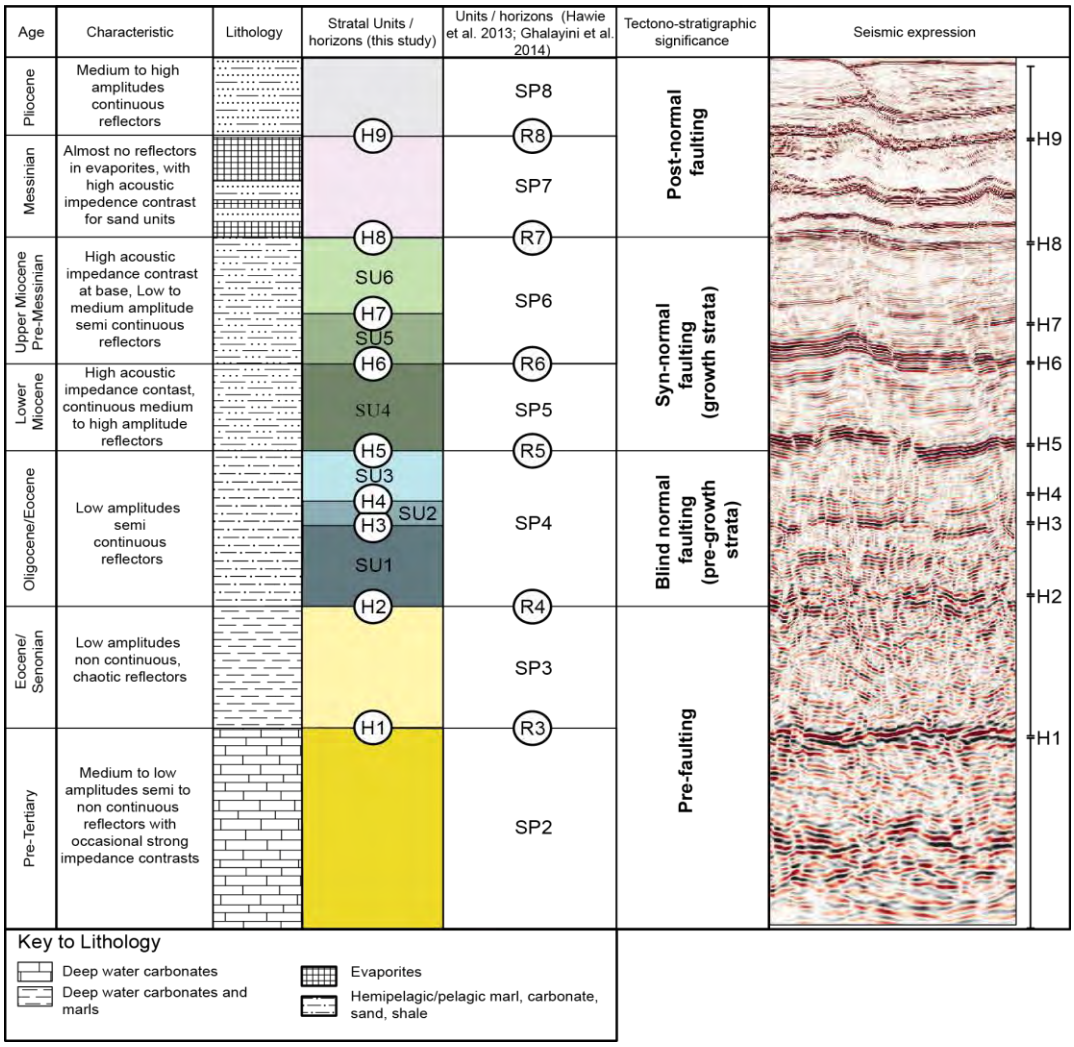

Figure 5.27: Local stratigraphic column showing the lithostratigraphy, key lithologies and seismic stratigraphic framework of the Cretaceous to Tertiary succession in the Levant Basin. SU = stratal units; H = horizon; R = reflector; SP = seismic package. This study focuses on the Oligo-Miocene unit, which was subdivided into six stratal units. Horizon interpretation is from Hawie *et al.* 2013b and Ghalayini *et al.* 2014.

Differential compaction along normal faults is susceptible of creating errors in displacement along fault planes. This could lead to underestimation of the total throw in the hanging wall if not corrected for accordingly [*Mansfield and Cartwright*, 1996; *Cartwright et al.*, 1998]. Since we are principally interested in the overall trend of displacement and variation of throw rather than the absolute throw, we have chosen not to correct for this phenomenon in this study. The displacement measurements are all taken on depth-converted profiles and not in two-way-time.

V. 2.5 Description of the normal fault array

Seismic stratigraphic framework

The normal fault array is confined within the Oligo-Miocene sedimentary units (SU1 to SU6; Figure 5.27). The base of the Oligo-Miocene units H2, is referred to as Eocene unconformity [*Lie et al.*, 2011; *Kosi et al.*, 2012]. The Oligocene (SU1, SU2 and SU3) units are believed to represent stacked deep-water clastic deposits in early lowstands at the base of the unit, transitioning upward to pelagic/hemipelagic sedimentation in deepwater settings [*Hawie et al.*, 2013; *Montadert et al.*, 2014]. A strong impedance contrast marks this transition whereby SU1 and SU3 are characterised by low to medium amplitude reflectors. SU2 unit is differentiated from SU1 and SU3 by a set of five strong and continuous reflectors across the entire basin.

Strong impedance contrast along H5 separates the Miocene from the Oligocene unit. SU4, SU5 and SU6 are characterised by high amplitude, moderate continuity reflectors, representing stacked deep-water clastic deposits in early lowstand [*Gardosh et al.*, 2008b; *Hawie et al.*, 2013; *Montadert et al.*, 2014]. They are separated by strong impedance contrasts along H6 and H7. Toward Lattakia Ridge, reflectors within SU5 and SU6 show increased amplitude, indicating lateral facies changes to the north of the basin (Fig 4 in Hawie *et al.* 2013b). For the purpose of this study, we separate the Oligo-Miocene units into the Oligocene "lower" tier (SU1, SU2 and SU3) and the Miocene "upper" tier (SU5 and SU6).

H8 consists of the upward boundary of the normal faults and is characterised by a strong impedance contrast marking the transition between the Miocene hemipelagic facies and the Messinian evaporite unit.

Distribution in the basin

The normal faults are documented in the center of the Levant basin offshore Lebanon. They disappear along the Levant's eastern margin, on top of the Saida-Tyr plateau (STP) [*Ghalayini et al.*, 2014], and on the Eratosthenes seamount (Figure 5.26). The available dataset allowed detailed mapping of the faults in only two seismic surveys (Figure 5.28). Regional mapping to know the detailed geographic distribution of these faults and their extent is inferred from available published materials only [*Dupin et al.*, 2012]. It has been previously advocated that these faults are also found offshore Cyprus

and Israel, and accumulate the biggest displacement offshore Lebanon [*Dupin et al.*, 2012]. This normal fault array hence appears to be regional and found within the whole Levant basin, over an area of about 70,000 Km^2.

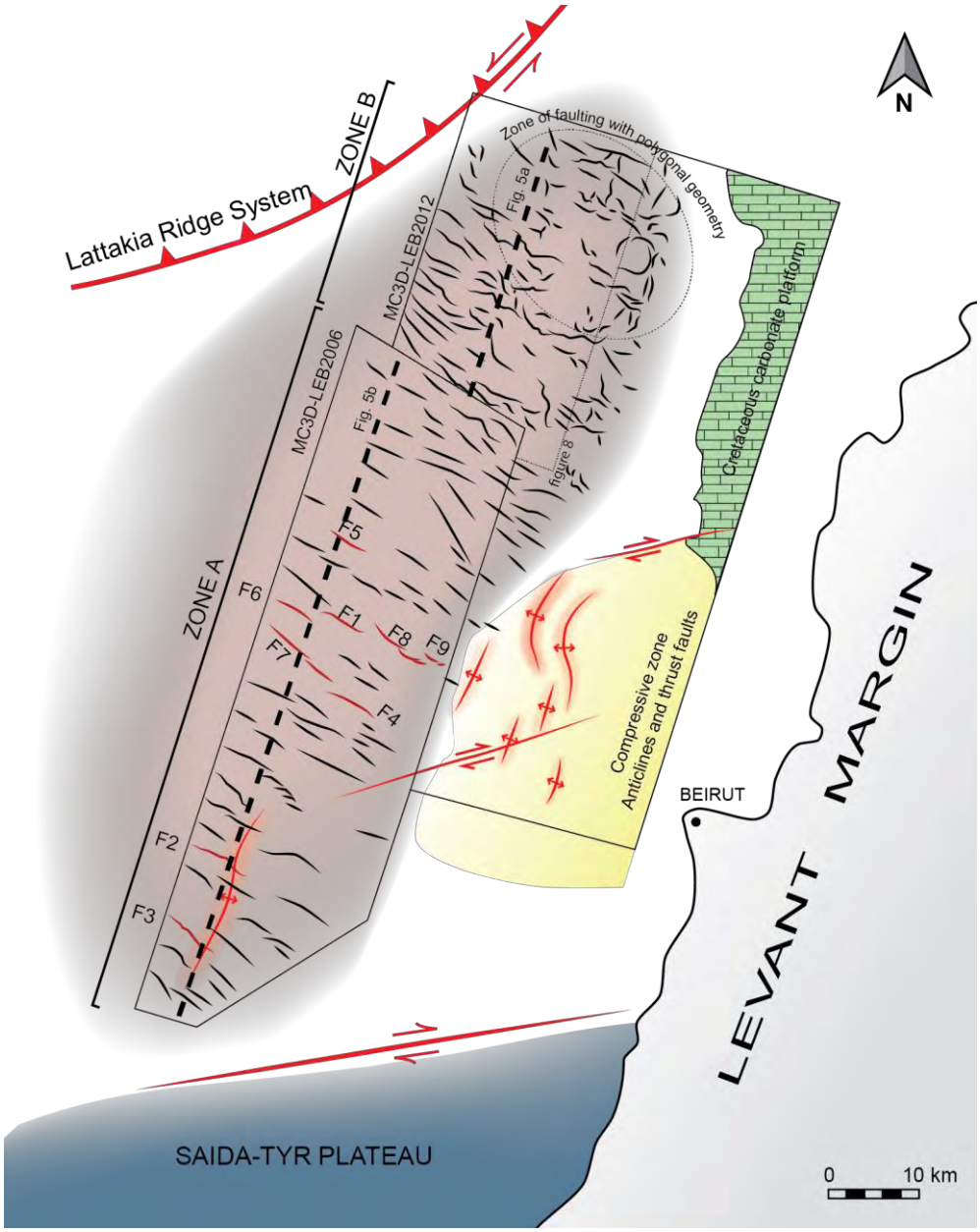

Figure 5.28: Schematic representation of the Base Miocene horizon (H5) showing the NW orientation of the normal faults in the study area. Faults acquire a gentle polygonal planform geometry close to the Lattakia Ridge in the NW corner of the survey, while in the rest of the basin the faults are linear and well-oriented. Investigated faults in this study are shown in red.

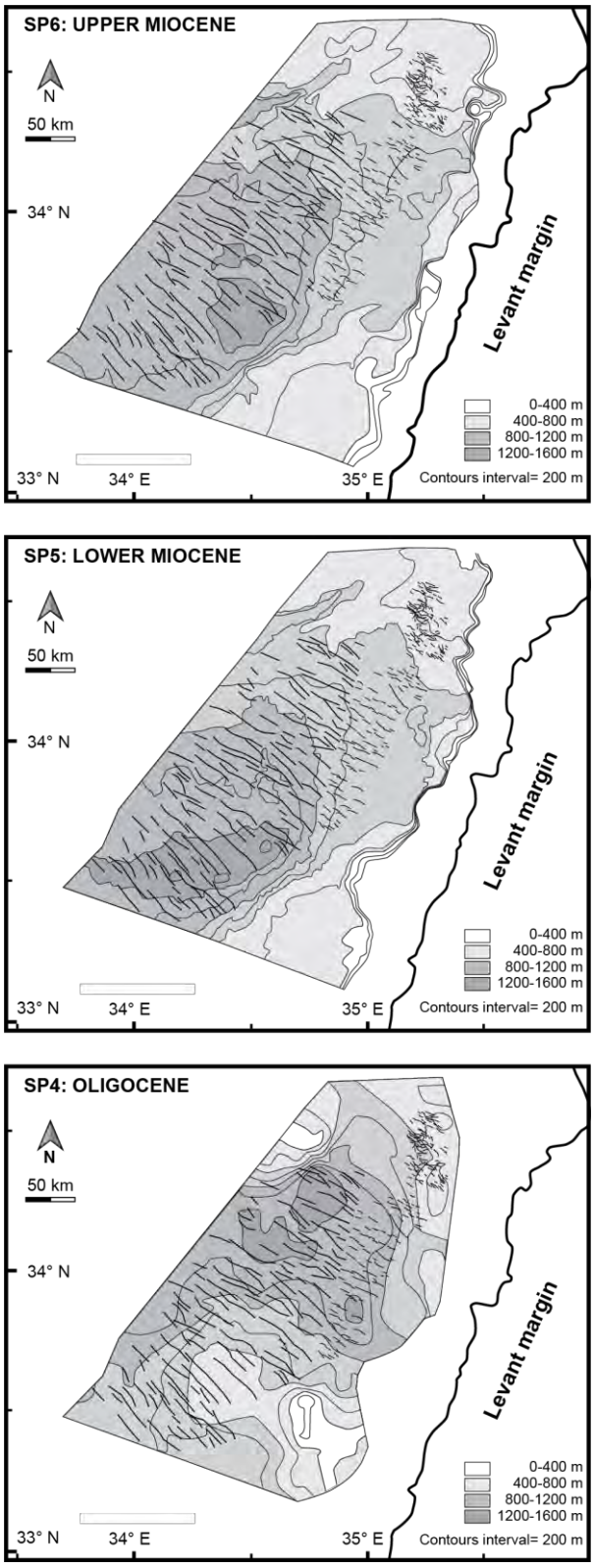

Figure 5.29 : Isopach maps of SP4, SP5 and SP6 with superposed fault mapping. The well-oriented normal faults are found where the Oligo-Miocene units are the thickest in the basin. The faults with polygonal planform geometry are restricted to the north of the basin whereby they occur in relatively thinner Oligo-Miocene thicknesses. Fault mapping is from Dupin *et al.* [2012]. SP5 and SP6 isopach maps are modified from Ghalayini *et al.* [2014] and SP4 isopach map is modified from Hawie *et al.* [2013].

Superposition of the distribution of these faults in the northern Levant basin offshore Lebanon on isopach maps of the Oligocene and Miocene units shows a correlation between the units thickness and the distribution of these faults [*Ghalayini et al.*, 2014] (Figure 5.29). They are predominantly developed where this sedimentary package is relatively thicker, mainly toward the basin's centre. At the Levant's eastern margin and over the STP, the thickness of the Oligo-Miocene is substantially reduced, and the normal faults disappear.

Geometry

The normal fault array in the Levant Basin can be divided in two regions based on the faults characteristics (orientation, length, maximum displacement …). The first (Zone A) consists of well-oriented NW trending normal faults, while the other (Zone B) consists of curved normal faults with a polygonal planform geometry (Figure 5.28).

Zone A

The NW trending normal faults are found in Zone A and are dipping 60°, either toward to NE or SW (Figure 5.30). All faults are typically 4-6 km long with an average aspect ratio of 1 (<1.3). The shape of fault planes is thus more or less square, in contrast with the ellipsoidal shape expected unrestricted normal faults [*Rippon*, 1984; *Barnett et al.*, 1987; *Walsh and Watterson*, 1988] (Figure 5.31). Faults at the seismic scale have a spacing of 3-5 km and at some places seem to interact with, or crosscut, other structures in the basin, like strike slip faults and anticlines [e.g. *Ghalayini et al.*, 2014]. Some faults in zone A interact with each other forming segmented faults with relay bends [*Kosi et al.*, 2012] (Figure 5.30).

The NW trending normal faults are layer-bound. They are found exclusively in the interpreted Oligo-Miocene units, dying out at the Eocene unconformity horizon (H2) at their lower tip (Figure 5.30). Along this horizon, few faults are terminating with tight rollover folds observed in their hangingwall (Figure 5.32). At their upper tip, the faults die out in the Messinian unit. Contrary to horizon H2, the Base Messinian horizon (H8) shows a small but varying amount of displacement along fault scarps, together with signs of erosion in the footwall (Figure 5.30). The strong and thick reflectors at the bottom of the Messinian unit show occasionally minor folding above H8.

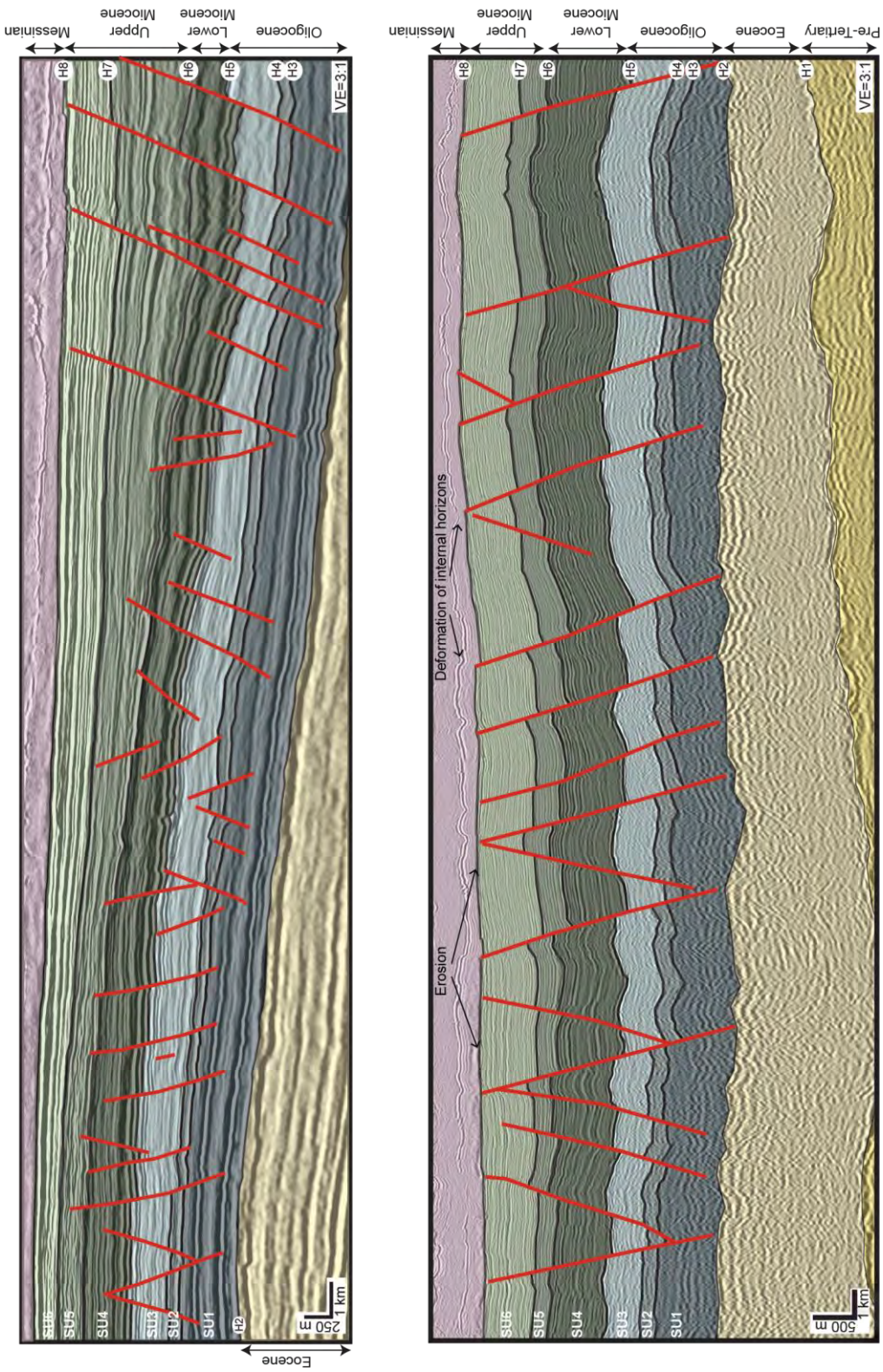

Figure 5.30 : Seismic lines showing in (a) the short and small faults with polygonal planform geometry in zone B and (b) the large contractional normal faults of zone A. The seismic lines were taken from the 3D seismic cubes. For location, see figure 5.28.

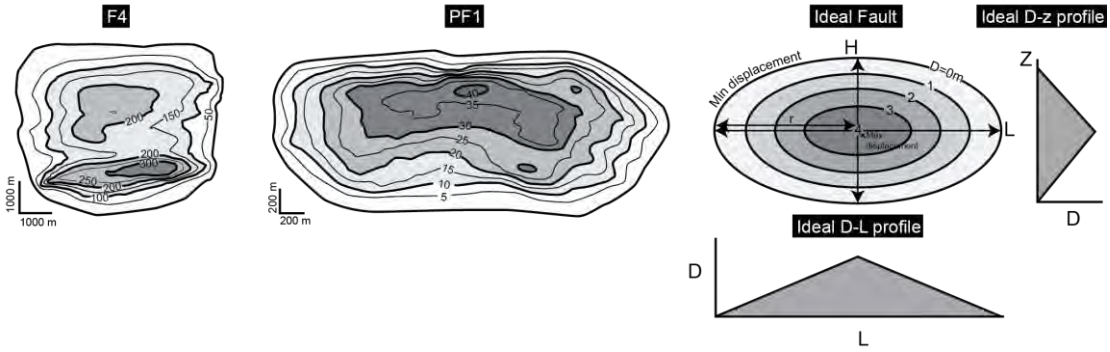

Figure 5.31: Schematic sketch comparing between (a) normal fault in the Levant Basin in zone A, (b) normal fault in zone B, and (c) an ideal normal fault. Note the presence of different aspect ratios between the faults of zone A and B, whereby the latter is closer to an ideal normal fault, while the former contains two displacement maxima. Mind the scale between the two faults.

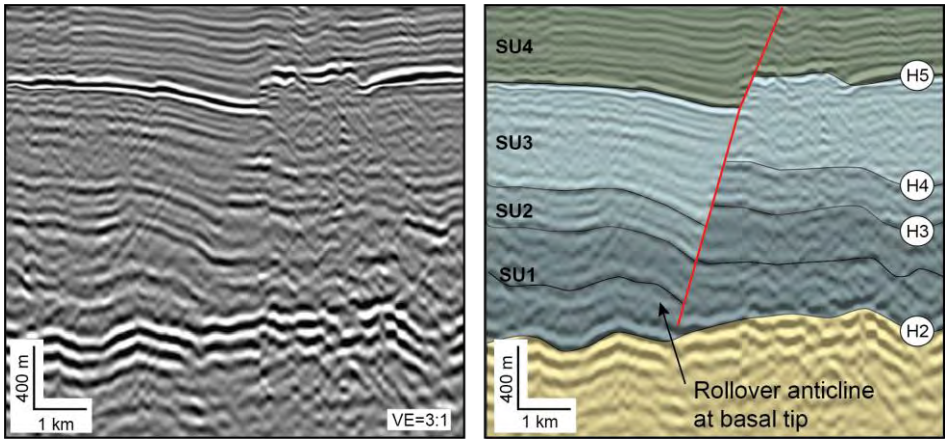

Figure 5.32: Seismic line taken from the MC3D-LEB2006 seismic cube showing a NW trending fault in zone A with a rollover anticline at its basal tip.

Zone B

The normal faults having a polygonal planform geometry are found in zone B and are best illustrated using a coherence attribute slice at H5 (base Miocene) in the MC3D-LEB2012 seismic cube (Figure 5.28). These faults are 2-3 km long, have a spacing of 1-2 km and a dip of 60°. They show a curved pattern (Figure 5.33), resembling an open, immature polygonal fault system with a high proportion of unrestricted lateral tips [e.g. *Cartwright et al.*, 2003; *Cartwright*, 2011].

These faults are predominant in SU3 and extend to SU1, SU2 and SU4 (Figure 5.30). They do not reach neither H2 (Eocene unconformity) nor H8 (base Messinian). Some faults are only found in the Oligocene tier and others also extend upward to the

Miocene tier, dying out before reaching H6 (Base mid-Miocene), terminating in monoclinal tipline folds. Depth sections at different horizons (Figure 5.33) illustrate well their distribution within the stratal units and their relative orientations.

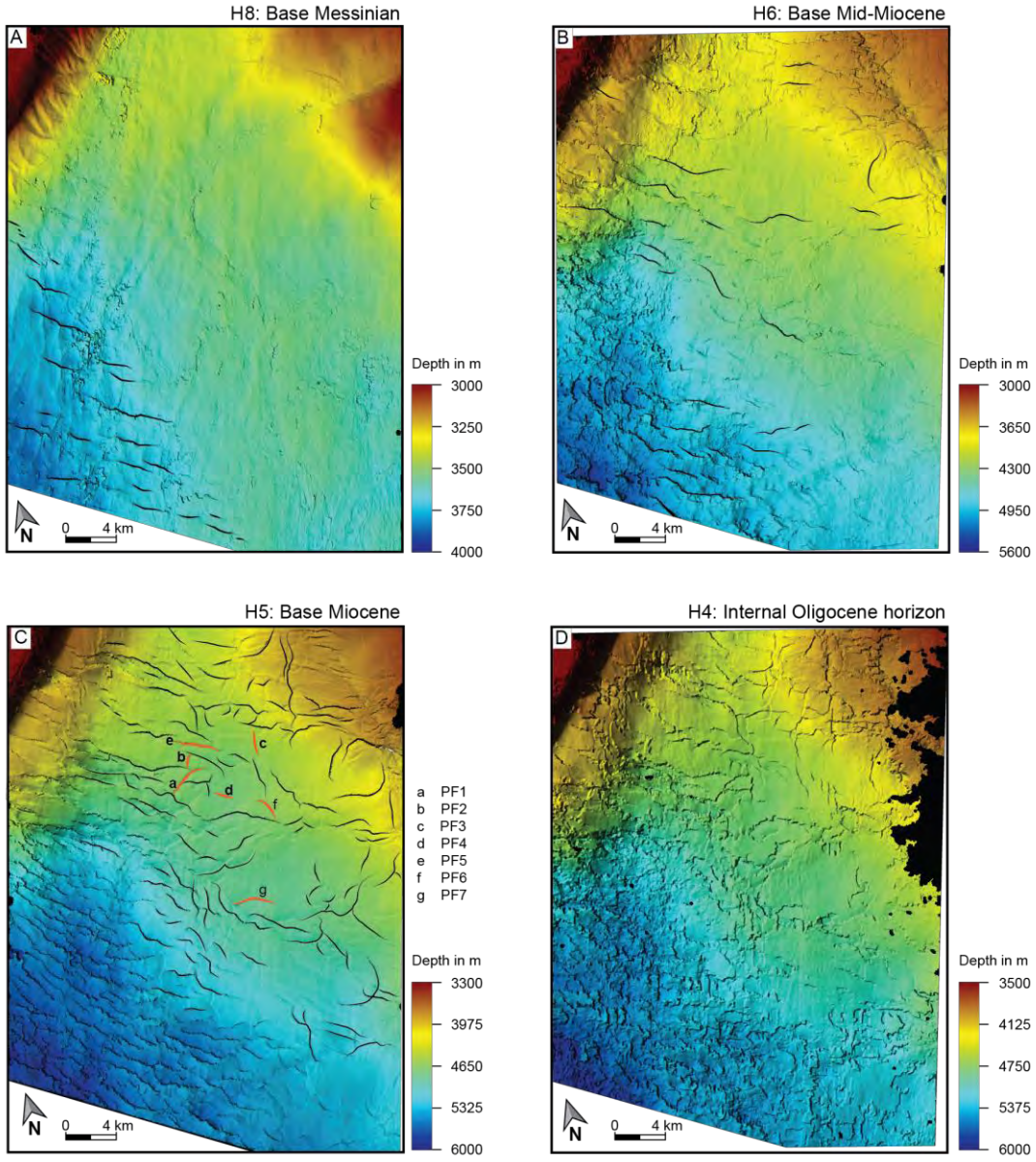

Figure 5.33: Depth structure maps of (a) Base Messinian showing the presence of limited NW trending normal faults crosscutting this horizon; (b) base mid-Miocene which is crosscut by few normal faults trending NW-SE; (c) base Miocene showing polygonal planform geometry of normal faults cross-cutting this horizon, and (d) an internal horizon in the Oligocene unit showing the distribution of normal faults with polygonal planform geometry, only found in the Oligocene unit. Thus, polygonal faults disappear in the Miocene unit, which is only characterised by NW trending normal faults. For location, see figure 5.28.

Thickness variation along fault planes

In order to understand the growth history along normal faults, expansion (EI) and growth indices (GI) plots were constructed following the method of Thorsen [1963] and Childs *et al.* [2003](Figure 5.34). These methods allow constraining the timing of activity along normal fault planes by comparing thickness variations of the same units between the hangingwall and footwall of faults.

In zone A, the calculated ratios indicate increased hanging wall thickness for SU4, SU5 and SU6 (interpreted Miocene units). In contrast the underlying SU2 and SU3 (interpreted Oligocene units) have an overall constant thickness while SU1 shows a negative ratio. Looking in details, very few faults show minor thickening along SU3.

In zone B, EI plots were constructed along 100 faults. All faults show no hangingwall thickening in SU1, SU2 and SU3 while ten show minor thickening in SU4.

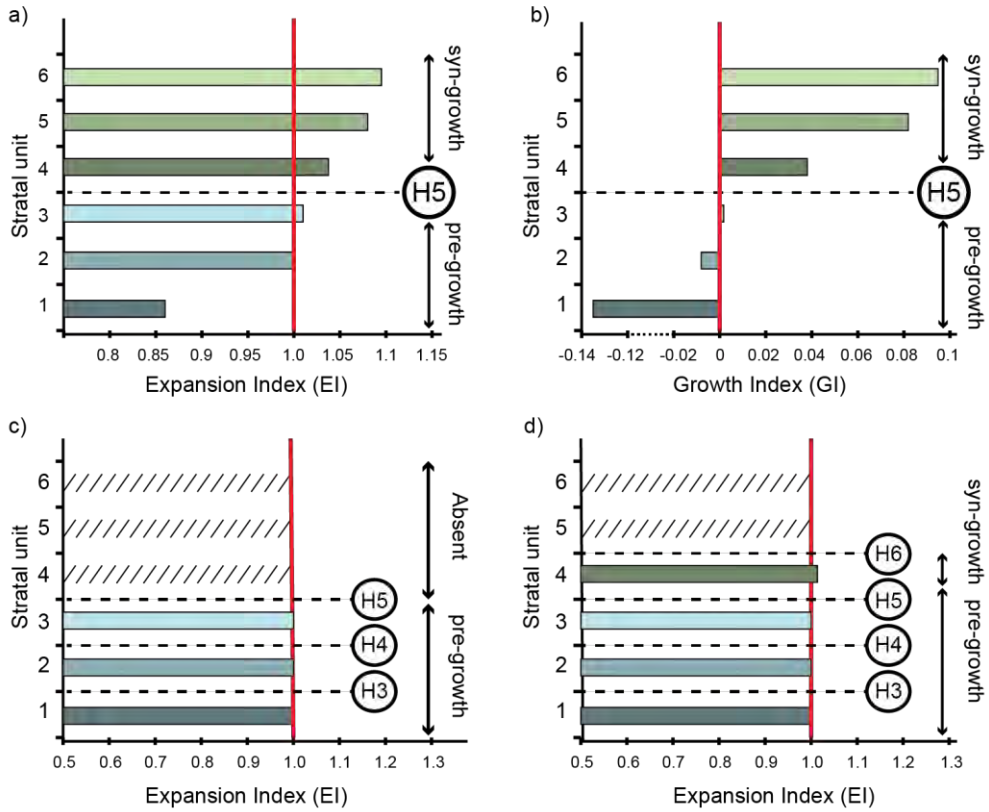

Figure 5.34: (a) Average expansion index (EI) and (b) growth index (GI) plots for faults in zone A showing thickening of units in SU4. Minor thickening is also noticed in SU3 over some faults. (c) average EI plot for faults only contained in the Oligocene tier (SU1, SU2 and SU3) of zone B, and (d) average EI plot for faults that are found in both the Miocene and Oligocene tiers (SU1, SU2, SU3 and SU4) of zone B. For (c) and (d), a total of 100 faults were averaged.

Displacement vs length relationship

Dmax/L diagrams for 100 faults in zone A and B were constructed on log-log and normal plots (Figure 5.35). Most of the faults used in this plot are single slip surface and are isolated, i.e. not forming relay geometries with nearby faults. We also included six segmented faults (including F7, F8 and F9) composed of two or three soft-linked segments forming relay bends geometries.

The log-log plot shows a linear relationship between the length of the faults in zone A and their displacement (Figure 5.35). This trend follows the scaling relation $D=0.03.L^{1.02}$ which is almost the same to the best fit curve $D=0.03.L^{1.06}$ calculated by Schlische *et al.* [1996] over a compilation of a global dataset from published materials (Figure 5.35a). On the normal plot, some scatter is observed in the data of zone A as faults with a large length (>8km) are under-displaced for their lengths (Figure 5.35b).

In contrast, the faults in zone B follow a different trend with a best fit line $D=0.64.L^{0.53}$ in the log-log plot (Figure 5.35a) with a slope value of 0.53 close to the one calculated by Nicol *et al.* [2003]. In the normal plot, the faults of zone B follow a best fit line of y=0.0083x+22 accumulating little displacement with increased length.

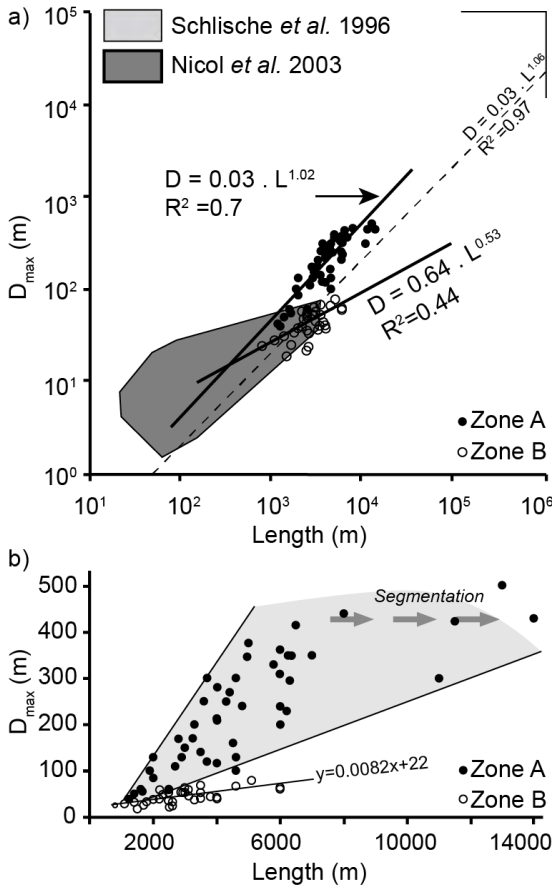

Figure 5.35: Dmax/Length plot for 100 faults from the Levant Basin, in both zone A and B. In (a), log/log plot showing a linear trend for faults in zone A with a best fit line of $D=0.03.L^{1.02}$ very close to the trend line of Schlische *et al.* [1996] over a global dataset. The faults in zone B follow a linear trend with a best fit line of $D=0.64.L^{0.53}$ which has a slope close to the one suggested by Nicol *et al.* [2003] of 0.6. Plots can be compared with those of Schlische *et al.* [1996] and Nicol *et al.* [2003] (shaded areas). Best fit line for data of zone A is shown as a heavy solid line while the best fit line of Schlische *et al.* [1996] is shown as a dashed line. In (b), normal plot for all faults in this study showing the effect of segmentation in zone A creating faults which are underdisplaced for their lengths.

Lateral variations in throw and throw gradients

Lateral variations in displacement were investigated along 13 faults in zone A and seven faults in zone B. Displacement/length (D-L) profiles were constructed within the six stratal units (SU1 to SU6) in order to map the variation of displacement within every tier. We chose to show profiles of SU3 and SU4 only as they are representative of the Oligocene and Miocene tiers respectively (Figures 5.36 and 5.37). The seismic sections were spaced every 100 m to map in detail the variation of displacement.

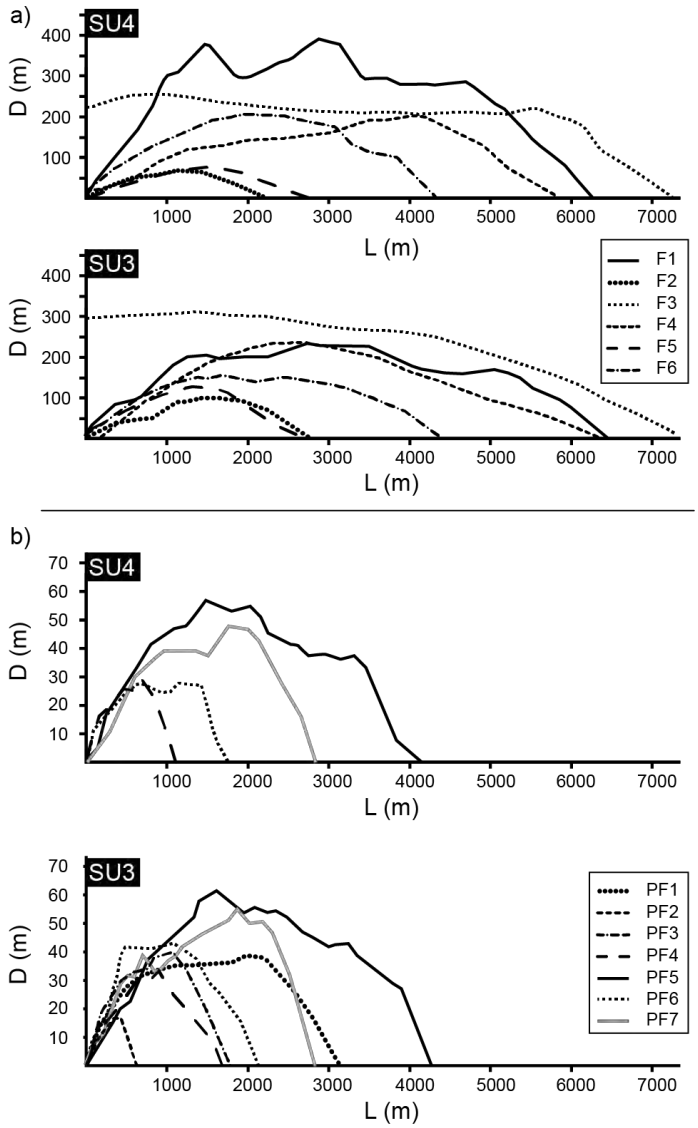

Figure 5.36: (a) displacement/Length (D-L) profiles of six faults in zone A taken along SU3 (Miocene) and SU4 (Oligocene). These profiles are flat-toped for lengths larger than 5000 m. (b) D-L profiles of seven faults in zone B taken along SU3 (Oligocene) and SU4 (Miocene). These profiles also look flat-topped.

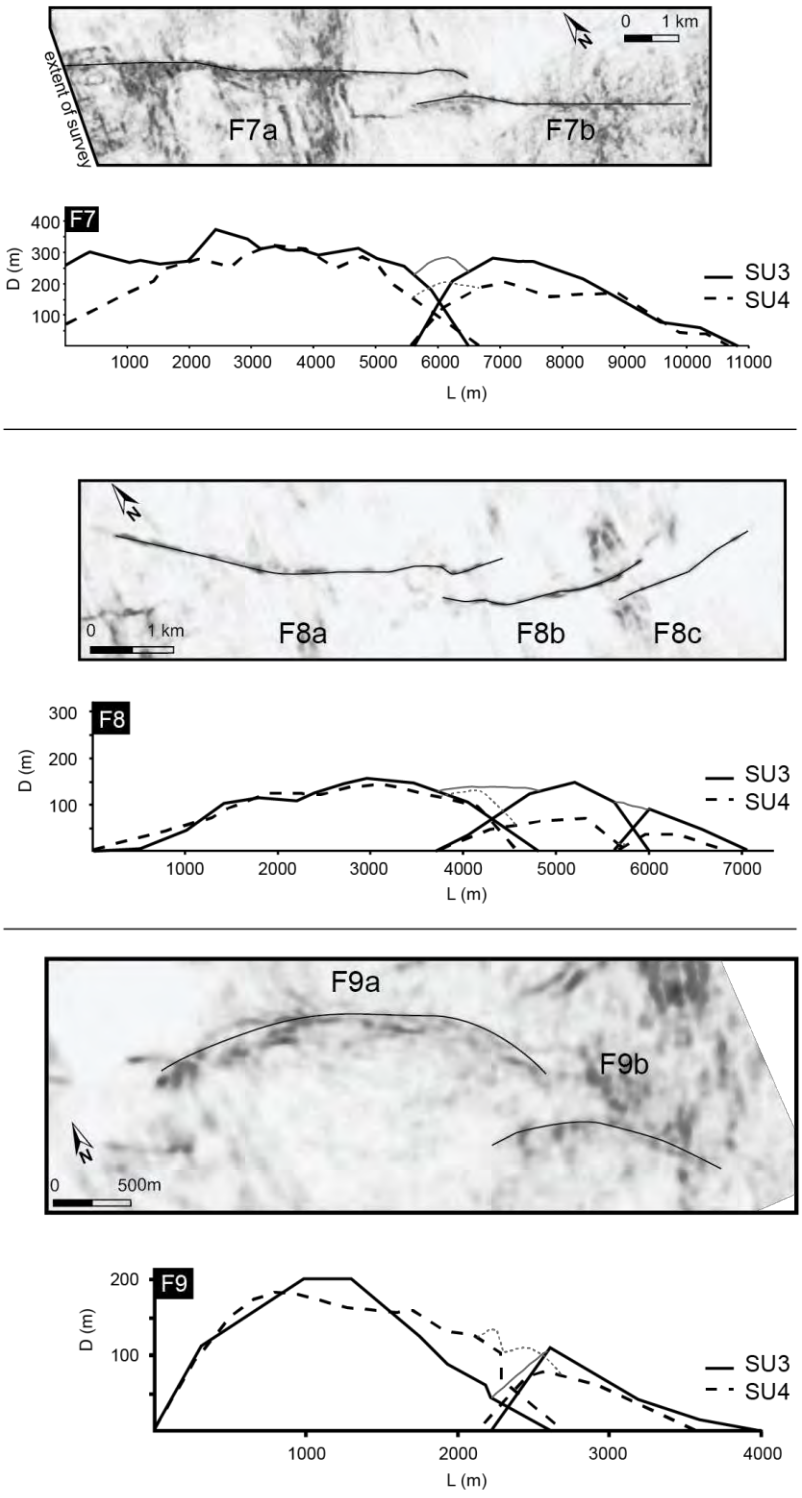

Figure 5.37: D-L profiles of three NW trending segmented faults in zone A taken along SU3 (Oligocene) and SU4 (Miocene). These faults are soft-linked in depth. After construction of the aggregate profile, the faults look like C-shaped, although individual segments are flat-topped.

Zone A

The maximum displacement recorded among investigated faults is 415 m, with a Dmax average of 200 m (Figure 5.36). It appears that faults shorter than 5km display a C shape profile whereas faults longer than 5km are generally flat-topped with an almost uniform throw distribution for >50% of the profile (Figure 5.36). This observation is valid for both the Oligocene and Miocene tiers.

The average displacement gradient within SU3 and SU4 was calculated for all the investigated faults (Figure 5.38). Away from the central part of the fault, displacement gradients vary between 0.1 and 0.13 towards both the SE and NW tips. A relatively high lateral displacement gradient (0.18) is particularly observed in SU5.

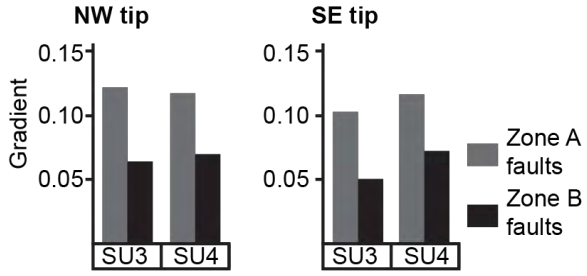

Figure 5.38: Average lateral tip gradients of the investigated faults in zone A and B. The faults of zone B exhibit a smaller lateral gradient than the faults of zone A which are considered as high gradients if compared to published literature.

Zone B

Faults on this zone show flat-topped D-L profiles [e.g. *Muraoka and Kamata*, 1983] (Figure 5.36). The maximum displacement observed is 63 m with an average of 40 m.

The average displacement gradient within the Oligocene and Miocene tiers (as observed in SU3 and SU4) varies between 0.05 and 0.075 (Figure 5.38) and are similar along either tip. The displacement gradient is slightly higher in the Miocene tier. These gradients are half those observed for faults in zone A.

Vertical variations in throw and throw gradients

Displacement-depth (D-z) profiles were constructed to investigate vertical variation of displacement along faults and their associated gradients (Figure 5.39). The profiles were constructed at the location of maximum displacement along the faults in both zones.

Zone A

The D-z profiles are M-shaped and are characterized by two distinctive displacement maxima along the fault plane at two separate structural levels: (i) in the Miocene tier, and (ii) in the Oligocene tier. These displacement maxima are separated by distinct displacement minima that occur close to H5 (base Miocene), even if the folding component due to breached monocline geometries (Figure 5.40) has been included in the displacement measurement.

Throw gradients were calculated on the upper and lower tips of D-z profiles (Figure 5.41) and are characterized by: (i) average throw gradient of 0.2 along the upper tip of faults, and (ii) average throw gradient of 0.37 along the lower tip of faults. This values are close to the upper bound of the published one, sometimes exceeding it [*Peacock and Sanderson*, 1991; *Nicol et al.*, 1996; *Roche et al.*, 2012b]. This is even more true for the lower tips that show abnormally high throw gradient values on some faults (0.56-0.57), larger than the throw gradients of the upper tip (5.41).

Zone B

D-z profiles along faults in zone B are C-shaped [e.g. Muraoka and Kamata, 1983] and show only one displacement maxima, in contrast with the faults of zone A. This displacement maxima is mainly located in the Oligocene tier with only one exception in fault PF4 (Figure 5.39).

The maximum displacement recorded on faults in zone B is 60 m, with an average of 35 m. This is strikingly smaller than the displacement of zone A. Displacement gradients were calculated on the upper and lower tips of D-z profiles and are characterised by average displacement gradient of 0.1 along the lower tips and 0.16 along the upper tips of faults (Figure 5.39). Such values are significantly lower than faults in zone A.

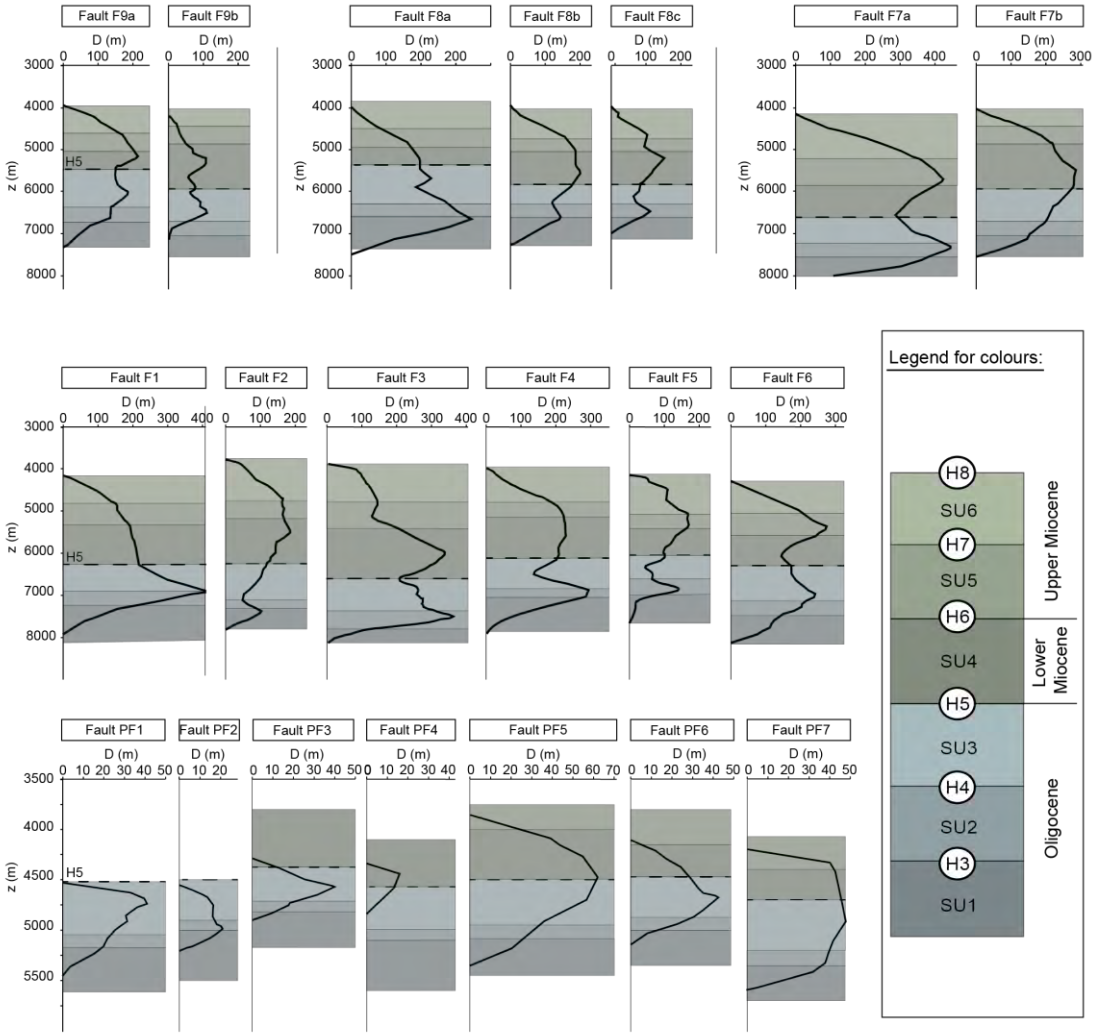

Figure 5.39: Displacement/depth (D-z) profiles of the 20 faults documented in this study. F9, F8 and F7 are segmented fault. F1, F2, F3, F4, F5, F6 and F7 are NW trending isolated faults in zone A. Their profiles show the presence of two displacement maxima. Faults PF1, PF2, PF3, PF4, PF5, PF6 and PF7 are faults with polygonal planform geometry in zone B. Their profiles show the presence of only one displacement maxima and have a C-shape distribution.

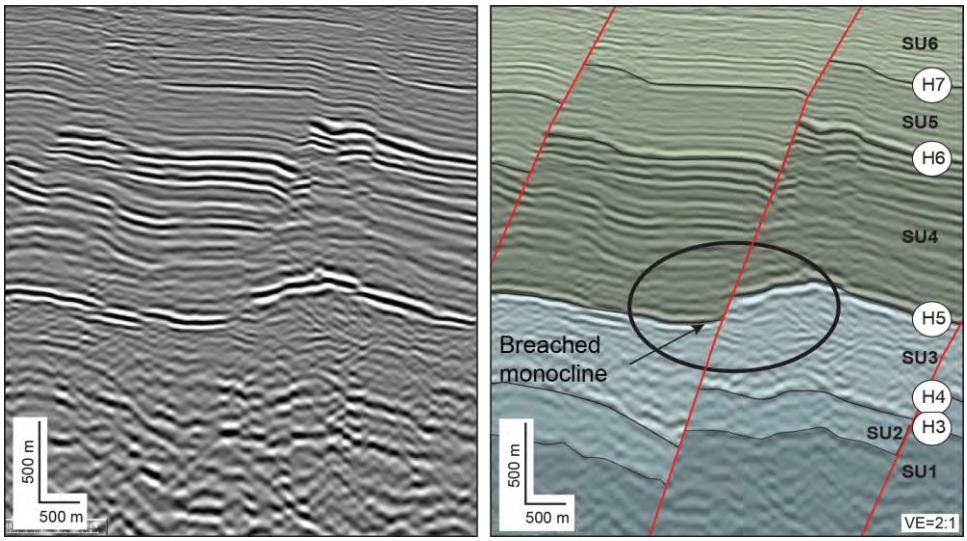

Figure 5.40: Seismic section taken from a NW trending normal fault in zone A showing the presence of breached monocline geometries commonly seen along H5 horizon.

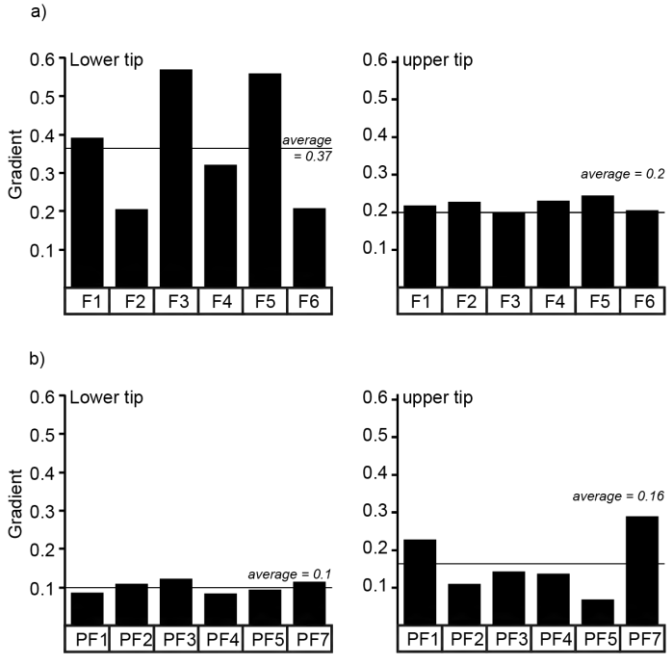

Figure 5.41: (a) Average vertical gradients of the investigated faults in zone A. These gradients are very high and indicate vertical restriction to fault propagation. (b) Average vertical gradients of the investigated faults in zone B. These gradients are smaller than faults in zone B.

V. 2.6 Evolution of the normal fault array

Trigger of faulting

In the previous section, we presented the characteristics of the normal faults array observed in the Levant Basin, which can be used to propose a model explaining their formation and growth. The key characteristics are as follow:

- Faults are layer-bound;
- They are regionally distributed and found in the whole Levant basin;
- Their distribution is correlated with the thickness of the host sediments;
- The host sediments are believed to consist of fine-grained sand;
- Faults are synsedimentary for almost half of their activity time in the basin;
- Basal tips show rollover anticlines in the hanginwall;
- A small region close to the Lattakia Ridge contains faults with a polygonal shape in map view.

The observations mentioned above are characteristic of polygonal faults in terms of timing and distribution [*Cartwright and Dewhurst*, 1998; *Cartwright et al.*, 2003; *Cartwright*, 2011]. The main difference with polygonal faults is their dominant NW trend. Such an aligned orientation is most likely a result of the NW-SE compressive stress field in the basin [*Barrier and Vrielynck*, 2008; *Ghalayini et al.*, 2014; *Montadert et al.*, 2014] causing a heterogeneous horizontal stress field. It is common for polygonal faults to be locally re-oriented in zones of subtle stress field variations [*Hansen et al.*, 2004; *Hansen and Cartwright*, 2006; *Cartwright*, 2011; *Carruthers et al.*, 2013], though such well oriented polygonal faults were never documented on a basin scale before. We suggest that the NW trending normal faults of the Levant Basin have a similar origin than classical polygonal faults but as they lack the typical polygonal planform geometry, we propose to call them 'contractional layer-bound normal faults' to avoid confusion.

This hypothesis is further supported by the presence of normal faults with typical polygonal planform geometry close to the Lattakia Ridge (Figure 5.28) [e.g. *Cartwright and Dewhurst*, 1998; *Lonergan et al.*, 1998; *Cartwright et al.*, 2003]. These faults are different from faults in zone A since they are smaller in length, shorter in height and with a markedly smaller displacement as we stated in previous paragraphs. They are found mainly in the Oligocene unit, and occasionally extend to the lower Miocene. This is not surprising because the Miocene is much thinner and most probably contains coarser sediments in the northern part of the basin due to its proximity to a northward sediment input source [*Hawie et al.*, 2013]. In contrast, the remainder of the basin was likely subject to sediments coming in from different sources during the Miocene, such as the Nile Delta [*Hawie et al.*, 2013]. In fact, thickness variations of individual tiers and sediment size have important effect on the

development of polygonal fault systems as faults are not developed in thin tiers and coarse-grained units [*Cartwright and Dewhurst*, 1998; *Cartwright et al.*, 2003; *Cartwright*, 2011]. The relationship between the faulting environment and the geometry of faults is summarised in table 5.3.

Table 5.3: *Relationship between fault geometries and host rock properties*

	Miocene Sediments	***Unit thickness***	***Fault geometry***
Zone A	Fine grained Pelagic to hemi-pelagic sediments	Miocene 2-3 km thick	Linear faults, oriented NW-SE probably due to a regional anisotropic stress field, cross-cut all Miocene
Zone B	Probable coarse grained lithology due to proximity to LRS	Miocene <1 km thick	Polygonally shaped faults probably due to local isotropic stress field close to LRS, Cross-cut mainly Oligocene and Lower Miocene

In summary, the lack of any regional extension documented in the Levant Basin during the Oligo-Miocene and the large geometric similarities between these faults and PFS, strongly suggest that these faults have a mechanism similar to that of PFS and related to volumetric contraction of the Oligo-Miocene (for a review see Goulty 2001, Goulty 2008, Cartwright *et al.* 2003, Cartwright 2011, Cartwright & Lonergan 1996).

Nucleation and mechanical stratigraphy

The following observations on the NW trending faults of zone A show a strong correlation with the layering of the sedimentary package where the faults are embedded:

- D-z plots and throw projection contours with two distinct displacement maxima in the Oligocene and Miocene tiers (Figure 5.39);
- More or less square shaped fault planes with aspect ratio close to 1 (Figure 5.31);
- Frequent breached monoclines close to H5 horizon (Figure 5.40).

Such observations are typical of dip linkage and/or reactivation of vertical fault segments [e.g. *Baudon and Cartwright*, 2008c; *Jackson and Rotevatn*, 2013; *Tvedt et al.*, 2013] (Figure 5.42). They demonstrate that the normal fault system in zone A was strongly influenced by mechanical stratigraphy (Figure 5.42).

The two distinct displacement maxima in the Miocene and Oligocene tiers (Figure 5.39) indicate that nucleation of faults could have happened in these two tiers independently. Such preferential nucleation is widely documented from dataset derived from outcrops at the meter scale [*Peacock and Zhang*, 1993; *Wilkins and Gross*, 2002; *Ferrill and Morris*, 2003]. Similarly, the aspect ratio of the NW-SE trending faults close to 1, and their square fault plane shape, are unusual for unrestricted normal faults that grew by radial tip propagation [*Rippon*, 1984; *Barnett et al.*, 1987; *Walsh and Watterson*, 1988]. Such observations can be explained by having two isolated fault segments growing by vertical propagation of the tip line as advocated by Mansfield & Cartwright (1996), which later joined to form a through-going fault as observed now.

This growth model with preferred nucleation of fault segments in two distinct tiers demonstrates that a strong mechanical contrast exists between these units (Figure 5.42). Even though such a scenario should result in a variation of fault dip in stronger and weaker layers leading to widely documented "staircase geometries" as seen on outcrops [*Ferrill and Morris*, 2003; *Schöpfer et al.*, 2007], the seismic resolution makes it challenging to look into that in our scale. The displacement minima and the monoclinal breaching seen along H5 indicate that this horizon might constitute the transition between units of differing mechanical properties, and hence a zone of linkage between hard-linked individual segments [*Peacock and Sanderson*, 1994; *Cartwright et al.*, 1995; *Gawthorpe et al.*, 1997; *Baudon and Cartwright*, 2008a] (Figure 5.42). The strong impedance contrast between low amplitude semi-continuous reflectors to continuous medium to high amplitude reflectors along H5 further supports a lithological change between the Oligocene and Miocene units, hence the mechanical decoupling between these units.

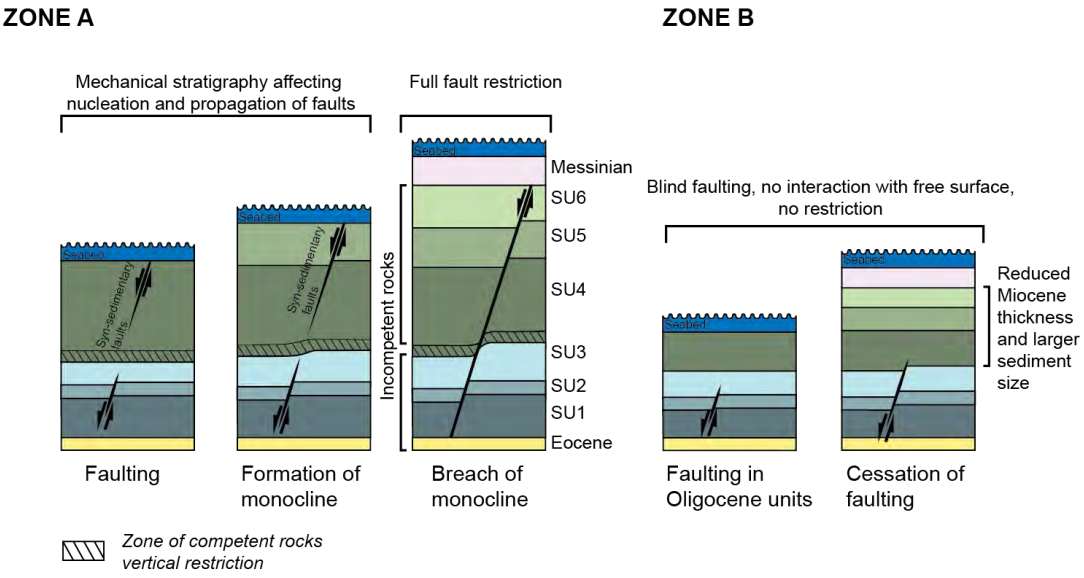

Figure 5.42: Proposed model for the evolution of the normal faults in the Levant Basin consisting of nucleation during the early Miocene in the Miocene and the Oligocene units simultaneously. This is due to anisotropic mechanical stratigraphy. The faults later propagated and vertically linked to form a sing throughgoing fault in zone A. In contrast, the faults in zone B were blind and unrestricted during their growth. In map, view, the orientation of these faults might be related to strong horizontal stress field anisotropy in zone A caused by the regional NW-SE compression during the Oligo-Miocene, while in zone B, the proximity to LRS might have caused local stress field fluctuations which resulted in polygonal planform geometry.

In contrast, the normal faults of zone B are more ellipsoidal and show only one displacement maxima (Figure 5.31 and 5.39). This could be related to lithological changes in this area influenced by the close proximity of the Lattakia Ridge shedding coarser sediments at the toe of the fold and thrust belt. Nucleation of faults has most likely occurred at the location of highest displacement in SU3 in this zone [e.g. *Walsh and Watterson*, 1989; *Cowie and Scholz*, 1992b] (Figure 5.42).

Timing and growth of the normal faults

The lack of growth strata in the faults of zone B implies that these structures never interacted with the free surface and hence limits our ability to constrain their age. However, we speculate that they grew during the early Miocene since some faults show minor amount of growth during this time. This is in accordance with observations on faults in zone A which show synsedimentary growth starting the early Miocene.

After proposing in previous paragraphs that the NW trending faults in zone A consisted of vertical linkage of segments, two models could hence be responsible for their evolution: (i) primary nucleation and blind propagation of faults segments in the Oligocene, followed by nucleation and syn-sedimentary propagation of fault segments in the Miocene, which also propagated downward and reactivated the Oligocene segments following the "reactivation by dip linkage" model of Baudon & Cartwright [2008b]; (ii) simultaneous nucleation during the early Miocene of faults segments in both the Oligocene and Miocene tiers due to anisotropic mechanical stratigraphy. The segments in both tiers grew by vertical propagation and joined together to form one fault system. In this model, the Miocene segment propagated upward as a growth fault while the Oligocene segment propagated upward as a blind fault (Figure 5.42).

Two key observations argue against Oligocene blind faulting followed by reactivation of fault segments during the Miocene in zone A: (i) no single normal fault is found only in the Oligocene unit (SU1, SU2 and SU3). If Miocene faulting reactivated existing faults, then we would expect a small number of faults to remain in the Oligocene inactive [*Baudon and Cartwright*, 2008c]. Instead, all faults are crosscutting the Oligocene and Miocene units entirely and fault segments are well aligned; and (ii) there is no proof for any faulting activity during the Oligocene. For this reason we postulate that the normal faults growth have initiated in the early Miocene.

The Base Messinian (H8) and the Eocene unconformity (H2) are key horizons in term of the fault growth. These horizons are not allowing the fault to propagate upward and downward, which is indicated by the high vertical tip gradients in D/Z profiles. This layer bound geometry is particularly observed along faults in zone A. Unable to propagate upward and downward due to this vertical restriction, the faults in zone A continue to propagate laterally till they interact with other NW trending faults, resulting in relatively high lateral tip gradients among all faults. Some faults, such as F7, F8 and F9, became even fully segmented in map view, consisting of soft-linked fault segments with relay bends in between. Segmentation of faults has most probably happened late in the faults history. D-L profiles show that faults with lengths >5,000 m exhibit flat-topped profiles, indicating that faults started to interact with each others when they reach a certain length, around 5,000 m. This is evidence that faults were radially propagating and were growing like blind faults [e.g. *Barnett et al.*, 1987; *Walsh and Watterson*, 1988].

During the Messinian, it is possible that the faults were still growing as evidenced by small deformation of Messinian markers (horizons with strong impedance

contrast) close to H8 (base Messinian) on top of big faults. The minor displacement along the base Messinian horizon (H8) along big faults, is another proof of syn-sedimentary activity mainly during the Miocene, and indicates that faulting have taken place before the deposition of the Messinian. However, the majority of faults in the basin are not segmented. Only few show a segmented geometry with horizontal relays between segments. This indicates that the faults reached an early stage of maturity, and became inactive in the early Messinian. If faults kept growing during the Messinian and Pliocene, then we would expect today to find a fully segmented fault pattern in the whole basin [e.g. *Walsh et al.*, 1999, 2003].

V. 2.7 Discussion

Volumetric contraction

In the previous sections, we presented the characteristics of the contractional normal fault array observed in the Levant Basin and proposed an evolution model for these faults. This model involves dip-linkage of normal fault segments nucleating in preferential units during the early Miocene. The planform geometry of these faults is very much affected by the presence of an anisotropic horizontal stress field, making them well-oriented and linear.

High vertical tip gradients (>0.2), especially in the Oligocene tier (average 0.37 and > 0.6 on two faults), measured at the faults in zone A is similar to other fault systems whereby high values were documented in incompetent units [*Wilkins and Gross*, 2002; *Wibberley et al.*, 2007; *Ferrill and Morris*, 2008; *Roche et al.*, 2012b]. Similarly, the 45° dip for faults in the Oligocene and Miocene tiers is in range for faults nucleating in soft and incompetent units [*Ferrill and Morris*, 2003; *Schöpfer et al.*, 2007; *Roche et al.*, 2012a]. Such observations suggest that the Oligocene and Miocene units consist of incompetent rocks at the time of faulting. The low seismic amplitude with continuous to chaotic reflectors observed in the Oligocene unit is also indicative of fine grained hemipelagic sediments [*Hawie et al.*, 2013]. The vertical restriction to propagation of faults into the underlying Eocene units has very likely contributed as well to the high displacement gradients. The Miocene unit shows relatively lower vertical tip gradients (average 0.2) close to the contact with the Messinian, suggesting a less pronounced vertical restriction and/or a slight facies change between the Miocene and the Oligocene. The latter is in accordance with the high amplitude continuous horizons observed in the Miocene sequences suggesting distal sheeted turbidite lobes

and basin floor fans [*Hawie et al.*, 2013] and indicating mud/clastic rich units [*Reading and Richards*, 1994; *Hawie et al.*, 2013] with potentially more clastic input. Such rock units were deposited during a period of uplift and erosion along the margin resulting in high sediment input and rapid deposition [*Hawie et al.*, 2013, 2014].

The fine-grained sedimentary facies characterising the Oligo-Miocene units in the Levant Basin are commonly associated with PFS worldwide [*Cartwright*, 2011]. Even though the mechanism behind PFS is still debated, we believe that volumetric contraction and eventual pressure change is responsible for the nucleation of these faults in the Levant Basin. Shallow diagenetic processes were suggested to explain such volumetric contraction in fine-grained rock sequences [*Shin et al.*, 2008; *Cartwright*, 2011], which lead to porosity reduction and shear failure. Such a model might explain the presence of contractional layer-bound normal faults in the Levant Basin, although well and core data are needed in order to check this hypothesis.

Between the Oligocene and Miocene tiers, displacement minima occur along H5 (Base Miocene horizon) along faults in zone A. The strong impedance contrast and the thick reflectors are likely the effect of a sandstone unit at the Base Miocene. If faults were caused by volumetric contraction and its associated mechanisms, which is directly related to the sedimentary facies, then sandy units will be barriers to fault propagation. With increasing displacement, faults will ultimately breach the sandy unit and join together. This has been documented offshore Norway whereby polygonal faults nucleating into two independent tiers separated by a thick sandy unit, were observed to transect the sand and join together [*Stuevold et al.*, 2003]. Such mechanical stratigraphy consists of faults nucleating in incompetent rocks (i.e. compliant and weak rocks like clays) while competent rocks are barriers to fault propagation [e.g. *Wilkins and Gross*, 2002; *Ferrill and Morris*, 2003]. This depends primarily on the strength, elastic parameters and relative proportions of the mechanical layers and the differential stress experienced by such layers [*Ferrill and Morris*, 2003; *Roche et al.*, 2013]. This is usually documented in detritic systems which is likely the case in the Oligo-Miocene sequence of the Levant Basin [*Hawie et al.*, 2013].

Generally, the PFS documented around the world contain faults smaller both in length and in height [*Cartwright*, 1994; *Lonergan et al.*, 1998; *Watterson et al.*, 2000; *Nicol et al.*, 2003; *Stuevold et al.*, 2003; *Hansen et al.*, 2004; *Shin et al.*, 2010; *Carruthers et al.*, 2013]. The normal faults in the Levant Basin accumulate large displacement (up to 400 m) and might thus be considered as the largest contractional layer-bound normal faults documented so far. We attribute this large fault size to be a product of vertical

linkage of individual segments due to mechanical stratigraphy and thick succession of suitable lithology (≈ 3 km) for the formation of such faults, allowing them to accumulate large displacement. The fact that smaller faults with classical polygonal geometry are found in a small region in the basin supports our hypothesis that a constitutive genetic mechanism explains the faults in both zone A and B (i.e. polygonal and linear faults). Thus it is not surprising if these faults will become preferentially reoriented and linear especially given that a regional anisotropic stress field is documented during the Oligo-Miocene [e.g. *Ghalayini et al.*, 2014].

Although we believe that local stress field variations resulted in faults with polygonal planform geometry close to the Lattakia ridge, this situation is in fact intriguing. In all the cases around the world, we find that isotropic horizontal stress fields result in classical polygonal faults in the basin, which become re-oriented and linear close to large geological structures (for a review see Cartwright, 2011). Why should we observe the opposite in the Levant Basin? An explanation could be that faults formed over a slope during the Oligo-Miocene resulting in faulting in preferred direction parallel to the slope while closer to the Lattakia Ridge the paleotopography was flat and faults are hence polygonal. However, this seems unlikely since the linear and well-oriented faults in zone A do not have a preferred dip direction. Thus, the most likely explanation is that large structures, such as the Lattakia Ridge, have increaseed Sh_{min} to equal Sh_{max} and created an isotropic horizontal stress field whereas the distal part of the basin underwent a normal stress regime.

Growth of contractional faults

The geometry and the displacement distribution along fault planes suggest that the faults were physically isolated and later grew by segment linkage which is in accordance with the isolated fault model [*Cartwright et al.*, 1995; *Mansfield and Cartwright*, 2001; *Baudon and Cartwright*, 2008a]. In zone A, the presence of mature soft-linked fully segmented faults together with immature isolated faults that just started to interact with nearby structures, proves that these faults did not link until relatively late in their history. The Dmax/L log/log plot shows that faults in zone A were accumulating displacement with length increase, following a best-fit line of $D=0.03.L^{1.02}$ (Figure 5.35). Such a value is very close the one calculated by Schlische *et al.* [1996] of $D=0.03.L^{1.06}$ by plotting a global dataset. They suggested that scaling relationship between length and displacement of faults is linear regardless of scale, which

necessitates that $n \approx 1$ in the $D=c.L^n$ law a value also suggested in other studies [*Kim and Sanderson*, 2005; *Soliva and Benedicto*, 2005; *Schultz et al.*, 2006; *Soliva et al.*, 2008]. By following the same trend line on the plot (Figure 5.35), the linear and well-oriented faults of zone A are not different than faults seen in different regions and hence grow by simultaneously accumulating length and displacement. The only difference is that the other faults are tectonic faults while the Levant Basin's are caused by volumetric contraction.

In the normal plot, some faults in zone A are underdisplaced for their lengths causing some scatter in the plot (Figure 5.35b). This is particularly observed for faults with L > 7000 m. These faults are segmented normal faults, consisting of two or three segments with soft relay bends in between. Thus, these faults gained considerable length after joining with nearby segments without accumulating much vertical displacement. This is in agreement with period of fault growth during which the D-L evolution is non linear [*Soliva and Benedicto*, 2004; *Roche et al.*, 2012b]. This explains some of the scatter in the dataset for particularly large faults [e.g. *Cartwright et al.*, 1995].

In zone B, however, Dmax/L plots follow a different trend than zone A. The trend line $D=0.64.L^{0.53}$ exhibits a slope value of 0.53 very similar to the one suggested by Nicol *et al.* [2003]. They calculated a best fine line of $D=0.09.L^{0.6}$ for a set of polygonal faults in the Lake Hope region of South Australia. The difference in our study is the *c* value of 0.64 compared with their lower value of 0.09. This could be due to some variations in rock types between both study areas as *c* is generally related to rock properties [*Schlische et al.*, 1996]. The slope value <1.0 over polygonal faults of Lake Hope was attributed to an increase in fault dimensions due to linkage which created underdisplaced faults [*Nicol et al.*, 2003]. Even though that the investigated faults in zone B were not linked as the one in Lake Hope, we believe that a certain degree of interaction and communication is established between faults early in their history. This is observed in D-L plots whereby some displacement profiles were flat-topped similar to other profiles of polygonal faults in literature [*Nicol et al.*, 2003; *Nelson*, 2006] indicating increase and tendency for linkage with maturity of the system [e.g. Cartwright 2011]. Regardless of this linkage from early on and potential early interaction, we believe that faults accumulated displacement with length and hence grow following the isolated fault model. A similar study by Nelson [2006], and to a lesser extent Stuevold *et al.* [2003], showed similar aspect ratios, elliptical shapes and concentric contour patterns as the faults in zone B (Figure 5.31) suggesting an early stage of fault evolution for these faults typical of blind and isolated normal faults [*Barnett et al.*, 1987; *Walsh and Watterson*, 1988]. It is also difficult to consider that faults were initially part of a coherent fault

system without having pre-existing structural grain and fault reactivation [*Walsh et al.*, 2002]. Instead, polygonal faults grow radially and start to interact quickly with nearby segments, hence the low $n < 1.0$ value.

The suggested growth models draw a similarity between the layer-bound contractional faults of the Levant Basin and global dataset. Where faults show a polygonal planform geometry, they exhibit similar D-L profiles and growth curves with other PFS [*Nicol et al.*, 2003; *Nelson*, 2006], which is caused by early linkage and interaction. However, when subject to an anisotropic horizontal stress field, the faults become linear and parallel in planform, and show a very similar growth pattern with tectonic normal faults elsewhere [*Cowie and Scholz*, 1992a; *Schlische et al.*, 1996]. We believe that such an anisotropic stress field has important effect on the growth of layer-bound contractional faults as it delays early linkage since faults are not curved. Instead, faults will accumulate displacement proportionally to length and link later on during their history. It's important that additional 3D seismic interpretation targets the displacement variation on contractional polygonal faults in general, and contractional linear faults in particular. This could be established by interpreting linear and well-oriented faults at the lateral end of PFS in some localities, in order to check if similar results and growth pattern are seen in contractional faults in other basins.

V. 2.8 Conclusion

This study has provided detailed analysis on the geometry and growth of a contractional layer-bound normal fault array in the Levant Basin. By performing various 3D interpretation techniques such as displacement-length, displacement-depth and expansion and growth indices, we were able to discuss and present the temporal and spatial evolution of this normal fault system. Observations indicate that these normal faults are caused by volumetric contraction or pressure changes and are very much affected by the presence of a regional NW-SE stress field, hence their orientation. These normal faults are thus a special type of stress induced well-oriented polygonal faults that we termed contractional layer-bound normal faults.

We propose that the normal faults nucleated during the early Miocene in the lower Miocene and Oligocene units simultaneously. Their displacement distribution attests to mechanical stratigraphy in the basin which controlled their preferred nucleation sites. This has also resulted in vertical dip-linkage of individual segments. Horizontal segment linkage took place later in their history, and some faults became

fully segmented. We concluded that the growth of contractional layer-bound normal faults follows the isolated fault growth model on a basin scale during their early history. When subject to a regional anisotropic horizontal stress field, they behave similarly to tectonic faults.

END OF ARTICLE 2

CHAPTER VI

DISCUSSION

Table of contents

VI. Discussion

"Read not to contradict and confute; nor to believe and take for granted; nor to find talk and discourse; but to weigh and consider" Sir Francis Bacon

This section summarises the different work undertaken in this project and correlates it with existing studies on the tectonic evolution of the Levant and north-western Arabian region. Seismic interpretations together with analogue modelling are integrated in order to provide a coherent geodynamic and structural model of the Levant region during the Cenozoic. The outcome of this contribution aims to understand a basin's structural deformation evolution and associated styles through looking at the development of a nearby major plate boundary. In other words, this understanding can be used to discuss to which extent the deformation recorded in a sedimentary basin is impacted by the tectonic activity of nearby plate-scale structures. This provides very examples of the imprints of plate boundary evolution on the deformations observed in surrounding basins. More specifically, this section will discuss how our integrated workflow serves to reduce uncertainty and provide an answer to major geological problems regarding the evolution of Levant Basin, bordering the Levant Fracture System, which is a major N-S transform fault forming the NW Arabian plate limit with Africa.

Very few studies were targeted to understand the tectonic setting of the offshore Levant region from geophysical data. Carton *et al.* [2009] argue that the LFS plate boundary extends offshore Lebanon, consisting there in a NNE trending offshore thrust system termed Mount Lebanon Thrust (MLT) ~10 km away from the Levant margin. They propose that this thrust system is currently active and responsible for the uplift of Mount Lebanon. Their hypothesis is based on the interpretation of shallow 2D seismic reflection lines. In the southern Levant Basin offshore Israel, more studies are available which resulted in better understanding of the tectonics of the Levant [e.g. *Gardosh and Druckman*, 2006; *Gardosh et al.*, 2008a, 2010; *Segev and Rybakov*, 2010] . Offshore Israel, the mapped structures are mostly NNE trending faults, horsts and grabens, interpreted

as Mesozoic rift structures reactivated during the Late Cretaceous and Tertiary [*Gardosh et al.*, 2010].

In this study, the tectonic setting of the Levant Basin is based on the interpretation of high quality ~12 sec twt industrial 2D and 3D seismic reflection data. The usage of 3D data had a great advantage as it allowed visualising structures in different orientations and in 3D. This had reduced uncertainty substantially and provided an opportunity to unravel the tectonics of the basin. Thus, a more refined and clearer scenario for the evolution of the Levant Basin could be proposed.

The study by [*Kosi et al.*, 2012] evidenced that the Levant basin is also deformed by a regional and dense normal fault spanning all over the basin but restricted to the Oligo-Miocene series As their approach was not targeted to explain the mechanism responsible for the nucleation and growth of these normal faults, they nonetheless made an interesting analogy with the Canyonlands faults. They suggest however, that the Levant's Basin normal faults were triggered by the Messinian Salinity Crisis [e.g. *Hsu et al.*, 1973] whereby the sudden pressure drop within the Cenozoic strata associated with the desiccation of the Mediterranean caused an isostatic rebound of the crust. The detailed geometry and characteristics of these faults coming out from this study evidenced that they developed earlier in Miocene time. We discuss bellow likely scenarios and mechanism for their nucleation and growth. As there are no well data in the basin, all the timings proposed in this study are not well-constrained and adopted from Hawie *et al.* [2013].

VI. 1 An updated structural model of the Levant region

VI. 1.1 Basin Geodynamics

Offshore LFS and successive Cenozoic plate-related deformation

The Levant Basin offshore Lebanon contains a variety of structures within a relatively thick Cenozoic rock sequence (reaching about 5 km). Disregarding the normal faults discussed in the following section, these include NNE trending folds and thrust faults, and ENE-WSW striking dextral strike-slip faults. All the structures appear to be intermittently active since the Mesozoic.

In this study, the largest movement on the NNE-SSW thrusts offshore northern Lebanon was documented to be before and during the Miocene whereas they were inactive during the Pliocene. An earlier movement is suspected in the Late Cretaceous and Eocene/Oligocene times. It is not clear what is the role of these thrusts in the uplift of the adjacent Levant margin (and Mount Lebanon), but it is very likely that they contributed to the structuration and minor uplift of the margin in the Oligocene.

Such an ancient structuration of the margin was proposed by Dubertret [1955] and more recently by Hawie *et al.* [2013a] who advocated that the Levant margin has been subject to minor uplift in Eocene and Oligocene. Their study is based on micropalaeontology and investigation of the Tertiary sedimentary facies. Indeed, the presence of open marine Miocene facies along the margin in contrast with restricted and continental Miocene facies in the Bekaa valley east of Mount Lebanon, indicate that there must have been a topographic barrier between the margin and the inner shelf (modern Bekaa valley and inland Syria) that explains this facies differentiation during the Miocene. Similarly, the angular unconformity between Lutetian and Burdgalian in northern Lebanon (Figure 6.1) and erosion of the majority of the Oligocene unit in Lebanon [*Boudagher-fadel and Clark*, 2006; *Homberg et al.*, 2010; *Müller et al.*, 2010; *Hawie et al.*, 2014] also attest to a minor orogenic phase during the Oligocene.

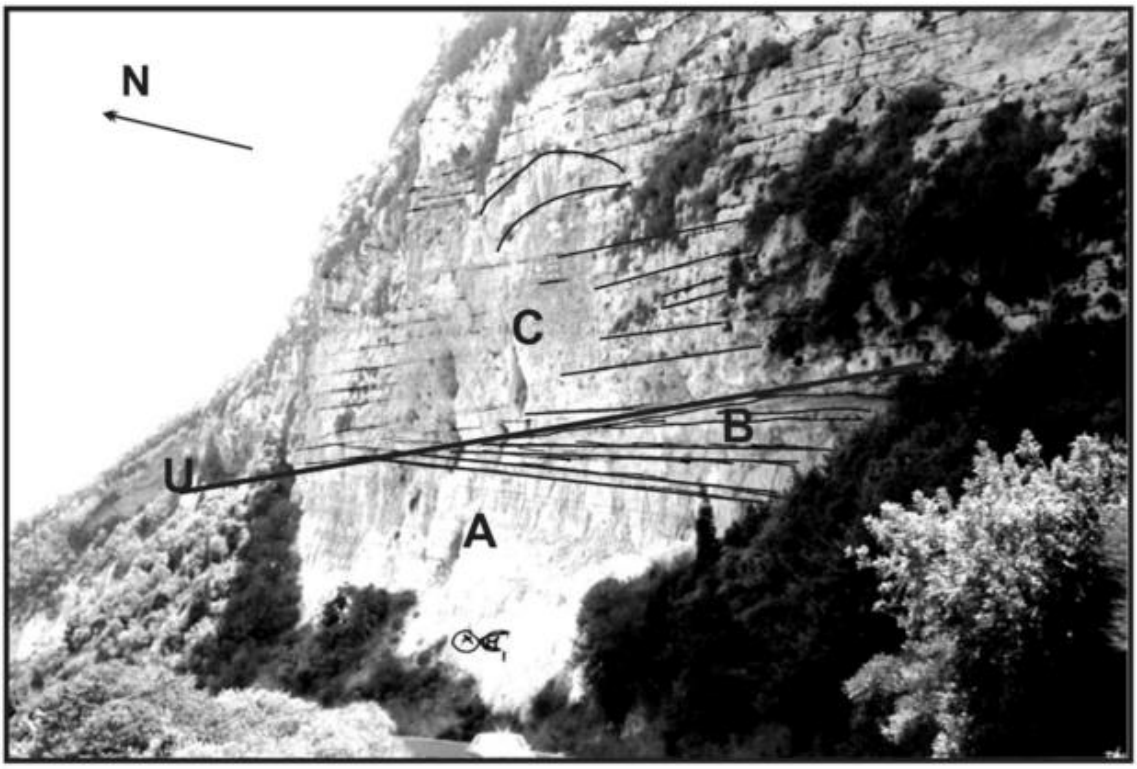

Figure 6.1 : Angular unconformity in northern Lebanon between the Early Lutetian (B) and the overlying Middle to Late Burdigalian (C). The angle of the unconfomirty is ~ 15°. From Boudagher-fadel and Clark [2006].

These observations indicate that the Levant margin has been deformed prior to the onset of the Levant Fracture System. Several authors argue that uplift and deformation took place exclusively in the Late Miocene as a result of transpression [*Butler et al.*, 1998; *Daëron et al.*, 2004; *Elias et al.*, 2007; *Gomez et al.*, 2007b]. Indeed, transpression caused a rapid uplift of Mount Lebanon starting the Late Miocene, but initial deformation started much earlier, probably by the Late Cretaceous. These tectonic movements are linked to major geodynamical events affecting the Arabian plates during the Eocene/Oligocene till Early Miocene. These times witnessed the initial collision between Arabia and Anatolia [*Allen and Armstrong*, 2008; *Barrier and Vrielynck*, 2008; *Frizon de Lamotte et al.*, 2011] coincident with the opening of the Red Sea [*Bellahsen et al.*, 2003; *Cochran and Karner*, 2007]. Thus, far field tectonic stresses have caused the contraction of the Levant margin and initial structuration of Mount Lebanon during the Oligocene/Early Miocene, synchronously with inversion in the Palmyrides [*Chaimov et al.*, 1990; *Brew et al.*, 2001b]. However, the ENE-WSW dextral strike-slip faults also show evidence for vertical movement during the Oligocene (Figure 3.12) synchronously with movement along the NNE-WSW striking thrust faults. The occurrence of both structures simultaneously active and under a NNW trending

compression is not mechanically easy. Thus, some periods of normal movements and localised extension might possibly be present during the Tertiary.

The NNE trending anticlines were folded during the Late Miocene and Messinian only, with no evidence for their current activity. They were linked to an evolving regional stress field caused by the Levant Fracture System (LFS). They thus serve to accommodate counter clockwise block rotations along the margin due to transpression. A major finding of this study is that the offshore part of the LFS also includes several kilometre long ENE-WSE dextral strike-slip faults with lateral offsets of 1-2 km. We could not observe direct arguments allowing to date their early movement, but a very recent activity is suggested by the deformation of the seabed coupled with active seismicity. Overall, the exact age of deformation along the LFS has been under debate especially in Lebanon. In Israel, transform activity postdates the 22 my old diabase dykes of Eyal *et al.*, [1981] and has most likely initiated during the Early Miocene [*Freund et al.*, 1970; *Steckler and ten Brink*, 1986]. In Lebanon, the activity along the Lebanese segment is only indicated through sporadic angular unconformities between Quaternary and Tertiary units, making the determination of the exact age of transpression slightly unclear. For example, it is known that the effects of the Levant Fracture System have initiated in the Late Miocene/Pliocene [*Walley*, 1988; *Butler et al.*, 1998; *Griffiths et al.*, 2000; *Daëron et al.*, 2004; *Gomez et al.*, 2006] in the form of transpression affecting the Lebanese mountain range. Similarly, the Yammouneh fault was initiated probably in the post-Langhian [*Homberg et al.*, 2010] or Pliocene [*Hancock and Atiya*, 1979; *Quennell*, 1984]. The results of this study indicated that the basin and the deformation of other structures were directly affected by activity on the restraining bend. This activity must have started in the late Miocene, prior to the Messinian event. Thus, this study provided an updated and clearer timing for the activity of the Levant Fracture System at the latitude of Lebanon.

Evolving regional dynamics during the Pliocene caused by continuous collision of Arabia and Eurasia [*Le Pichon and Kreamer*, 2010], together with the westward escape of Anatolia [*Sengor et al.*, 1985] and the sinistral reactivation of the Lattakia Ridge System [*Hall et al.*, 2005a] had all large impacts on the entire NW Arabian plate. In this study, the Levant Basin was investigated and the interpreted structures were linked to this regional geodynamic evolution. Notably, the cessation of folding and thrusting in the basin was correlated with these regional events and provided further constraints on the activity of the LFS in Lebanon. Thus, the second phase of LFS movement is very likely to have initiated during the Pliocene. In the basin, this activity is evidenced by ENE-WSW dextral strike-slip faulting along old reactivated faults only.

The cessation of folding in the basin during the second phase of LFS activity in the Pliocene suggests that either no regional NW-SE compressive stress field is prevalent in the basin during this time, or that the stress field was not strong enough to cause shortening. If such compression is still ongoing with the same rates as during the Oligocene, it should be expected that the folds in the basin were still deforming. However, this NW-SE compression, which started in the Late Cretaceous, shows no evidence of its persistence till the Pliocene and modern times, whereby the stress field probably became isotropic away from the LFS. It is likely that the NW-SE or the NNW-SSE compression is absent in the basin and is only evidenced along the margin during the Pliocene and is related to transpression along the LFS [*Eyal and Reches*, 1983; *Eyal*, 1996; *Homberg et al.*, 2010].

Deformation in the deep Levant Basin

The normal faults were described in detail in chapter 5. Several explanations can be taken into account, the most important scenarios are discussed below and summarised in the following table 6.1.

Table 6.1: *some mechanisms that might results in the occurrence of normal faults in the basin*

Mechanism	*Arguments for*	*Arguments against*
Rifting	Synchronous extension and rifting in the Red Sea	No crustal faults, absence of extension onshore, Red Sea did not propagate through Gulf of Suez
Tectonic flexure	Mantle plume regional uplift documented during the Eocene and Miocene	No crustal faults, faults are well oriented and not concentric
Gravity driven detachment	Faults are detached on the Eocene Unconformity horizon	Faults are not parallel with the slope of the margin
Messinian related isostasy	Crustal uplift is triggered by removal of ~ 2 km of water column	Faults nucleated during the Early Miocene in the basin before the Messinian times, no crustal faults

The most evident mechanism for the occurrence of normal faults in general is related to extension and rifting caused by tectonic plates movement. In fact, the western edge of the Arabian plate is marked by rifting along the Red Sea starting in the Oligocene [*McKenzie et al.*, 1970; *Cochran and Karner*, 2007]. The NW-SE direction of the Red Sea rift is parallel to the trend of the normal faults array of the Levant Basin and thus we can argue that the rifting has extended northward to the Levant Basin causing minor NE-SW extension and faulting. However, two arguments disprove this scenario: (1) for rifting related extension and normal faulting, faults must be deep and found along at least the whole upper crust. In the Levant Basin the faults are layer-bound and confined to the Oligo-Miocene units only. No normal faulting is observed in the underlying units. (2) The Red Sea rift was not able to propagate through the Suez and to the Mediterranean due to differing lithospheric mechanical strength between the Mediterranean and the Sinai/Red Sea [*Steckler and ten Brink*, 1986]. Instead, the rift shifted northward to Aqaba and initiated the LFS. If rifting between Arabia and Africa propagated to the Mediterranean, then the LFS would not have been present today and the plate boundary will be in the Mediterranean.

Another scenario for the evolution of these faults might be related to crustal flexuration in the East Mediterranean. Analysis of isopach maps of the Tertiary sequence in the Levant Basin indicate a different sedimentary depocenter location in the Eocene/Oligocene and Miocene (Figures 3.9 and 5.29). During the Eocene, the depocenter was located at the north of the basin close to the Lattakia ridge while in the Miocene it shifted to the center of the basin (Figure 5.29). Such observation might indicate a certain plate flexure followed by subsidence by Miocene times in order to explain such thickness variations. Could there be a large flexure in the Late Cretaceous/Early Tertiary that affected the style of sedimentation and caused the observed thickening and thinning of strata? The subduction of the African lithosphere below the Eurasian one started in the Late Cretaceous [*Frizon de Lamotte et al.*, 2011]. Thus, thickening of Lower Tertiary units close to the Lattakia Ridge is expected. By the Early Miocene, collision of Arabia with Anatolia has affected the geodynamics of the region and has probably caused subsidence in the Levant Basin, which explains the thickening of Miocene sediments. However, subsidence should result in faults having no particular orientation, in contrast with the linear orientation of the normal faults in the Levant Basin. Furthermore, the faults should also be crustal and not confined to particular units, which is not the case. Thus, this scenario is unlikely to have been responsible for normal faulting in the Levant.

The third scenario is gravity sliding. The normal faults die out on the Eocene unconformity horizon, which is a detachment surface (Figure 5.30) [*Lie et al.*, 2011; *Hawie et al.*, 2013; *Montadert et al.*, 2014]. During the Miocene and up till modern times, the Levant margin has been under quick uplift resulting in the tilting of the margin along an E-W direction [*Sanlaville*, 1974; *Gomez et al.*, 2006; *Hawie et al.*, 2013]. Thus, the Eocene unit is expected to dip westward, hence generating NNE trending normal faults that are parallel to the direction of dip [e.g. *Cartwright*, 2011]. However, the faults in the Levant Basin are trending perpendicular to the dip of the Eocene, hence negating any gravity effect on the nucleation and orientation of faults. Furthermore, the Eocene unit is only dipping along the margin where these faults are absent, and in the basin where these faults are abundant it is nearly flat. These faults do not show as well any preferential or regular dip orientation (Figure 5.30). Thus, gravity sliding is an unlikely mechanism for the nucleation of normal faults in the Levant.

Kosi *et al.* [2012] argue that the desiccation of the Mediterranean sea during the Messinian [*Hsu et al.*, 1973] has triggered the nucleation of normal faults. The evaporation of 2 km water-column during the Messinian could result in isostatic rebound due to decreasing weight on the crust. However, Ryan [2009] demonstrated that water unloading should be compensated by rapid salt precipitation refuting any significant rebound effect. Regardless of the amplitude of isostasy during the Messinian, this event requires that faults nucleate during the Messinian times, i.e. in the very Late Miocene, and requires also that the faults should be crustal. This is in contrast with observations on unit thickness variations along fault planes revealing that faults have nucleated in the Early Miocene (Figure 5.34). Furthermore, if the entire Mediterranean was desiccated and the Mediterranean crust underwent isostatic rebound, it should be expected that the whole Mediterranean should exhibit similar fault patterns, which is not generally the case. Thus, the Messinian event is unlikely to have been responsible for generating these faults, as they have nucleated much earlier.

Having discussed the different nucleation mechanisms in which the normal faults might have been associated with, it is very likely that the genetic mechanism must be constitutive rather than externally imposed. That means that nucleation of faults is related to the sedimentologic character of the Oligo-Miocene unit rather than being dictated by regional tectonics or crustal processes. This mechanism, discussed in detail in chapter 5 and described in a generic way under the term ‘volumetric contraction’ [e.g. *Cartwright*, 2011], entails important consequences on our understanding of the geodynamics of the basin and the nature of sediments during the Cenozoic in general

and the Oligo-Miocene in particular especially when combined with observations of other structures.

Synthesis: tectonic provinces in the Levant Basin and Mesozoic inheritance

Having discussed the occurrence of the various structures in the basin, several points were highlighted from the discussion above and are summarised in this section and in figure 6.2:

- Two important trends of structures are found in the basin (NNE-SSW and ENE-WSW) and attest to an old and well-marked structuration, probably dating back to Mesozoic times. These structures were intermittently active throughout geologic times, when reactivation conditions were favourable. During the Cenozoic, the Levant basin was divided into three provinces in relation with the transmission of the plate movement related stresses. The Mesozoic basin margin (eastern part) was incorporated in the LFS, the most north-western part (Lattakia ridge) accommodated the convergence between the African and Eurasian plates, whereas the deep Levant Basin was directly affected by the stresses from the adjacent major structures.

- A regional NW-SE compressive stress field is prevalent in the Levant Basin and probably the Lattakia ridge during the Oligo-Miocene. Today, there is no indication of shortening in this area but a NW-SE strike-slip regime may continue to exist. Eastward, the maximal horizontal stress curved to a NNW-SSE direction [*Homberg et al.*, 2010], probably highlighting stress deflection in Neogene times along the main NNE-SSW LFS faults.

- The deep Levant Basin was likely in a passive margin setting during and shortly prior to the Oligo-Miocene. No tectonic events have marked the deep basin during the Cenozoic. This has contributed to the development at regional scale of the dense network of layer-bound normal faults in the Oligo-Miocene. Such fault systems are widely documented worldwide in passive margin and foreland basins [*Stuevold et al.*, 2003; *Hansen et al.*, 2004; *HE et al.*, 2010; *Andersen and Huuse*, 2011; *Preto et al.*, 2011].

- The margin underwent accelerated uplift since at least the Miocene and probably in the Eocene as indicated by rapid sedimentation and deposition of materials eroded from the margin during the Eocene, Oligocene and Miocene

times. Such an uplifted was probably facilitated by the presence of NNE-SSW thrust faults along the Lebanese shoreline.

- Toward the Late Miocene, NNE trending anticlines were folded synchronously with the 1st phase of activity along the LFS. Their activity ceased, together with the thrust faults, in the Messinian or early Pliocene synchronously with major geodynamic changes in the region and the 2nd phase of activity along the LFS.
- The occurrence of the layer-bound normal faults necessitates that the Oligo-Miocene units should be composed of fine-grained sediments, such as clay and silt and fine-grained sand. Such lithologies were proposed by [*Hawie et al.*, 2013] based on seismic facies analysis. The Eocene is documented to be generally composed of compacted shale [*Lie et al.*, 2011; *Hawie et al.*, 2013; *Montadert et al.*, 2014] serving as a detachment surface for these faults.
- The only active structures today are ENE-WSW dextral strike-slip faults, which accommodate the counterclockwise block rotation of the margin as a result of transpression.

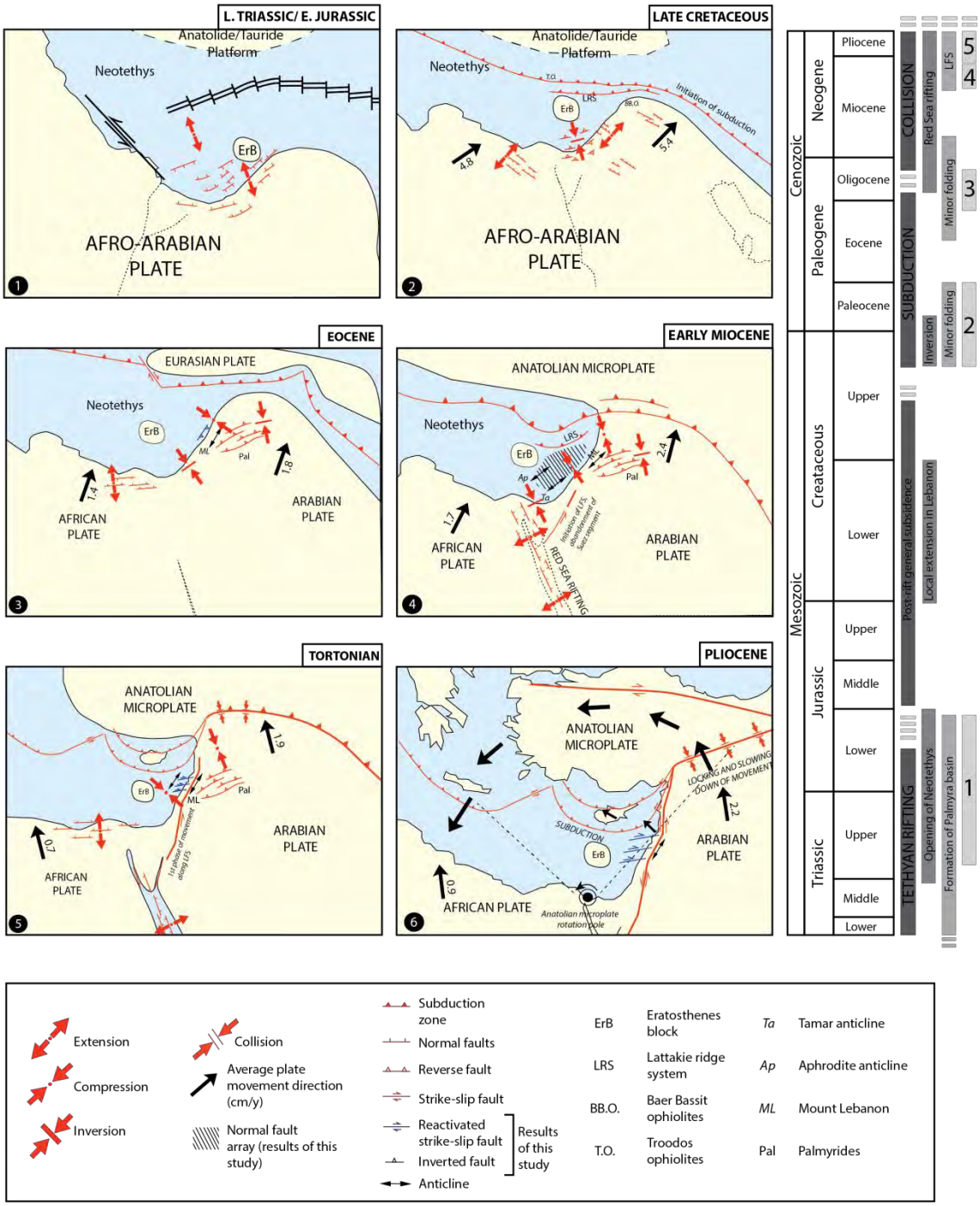

Figure 6.2 : Paleogeographic maps of the Levant region summarising the results of this study especially during the Cenozoic. The location of subduction zones, paleocostlines, and structures outside the study area are taken from Barrier and Vrielynck [2008]. (1) refers to the Mesozoic rifting event, (2) refers to the start of closure of Neotethys and convergence tectonics, (3) the initial structuration and folding along the Levant margin and Palmyra, (4) 1st stage of LFS movement and establishment of the restraining bend in Lebanon, and (5) 2nd stage of LFS movement and rapid uplift of the Levant margin.

VI. 1.2 Role of structural inheritance and the westward extension of the Palmyra Basin

Following the discussion over the tectonic history of the Levant basin, it is essential to complete the picture by looking at the evolution of its margin. Initial structuration of the margin started during the Mesozoic by the creation of small faulted blocks oriented roughly E-W with a gentle topography [*Dubertret*, 1955]. Following this idea, Collin *et al.* [2010] emphasizes the role of Late Jurassic structuration by documenting several E-W faults with Late Jurassic basalt in their fault plane, which confirms their activity during the Late Jurassic.

An important aspect of the geology of the margin that has long been overlooked is its close geographic location to the Palmyra Basin (Figures 1.1 and 2.2). This latter basin is an intracontinental rift in the north-western Arabian plate that initiated in the late Paleozoic. Mesozoic subsidence and Cenozoic basin inversion shortly followed rifting, and resulted in a fold and thrust belt termed the 'Palmyrides fold belt'. It must have had significant impacts on the evolution of the Levant margin, where both geological provinces intersect. The implications of the modelling performed in this study is important, as few authors tried to extend the Palmyra Basin westward to Lebanon [e.g. *Searle*, 1994; *Walley*, 1998; *Nader*, 2011] while most of the authors prefer to separate Lebanon from the Palmyra Basin, and choose to stop the Palmyrides ranges at the current border between Lebanon and Syria. The Levant margin in Lebanon is too small to be a geological province in itself. It certainly must have been affected by regional tectonics and was most likely part of larger geologic provinces such as the Palmyra Basin, transitioning to the Levant Basin further westward. The pre-existing structures must have played an important role in affecting the style of deformation along the margin, and resulted in the complex structural setting of the Levant region.

Rifting in Palmyra initiated in the Late Paleozoic and continued through the Late Triassic/Early Jurassic [*Ponikarov*, 1966; *Brew et al.*, 2001b; *Sawaf et al.*, 2001]. Subsequent subsidence was documented in the Jurassic and Early Cretaceous resulting in normal faulting [*Best et al.*, 1993]. At the end of the Cretaceous, the closure of the Neo-Tethys along the northern margin of the Arabian platform resulted in a compressive environment in Palmyra. This has resulted in the inversion of the Palmyrides fold belt in three distinct time periods [*Chaimov et al.*, 1992] (table 6.2).

Table 6.2: *the three inversion times documented in the Palmyra basin as a result of the closure of Neo-Tethys*

Time	*Effect*
Late Cretaceous	Minor, caused slight uplift of the SE Palmyrides
Middle Eocene	Minor, caused some Paleogene thickness variations
Early Miocene	Major, responsible for the uplift and erosion of the Palmyrides

The sedimentary sequence in Palmyra is 11 km thick with a depth to Moho of ~40 km [*Brew et al.*, 2001b]. The thickness of the crust gradually decreases westward to the Levant Basin, with ~35 km beneath the anti-Lebanon ranges, ~27 km beneath Mount Lebanon [*Khair et al.*, 1993] and ~20 km beneath the Levant Basin [*Hirsch et al.*, 1995; *Khair and Tsokas*, 1999; *Ben-Avraham et al.*, 2002]. Northern and southern Syria are two different crustal blocks sutured along the Palmyrides trend [*Al-Saad et al.*, 1992; *Sawaf et al.*, 1993; *Brew et al.*, 2001b], whereby bouguer gravity maps show variations in crustal properties between the north and the south of Syria (Figure 2.15).

The previous observations point to a common geologic history between the margin of the Levant in Lebanon and the Palmyra Basin. Both witnessed similar tectonic events with rifting and inversion. Several arguments, discussed in previous sections, point that the Levant margin was deformed and uplifted in the Lower Miocene similarly to the Palmyrides ranges. The crust is thinning to the west, indicating continuity in the Palmyrides trend toward the Levant Basin. Thus, it is not surprising if the Palmyra Basin extends westward to Lebanon, or at least to southern Lebanon if the sinistral 100 km displacement is taken into account [e.g. *Walley*, 1998], as they are both geographically very close and share similar geological history (Figure 4.7).

This hypothesis was tested by means of analogue modelling performed in this study, to particularly investigate the effects of the intersected Palmyra/Levant on the growth of the Levant Fracture System. First Results indicated geometrical similarities between the Levant restraining bend and that of the model, emphasizing the role of existing structures on the evolution of the restraining bend (Figure 4.14). These existing structures are very likely related to the structures in the Palmyra Basin, being remnant of the Mesozoic rifting event.

The segmentation of the LFS and the results of analogue modelling provide insights on the evolution of restraining bends in general. Initial structuration has important effects on the geometry of the popup. The orientations of existing structures

play an key role in controlling whether the structures will be reactivated or not. This study completes the one by Mattioni *et al.* [2007] whereby they tested the effect of pre-existing structures that are parallel to the main sinistral strike-slip and their reactivation. The modelling performed in this study investigated the effect of oblique structuration instead, and revealed to which degree they might affect the restraining bend. A future study should test the effect of existing folds and whether they affect the final geometry of the popup, and include the mantle in the model parameters.

VI. 2 Toward an integrated petroleum system model for the Levant Basin

The discovery of commercial quantities of hydrocarbons in the southern Levant Basin offshore Israel and Cyprus (~38 tcf of natural gas, www.noblenergy.inc) has made this area a frontier petroleum province. Nevertheless, the Levant Basin offshore Lebanon has never been drilled and still contains uncertainties for what concerns its petroleum reserves. For this reason, thorough and integrated geological investigations of the Levant Basin offshore Lebanon might reduce uncertainties on the petroleum system and provide preliminary ideas on potential plays.

Petroleum systems analysis should integrate the sedimentary and structural history of a basin, in order to better assess the prospectivity of frontier hydrocarbon provinces, such as the Levant Basin. Typical petroleum investigations are classified according to a hierarchy with an increasing economics significance [*Magoon and Dow*, 1994] (Figure 6.3):

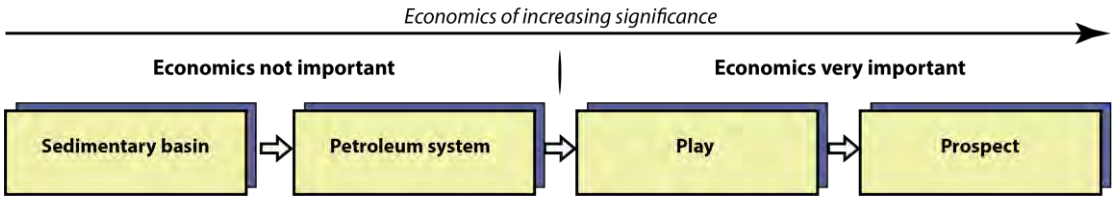

Figure 6.3: The four levels of petroleum investigation of Magoon and Dow [1994] defining the hierarchy in petroleum exploration relative to scale and economics.

The following sections discuss the existing literature regarding the source rocks and stratigraphy of the Levant Basin and the impact of structural interpretation on the petroleum system.

VI. 2.1 Review of the Levant petroleum system

The sedimentology and stratigraphy of the Levant Basin has been recently investigated by Hawie *et al.* [2014]. Through seismic interpretation, fieldwork in Lebanon and forward stratigraphic modelling of the sedimentary filling, a source to sink study was applied leading to a better understanding of the stratigraphic architecture and evolution of the basin. Hawie [2014] argues that its filling in the Miocene, has been achieved through several sources, namely a proto Nile delta, the Levant margin and Lattakia/Syrian coasts. This hypothesis has great implications on the expected Miocene sedimentary facies distribution throughout the basin, which are further constrained by seismic interpretation.

The source rocks of the Levant may consist of deeply-buried Triassic succession along the Levant margin possessing good characteristics. This unit may also contain evaporitic caprocks equivalent to those in Syria [*Nader and Swennen*, 2004]. Geochemical studies in the Turonian-Upper Campanian successions onshore northern Lebanon and Santonian-Paleocene in southern Lebanon revealed the presence of oil-prone type II kerogen-rich fine-grained carbonates and marls with very good source rock potentials [*Bou Daher et al.*, 2014, 2015]. However, they are not mature to generate hydrocarbon onshore. It is likely that more toward the west, this succession upon burial becomes more matured in the basin and hence could constitute a viable source rock. Bou Daher *et al.* [2015] suggest that the Upper Cretaceous succession has decreasing source rock properties and a shift in kerogen type toward the deeper parts of the basin. Thus, the Levant margin and inner shelf have the best Upper Cretaceous source rocks in terms of TOC and maturation upon burial when compared with the Levant Basin, and are thus classified as thermogenic source rocks. Other potential source rocks present in the basin are believed to include Lower Miocene shales [*Dolson et al.*, 2005; *Gardosh and Druckman*, 2006]. These source rocks could be of biogenic origin, in contrast with thermogenic sources of deeper units.

The complex faulting along the margin might constitute a pathway for petroleum charge from the deep basin to the margin onshore Lebanon (Figure 6.4). Onshore, potential traps might be the Qartaba structures and other anticlines, if a

proper seal is found and is capable to accumulate hydrocarbons [*Beydoun*, 1977]. In fact, a deep conductive layer in the Triassic rocks is suggested 650 m below the oldest outcrops in Lebanon [*Renouard*, 1955] and is interpreted to the analogue of the Triassic Kurrachine evaporites in Syria [*Beydoun*, 1977]. Thus, a regionally extent evaporite layer in the Triassic might be sealing all the pre-Jurassic strata along the margin. The Jurassic itself might not host any hydrocarbon accumulations because it was affected by an early phase of emergence and invasion by meteoric waters during the late Jurassic and by later meteoric flushing in the Cenozoic making it very permeable onshore Lebanon [*Nader and Swennen*, 2004].

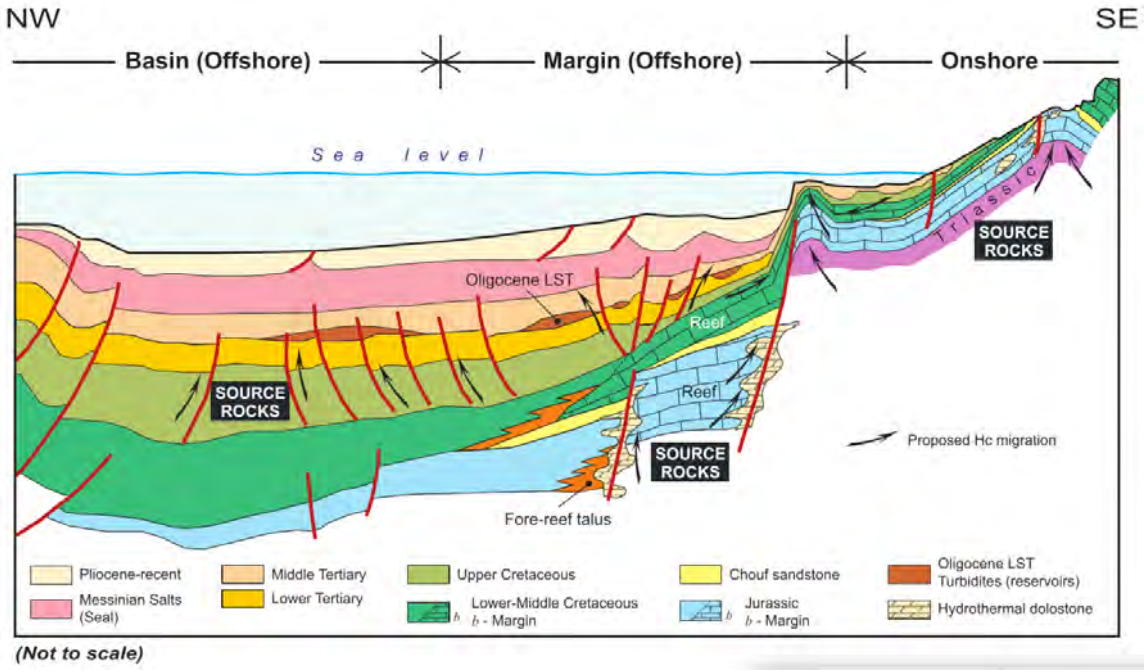

Figure 6.4: Simplified showing the effect of structures along the margin in hydrocarbon migration from the basin to the margin. The intense and inherited deformation along the margin should make these structres important fluid conduits since at least the Mesozoic. From [*Nader*, 2011].

VI. 2.2 Timing of trap formation

The NE trending anticlines form a series of 4-way dip closures and might thus constitute traps sealed by the Messinian evaporites. These structures were created during the Late Miocene and hence require a syn/post-Messinian charge. They could hold ~450 m of hydrocarbon column if they are filled-to-spill according to their amplitude. A key question is regarding the source rocks if a charge is capable of filling these structures to spill during the Messinian and Pliocene alone and whether the seals are capable of holding such a large hydrocarbon column.

ENE-WSW striking strike-slip faults create 2-way and 3-way closures sealed laterally by the fault itself. In the Upper Miocene and Pliocene, some faults result in Riedel-like folds resulting in 4-way dip closures. As these structures were active in the Late Miocene, they require a syn/post late Miocene charge. The ENE-WSW dextral strike-slip faults were inherited from Mesozoic times. Thus, their effect on the petroleum system might date as far back as the Jurassic time, being migration conduits for deeper Mesozoic source rocks.

Other structures such as NNE-SSW striking thrust faults also create 2-way and 3-way dip closures sealed laterally by these faults and by the Messinian evaporites on top. The thrust faults were active during the early Tertiary or Eocene, thus necessitating a charge that is syn/post Eocene. These hydrocarbon leads are perhaps more promising than the Late-Miocene 4-way and 2-way dip closures associated with the anticlines and the strike-slip faults since they have a longer charge period.

The normal faults may constitute a characteristic petroleum play known as 'tilted fault blocks' initiated in the Lower Miocene. It consists of Miocene reservoirs sealed either by intra-Miocene impermeable rocks or by the Messinian evaporites. The normal faults will thus serve as lateral barriers and seals, with important compartmentalisation effect as discussed in the following sub-section. The amount of hydrocarbon captured in these reservoirs is dependent on how much oil will be generated from the source rocks. As stated earlier, the Upper Cretaceous thermogenic source rocks are thought to have lower TOC and maturity in the basin [*Bou Daher et al.*, 2014, 2015]. Thus, it is unlikely that they could contribute much to charging Miocene reservoirs. However, other source rocks in the basin, such as biogenic Miocene shale, might charge the reservoirs in the Miocene rocks. The normal faults will also be conduits for vertical hydrocarbon migration, while being barriers to lateral flow causing strong compartmentalisation of the reservoirs (see below).

VI. 2.3 Implication of normal faulting

The 3D seismic characterisation of the normal faults revealed an effect of mechanical stratigraphy on their growth and evolution. They nucleated in incompetent units and joined vertically later along competent units. The location whereby these faults have joined are marked by thick reflectors with a strong impedance contrast, mappable throughout all the basin. Even though mechanical stratigraphy indicates units of varying mechanical strength and not absolute lithological units since several

lithologies could display similar mechanical strength, we believe that the competent units likely consist of sand. This interpretation is based on strong resemblance with published data with similar deformational patterns in the North Sea [*Stuevold et al.*, 2003]. Similarly, the adopted volumetric contraction model for the nucleation of these faults does not favour faulting in coarse grained sediments [*Cartwright and Dewhurst*, 1998; *Lonergan and Cartwright*, 1999]. Thus, the base of the Miocene unit could consist of a small sand unit ~100 m thick that might constitute a potential reservoir.

It is suggested that the contrast in fault densities could serve as a quick and efficient exploration tool to identify and locate coarser sand bodies in the fine-grained clay dominated units where these faults occur. Such mapping of sand becomes clearer when combined with other geophysical approaches, such as seismic amplitude and attributes analyses [e.g. *Lonergan and Cartwright*, 1999]. Thus, when the normal faults disappear in the Upper Miocene toward the north of the Levant Basin, it is possibly a result of sandy units in this region preventing their growth. A likely interpretation is that the proximity to a northern sediment source close to the Lattakia Ridge has resulted in coarser sediments in the Upper Miocene. This converges with the model of Hawie *et al.* [2013] who advocates a northern sedimentary source for the filling of the Levant Basin, hence the coarser units close to that source.

A direct and important effect of these faults is their ability to be important fluid pathways and to compartmentalise the reservoirs. The intersections between faults, especially in the north of the basin were they acquire a polygonal geometry, are likely to be sites for preferential fluid communication due to their branching. However, the occurrence of these faults in fine-grained sediments and clay, complicates the situation whereby the fault zone might contain what is referred to as 'shale smear' [*Aydin and Eyal*, 2002]. This shale will be incorporated in the fault zone and prohibits fluids circulation due to its low permeability. Since these faults are most likely caused by volumetric contraction of the host rock unit, it is expected that a large number of subseismic faults will be found in the Oligo-Miocene sequence. Having noted the low permeability that is likely associated with these faults, the reservoirs will thus be severely compartmentalised. A 3D representation of the base Messinian horizon shows how the anticlines are crosscut by these faults, probably making several smaller reservoir intervals, vertically displaced and hydraulically dissociated (Figures 6.5 and 6.6).

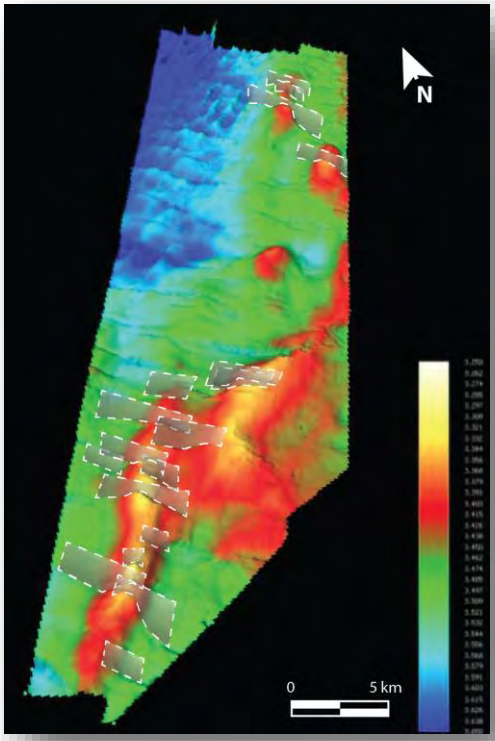

Figure 6.5 : Base Messinian horizon showing how anticlines are crosscut and segmented by the normal faults. The latter are creating compartments in the anticlines that are probably isolated and not hydraulically connected. Seismic figure courtesy of PGS.

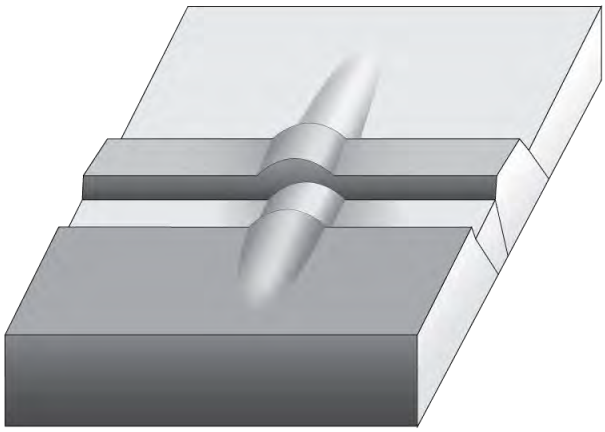

Figure 6.6 : Conceptual sketch showing the effect of the normal faults on segmenting the NNE-SSW trending anticlines, and compartmentalise reservoirs by vertically displacing and isolating them.

The generation of layer-bound normal faults in fine-grained strata will generate an extensive amount of fractures in the host rocks [*Cartwright*, 2011]. Hurst *et al.* [2003] argue that such fractures will facilitate the development of sand injectites, which are small lobes of sand formed by remobilization of sand from depositional units by fluidization. It is advocated that the mechanism of nucleation of layer-bound faults could result in sand injections [*Lonergan and Cartwright*, 1999]. Thus, these features might be present in the Levant Basin in association with layer-bound normal faulting, and are usually considered as good sand-rich reservoirs [*MacLeod et al.*, 1999].

VI. 2.4 Active faulting

The complex deformation history along the margin and the intermittent reactivation of the mapped structures result in a complex fault pattern both in the basin and along the margin. Some faults, such as the ENE-WSW striking strike-slip faults, show evidence of current activity. Their ongoing activity might result in continuous deformation in the adjacent reservoirs, causing hydrocarbon leakage [*Wiprut and Zoback*, 2002]. Furthermore, the salt motion in the Levant Basin, driven by gravity gliding due to continuous uplift of the margin [*Sanlaville*, 1974; *Gomez et al.*, 2006] and rapid Pliocene sediments deposition [*Gradmann et al.*, 2005; *Bertoni and Cartwright*, 2007; *Hawie et al.*, 2013] causes migration of salt towards the deep basin resulting in intense growth faulting in the Pliocene sequence along the margin [*Baudon and Cartwright*, 2008b; *Gvirtzman et al.*, 2014]. These two tectonic processes are the reason why the Levant margin offshore Lebanon is seismically active and provides a hazard for the positioning of offshore oilrigs. Large earthquakes offshore Lebanon were recorded in history causing significant damages along the coastline [*Elias et al.*, 2007]. If such seismic events occur during exploration or production, they could have devastating effects on oil infra-structures and the environment by spewing oil into the sea.

CHAPTER VII

CONCLUSION

VII. Conclusions

"If learning the truth is the scientist's goal, then he must make himself the enemy of all that he reads" Ibn Al-Haytham

Seismic data interpretation in the Levant Basin offshore Lebanon unveiled the presence of a multitude of structures, whose detailed investigation yielded new information on the basin evolution during the Cenozoic. The majority of these structures are old inherited, which have been intermittently active throughout geological times. These structures include:

- ENE-WSW striking dextral strike-slip faults. These faults are inherited from Mesozoic times and were reactivated into a dextral strike-slip regime in the Late Miocene as a result of the propagation of LFS in the margin. They are the only structures with evidence for their current activity at the present day, accommodating the counter-clockwise block rotation caused by transpression onshore.
- NNE-SSW striking thrust faults, found offshore Beirut and Tripoli. These structures were active in the early Tertiary and are inactive in the Pliocene. Their presence close to the margin and parallel to Mount Lebanon is most likely indicative for an early emergence and minor uplift of Mount Lebanon before the onset of transpression, during the Oligocene/Early Miocene.
- A large NW trending normal fault array found in the majority of the Levant Basin offshore Lebanon, Cyprus and Israel. The faults are layer bound, comprised in the Oligocene and Miocene units only. They are mostly parallel, although in the vicinity of the Lattakia Ridge System, they acquire a polygonal geometry. All evidence point to a nucleation mechanism that is not tectonic related. It is rather most likely associated to the specificities of sedimentary facies of the Oligo-Miocene units. These faults are caused by volumetric contraction of the host rock units and thus resemble the previously documented 'polygonal faults'.

- NNE trending anticlines folded during the Late Miocene prior to the Messinian event. Their activity ceased by the Pliocene times due to changes in the regional geodynamics and the evolution of the LFS. These anticlines are believed to overly deep structures, which are causing thickness variations of the Eocene strata and preferentially localising the anticlines.

The intermittent activity of the mapped structures, with the exception of the normal faults, is related to the multiple phases of tectonic deformation in the Levant region. The Mesozoic rifting event has resulted in a pre-existing structural fabric that was reactivated and inverted during subsequent tectonic events. Namely, the Late Cretaceous convergence of Arabia and Eurasia and the Early Miocene collision and suturing have caused the initial structures to be reactivated. The most important event is most likely the Late Miocene propagation of the LFS into Lebanon. The resulting transpression along the central LFS segment in Lebanon has affected the structures in the basin by stopping activity on some, namely the NNE-SSW thrust faults, and reactivating others such as the ENE-WSW strike-slip faults and ENE trending anticlines. Similarly, the final suturing of Arabia and Anatolia in the early Pliocene strongly affected the regional geodynamics, whereby the LFS started its second phase of movement and the structures in the basin were greatly affected. Only the ENE-WSW dextral strike-slip faults are still active today accommodating counter-clockwise block rotations in the Levant restraining bend.

The evolution of the margin and the Levant restraining bend was investigated through analogue modelling. The examined conceptual model involved creating pre-existing structures in an obliquely oriented graben to test their reactivation during sinistral strike-slip faulting. The resulting model geometry was greatly affected by the presence of existing structures, which were reactivated into dextral strike-slip faults. The restraining bend in the model was also segmented by these faults and resembles to a certain extent the Levant restraining bend. This resemblance between the model and Mount Lebanon strongly suggest that the latter is affected by pre-existing structuration that is likely part of the Palmyra Basin extending westward to the Levant Basin.

In consequence, the initial structuration of the margin, which is thought to have initiated in the Mesozoic, is most likely a part of Palmyra, which is the back-drop to the Levant Basin part of the Tethyan realm. The similar deformation time and geologic history are all favourable for this geologic scenario emphasizing the link between the Levant margin in Lebanon and the Palmyra Basin in Syria. For this reason, the Triassic,

Jurassic and Cretaceous successions thicken westward towards the Mediterranean, together with gradual thinning of the crust.

The availability of 3D seismic data in the Levant Basin provided an excellent opportunity to study the growth and evolution of normal faults, by qualitative seismic interpretation of these structures in the Oligo-Miocene unit. Their geometry, displacement distribution and interaction with each other all point to faulting initiated in the early Miocene through volumetric contraction of the host rock unit. The occurrence of two different plan view geometries, namely collinear or parallel in the basin and polygonal close to the Lattakia Ridge, indicate a link between the growth of these faults and the regional stress field. NW-SE compression is documented in the Levant region during the early Miocene and is the cause of why the faults are well oriented in the basin. When close to the Lattakia Ridge, stress field fluctuations probably result in horizontal isotropic stress applied on the faults explaining their polygonal plan view geometries in this zone in particular. The growth of the well-oriented normal faults in the basin and the faults close to the Lattakia Ridge strongly resembles the growth of tectonic faults and of polygonal faults respectively. They both accumulate displacement with increased length emphasizing the isolated fault growth model at basin scales.

The effect of the mapped structures on the petroleum system is significant. Most importantly, the mapped structures provided a clear timing for the creation of traps, being Late Miocene for the 4-way dip closures, early Miocene for the tilted fault blocks and early Tertiary for the 2-way dip closures along thrust faults. The Oligo-Miocene normal faults have important consequences on the petroleum system, as their occurrence indicate that the Oligo-Miocene units are formed of mostly fine-grained sediments. However, such faults might be associated with sand injections, which are usually considered as good reservoirs. Close to the Lattakia Ridge and to the eastern Levant margin, the absence of these faults in the Miocene intervals could point to an increase in the sandy content of these units, thus enhancing reservoir qualities. Their fault planes could contain shale smear, and might thus be impermeable laterally causing strong reservoir compartmentalisation. In contrast, they might increase vertical permeability and act as conduits for hydrocarbon migration from source rocks in the basin. Similarly, faults active throughout the whole Cenozoic along the margin could be important conduits for hydrocarbon migration from source rocks in the basin toward the margin and onshore. Active structures can be potential geohazards, especially that active faults can be permeable and cause petroleum leakage from reservoirs.

The final outcome of this PhD project consisted of proposing a geological model for the tectonic evolution of the Levant area during the Cenozoic. This model is based on new interpretation of the structures in the basin based on seismic data, which has allowed associating them with the regional geodynamics of the region. This area has undergone a long and complex history of deformation, resulting in a mosaic of structures all related to each other. Our new interpretation of the long lasting deformation in the basin, coupled with its regional interpretation, shed the light on the impact of plate movements in general, and the adjacent Levant Fracture System in particular, on the development of the Levant Basin. In consequence, basins that are close to plate boundaries could record related deformations and would therefore help in further understanding the evolution of such plate boundaries.

VII. 1 Future work and perspectives

Several points are recommended and proposed for future research venues regarding structural aspects in Levant Basin. Some of which will consolidate the above conclusions, others are new ideas that sparked out of the present study:

- *Salt tectonics:* In this project, salt tectonics has not been investigated. The Messinian sequence is heavily deformed with a variety of structures within the salt. The overlying Pliocene sequence exhibits extensional structures associated with salt and indicating salt flow toward the basin. A detailed and intricate investigation of the Messinian sequence would provide more constrains on the uplift of Mount Lebanon in the Messinian and Pliocene times.

- *Evolution of segment linkage in normal faults:* the normal faults have complex interaction with each other. Some faults have breached relay segments while others exhibit classical relay segments with gentle monoclinal geometries between faults. The excellent quality of seismic data and the clear fault plane provide an opportunity to study the spatial and temporal evolution of segmented and non-segmented normal faults. Furthermore, this investigation will provide more insight on the evolution of the normal faults in the basin and the interaction between them. This will also serve to better understand the effect of these faults on the petroleum system of the Levant basin.

- *Integration of results with gravity and magnetic surveys:* recently acquired air-born gravity data onshore will refine our understanding of the subsurface along

the Levant margin. Magnetic surveys are not available onshore and offshore Lebanon, but when acquired their integration with gravity will provide a great enhancement for the 3D geological model proposed in this study.

- *Integration with fieldwork and seismic data onshore:* a number of 2D seismic lines were recently acquired onshore Lebanon across Mount Lebanon. A big challenge in this PhD was to build the onshore cross-section due to large uncertainties on the subsurface geology. Fieldwork in Lebanon for detailed structural investigations over the E-W faults and other structures, coupled with an interpretation of these seismic lines will provide a great enhancement to the cross-sections across Mount Lebanon by limiting uncertainties.

- *Evolution of faulted anticlines:* the anticlines in the Levant Basin are cross-cut by the Oligo-Miocene normal faults. These faults are believed to predate the folding of these anticlines. A scientific question is what is the role of pre-existing oblique faults on folding of strata. An investigation of this question involves detailed spatial and temporal characterisation of faults cross-cutting the anticline. Furthermore, it will provide a clearer understanding of these anticlines in terms of their effect of the petroleum system and the effect of these faults on the compartmentalisation of reservoirs.

- *Analogue modelling:* experimental modelling is limited in terms of procedures and parameters. It is important to add on to the already undertaken experiments by trying to change the parameters. For example, investigation the effects of detachments surfaces within the sand, or testing the effect of pre-existing folds prior to strike-slip displacement and transpression. Most importantly, the effect of the mantle was not tested in experiments in this work. It is important to add honey below the silicone to simulate the rheology of the mantle, and test its effect of fault crustal reactivation.

- *Numeric modelling:* having proposed a conceptual model for the evolution of normal faults, it is important to test this scenario by numerical modelling and structural restoration. The importance of this step is to understand, through testing of conceptual models, the effect of these faults on fluid flow and the petroleum system. The normal faults have a large impact on the petroleum system of the Levant Basin. Their extensive distribution in the basin implies a strong effect on reservoirs and migration of petroleum. The lack of well data, however, is very restricting when trying to investigate the impact these faults have on the petroleum system of the basin, hence the advantage of using

numerical and mechanical models. 3D restoration will also provide additional insight on their evolution at a basin scale.

- *Integration with other projects:* the results of this project regarding the timing of the structures and their effect on the petroleum system should be integrated with other studies targeted to understand the stratigraphy and source rocks of the Levant Basin. The combination of the results of these projects will culminate in a large geologic model of the Levant Basin, allowing to restrain uncertainties on the petroleum system of the basin.

- *Integration of results in DionisosFlow and TemisFlow:* The results of this work should be integrated in DionisosFlow in order to refine the forward stratigraphic model of Hawie [2014] by confirming the proposed fine-grained facies for the Oligo-Miocene unit. Similarly, the timing of the structures interpreted in this work should be integrated in TemisFlow model constructed during the PhD project of Samer Bou Daher to assess their impact on charging or migrating petroleum and refining this model.

References

"It is the mark of an educated mind to be able to entertain a thought without accepting it"
Plato

Al Abdalla, A., É. Barrier, A. Matar, and C. Müller (2010), Late Cretaceous to Cenozoic tectonic evolution of the NW Arabian platform in NW Syria, in *Evolution of the Levant margin and western Arabia platform since the Mesozoic*, vol. 341, edited by C. Homberg and M. Bachmann, pp. 305–327, Geological Society Special Publications, London.

Agudelo, W., J. F. Gamboa, S. Guevara, C. Piedratha, L. E. Rojas, M. Morales, and H. Alfonso (2009), Combining PSDM and Seismic Modeling to reduce uncertainties in time structural interpretation, in *X simposio Bolivariano exploracion Petrolera*, pp. 1–3.

Al-Saad, D., T. Sawaf, A. Gebran, M. Barazangi, J. A. Best, and T. A. Chaimov (1992), Crustal structure of central Syria: The intracontinental Palmyride mountain belt, *Tectonophysics*, *207*(3-4), 345–358, doi:10.1016/0040-1951(92)90395-M.

Allen, M. B., and H. A. Armstrong (2008), Arabia–Eurasia collision and the forcing of mid-Cenozoic global cooling, *Palaeogeogr. Palaeoclimatol. Palaeoecol.*, *265*(1-2), 52–58, doi:10.1016/j.palaeo.2008.04.021.

Allen, M. B., J. A. Jackson, and R. Walker (2004), Late Cenozoic reorganization of the Arabia-Eurasia collision and the comparison of short-term and long-term deformation rates, *Tectonics*, *23*(2), doi:10.1029/2003TC001530.

Alsharhan, A. S., and A. E. M. Nairn (2003), *Sedimentary Basins and Petroleum Geology of the Middle East*, 2nd ed., Elsevier.

Alsharhan, A. S., and M. G. Salah (1996), Geologic setting and hydrocarbon potential of north Sinai , Egypt, *Bull. Can. Pet. Geol.*, *44*(4), 615–631.

Andersen, K. J., and M. Huuse (2011), " Bulls-eye " pockmarks and polygonal faulting in the Lower Congo Basin : Relative timing and implications for fluid expulsion during shallow burial, *Mar. Geol.*, *279*, 111–127, doi:10.1016/j.margeo.2010.10.016.

Anderson, E. M. (2012), Facsimile reproduction of The Dynamics of Faulting by E. M. Anderson, in *Faulting, Fracturing and Igneous intrusion in the Earth's crust*, vol. 367, edited by D. Healy, R. W. H. Butler, Z. K. Shipton, and R. H. Sibson, pp. 231–246, Geological Society Special Publications, London.

Arsenikos, S., D. Frizon De Lamotte, N. Chamot-Rooke, G. Mohn, M. C. Bonneau, and C. Blanpied (2013), Mechanism and timing of tectonic inversion in Cyrenaica (Libya): Integration in the geodynamics of the East Mediterranean, *Tectonophysics*, *608*, 319–329, doi:10.1016/j.tecto.2013.09.025.

Aydin, A., and Y. Eyal (2002), Anatomy of a normal fault with shale smear: implications for fault seal, *Am. Assoc. Pet. Geol. Bull.*, *86*(8), 1367–1381.

Bahorich, M., and S. Farmer (1995), 3D seismic discontinuity for faults and stratigraphic features: The coherence cube, *Lead. edge*, (October), 1053–1058.

Barnett, J. A., J. Mortimer, J. H. Rippon, J. J. Walsh, and J. Watterson (1987), Displacement Geometry in the Volume Containing a Single Normal Fault, *Am. Assoc. Pet. Geol. Bull.*, *71*(8), 925–937.

Barrier, É., and B. Vrielynck (2008), Paleotectonic maps of the Middle East: Tectono-sedimentary-palinspatic maps from Late Norian to Pliocene, 14 maps, *Comm. la Cart. Geol. du monde*.

Baudon, C., and J. A. Cartwright (2008a), 3D seismic characterisation of an array of blind normal faults in the Levant Basin, Eastern Mediterranean, *J. Struct. Geol.*, *30*(6), 746–760, doi:10.1016/j.jsg.2007.12.008.

Baudon, C., and J. A. Cartwright (2008b), Early stage evolution of growth faults: 3D seismic insights from the Levant Basin, Eastern Mediterranean, *J. Struct. Geol.*, *30*(7), 888–898, doi:10.1016/j.jsg.2008.02.019.

Baudon, C., and J. A. Cartwright (2008c), The kinematics of reactivation of normal faults using high resolution throw mapping, *J. Struct. Geol.*, *30*, 1072–1084, doi:10.1016/j.jsg.2008.04.008.

Bein, A., and G. Gvirtzman (1977), A mesozoic fossil edge of the Arabian plate along the Levant coastline and its bearing on the evolution of the eastern mediterranean, in *International symposium on the structural history of the Mediterranean basins*, edited by B. Biju-Duval and L. Montadert, pp. 95–110, Paris.

Bellahsen, N., C. Faccenna, F. Funiciello, J. M. Daniel, and L. Jolivet (2003), Why did Arabia separate from Africa? Insights from 3-D laboratory experiments, *Earth Planet. Sci. Lett.*, *216*, 365–381, doi:10.1016/S0012-821X(03)00516-8.

Ben-Avraham, Z. (1985), Structural framework of the gulf of Elat (Aqaba), northern Red Sea, *J. Geophys. Res.*, *90*(B1), 703–726.

Ben-Avraham, Z., and U. S. ten Brink (1989), Transverse faults and segmentation of basins within the Dead Sea Rift, *J. African Earth Sci.*, *8*(2/3), 603–616.

Ben-avraham, Z., and J. Charrach (1990), Transverse faults at the northern end of the southern basin of the Dead Sea graben, *Tectonophysics*, *180*, 37–47.

Ben-Avraham, Z., A. Ginzburg, J. Makris, and L. Eppelbaum (2002), Crustal structure of the Levant Basin, eastern Mediterranean, *Tectonophysics*, *346*(1-2), 23–43, doi:10.1016/S0040-1951(01)00226-8.

Bentham, P. A., I. HAnbal, J. Cotton, M. B. Longacre, and R. Edwards (2007), Crustal Structure and Early Opening of the Eastern Mediterranean Basin - Key Observations from Offshore Northern Egypt, in *3rd North African/Mediterranean Petroleum & Geosciences conference and exhibition*, Tripoli, Lybia.

Bertoni, C., and J. A. Cartwright (2007), Clastic depositional systems at the base of the late Miocene evaporites of the Levant region, Eastern Mediterranean, in *Evaporites through space and time*, vol. 285, edited by B. C. Schreiber, S. Lugli, and M. Babel, pp. 37–52, Geological Society Special Publications, London.

Best, J. A., M. Barazangi, D. Al-Saad, T. Sawaf, and A. Gebran (1993), Continental margin evolution of the Northern Arabian Platform in Syria, *Am. Assoc. Pet. Geol. Bull.*, *77*(2), 173–193.

Beydoun, Z. R. (1977), Petroleum Prospects of Lebanon: Reevaluation, *Am. Assoc. Pet. Geol. Bull.*, *61*(I), 43–64, doi:10.1306/C1EA3BF4-16C9-11D7-8645000102C1865D.

Beydoun, Z. R. (1981), Some Open Questions Relating To the Petroleum Prospects of Lebanon*, *J. Pet. Geol.*, *3*, 303–314, doi:10.1306/BF9AB5CA-0EB6-11D7-8643000102C1865D.

Beydoun, Z. R. (1988), *The Middle East: regional geology and petroleum ressources*, Scientific Press, Beaconsfield.

Beydoun, Z. R. (1993), Evolution of the northeastern arabian plate margin and shelf: hydrocarbon habitat and conceptual future potential, *Rev. l'institut Fr. du Pet.*, *48*(4), 311–345.

Beydoun, Z. R. (1999), Evolution and development of the Levant (Dead Sea Rift) Transform System: A historical-chronological review of a structural controversy, in *Continental Tectonics*, vol. 164, edited by C. Mac Niocaill and P. D. Ryan, pp. 239–255, Geological Society Special Publications, London.

Beydoun, Z. R., and J. G. Habib (1995), Lebanon revisited: new insights into Triassic

hyrocarbon prospects, *J. Pet. Geol.*, *18*(1), 75–90.

Bonini, M., F. Sani, and B. Antonielli (2012), Basin inversion and contractional reactivation of inherited normal faults: A review based on previous and new experimental models, *Tectonophysics*, *522-523*, 55–88, doi:10.1016/j.tecto.2011.11.014.

Bou Daher, S., F. H. Nader, H. Strauss, and R. Littke (2014), Depositional environment and source-rock characterisation of organic-matter rich Upper Santonian-Upper Campanian carbonates, northern Lebanon, *J. Pet. Geol.*, *37*(January), 5–24.

Bou Daher, S., F. H. Nader, C. Müller, and R. Littke (2015), Geochemical and petrographic characterization of Campanian – Lower Maastrichtian calcareous petroleum source rocks of Hasbayya, South Lebanon, *Mar. Pet. Geol.*, *64*, 304–323, doi:10.1016/j.marpetgeo.2015.03.009.

Boudagher-fadel, M., and G. N. Clark (2006), Stratigraphy , paleoenvironment and paleogeography of Maritime Lebanon : a key to Eastern Mediterranean Cenozoic history, *Stratigraphy*, *3*(2), 1–38.

Bowman, S. A. (2011), Regional seismic interpretation of the hydrocarbon prospectivity of offshore Syria, *GeoArabia*, *16*(3), 95–124.

Brew, G. E. (2001), Tectonic evolution of Syria interpreted from integrated geophysical and geological analysis, Cornell University.

Brew, G. E., J. Lupa, M. Barazangi, T. Sawaf, A. Al-Imam, and T. Zaza (2001a), Structure and tectonic development of the Ghab basin and the Dead Sea fault system, Syria, *J. Geol. Soc. London.*, *158*(4), 665–674, doi:10.1144/jgs.158.4.665.

Brew, G. E., M. Barazangi, A. K. Al-Maleh, and T. Sawaf (2001b), Tectonic and Geologic Evolution of Syria, *GeoArabia*, *6*(4), 573–616.

Brew, G. E., J. A. Best, M. Barazangi, and T. Sawaf (2003), Tectonic evolution of the NE Palmyride mountain belt, Syria: the Bishri crustal block, *J. Geol. Soc. London.*, *160*(5), 677–685, doi:10.1144/0016-764902-161.

Brinker, J. C., and G. W. Scherer (1990), *Solg-Gel Sience: the physics and chemistry of sol-gel processing*, Academic Press.

Brun, J., and T. Nalpas (1996), Graben inversion in nature and experiments, *Tectonics*, *15*(2), 677, doi:10.1029/95TC03853.

Butler, R. W. H., S. Spencer, and H. M. Griffiths (1997), Transcurrent fault activity on the Dead Sea Transform in Lebanon and its implications for plate tectonics and seismic hazard, *J. Geol. Soc. London.*, *154*(5), 757–760, doi:10.1144/gsjgs.154.5.0757.

Butler, R. W. H., S. Spencer, and H. M. Griffiths (1998), The structural response to evolving plate kinematics during transpression: evolution of the Lebanese restraining bend of the Dead Sea Transform, in *Continental transpressional and transtensional tectonics*, vol. 135, edited by R. E. Holdsworth, R. A. Strachan, and J. F. Dewey, pp. 81–106, Geological Society Special Publications, London.

Carruthers, D., J. A. Cartwright, M. P. a. Jackson, and P. Schutjens (2013), Origin and timing of layer-bound radial faulting around North Sea salt stocks: New insights into the evolving stress state around rising diapirs, *Mar. Pet. Geol.*, *48*, 130–148, doi:10.1016/j.marpetgeo.2013.08.001.

Carton, H. et al. (2009), Seismic evidence for Neogene and active shortening offshore of Lebanon (Shalimar cruise), *J. Geophys. Res.*, *114*, 15–18, doi:10.1029/2007JB005391.

Cartwright, J. A. (1994), Episodic basin-wide hydrofracturing of overpressured Early Cenozoic mudrock sequences in the North Sea Basin, *Mar. Pet. Geol.*, *11*(5), 587–607, doi:0264-8172/94/05/0587-21.

Cartwright, J. A. (2011), Diagenetically induced shear failure of fine-grained sediments and the development of polygonal fault systems, *Mar. Pet. Geol.*, *28*(9), 1593–1610, doi:10.1016/j.marpetgeo.2011.06.004.

Cartwright, J. A., and D. N. Dewhurst (1998), Layer-bound compaction faults in fine-grained sediments, *Geol. Soc. Am. Bull.*, *110*(10), 1242–1257, doi:10.1130/0016-7606(1998)110<1242.

Cartwright, J. A., and L. Lonergan (1996), Volumetric contraction during the compaction of mudrocks: A mechanism for the development of regional-scale polygonal fault systems, *Basin Res.*, *8*(September), 183–193.

Cartwright, J. A., B. D. Trudgill, and C. S. Mansfield (1995), Fault growth by segment linkage: an explanation for scatter in maximum displacement and trace length data from the Canyonlands Grabens of SE Utah, *J. Struct. Geol.*, *17*(9), 1319–1326.

Cartwright, J. A., R. Bouroullec, D. James, and H. Johnson (1998), Polycyclic motion history of some Gulf Coast growth faults from high-resolution displacement analysis, *Geology*, *26*(9), 819–822, doi:10.1130/0091-7613(1998)026<0819.

Cartwright, J. A., D. James, and A. Bolton (2003), The genesis of polygonal fault systems: a review, in *Subsurface sediment mobilization*, vol. 216, edited by P. Van Rensbergen, R. R. Hillis, A. J. Maltman, and C. K. Morley, pp. 223–243, Geological Society Special Publications, London.

Casas, A. M., D. Gapais, T. Nalpas, K. Besnard, and T. Roman-Berdiel (2001), Analogue models of transpressive systems, *J. Struct. Geol.*, *23*, 733–743.

Chaimov, T. A., M. Barazangi, D. Al-Saad, T. Sawaf, and A. Gebran (1990), Crustal shortening in the Palmyride fold belt, Syria, and implications for movement along the Dead Sea fault system, *Tectonics*, *9*, 1369–1386.

Chaimov, T. A., M. Barazangi, D. Al-Saad, T. Sawaf, and A. Gebran (1992), Mesozoic and Cenozoic deformation inferred from seismic stratigraphy in the southwestern intracontinental Palmyride fold-thrust belt, Syria, *Geol. Soc. Am. Bull.*, *104*(6), 704–715, doi:10.1130/0016-7606(1992)104<0704:MACDIF>2.3.CO;2.

Chaimov, T. A., M. Barazangi, D. Al-Saad, T. Sawaf, and M. Khaddour (1993), Seismic fabric and 3-D structure of the southwestern intracontinental Palmyride fold belt, Syria, *Am. Assoc. Pet. Geol. Bull.*, *77*(12), 2032–2047.

Childs, C., J. Watterson, and J. J. Walsh (1995), Fault overlap zones within developing normal fault systems, *J. Geol. Soc. London.*, *152*(3), 535–549, doi:10.1144/gsjgs.152.3.0535.

Childs, C., A. Nicol, J. J. Walsh, and J. Watterson (1996), Growth of vertically segmented normal faults, *J. Struct. Geol.*, *18*(12), 1389–1397, doi:10.1016/S0191-8141(96)00060-0.

Childs, C., A. Nicol, J. J. Walsh, and J. Watterson (2003), The growth and propagation of synsedimentary faults, *J. Struct. Geol.*, *25*(4), 633–648, doi:10.1016/S0191-8141(02)00054-8.

Clausen, J. A., R. H. Gabrielsen, P. A. Reksnes, and E. Nysaether (1999), Development of intraformational (Oligocene-Miocene) faults in the northern North Sea: influence of remote stresses and doming of Fennoscandia, *J. Struct. Geol.*, *21*, 1457–1475.

Cloos, E. (1968), Experimental analysis of gulf coast fracture patterns, *Am. Assoc. Pet. Geol. Bull.*, *52*(3), 420–444.

Cloos, H. (1928), Experimente zur inneren Tektonik, *Cent. für Mineral.*, *12*, 609–621.

Cochran, J. R. (1983), A Model for Development of Red Sea, *Am. Assoc. Pet. Geol. Bull.*, *67*(1), 41–69.

Cochran, J. R., and G. D. Karner (2007), Constraints on the deformation and rupturing of continental lithosphere of the Red Sea: the transition from rifting to drifting, in *Imaging, mapping and modelling continental lithosphere extension and breakup*, vol. 282, edited by G. D. Karner, G. Manatschal, and L. M. Pinheiro, pp. 265–289, Geological Society Special Publications, London.

Colletta, B., P. Bale, J. F. Ballard, J. Letouzey, and R. Pinedo (1991), Computerized X-ray tomography analysis of sandbox models: examples of thin-skinned thrust systems, *Geology*, *19*, 1063–1067.

Collin, P. Y., A. Mancinelli, M. Chiocchini, M. Mroueh, W. Hamdan, and F. Higazi (2010), Middle and Upper Jurassic stratigraphy and sedimentary evolution of Lebanon (Levantine margin): palaeoenvironmental and geodynamic implications, in *Evolution of the Levant margin and western Arabia platform since the Mesozoic*, vol. 341, edited by C. Homberg and M. Bachmann, pp. 227–244,

Geological Society Special Publications, London.

Cowie, P. A., and C. H. Scholz (1992a), Displacement-length scaling relationship for faults: data synthesis and discussion, *J. Struct. Geol.*, *14*(10), 1149–1156.

Cowie, P. A., and C. H. Scholz (1992b), Growth of faults by accumulation of seismic slip, *J. Geophys. Res.*, *97*(B7), 11085–11095.

Cowie, P. A., and Z. K. Shipton (1998), Fault tip displacement gradients and process zone dimensions, *J. Struct. Geol.*, *20*(8), 983–997.

Crognier, N. (2013), Etudes sédimentologiques et biostratigraphiques de la série Turono-Miocène du Nord Liban : Contraintes pour la modélisation stratigraphique sur Dionisos, Memoire de these, Universite Pierre et Marie Curie.

Cunningham, W. D., and P. Mann (2007), Tectonics of strike-slip restraining and releasing bends, in *Tectonics of strike-slip restraining and releasing bends*, vol. 290, edited by W. D. Cunningham and P. Mann, pp. 1–12, Geological Society Special Publications, London.

D'Acremont, E., S. Leroy, M.-O. Beslier, N. Bellahsen, M. Fournier, C. Robin, M. Maia, and P. Gente (2005), Structure and evolution of the eastern Gulf of Aden conjugate margins from seismic reflection data, *Geophys. J. Int.*, *160*(3), 869–890, doi:10.1111/j.1365-246X.2005.02524.x.

Daeron, M. (2005), comportement sismique à long terme de la faille de Yammoûneh, PhD thesis, Institut du Physique du Globe de Paris.

Daëron, M., L. Benedetti, P. Tapponnier, A. Sursock, and R. C. Finkel (2004), Constraints on the post ~25-ka slip rate of the Yammoûneh fault (Lebanon) using in situ cosmogenic 36Cl dating of offset limestone-clast fans, *Earth Planet. Sci. Lett.*, *227*(1-2), 105–119, doi:10.1016/j.epsl.2004.07.014.

Daëron, M., Y. Klinger, P. Tapponnier, A. Elias, E. Jacques, and A. Sursock (2005), Sources of the large A.D. 1202 and 1759 Near East earthquakes, *Geology*, *33*(7), 529, doi:10.1130/G21352.1.

Daëron, M., Y. Klinger, P. Tapponnier, A. Elias, E. Jacques, and A. Sursock (2007), 12,000-Year-Long Record of 10 to 13 Paleoearthquakes on the Yammouneh Fault, Levant Fault System, Lebanon, *Bull. Seismol. Soc. Am.*, *97*(3), 749–771, doi:10.1785/0120060106.

Davies, R. J., and M. T. Ireland (2011), Initiation and propagation of polygonal fault arrays by thermally triggered volume reduction reactions in siliceous sediment, *Mar. Geol.*, *289*(1-4), 150–158, doi:10.1016/j.margeo.2011.05.005.

Davy, P. (1986), Modelisation thermo-mecanique de la collision continentale, PhD thesis, Universite de Rennes 1.

Dawers, N. H., and M. H. Anders (1995), Displacement-length scaling and fault linkage, *J. Struct. Geol.*, *17*(5), 607–614.

Dewey, J. F., W. C. I. Pitman, W. B. F. Ryan, and J. Bonin (1973), Plate Tectonics and the Evolution of the Alpine System, *Geol. Soc. Am. Bull.*, *84*, 3137–3180, doi:10.1130/0016-7606(1973)84<3137.

Dewey, J. F., M. R. Hempton, W. S. F. Kidd, F. Saroglu, and A. M. C. Sengor (1986), Shortening of continental lithosphere: the neotectonics of Eastern Anatolia -- a young collision zone, in *Collision tectonics*, vol. 19, edited by M. P. Coward and A. C. Ries, pp. 1–36, Geological Society Special Publications, London.

Dewhurst, D. N., J. A. Cartwright, and L. Lonergan (1999), The development of polygonal fault systems by syneresis of colloidal sediments, *Mar. Pet. Geol.*, *16*, 793–810.

Dickinson, W. R. (1996), Kinematics of transrotational tectonism in the California Transverse Ranges and its contribution to cumulative slip along the San Andreas transform fault system, *Geol. Soc. Am.*, *305*, 1–46, doi:10.1130/0-8137-2305-1.1.

Dolson, J. C., P. J. Boucher, J. Siok, and P. D. Heppard (2005), Key Challenges to realizing full potential in an emerging giant gas province: Nile Delta/Mediterranean offshore, deep water, Egypt, in *Petroleum Geology: North-West Europe and Global Perspectives - Proceedings of the 6th Petroleum geology conference*, edited by A. G. Doré and B. A.

Vining, pp. 607–624, Geological Society Special Publications, London.

Dooley, T. P., and G. Schreurs (2012), Analogue modelling of intraplate strike-slip tectonics: A review and new experimental results, *Tectonophysics*, *574-575*, 1–71, doi:10.1016/j.tecto.2012.05.030.

Dooley, T. P., K. R. Mcclay, and M. Bonora (1999), 4D evolution of segmented strike-slip fault systems : applications to NW Europe, in *Petroleum geology of Northwest Europe: Proceedings of the 5th conferece*, edited by A. J. Fleet and S. A. R. Boldy, pp. 215–225, Geological Society Special Publications, London.

Druckman, Y. (1981), Comments on the structural reversal model as a factor of the geological evolution of Israel, *Isr. J. Earth Sci.*, *30*, 44–48.

Druckman, Y. (1984), Evidence for Early-Middle Triassic faulting and possible rifting from the Helez Deep Borehole in the coastal plain of Israel, in *The geological evolution of the Eastern Mediterranean*, vol. 17, edited by J. E. Dixon and A. H. F. Robertson, pp. 203–212, Geological Society Special Publications, London.

Druckman, Y., F. Hirsch, and T. Weissbrod (1982), The Triassic of the southern margin of the Tethys in the Levant and its correlation across the Jordan Rift Valley, *Geol. Rundschau*, *71*(3), 919–936, doi:10.1007/BF01821111.

Druckman, Y., B. Buchbinder, G. M. Martinotti, R. Siman Tov, and P. Aharon (1995), The buried Afiq Canyon (eastern Mediterranean , Israel): a case study of a Tertiary submarine canyon exposed in Late Messinian times, *Mar. Geol.*, *123*, 167–185.

Dubertret, L. (1955), Carte Geologique du Liban au 1/200000, , 74.

Dubertret, L. (1972), Sur la dislocation de l'ancienne plaque sialique afrique sinai peninsule arabique.pdf, *Notes Mem. sur le Moyen Orient*, *12*(2), 227–243.

Dubois, A., F. Odonne, G. Massonnat, T. Lebourg, and R. Fabre (2002), Analogue modelling of fault reactivation: tectonic inversion and oblique remobilisation of grabens, *J. Struct. Geol.*, *24*(11), 1741–1752, doi:10.1016/S0191-8141(01)00129-8.

Dupin, I., J. Brahami, Y. Gou, and L. Montadert (2012), Petroleum assessment of the offshore Lebanon based on the seismic interpretation and the regional geological framework, in *Lebanon International Petroleum Exploration forum and exhibition*, Lebanese Republic ministry of energy and water, Beirut.

Eisenstadt, G., and M. O. Withjack (1995), Estimating inversion: results from clay models, in *Basin inversion*, vol. 88, edited by J. G. Buchanan and P. G. Buchanan, pp. 119–136, Geological Society Special Publications, London.

Elias, A. et al. (2007), Active thrusting offshore Mount Lebanon: Source of the tsunamigenic A.D. 551 Beirut-Tripoli earthquake, *Geology*, *35*(8), 755, doi:10.1130/G23631A.1.

Eyal, M., Y. Eyal, Y. Bartov, and G. Steinitz (1981), The tectonic development gulf of elat (aqaba) rift of the western margin of the Gulf of Elat (Aqaba) rift, *Tectonophysics*, *80*, 39–66.

Eyal, Y. (1996), Stress field fluctuations along the Dead Sea rift since the Middle Miocene, *Tectonics*, *15*(1), 157–170.

Eyal, Y., and Z. Reches (1983), Tectonic analyses of the Dead Sea rift region since the Late-Cretaceous based on mesostructures, *Tectonics*, *2*(2), 167–185.

Ferrill, D. A., and A. P. Morris (2001), Displacement gradient and deformation in normal fault systems, *J. Struct. Geol.*, *23*, 619–638.

Ferrill, D. A., and A. P. Morris (2003), Dilational normal faults, *J. Struct. Geol.*, *25*, 183–196.

Ferrill, D. A., and A. P. Morris (2008), Fault zone deformation controlled by carbonate mechanical stratigraphy, Balcones fault system, Texas, *Am. Assoc. Pet. Geol. Bull.*, *92*(3), 359–380, doi:10.1306/10290707066.

Ford, M., C. Le Carlier de Veslud, and O. Bourgeois (2007), Kinematic and geometric analysis of fault-related folds in a rift setting: The Dannemarie basin, Upper Rhine Graben, France, *J. Struct. Geol.*, *29*(11), 1811–1830, doi:10.1016/j.jsg.2007.08.001.

Fossen, H. (2010), *Structural Geology*, Cambridge University Press.

Fournier, M., P. Patriat, S. Leroy, and M. Curie (2001), Reappraisal of the Arabia-India-Somalia triple junction kinematics, *Earth Planet. Sci. Lett.*, *189*, 103–114.

Fournier, M. et al. (2010), Arabia-Somalia plate kinematics, evolution of the Aden-Owen-Carlsberg triple junction, and opening of the Gulf of Aden, *J. Geophys. Res.*, *115*(B4), B04102, doi:10.1029/2008JB006257.

Frei, L. S., and R. Freund (1990), Spatial and temporal relationships between two sets of strike-slip faults in southeastern Sinai, *Tectonophysics*, *180*, 111–121.

Freund, R. (1965), A model of the structural development of Israel and adjacent areas since Upper Cretaceous times, *Geol. Mag.*, *102*(3).

Freund, R. (1974), Kinematics of transform and transcurrent faults, *Tectonophysics*, *21*, 93–134.

Freund, R., Z. Garfunkel, I. Zak, M. Goldberg, T. Weissbrod, B. Derin, F. Bender, F. E. Wellings, and R. W. Girdler (1970), The Shear along the Dead Sea Rift [and Discussion], *Philos. Trans. R. Soc. A Math. Phys. Eng. Sci.*, *267*(1181), 107–130, doi:10.1098/rsta.1970.0027.

Frizon de Lamotte, D., C. Raulin, N. Mouchot, J. Christophe, W. Daveau, C. Blanpied, and J. C. Ringenbach (2011), The southernmost margin of the Tethys realm during the Mesozoic and Cenozoic : Initial geometry and timing of the inversion processes, *Tectonics*, *30*, 1–22, doi:10.1029/2010TC002691.

Gardosh, M., and Y. Druckman (2006), Seismic stratigraphy, structure and tectonic evolution of the Levantine Basin, offshore Israel, in *Tectonic Development of the Eastern Mediterranean Region*, vol. 260, edited by A. H. F. Robertson and D. Mountrakis, pp. 201–227, Geological Society Special Publications, London.

Gardosh, M., Y. Druckman, B. Buchbinder, and M. Rybakov (2006), *The Levant Basin Offshore Israel : Stratigraphy , Structure , Tectonic Evolution and Implications for Hydrocarbon Exploration.*

Gardosh, M., Y. Druckman, B. Buchbinder, and M. Rybakov (2008a), *The Levant Basin Offshore Israel : Stratigraphy , Structure , Tectonic Evolution and Implications for Hydrocarbon Exploration.*

Gardosh, M., Y. Druckman, B. Buchbinder, and R. Calvo (2008b), *The Oligo-Miocene deepwater system of the Levant Basin.*

Gardosh, M., Z. Garfunkel, Y. Druckman, and B. Buchbinder (2010), Tethyan rifting in the Levant Region and its role in Early Mesozoic crustal evolution, in *Evolution of the Levant margin and western Arabia platform since the Mesozoic*, vol. 341, edited by C. Homberg and M. Bachmann, pp. 9–36, Geological Society Special Publication, London.

Gardosh, M., P. Weimer, and A. Flexer (2011), The sequence stratigraphy of Mesozoic successions in the Levant margin, southwestern Israel: A model for the evolution of southern Tethys margins, *Am. Assoc. Pet. Geol. Bull.*, *95*(10), 1763–1793, doi:10.1306/02081109135.

Garfunkel, Z. (1981), Internal structure of the Dead Sea leacky transform (rift) in relation to plate kinematics, *Tectonophysics*, *80*, 81–108, doi:0040-1951/81/0000.

Garfunkel, Z. (1998), Constrains on the origin and history of the Eastern Mediterranean basin, *Tectonophysics*, *298*(1-3), 5–35, doi:10.1016/S0040-1951(98)00176-0.

Garfunkel, Z. (2004), Origin of the Eastern Mediterranean basin: a reevaluation, *Tectonophysics*, *391*(1-4), 11–34, doi:10.1016/j.tecto.2004.07.006.

Garfunkel, Z., and B. Derin (1984), Permian-early Mesozoic tectonism and continental margin formation in Israel and its implications for the history of the Eastern Mediterranean, in *The geological evolution of the Eastern Mediterranean*, vol. 17, edited by R. J. Dixon and A. H. F. Robertson, pp. 187–201, Geological Society, London, Special Publications.

Garfunkel, Z., and R. Freund (1981), Active faulting in the Dead Sea rift, *Tectonophysics*, *80*, 1–26.

Gawthorpe, R. L., I. Sharp, J. R. Underhill, and S. Gupta (1997), Linked sequence stratigraphic

and structural evolution of propagating normal faults, *Geology*, *25*(9), 795, doi:10.1130/0091-7613(1997)025<0795:LSSASE>2.3.CO;2.

Gedeon, M. (1999), Structural analysis of latitudinal faults in the Mount Lebanon north of Beirut: their kinematic and their role in the tectonic evolution of Lebanon, MSc thesis, American University of Beirut.

Ghalayini, R., J.-M. Daniel, C. Homberg, F. H. Nader, and J. E. Comstock (2014), Impact of Cenozoic strike-slip tectonics on the evolution of the northern Levant Basin (offshore Lebanon), *Tectonics*, *33*(11), 2121–2142, doi:10.1002/2014TC003574.

Girdler, R. W. (1990), The Dead Sea transform fault system, *Tectonophysics*, *180*(1), 1–13, doi:10.1016/0040-1951(90)90367-H.

Glennie, K. W., M. G. A. Boeuf, M. W. Hughes Clarke, M. Moody-Stuart, W. F. H. Pilaar, and B. M. Reinhardt (1973), Late Cretaceous Nappes in Oman Mountains and Their Geologic Evolution ', *Am. Assoc. Pet. Geol. Bull.*, *57*(1), 5–27.

Gomez, F., M. Meghraoui, A. N. Darkal, R. Sbeinati, R. Darawcheh, C. Tabet, M. Khawlie, M. Charabe, K. Khair, and M. Barazangi (2001), Coseismic displacements along the Serghaya fault: an active branch of the Dead Sea fault system in Syria and Lebanon, *J. Geol. Soc. London.*, *158*, 405–408.

Gomez, F., M. Meghraoui, A. N. Darkal, F. Hijazi, M. Mouty, Y. Suleiman, R. Sbeinati, R. Darawcheh, R. Al-Ghazzi, and M. Barazangi (2003), Holocene faulting and earthquake recurrence along the Serghaya branch of the Dead Sea fault system in Syria and Lebanon, *Geophys. J. Int.*, *153*(3), 658–674, doi:10.1046/j.1365-246X.2003.01933.x.

Gomez, F., M. Khawlie, C. Tabet, A. N. Darkal, K. Khair, and M. Barazangi (2006), Late Cenozoic uplift along the northern Dead Sea transform in Lebanon and Syria, *Earth Planet. Sci. Lett.*, *241*(3-4), 913–931, doi:10.1016/j.epsl.2005.10.029.

Gomez, F., G. Karam, M. Khawlie, S. McClusky, P. Vernant, R. Reilinger, R. Jaafar, C. Tabet, K. Khair, and M. Barazangi (2007a), Global Positioning System measurements of strain accumulation and slip transfer through the restraining bend along the Dead Sea fault system in Lebanon, *Geophys. J. Int.*, *168*(3), 1021–1028, doi:10.1111/j.1365-246X.2006.03328.x.

Gomez, F., T. Nemer, C. Tabet, M. Khawlie, M. Meghraoui, and M. Barazangi (2007b), Strain partitioning of active transpression within the Lebanese restraining bend of the Dead Sea Fault (Lebanon and SW Syria), in *Tectonics of strike-slip restraining and releasing bends*, vol. 290, edited by W. D. Cunningham and P. Mann, pp. 285–303, Geological Society, London, Special Publications.

Goulty, N. R. (2001), Mechanics of layer-bound polygonal faulting in fine-grained sediments, *J. Geol. Soc. London.*, *159*, 239–246, doi:10.1144/0016-764901-111.

Goulty, N. R. (2008), Geomechanics of polygonal fault systems: a review, *Pet. Geosci.*, *14*(4), 389–397, doi:10.1144/1354-079308-781.

Gradmann, S., C. Hübscher, Z. Ben-Avraham, D. Gajewski, and G. Netzeband (2005), Salt tectonics off northern Israel, *Mar. Pet. Geol.*, *22*(5), 597–611, doi:10.1016/j.marpetgeo.2005.02.001.

Griffiths, H. M., R. a. Clark, K. M. Thorp, and S. Spencer (2000), Strain accommodation at the lateral margin of an active transpressive zone: geological and seismological evidence from the Lebanese restraining bend, *J. Geol. Soc. London.*, *157*(2), 289–302, doi:10.1144/jgs.157.2.289.

Gross, M. R. (1995), Fracture partitioning: Failure mode as a function of lithology in the Monterey Formation of coastal California, *Geol. Soc. Am. Bull.*, *107*(7), 779–792, doi:10.1130/0016-7606(1995)107<0779:FPFMAA>2.3.CO;2.

Gross, M. R., G. Gutie´rrez-Alonso, T. Bai, M. a. Wacker, K. B. Collinsworth, and R. J. Behl (1997), Influence of mechanical stratigraphy and kinematics on fault scaling relations, *J. Struct. Geol.*, *19*(2), 171–183, doi:10.1016/S0191-8141(96)00085-5.

Le Guerroué, E., and P. R. Cobbold (2006), Influence of erosion and sedimentation on strike-slip fault systems: insights from analogue models, *J.*

Struct. Geol., *28*(3), 421–430, doi:10.1016/j.jsg.2005.11.007.

Guiraud, R., and W. Bosworth (1997), Senonian basin inversion and rejuvenation of rifting in Africa and Arabia: synthesis and implications to plate-scale tectonics, *Tectonophysics*, *282*(1-4), 39–82, doi:10.1016/S0040-1951(97)00212-6.

Guiraud, R., and W. Bosworth (1999), Phanerozoic geodynamic evolution of northeastern Africa and the northwestern Arabian platform, *Tectonophysics*, *315*, 73–108.

Gupta, A., and C. H. Scholz (2000), A model of normal fault interaction based on observations and theory, *J. Struct. Geol.*, *22*, 865–879.

Gvirtzman, Z., E. Zilberman, and Y. Folkman (2008), Reactivation of the Levant passive margin during the late Tertiary and formation of the Jaffa basin offshore central Israel, *J. Geol. Soc. London.*, *165*, 563–578.

Gvirtzman, Z., M. Reshef, O. Buch-Leviatan, G. Groves-Gidney, Z. Karcz, Y. Makovsky, and Z. Ben-Avraham (2014), Bathymetry of the Levant basin: Interaction of salt-tectonics and surficial mass movements, *Mar. Geol.*, *360*, 25–39, doi:10.1016/j.margeo.2014.12.001.

Hall, J. T., T. J. Calon, A. E. Aksu, and S. R. Meade (2005a), Structural evolution of the Latakia Ridge and Cyprus Basin at the front of the Cyprus Arc , Eastern Mediterranean Sea, *Mar. Geol.*, *221*, 261–297, doi:10.1016/j.margeo.2005.03.007.

Hall, J. T., A. E. Aksu, T. J. Calon, and D. Yaşar (2005b), Varying tectonic control on basin development at an active microplate margin: Latakia Basin, Eastern Mediterranean, *Mar. Geol.*, *221*(1-4), 15–60, doi:10.1016/j.margeo.2004.05.034.

Hancock, P. L., and M. S. Atiya (1979), Tectonic significance of mesofracture systems associated with the Lebanese segment of the Dead Sea transform fault, *J. Struct. Geol.*, *1*(2), 143–153, doi:10.1016/0191-8141(79)90051-8.

Handin, J. (1969), On the Coulomb-Mohr failure criterion, *J. Geophys. Res.*, *74*(22), 5343–5348.

Hansen, D. M., and J. A. Cartwright (2006), The three-dimensional geometry and growth of forced folds above saucer-shaped igneous sills, *J. Struct. Geol.*, *28*, 1520–1535, doi:10.1016/j.jsg.2006.04.004.

Hansen, D. M., J. W. Shimeld, M. A. Williamson, and H. Lykke-Andersen (2004), Development of a major polygonal fault system in Upper Cretaceous chalk and Cenozoic mudrocks of the Sable Subbasin, Canadian Atlantic margin, *Mar. Pet. Geol.*, *21*(9), 1205–1219, doi:10.1016/j.marpetgeo.2004.07.004.

Hardy, C., C. Homberg, Y. Eyal, É. Barrier, and C. Müller (2010), Tectonic evolution of the southern Levant margin since Mesozoic, *Tectonophysics*, *494*(3-4), 211–225, doi:10.1016/j.tecto.2010.09.007.

Hatem, A. E., M. L. Cooke, and E. H. Madden (2015), Evolving efficiency of restraining bends within wet kaolin analog experiments, *J. Geophys. Res. Solid Earth*, n/a–n/a, doi:10.1002/2014JB011735.

Hawie, N. (2014), Architecture, geodynamic evolution and sedimentary filling of the Levant Basin: a 3D quantitative approach based on seismic data, PhD thesis, Universite Pierre et Marie Curie.

Hawie, N., C. Gorini, R. Deschamps, F. H. Nader, L. Montadert, D. Granjeon, and F. Baudin (2013), Tectono-stratigraphic evolution of the northern Levant Basin (offshore Lebanon), *Mar. Pet. Geol.*, *48*, 392–410, doi:10.1016/j.marpetgeo.2013.08.004.

Hawie, N., R. Deschamps, F. H. Nader, C. Gorini, C. Müller, D. Desmares, A. Hoteit, D. Granjeon, L. Montadert, and F. Baudin (2014), Sedimentological and stratigraphic evolution of northern Lebanon since the Late Cretaceous: implications for the Levant margin and basin, *Arab. J. Geosci.*, *7*(4), 1323–1349, doi:10.1007/s12517-013-0914-5.

He, C., L. Tang, D. Huang, and S. Shi (2010), Polygonal faults in the Sanzhao sag of the Songliao basin: their significance in hydrocarbon accumulation, *Min. Sci. Technol.*, *20*(2), 300–305, doi:10.1016/S1674-5264(09)60202-7.

Hempton, M. R. (1987), Constraints on Arabian Plate motion and extensional history of the Red Sea,

Tectonics, *6*(6), 687, doi:10.1029/TC006i006p00687.

Henriet, J. P., M. De Batist, and M. Verschuren (1991), Early fracturing of Paleogene clays, southernmost North Sea: Relevance to mechanisms of primary hydrocarbon migration, in *Generation, accumulation and production of Europe's hydrocarbon*, edited by A. M. Spencer, pp. 217–227, European association of petroleum geologists, special publication 1.

Henry, B., C. Homberg, M. Mroueh, W. Hamdan, and F. Higazi (2010), Rotations in Lebanon inferred from new palaeomagnetic data and implications for the evolution of the Dead Sea Transform system, in *Geological Society, London, Special Publications*, vol. 341, edited by C. Homberg and M. Bachmann, pp. 269–285, Geological Society, London, Special Publications.

Higgs, W. G., and K. R. Mcclay (1993), Analogue sandbox modelling of Miocene extensional faulting in the Outer Moray Firth, in *Tectonics and seismic sequence stratigraphy*, vol. 71, edited by G. D. Williams, pp. 141–162, Geological Society, London, Special Publications.

Hildebrand-Mittlefehldt, N. (1979), Deformation near a fault termination, in a clay experiment part 1: a fault in a clay experiment, *Tectonophysics*, *57*, 131–150.

Hirsch, F., A. Flexer, A. Rosenfeld, and A. Yellin-Dror (1995), Palinspastic and crustal setting of the eastern Mediterranean, *J. Pet. Geol.*, *18*(2), 149–170.

Hirsch, F., J.-P. Bassoulet, E. Cariou, B. Conway, H. R. Feldman, L. Grossowicz, A. Honigstein, E. F. Owen, and A. Rosenfeld (1998), The jurassic of the southern levant biostratgraphy paleogeography and cyclic events, in *Peri-Tethys Memoir 4: epicratonic basins of Peri-Tethyan platforms*, edited by S. Crasquin-Soleau and E. Barrier, pp. 213–235, Memoire du Museum national d'histoire naturelle, Paris.

Hofstetter, R., Y. Klinger, A.-Q. Amrat, L. Rivera, and L. Dorbath (2007), Stress tensor and focal mechanisms along the Dead Sea fault and related structural elements based on seismological data, *Tectonophysics*, *429*(3-4), 165–181, doi:10.1016/j.tecto.2006.03.010.

Homberg, C., É. Barrier, M. Mroueh, W. Hamdan, and F. Higazi (2009), Basin tectonics during the Early Cretaceous in the Levant margin, Lebanon, *J. Geodyn.*, *47*(4), 218–223, doi:10.1016/j.jog.2008.09.002.

Homberg, C., É. Barrier, M. Mroueh, C. Müller, W. Hamdan, and F. Higazi (2010), Tectonic evolution of the central Levant domain (Lebanon) since Mesozoic time, in *Evolution of the Levant margin and western Arabia platform since the Mesozoic*, vol. 341, edited by C. Homberg and M. Bachmann, pp. 245–268, Geological Society, London.

Horsfield, W. T. (1977), An experimental approach to basement-controlled faulting, *Geologie*, *56*(4), 363–370.

Hounsfield, G. N. (1973), Computerized transverse axial scanning (tomography), *Br. J. Radiol.*, *46*, 1016–1022.

Hsu, K. J., W. B. F. Ryan, and M. B. Cita (1973), Late Miocene Desiccation of the Mediterranean, *Nature*, *242*, 240–244.

Hubbert, M. K. (1937), Theory of scale models as applied to the study of geologic structures, *Geol. Soc. Am. Bull.*, *48*, 1459–1520.

Hurst, A., J. A. Cartwright, and D. Duranit (2003), Fluidization structures produced by upward injection of sand through a sealing lithology, in *Subsurface sediment mobilization*, edited by P. Van Rensbergen, R. R. Hillis, A. J. Maltman, and C. K. Morley, pp. 123–137, Geological Society, London, Special Publications.

Jackson, C. A. L., and A. Rotevatn (2013), 3D seismic analysis of the structure and evolution of a salt-influenced normal fault zone: A test of competing fault growth models, *J. Struct. Geol.*, *54*, 215–234, doi:10.1016/j.jsg.2013.06.012.

Jackson, J. A. (1987), Active normal faulting and crustal extension, in *Continental extensional tectonics*, vol. 28, edited by M. P. Coward, J. F. Dewey, and P. L. Hancock, pp. 3–17, Geological Society, London, Special Publications.

Jeager, J. C., and N. G. W. Cook (1976), *Fundamentals of Rock Mechanics*, Chapman & Hall, Wiley, New York.

Joffe, S., and Z. Garfunkel (1987), Plate kinematics of the circum Red Sea-a, *Tectonophysics*, *141*, 5–22.

Jolivet, L., and C. Faccenna (2000), Mediterranean extension and the Africa-Eurasia collision, *Tectonics*, *19*(6), 1095–1106.

Joseph-Hai, N., Y. Eyal, and R. Weinberger (2010), Mesoscale folds and faults along a flank of a Syrian Arc monocline, discordant to the monocline trend, in *Evolution of the Levant margin and western Arabia platform since the Mesozoic*, vol. 341, edited by C. Homberg and M. Bachmann, pp. 211–226, Geological Society, London, Special Publications.

Kane, K. E., C. A. L. Jackson, and E. Larsen (2010), Normal fault growth and fault-related folding in a salt-influenced rift basin: South Viking Graben, offshore Norway, *J. Struct. Geol.*, *32*(4), 490–506, doi:10.1016/j.jsg.2010.02.005.

Khair, K. (2001), Geomorphology and seismicity of the Roum fault as one of the active branches of the Dead Sea fault system in Lebanon, *J. Geophys. Res.*, *106*(2001), 4233–4245.

Khair, K., and G. N. Tsokas (1999), Nature of the Levantine (eastern Mediterranean) crust from multiple-source Werner deconvolution of Bouguer gravity anomalies, *J. Geophys. Res.*, *104*(B11), 25469–25478, doi:10.1029/1999JB900228.

Khair, K., M. Khawlie, F. Haddad, M. Barazangi, D. Seber, and T. A. Chaimov (1993), Bouguer gravity and crustal structure of the Dead Sea transform fault and adjacent mountain belts in Lebanon, *Geology*, *21*, 739–742.

Khair, K., G. N. Tsokas, and T. Sawaf (1997), Crustal structure of the northern Levant region: multiple source Werner deconvolution estimates for Bouguer gravity anomalies, *Geophys. J. Int.*, *128*(3), 605–616, doi:10.1111/j.1365-246X.1997.tb05322.x.

Kim, Y.-S., and D. J. Sanderson (2005), The relationship between displacement and length of faults: a review, *Earth-Science Rev.*, *68*(3-4), 317–334, doi:10.1016/j.earscirev.2004.06.003.

Kosi, W., G. Tari, F. H. Nader, C. Skiple, B. D. Trudgill, and D. Lazar (2012), Structural analogy between the "piano key faults" of deep-water Lebanon and the extensional faults of the Canyonlands grabens, Utah, United States, *Lead. edge*, (July), 824–830.

Krantz, R. W. (1991), Measurements of friction coefficients and cohesion for faulting and fault reactivation in laboratory models using sand and sand mixtures, *Tectonophysics*, *188*, 203–207.

Lie, O., C. Skiple, and C. Lowry (2011), New insights into the Levantine basin, *GeoExpro*, *8*(1).

Litak, R. K., M. Barazangi, G. E. Brew, T. Sawaf, A. Al-imam, and W. Al-Youssef (1998), Structure and Evolution of the Petroliferous Euphrates Graben System, Southeast Syria, *Am. Assoc. Pet. Geol. Bull.*, *82*(6), 1173–1190.

Lonergan, L., and J. A. Cartwright (1999), Polygonal Faults and Their Influence on Deep-Water Sandstone Reservoir Geometries , Alba Field , United Kingdom Central North Sea, *Am. Assoc. Pet. Geol. Bull.*, *83*(3), 410–432.

Lonergan, L., J. A. Cartwright, and R. Jolly (1998), The geometry of polygonal fault systems in Tertiary mudrocks of the North Sea, *J. Struct. Geol.*, *20*(5), 529–548.

Lundin, E. R. (1992), Thin-skinned extensional tectonics on a salt detachment, northern Kwanza Basin, Angola, *Mar. Pet. Geol.*, *9*(October 1991), 405–411.

Lyberis, N. (1988), Tectonic evolution of the Gulf of Suez and the Gulf of Aqaba, *Tectonophysics*, *153*(1-4), 209–220, doi:10.1016/0040-1951(88)90016-9.

MacLeod, M. K., R. a. Hanson, C. R. Bell, and S. McHugo (1999), The Alba Field ocean bottom cable seismic survey: Impact on development, *Lead. Edge*, *18*, 1306, doi:10.1190/1.1438206.

Magoon, L. B., and W. G. Dow (1994), The petroleum system, in *The petroleum system from source to trap*, edited by W. G. Dow and L. B. Magoon, pp. 3–24, AAPG memoir 60.

Mahmoud, S., R. Reilinger, S. Mcclusky, P. Vernant, and A. Tealeb (2005), GPS evidence for

northward motion of the Sinai Block: Implications for E. Mediterranean tectonics, *Earth Planet. Sci. Lett.*, *238*, 217–224, doi:10.1016/j.epsl.2005.06.063.

Makris, J., and C. Stobbe (1984), Physical properties and state of the crust and upper mantle of the eastern Mediterranean sea deduced from geophysical data, *Mar. Geol.*, *55*(1984), 347–363.

Makris, J., Z. Ben-Avraham, A. Behle, A. Ginzburg, P. Giese, L. Steinmetz, R. B. Whitmarsh, and S. Eleftheriou (1983), Seismic refraction profiles between Cyprus and Israel and their interpretation, *Geophys. J. Int.*, *75*, 575–591.

Mann, P. (2007), Global catalogue , classification and tectonic origins of restraining- and releasing bends on active and ancient strike-slip fault systems, in *Tectonics of strike-slip restraining and releasing bends*, edited by W. D. Cunningham and P. Mann, pp. 13–142, Geological Society, London, Special Publications.

Mann, P., M. R. Hempton, D. C. Bradley, and K. Burke (1983), Development of pull-apart basins, *J. Geol.*, *91*(5), 529–5541.

Mansfield, C. S., and J. A. Cartwright (1996), High resolution fault displacement mapping from three-dimensional seismic data: evidence for dip linkage during fault growth, *J. Struct. Geol.*, *18*(2/3), 249–263.

Mansfield, C. S., and J. A. Cartwright (2001), Fault growth by linkage: observations and implications from analogue models, *J. Struct. Geol.*, *23*, 745–763.

Mart, Y. (1984), The tectonic regime of the southeastern Mediterranean continental margin, *Mar. Geol.*, *55*(3-4), 365–386, doi:10.1016/0025-3227(84)90077-X.

Mart, Y. (1991), The Dead Sea Rift: from continental rift to incipient ocean, *Tectonophysics*, *197*(2-4), 155–179, doi:10.1016/0040-1951(91)90039-U.

Mart, Y. (1994), Ptolemdis basin : The tectonic origin of a Senonian marine basin underneath the southeastern Mediterranean Sea, *Tectonophysics*, *234*, 5–17.

Mart, Y., and P. D. Rabinowitz (1986), The Red Sea is approximately 2300 km long and up to 350 km wide with depths reaching up to 2600 m . Its bathyal zone , which is bounded by the faulted continentai margins , is built of two coaxial troughs-an inner or axial trough and an outer or main trou, *Tectonophysics*, *124*, 85–113.

Martinez, F., and J. R. Cochran (1988), Structure and tectonics of the northern Red Sea: catching a continental margin between rifting and drifting, *Tectonophysics*, *150*, 1–32, doi:10.1016/0040-1951(88)90293-4.

Mattioni, L., W. Sassi, and J. Callot (2007), Analogue models of basin inversion by transpression: role of structural heterogeneity, in *Deformation of the continental crust: the legacy of Mike Coward*, vol. 272, edited by A. C. Ries, R. W. H. Butler, and R. H. Graham, pp. 397–417, Geological Society, London, Special Publications.

McClay, K. R. (1989), Analogue models of inversion tectonics, in *Inversion tectonics*, vol. 44, edited by M. A. Cooper and G. D. Williams, pp. 41–59, Geological Society, London, Special Publications.

McClay, K. R. (1990), Extensional fault systems in sedimentary basins: a review of analogue model studies, *Mar. Pet. Geol.*, *7*, 206–233.

McClay, K. R. (1996), Recent advances in analogue modelling: uses in section interpretation and validation, in *Modern developments in structural interpretation, validation and modelling*, vol. 99, edited by P. G. Buchanan and D. A. Nieuwland, pp. 201–225, Geological Society, London, Special Publications.

Mcclay, K. R., and M. Bonora (2001), Analog models of restraining stepovers in strike-slip fault systems, *Am. Assoc. Pet. Geol. Bull.*, *85*(2), 233–260.

Mcclay, K. R., and P. G. Ellis (1987), Analogue models of extensional fault geometries, in *Continental extensional tectonics*, vol. 28, edited by M. P. Coward, J. F. Dewey, and P. L. Hancock, pp. 109–125, Geological Society, London, Special Publications.

McClusky, S., R. Reilinger, S. Mahmoud, D. Ben Sari, and A. Tealeb (2003), GPS constraints on

Africa (Nubia) and Arabia plate motions, *Geophys. J. Int.*, *155*, 126–138.

Mcgrath, A. G., and I. Davison (1995), Damage zone geometry around fault tips, *J. Struct. Geol.*, *17*(7), 1011–1024.

McKenzie, D. . (1970), The development of the Red Sea and Gulf of Aden in relation to plate tectonicst (summary only), *Philos. Trans. R. Soc. London*, *267*, 393–395.

McKenzie, D. ., and J. A. Jackson (1986), A block model of distributed deformation by faulting, *J. Geol. Soc. London.*, *143*(2), 349–353, doi:10.1144/gsjgs.143.2.0349.

McKenzie, D. ., D. Davis, and P. Molnar (1970), Plate tectonics of the Red Sea and East Africa, *Nature*, *226*, 243–248.

Miller, J. F., and S. Mitra (2011), Deformation and secondary faulting associated with basement-involved compressional and extensional structures, *Am. Assoc. Pet. Geol. Bull.*, *95*(4), 675–689, doi:10.1306/09131010007.

Mitra, S. (1993), Geometry and kinematic evolution of inversion structures, *Am. Assoc. Pet. Geol. Bull.*, *77*(7), 1159–1191.

Mitra, S., and D. Paul (2011), Structural geometry and evolution of releasing and restraining bends: Insights from laser-scanned experimental models, *Am. Assoc. Pet. Geol. Bull.*, *95*(7), 1147–1180, doi:10.1306/09271010060.

Montadert, L., P. H. Semb, O. Lie, and S. Kassinis (2010), New seismic may put offshore Cyprus hydrocarbon prospects in the spotlight, *First Break*, *28*(April), 91–101.

Montadert, L., S. Nicolaides, P. H. Semb, and O. Lie (2014), Petroleum Systems offshore Cyprus, in *Petroleum systems of the Tethyan region*, edited by L. Marlow, C. Kendall, and L. Yose, pp. 301–334, AAPG special publication, Tulsa.

Morhange, C., P. a. Pirazzoli, N. Marriner, L. F. Montaggioni, and T. Nammour (2006), Late Holocene relative sea-level changes in Lebanon, Eastern Mediterranean, *Mar. Geol.*, *230*(1-2), 99–114, doi:10.1016/j.margeo.2006.04.003.

Moustafa, A. R. J. (2010), Structural setting and tectonic evolution of North Sinai folds, Egypt, in *Evolution of the Levant margin and western Arabia platform since the Mesozoic*, vol. 341, edited by C. Homberg and M. Bachmann, pp. 37–63, Geological Society, London, Special Publications.

Moustafa, A. R. J., and M. H. Khalil (1994), Rejuvenation of the eastern Mediterranean passive continental margin in northern and central Sinai : new data from the Themed Fault, *Geol. Mag.*, *131*(4), 435–448.

Müller, C., F. Higazi, W. Hamdan, and M. Mroueh (2010), Revised stratigraphy of the Upper Cretaceous and Cenozoic series of Lebanon based on nannofossils, in *Geological Society, London, Special Publications*, vol. 341, edited by C. Homberg and M. Bachmann, pp. 287–303, Geological Society, London, Special Publications.

Muraoka, H., and H. Kamata (1983), Displacement distribution along minor fault traces, *J. Struct. Geol.*, *5*(5), 483–495.

Nader, F. H. (2003), Petrographic and Geochemical Study of the Kesrouane Formation (Jurassic), Mount Lebanon : Implications on Dolomitization and Petroleum Geology, PhD thesis, Katholieke Universiteit Leuven.

Nader, F. H. (2011), The petroleum prospectivity of Lebanon: an overview, *J. Pet. Geol.*, *34*(April), 135–156.

Nader, F. H., and R. Swennen (2004), The hydrocarbon potential of Lebanon: new insights from regional correlations and studies of Jurassic dolimitization, *J. Pet. Geol.*, *27*(3), 253–275.

Nalpas, T., S. Le Douaran, J.-P. Brun, P. Unternehr, and J.-P. Richert (1995), Inversion of the Broad Fourteens Basin (offshore Netherlands), a small-scale model investigation, *Sediment. Geol.*, *95*(94), 237–250, doi:10.1016/0037-0738(94)00113-9.

Nelson, M. (2006), 3D geometry and kinematics of non-colinear fault intersections, PhD thesis, Cardiff University.

Nemer, T. (1999), The roum fault: extent and associated structures, MSc thesis, American University of Beirut.

Nemer, T., and M. Meghraoui (2006), Evidence of coseismic ruptures along the Roum fault (Lebanon): a possible source for the AD 1837 earthquake, *J. Struct. Geol.*, *28*(8), 1483–1495, doi:10.1016/j.jsg.2006.03.038.

Netzeband, G., K. Gohl, C. Hübscher, Z. Ben-Avraham, G. a. Dehghani, D. Gajewski, and P. Liersch (2006), The Levantine Basin—crustal structure and origin, *Tectonophysics*, *418*(3-4), 167–188, doi:10.1016/j.tecto.2006.01.001.

Nicol, A., J. Watterson, J. J. Walsh, and C. Childs (1996), The shapes, major axis orientations and displacement patterns of fault surfaces, *J. Struct. Geol.*, *18*(2/3), 235–248.

Nicol, A., J. J. Walsh, J. Watterson, P. A. R. Nell, and P. G. Bretan (2003), The geometry, growth and linkage of faults within a polygonal fault system from South Australia, in *Subsurface sediment mobilization*, vol. 216, edited by P. Van Rensbergen, R. R. Hillis, A. J. Maltman, and C. K. Morley, pp. 245–261, Geological Society, London, Special Publications.

Oertel, G. (1965), The mechanism of faulting in clay experiments, *Tectonophysics*, *2*(5), 343–393.

Okay, A. I. (2008), Geology of Turkey : A Synopsis, *Anschnitt*, *21*, 19–42.

Pascoe, R., R. Hooper, K. Storhaug, and H. Harper (1999), Evolution of extensional styles at the southern termination of the Nordland ridge, Mid-Norway: a response to variations in coupling above Triassic salt, in *Petroleum geology of Northwest Europe: Proceedings of the 5th conferece*, edited by A. J. Fleet and S. A. R. Boldy, pp. 83–90, Geological Society, London.

Peacock, D. C. P., and D. . Sanderson (1991), Displacements, segment linkage and relay ramps in normal fault zones, *J. Struct. Geol.*, *13*(6), 721–733, doi:10.1016/0191-8141(91)90033-F.

Peacock, D. C. P., and D. J. Sanderson (1992), Effects of layering and anisotropy on fault geometry, *J. Geol. Soc. London.*, *149*(5), 793–802, doi:10.1144/gsjgs.149.5.0793.

Peacock, D. C. P., and D. J. Sanderson (1994), Geometry and Development of Relay Ramps in Normal Fault Systems, *Am. Assoc. Pet. Geol. Bull.*, *2*(2), 147–165.

Peacock, D. C. P., and X. Zhang (1993), Field examples and numerical modelling of oversteps and bends along normal faults in cross-section, *Tectonophysics*, *234*(1993), 147–167.

Le Pichon, X., and J.-M. Gaulier (1988), The rotation of Arabia and the Levant fault system, *Tectonophysics*, *153*(1-4), 271–294, doi:10.1016/0040-1951(88)90020-0.

Le Pichon, X., and C. Kreamer (2010), The Miocene-to-Present Kinematic Evolution of the Eastern Mediterranean and Middle East and Its Implications for Dynamics, *Annu. Rev. Earth Planet. Sci.*, *38*, 323–351, doi:10.1146/annurev-earth-040809-152419.

Ponikarov, V. P. (1966), *The geological map of Syria scale 1:1000000 explanatory notes*, Syrian Arab Republic Ministry of Industry, Damascus.

Preto, N., M. Franceschi, G. Gattolin, M. Massironi, A. Riva, P. Gramigna, L. Bertoldi, and S. Nardon (2011), The Latemar: A Middle Triassic polygonal fault-block platform controlled by synsedimentary tectonics, *Sediment. Geol.*, *234*(1-4), 1–18, doi:10.1016/j.sedgeo.2010.10.010.

Quennell, A. M. (1958), the Structural and Geomorphic Evolution of the Dead Sea Rift, *Q. J. Geol. Soc.*, *114*(1-4), 1–24, doi:10.1144/gsjgs.114.1.0001.

Quennell, A. M. (1984), The Western Arabia rift system, in *The geological evolution of the Eastern Mediterranean*, vol. 17, edited by R. J. Dixon and A. H. F. Robertson, pp. 775–788, Geological Society, London, Special Publications, London.

Raleigh, C. B., and S. Paterson (1965), Experimental Deformation of Serpentinite and Its Tectonic Implications, *J. Geophys. Res.*, *70*(16), 3965–3985.

Ramberg, H. (1967), *Gravity, Deformation and the Earth's Crust*, Academic Press, New York.

Rank-Friend, M., and C. F. Elders (2004), The Evolution and Growth of Central Graben Salt Structures, Salt Dome Province, Danish North Sea, in *3D seismic technology: application to the exploration of sedimentary basins*, vol. 29, edited by R. J. Davies, J. A. Cartwright, S. A. Stewart, M. Lappin, and J. R. Underhill, pp. 149–164, Geological Society, London, Memoirs, London.

Reading, H. G., and M. Richards (1994), Turbidite Systems in Deep-Water Basin Margins Classified by Grain Size and Feeder System 1, *Am. Assoc. Pet. Geol. Bull.*, *78*(5), 792–822.

Reches, Z. (1988), Evolution of fault patterns in clay experiments, *Tectonophysics*, *145*, 141–156.

Reilinger, R. et al. (2006), GPS constraints on continental deformation in the Africa-Arabia-Eurasia continental collision zone and implications for the dynamics of plate interactions, *J. Geophys. Res.*, *111*(B5), B05411, doi:10.1029/2005JB004051.

Renouard, G. (1955), Oil prospects of Lebanon, *Am. Assoc. Pet. Geol. Bull.*, *39*(11), 2125–2169.

Richard, P. (1990), Champs de failles au dessus d'un decrochement de socle: modelisation experimentale, PhD thesis, Universite de Rennes.

Richard, P., B. Mocquet, and P. R. Cobbold (1991), Experiments on simultaneous faulting and folding above a basement wrench fault, *Tectonophysics*, *188*, 133–141.

Riedel, W. (1929), Zur Mechanik geologischer Brucherscheinungen, *Cent. für Mineral.*, (Abteilung B), 354–368.

Rippon, J. H. (1984), Contoured patterns of the throw and hade of normal faults in the Coal Measures (Westphalian) of north-east Derbyshire, *Proc. Yorksh. Geol. Soc.*, *45*(3), 147–161, doi:10.1144/pygs.45.3.147.

Roberts, G., and D. Peace (2007), Hydrocarbon plays and prospectivity of the Levantine Basin , offshore Lebanon and Syria from modern seismic data, *GeoArabia*, *12*(3).

Robertson, A. H. F. (1998a), Mesozoic-Tertiary tectonic evolution of the Easternmost Mediterranean area: integration of marine and land evidence, *Proc. Ocean Drill. program, Sci. results*, *160*.

Robertson, A. H. F. (1998b), Tectonic significance of the Eratosthenes Seamount: a continental fragment in the process of collision with a subduction zone in the eastern Mediterranean (Ocean Drilling Program Leg 160), *Tectonophysics*, *298*(1-3), 63–82, doi:10.1016/S0040-1951(98)00178-4.

Robertson, A. H. F. (2006), Sedimentary evidence from the south Mediterranean region (Sicily, Crete, Peloponnese, Evia) used to test alternative models for the regional tectonic setting of Tethys during Late Palaeozoic-Early Mesozoic time, in *Tectonic Development of the Eastern Mediterranean Region*, vol. 260, edited by A. H. F. Robertson and D. Mountrakis, pp. 91–154, Geological Society, London, Special Publications.

Robertson, A. H. F. (2007), Overview of tectonic settings related to the rifting and opening of Mesozoic ocean basins in the Eastern Tethys: Oman, Himalayas and Eastern Mediterranean regions, in *Imaging, mapping and modelling continental lithosphere extension and breakup*, vol. 282, edited by G. D. Karner, G. Manataschal, and L. M. Pinheiro, pp. 325–388, Geological Society, London, Special Publications.

Robertson, A. H. F., and J. E. Dixon (1984), Introduction: aspects of the geological evolution of the Eastern Mediterranean Introduction: aspects of the geological evolution of the Eastern Mediterranean, in *The geological evolution of the Eastern Mediterranean*, vol. 17, edited by A. H. F. Robertson and J. E. Dixon, pp. 1–74, Geological Society, London, Special Publications.

Robertson, A. H. F., and D. Mountrakis (2006), Tectonic development of the Eastern Mediterranean region: an introduction, in *Tectonic Development of the Eastern Mediterranean Region*, vol. 260, edited by A. H. F. Robertson and D. Mountrakis, pp. 1–9, Geological Society, London, Special Publications.

Robertson, A. H. F., J. E. Dixon, S. Brown, A. Collins, A. P. Morris, E. Pickett, I. R. Sharp, and T. Ustaomer (1996), Alternative tectonic models

for the Late Palaeozoic-Early Tertiary development of Tethys in the Eastern Mediterranean region, in *Palaeomagnetism and tectonics of the Mediterranean region*, vol. 105, edited by A. Morris and D. H. Tarling, pp. 239–263, Geological Society, London, Special Publications.

Roche, V. (2011), Architecture et croissance des failles dans les alternances argilo-calcaires, PhD thesis, Universite Pierre et Marie Curie.

Roche, V., C. Homberg, and M. Rocher (2012a), Architecture and growth of normal fault zones in multilayer systems : A 3D field analysis in the South-Eastern Basin , France, *J. Struct. Geol.*, *37*, 19–35, doi:10.1016/j.jsg.2012.02.005.

Roche, V., C. Homberg, and M. Rocher (2012b), Fault displacement profiles in multilayer systems: from fault restriction to fault propagation, *Terra Nov.*, *24*(6), 499–504, doi:10.1111/j.1365-3121.2012.01088.x.

Roche, V., C. Homberg, and M. Rocher (2013), Fault nucleation, restriction, and aspect ratio in layered sections: Quantification of the strength and stiffness roles using numerical modeling, *J. Geophys. Res. Solid Earth*, *118*(8), 4446–4460, doi:10.1002/jgrb.50279.

Roche, V., C. Homberg, C. David, and M. Rocher (2014), Normal faults, layering and elastic properties of rocks, *Tectonophysics*, *622*, 96–109, doi:10.1016/j.tecto.2014.03.006.

Ron, H. (1987), Deformation along the Yammuneh the restaining bend of the Dead Sea Transform: paleomagnetic data and kinematic implications, *Tectonics*, *6*(5), 653–666.

Ron, H., and Y. Eyal (1985), Intraplate deformation by block rotation and mesostructures along the Dead Sea transform, northern Israel, *Tectonics*, *4*(1), 85–105.

Ron, H., R. Freund, Z. Garfunkel, and A. Nur (1984), Block rotation by strike-slip faulting: structural and paleomagnetic evidence, *J. Geol. Res.*, *89*(B7), 6256–6270.

Ron, H., A. Nur, and Y. Eyal (1990), Multiple strike-slip fault sets: a case study from the Dead Sea Transform, *Tectonics*, *9*(6), 1421–1431.

Ryan, W. B. F. (2009), Decoding the mediterranean salinity crisis, *Sedimentology*, *56*, 95–136, doi:10.1111/j.1365-3091.2008.01031.x.

Sabbagh, G. (1961), Stratigraphie et tectonique du liban generalites: exemple de deux structures anticlinales, Memoire de these, Faculte de Science de Grenoble.

Sabbagh, G. (1962), Geological cross-section across northern and southern Mount Lebanon, *Am. Univ. Beirut, Arch.*

Salel, J. F., and M. Seguret (1994), Late Cretaceous to Palaeogene thin-skinned tectonics of the Palmyrides belt (Syria), *Tectonophysics*, *234*, 265–290.

Sanlaville, P. (1974), Le rôle de la mer dans les aplanissements côtiers du Liban, *Rev. Geogr. Lyon*, *49*(4), 295–310.

Sassi, W., and B. Colletta (1993), Modelling of structural complexity in sedimentary basins : the role of pre-existing faults in thrust tectonics, *Tectonophysics*, *226*, 97–112.

Sawaf, T., D. Al-Saad, A. Gebran, M. Barazangi, J. A. Best, and T. A. Chaimov (1993), Stratigraphy and structure of eastern Syria across the Euphrates depression, *Tectonophysics*, *220*(1-4), 267–281, doi:10.1016/0040-1951(93)90235-C.

Sawaf, T., G. E. Brew, R. K. Litak, and M. Barazangi (2001), Geologic evolution of the intraplate palmyride basin and euphrates fault system syria, in *Peri-Tethys Memoir 6: Peri-Tethyan rift/Wrench basins and passive margins*, edited by P. A. Ziegler, W. Cavazza, A. H. F. Robertson, and S. Crasquin-Soleau, pp. 441–467, Memoire du Museum national d'histoire naturelle, Paris.

Schellart, W. P. (2000), Shear test results for cohesion and friction coefficients for different granular materials: scaling implications for their usage in analogue modelling, *Tectonophysics*, *324*, 1–16.

Schlagenhauf, A., I. Manighetti, J. Malavieille, and S. Dominguez (2008), Incremental growth of normal faults : Insights from a laser-equipped analog experiment, *Earth Planet. Sci. Lett.*, *273*, 299–311, doi:10.1016/j.epsl.2008.06.042.

Schlische, R. W., S. S. Young, R. V Ackermann, and A. Gupta (1996), Geometry and scaling relations of a population of very small rift-related normal faults, *Geology*, *24*(8), 693–686, doi:10.1130/0091-7613(1996)024<0683.

Scholz, C. H. (1982), Scaling laws for large earthquakes: consequences for physical models, *Bull. Seismol. Soc. Am.*, *72*(1).

Schöpfer, M. P. J., C. Childs, and J. J. Walsh (2006), Localisation of normal faults in multilayer sequences, *J. Struct. Geol.*, *28*(5), 816–833, doi:10.1016/j.jsg.2006.02.003.

Schöpfer, M. P. J., C. Childs, J. J. Walsh, T. Manzocchi, and H. a. Koyi (2007), Geometrical analysis of the refraction and segmentation of normal faults in periodically layered sequences, *J. Struct. Geol.*, *29*(2), 318–335, doi:10.1016/j.jsg.2006.08.006.

Schreurs, G., and B. Colletta (1998), Analogue modelling of faulting in zones of continental transpression and transtension, in *Continental transpressional and transtensional tectonics*, edited by R. E. Holdsworth, R. A. Strachan, and J. F. Dewey, pp. 59–79, Geological Society, London, Special Publications, London.

Schueller, S. (2004), Localisation de la deformation et fracturation associee, PhD thesis, Universite de Rennes 1.

Schultz, R. A., and H. Fossen (2002), Displacement–length scaling in three dimensions: the importance of aspect ratio and application to deformation bands, *J. Struct. Geol.*, *24*(9), 1389–1411, doi:10.1016/S0191-8141(01)00146-8.

Schultz, R. A., C. H. Okubo, and S. J. Wilkins (2006), Displacement-length scaling relations for faults on the terrestrial planets, *J. Struct. Geol.*, 1–12, doi:10.1016/j.jsg.2006.03.034.

Searle, M. P. (1994), Structure of the intraplate eastern Palmyride fold belt, Syria, *Geol. Soc. Am. Bull.*, *106*, 1332–1350, doi:10.1130/0016-7606(1994)106<1332.

Searle, M. P., S.-L. Chung, and C.-H. Lo (2010), Geological offsets and age constraints along the northern Dead Sea fault, Syria, *J. Geol. Soc. London.*, *167*(5), 1001–1008, doi:10.1144/0016-76492010-009.

Segev, A., and M. Rybakov (2010), Effects of Cretaceous plume and convergence, and Early Tertiary tectonomagmatic quiescence on the central and southern Levant continental margin, *J. Geol. Soc. London.*, *167*(4), 731–749, doi:10.1144/0016-76492009-118.

Segev, A., M. Rybakov, V. Lyakhovsky, A. Hofstetter, G. Tibor, V. Goldshmidt, and Z. Ben-avraham (2006), The structure, isostasy and gravity field of the Levant continental margin and the southeast Mediterranean area, *Tectonophysics*, *425*(1-4), 137–157, doi:10.1016/j.tecto.2006.07.010.

Segev, A., U. Schattner, and V. Lyakhovsky (2011), Middle–Late Eocene structure of the southern Levant continental margin — Tectonic motion versus global sea-level change, *Tectonophysics*, *499*(1-4), 165–177, doi:10.1016/j.tecto.2011.01.006.

Sengor, A. M. C., and W. S. F. Kidd (1979), Post-collisional tectonics of the turkish-iranian plateau and a comparison with tibet, *Tectonophysics*, *55*, 361–376.

Sengor, A. M. C., and Y. Yilmaz (1981), Tethyan evolution of Turkey: a plate tectonic approach, *Tectonophysics*, *75*, 181–241.

Sengor, A. M. C., Y. Yilmaz, and O. Sungurlu (1984), Tectonics of the Mediterranean Cimmerides: nature and evolution of the western termination of Palaeo-Tethys, in *The geological evolution of the Eastern Mediterranean*, vol. 17, edited by J. E. Dixon and A. H. F. Robertson, pp. 77–112, Geological Society Special Publications, London.

Sengor, A. M. C., N. Gorur, and F. Saroglu (1985), Strike slip faulting and related basin formation in zones of tectonic escape: Turkey as a case study, *Soc. Econ. Paleontol. Mineral.*, 227–264.

Shahar, J. (1994), The Syrian arc system: an overview, *Palaeogeogr. Palaeoclimatol. Palaeoecol.*, *112*, 125–142.

Shin, H., J. C. Santamarina, and J. a. Cartwright (2008), Contraction-driven shear failure in compacting uncemented sediments, *Geology*, *36*(12), 931, doi:10.1130/G24951A.1.

Shin, H., J. C. Santamarina, and J. A. Cartwright (2010), Displacement field in contraction-

driven faults, *J. Geophys. Res.*, *115*(B7), 1–13, doi:10.1029/2009JB006572.

Soliva, R., and A. Benedicto (2004), A linkage criterion for segmented normal faults, *J. Struct. Geol.*, *26*, 2251–2267, doi:10.1016/j.jsg.2004.06.008.

Soliva, R., and A. Benedicto (2005), Geometry, scaling relations and spacing of vertically restricted normal faults, *J. Struct. Geol.*, *27*, 317–325, doi:10.1016/j.jsg.2004.08.010.

Soliva, R., A. Benedicto, and L. Maerten (2006), Spacing and linkage of confined normal faults: Importance of mechanical thickness, *J. Geophys. Res.*, *111*(October 2004), 1–17, doi:10.1029/2004JB003507.

Soliva, R., A. Benedicto, D. D. Schultz-Ela, L. Maerten, and L. Micarelli (2008), Displacement and interaction of normal fault segments branched at depth: Implications for fault growth and potential earthquake rupture size, *J. Struct. Geol.*, *30*(10), 1288–1299, doi:10.1016/j.jsg.2008.07.005.

Stampfli, G. M., and G. D. Borel (2002), A plate tectonic model for the Paleozoic and Mesozoic constrained by dynamic plate boundaries and restored synthetic oceanic isochrons, *Earth Planet. Sci. Lett.*, *196*, 17–33.

Stampfli, G. M., and C. Hochard (2009), Plate tectonics of the Alpine realm, in *Ancient orogens and modern analogues*, vol. 327, edited by J. B. Murphy, J. D. Keppie, and A. J. Hynes, pp. 89–111, Geological Society Special Publication, London.

Steckler, M. S., and U. S. ten Brink (1986), Lithospheric strength variations as a control on new plate boundaries: examples from the northern Red Sea region, *Earth Planet. Sci. Lett.*, *79*(1-2), 120–132, doi:10.1016/0012-821X(86)90045-2.

Steckler, M. S., F. Berthelot, N. Lyberis, and X. Le Pichon (1988), Subsidence in the Gulf of Suez : implications for rifting and plate kinematics, *Tectonophysics*, *153*, 249–270.

Stewart, S. A. (2006), Implications of passive salt diapir kinematics for reservoir segmentation by radial and concentric faults, *Mar. Pet. Geol.*, *23*(8), 843–853, doi:10.1016/j.marpetgeo.2006.04.001.

Stuevold, L. M., R. B. Faerseth, L. Arnesen, J. A. Cartwright, and N. Möller (2003), Polygonal faults in the Ormen Lange Field, Møre Basin, offshore Mid Norway, in *Subsurface sediment mobilization*, vol. 216, edited by P. Van Ransbergem, R. R. Hillis, A. J. Maltman, and C. K. Morley, pp. 263–281, Geological Society, London, Special Publications.

Sylvester, A. G. (1988), Strike-slip faults, *Geol. Soc. Am.*, *100*(November), 1666–1703.

Tchalenko, J. S. (1970), Similarities between Shear zones of different magnitudes, *Geol. Soc. Am. Bull.*, *81*(June), 1625–1640.

Thorsen, C. E. (1963), Age of growth faulting in the southeast Louisiana, *Trans. Gulf Coast Assoc. Geol. Soc.*, *13*, 103–110.

Tvedt, A. B. M., A. Rotevatn, C. A. L. Jackson, H. Fossen, and R. L. Gawthorpe (2013), Growth of normal faults in multilayer sequences: A 3D seismic case study from the Egersund Basin, Norwegian North Sea, *J. Struct. Geol.*, *55*, 1–20, doi:10.1016/j.jsg.2013.08.002.

Twiss, R. J., and E. M. Moore (1992), *Structural geology*, W. H. Freeman and company, New York.

Vendeville, B., P. R. Cobbold, P. Davy, J. P. Brun, and P. Choukroune (1987), Physical models of extensional tectonics at various scales, in *Continental extensional tectonics*, edited by M. P. Coward, J. F. Dewey, and P. L. Hancock, pp. 95–107, London.

Vendeville, B. C., and M. P. a. Jackson (1992a), The fall of diapirs during thin-skinned extension, *Mar. Pet. Geol.*, *9*(March 1991), 354–371.

Vendeville, B. C., and M. P. a. Jackson (1992b), The rise of diapirs during thin-skinned extension, *Mar. Pet. Geol.*, *9*, 331–353.

Vidal, N., J. Alvarez-Marron, and D. Klaeschen (2000), Internal configuration of the Levantine Basin from seismic reflection data (eastern Mediterranean), *Earth Planet. Sci. Lett.*, *180*, 77–89.

Viola, G., F. Odonne, and N. . Mancktelow (2004), Analogue modelling of reverse fault reactivation in strike–slip and transpressive regimes: application to the Giudicarie fault system, Italian Eastern Alps, *J. Struct. Geol.*, *26*(3), 401–418, doi:10.1016/j.jsg.2003.08.014.

Walley, C. D. (1988), A braided strike-slip model for the northern continuation of the Dead Sea Fault and its implications for Levantine tectonics, *Tectonophysics*, *145*(1-2), 63–72, doi:10.1016/0040-1951(88)90316-2.

Walley, C. D. (1998), Some outstanding issues in the geology of Lebanon and their importance in the tectonic evolution of the Levantine region, *Tectonophysics*, *298*(1-3), 37–62, doi:10.1016/S0040-1951(98)00177-2.

Walley, C. D. (2001), The Lebanon passive margin and the evolution of the Levantine Neo-Tethys, in *Peri-Tethys Memoir 6: Peri-Tethyan rift/Wrench basins and passive margins*, edited by P. A. Ziegler, W. Cavazza, A. H. F. Robertson, and S. Crasquin-Soleau, pp. 407–439, Memoire du Museum national d'histoire naturelle, Paris.

Walsh, J. J., and J. Watterson (1987), Distributions of cumulative displacement and seismic slip on a single normal fault surface, *J. Struct. Geol.*, *9*(8), 1039–1046.

Walsh, J. J., and J. Watterson (1988), Analysis of the relationship between displacements and dimensions of faults, *J. Struct. Geol.*, *10*(3), 239–247.

Walsh, J. J., and J. Watterson (1989), Displacement gradients on fault surfaces, *J. Struct. Geol.*, *11*(3), 307–316.

Walsh, J. J., and J. Watterson (1991), Geometric and kinematic coherence and scale effects in normal fault systems, in *The geometry of normal faults*, vol. 56, edited by A. M. Roberts, G. Yielding, and B. Freeman, pp. 193–203, Geological Society, London, Special Publications.

Walsh, J. J., J. Watterson, W. R. Bailey, and C. Childs (1999), Fault relays , bends and branch-lines, *J. Struct. Geol.*, *21*, 1019–1026.

Walsh, J. J., A. Nicol, and C. Childs (2002), An alternative model for the growth of faults, *J. Struct. Geol.*, *24*, 1669–1675.

Walsh, J. J., W. R. Bailey, C. Childs, A. Nicol, and C. G. Bonson (2003), Formation of segmented normal faults: a 3-D perspective, *J. Struct. Geol.*, *25*(8), 1251–1262, doi:10.1016/S0191-8141(02)00161-X.

Watterson, J. (1986), Fault dimensions, displacements and growth, *Pure Appl. Geophys.*, *124*(1/2), 365–373.

Watterson, J., J. J. Walsh, A. Nicol, P. A. R. Nell, and P. G. Bretan (2000), Geometry and origin of a polygonal fault system, *J. Geol. Soc. London.*, *157*(1995), 151–162.

Wdowinski, S., Y. Bock, G. Baer, L. Prawirodirdjo, N. Bechor, S. Naaman, R. Knafo, Y. Forrai, and Y. Melzer (2004), GPS measurements of current crustal movements along the Dead Sea Fault, *J. Geophys. Res.*, *109*, doi:10.1029/2003JB002640.

Weijermars, R. (1986), Flow behaviour and physical chemistry of bouncing putties and related polymers in view of tectonic laboratory applications, *Tectonophysics*, *124*, 325–358.

Welch, M. J., R. K. Davies, R. J. Knipe, and C. Tueckmantel (2009), A dynamic model for fault nucleation and propagation in a mechanically layered section, *Tectonophysics*, *474*(3-4), 473–492, doi:10.1016/j.tecto.2009.04.025.

Wells, D. L., and K. J. Coppersmith (1994), New Empirical Relationships among Magnitude , Rupture Length , Rupture Width , Rupture Area , and Surface Displacement, *Bull. Seismol. Soc. Am.*, *84*(4), 974–1002.

Westaway, R. (2004), Kinematic consistency between the Dead Sea Fault Zone and the Neogene and Quaternary left-lateral faulting in SE Turkey, *Tectonophysics*, *391*, 203–237, doi:10.1016/j.tecto.2004.07.014.

Wibberley, C. A. J., J. Petit, and T. Rives (2007), The effect of tilting on fault propagation and network development in sandstone – shale sequences : a case study from the Lodève Basin, southern France, *J. Geol. Soc. London.*, *164*, 599–608, doi:10.1144/0016-76492006-047.

Wilkins, S. J., and M. R. Gross (2002), Normal fault growth in layered rocks at Split Mountain, Utah: influence of mechanical stratigraphy on dip linkage, fault restriction and fault scaling, *J. Struct. Geol.*, *24*, 1413–1429.

Wiprut, D., and M. D. Zoback (2002), Fault reactivation, leakage potential, and hydrocarbon column heights in the northern North Sea, in *Hydrocarbon seal quantification*, edited by A. G. Koestler and R. Hunsdale, pp. 203–219, Elsevier, Amsterdam.

Withjack, M. O., and S. Callaway (2000), Active Normal Faulting Beneath a Salt Layer: An Experimental Study of Deformation Patterns in the Cover Sequence, *Am. Assoc. Pet. Geol. Bull.*, *5*(5), 627–651.

Woodcock, N. H. (1986), The role of strike-slit fault systems at plate boundaries, *Philos. Trans. R. Soc. London*, *317*(1539), 13–29.

Yousef, M., A. R. J. Moustafa, and M. Shann (2010), Structural setting and tectonic evolution of offshore North Sinai, Egypt, in *Evolution of the Levant margin and western Arabia platform since the Mesozoic*, vol. 341, edited by C. Homberg and M. Bachmann, pp. 65–84, Geological Society, London, Special Publications.

Zoback, M. D. (1991), State of stress and crustal deformation along weak transform faults, *Philos. Trans. R. Soc. A Math. Phys. Eng. Sci.*, *337*(1645), 141–150.

Zoback, M. D. (2010), *Reservoir Geomechanics*, Cambridge University Press.

Zviely, D., E. Galili, A. Ronen, A. Salamon, and Z. Ben-Avraham (2009), Reevaluating the tectonic uplift of western Mount Carmel, Israel, since the middle Pleistocene, *Quat. Res.*, *71*(2), 239–245, doi:10.1016/j.yqres.2008.11.008.

APPENDIX

Table showing the different amount of slip recorded by many authors using different techniques over the regional Arabian-African plate boundary and the different structures along this plate boundary.

	STRUCTURES					
	ARABIAN AFRICAN PLATE	**YAMMOUNEH**	**SERGHAYA**	**ROUM**	**MISSYAF FAULT**	**TOTAL LEBANESE RESTRAINING BEND**
Freund *et al.* 1965 Garfunkel 1981	>5.8 mm/a (time span: <18Ma, method used: geological offsets)					
Freund *et al.* 1965 Garfunkel 1981	8.5 ± 0.5 mm/a (time span: <18Ma, method used: geological offsets between Zahle and dead sea)					
Garfunkel 1981	0.5-1.0 cm/a (time span: last 20 Ma)					
Chu & Gordon 1998	8.4 ± 2.8 mm/a (time span: 3.2 Ma, method used: red sea seafloor spreading)					
Klinger *et al.* 2000	4.0 ± 2.0 mm/a (time span: >25ka, method used: geomorphology of Araba valley)					
Nemer & Meghraoui 2006				0.9 ± 0.2 mm/a (time span: since 6400-8500BC, method used: consistent offsets of small streams that incise a caliche horizon)		
Meghraoui *et al.* 2003				1 mm/a (method used: paleaoseismology over Roum fault	6.9 ± 0.1 mm/a (time span: ≈2 ka, method used: paleoseismology)	
Joffe & Garfunkel 1987	4.0-8.0 mm/a (method used: plate tectonic model)					
Ginat 1998		3.0 to 7.5 mm/a (method used: pleistocene drainage systems)				
McCluksy 2003	6.0 ± 2.0 mm/a (time span: 10 yr, method used: GPS)					

APPENDIX I

reilinger *et al* 2006	4.8 ± 0.4 mm/a (method used: GPS)				
Daeron *et al.* 2004		3.8 to 6.4 mm/a (time span: 25ka, method used: field observations, air and satellite images, topo maps of alluvial fans			
Gomez *et al.* 2007			3.9-6.1 mm/a (method used: cosmogenic dating of faulted alluvial fans)	1-2.0 mm/a	0.6-0.8 mm/a (method used: geometric calculations based on 0.8-1.1mm/a slip rate on yammouneh)
Gomez *et al.* 2007, 2003			1.4±0.2 mm/a		
Gomez *et al.* 2006		3.3-4.0 mm/a (time span: Pliocene/Quaternary, method used: offset of Barshin volcano in Syria)	1 mm/a (time span: since late Tortonian/Messinian, method used: mapping notched rivers over anti-lebanon)		
Gomez *et al.* 2007	4-5 mm/a (method used: GPS)				
Wdowinsky 2004	4-6 mm/a (method used: Geodetic estimates)				
Mahmoud 2005	4-6 mm/a (method used: Geodetic estimates)				
Westaway 2004 walley 1988		4-5 mm/a (method used: correlation of litani incision with inferred regional fluvial incision in northern arabian platform and eastern turkey)			
Westaway 1994	6.0 to 10.0 mm/a (time span: historic, method used: inferring seismic moment and historically documented earthquakes)				
Dubertret 1970 Hancock & Attiya 1979		7-11 km (time span: since late Miocene)			

Table showing the different experiments with variable parameters undertaken in this study. These consist of changing the materials, compression rate, velocity and geometry of the underlying plates. Nb = number of the experiment, SS = strike-slip and sil = silicone.

Date	Nb	Scanner	box	strike-slip (cm)	compression (cm)	velocity S-S	velocity comp	size stepover	Sil thickness (cm)	Sil size	sand thickness (cm)
17/03/2014	1	N	big	9	4.5 (2.25 each side)	10 cm/h	2.5 cm/h	5 x 1.9	/	/	5
18/03/2014	2	N	big	9	/	20 cm/h	/	5 x 1.9	/	/	3
18/03/2014	3	N	big	9	4.5 (2.25 each side)	20 cm/h	5 cm/h	5 x 1.9	/	/	3
21/03/2014	4	N	big	9	4.5 (2.25 each side)	20 cm/h	5 cm/h	5 x 1.9	/	/	3
26/03/2014	5	N	big	9	4.5 (2.25 each side)	20 cm/h	5 cm/h	9 x 4.5	/	/	3
15/05/2014	6	N	big	9	4.5 (2.25 each side)	20 cm/h	5 cm/h	9 x 3	/	/	3
16/05/2014	6 b	N	big	9	4.5 (2.25 each side)	20 cm/h	5 cm/h	9 x 3	/	/	3
21/05/2014	7	N	big	9	4.5 (2.25 each side)	40 cm/h	10 cm/h	9 x 3	1.5	70x41cm	3
22/05/2014	8	N	big	9	4.5 (2.25 each side)	20 cm/h	5 cm/h	9 x 3	1.3	70x41cm	3
22/05/2014	9	N	big	9	4.5 (2.25 each side)	10 cm/h	5 cm/h	9 x 3	1.5	64 x 41.5	3
08/07/2014	10	N	big	9	4.5 (2.25 each side)	40 cm/h	10 cm/h	9 x 3	1	65 x 38.5	3
09/07/2014	11	N	big	9	4.5 (2.25 each side)	40 cm/h	10 cm/h	9 x 3	1	65 x 41	2
10/07/2014	12	N	big	9	4.5 (2.25 each side)	50 cm/h	12.5 cm/h	9 x 3	1	65 x 41	2
11/07/2014	13	N	big	9	4.5 (2.25 each side)	5 cm/h	1.25 cm/h	9 x 3	1	65 x 41	2
11/07/2014	14	N	big	9	/	50 cm/h	/	9 x 3	1	65 x 41	2
17/07/2014	15	Y 5238	big	9	/	50 cm/h	/	9 x 3	1	65 x 41	0.9 + 0.2 (pyrex) +0.9
22/07/2014	16	N	small	/	10 cm	0	50 cm/h	/	1	75 x 39	2
23/07/2014	17	Y 5244	big	9	4.5 (2.25 each side)	50 cm/h	12.5 cm/h	9 x 3	1	65 x 41	0.9 + 0.2 (pyrex) +0.9
29/07/2014	18	Y 5252	big	9	/	50 cm/h	/	9 x 3	1	65 x 41	0.9 + 0.2 (pyrex) +0.9
31/07/2014	19	N	big	9	4.5 (2.25 each side)	50 cm/h	12.5 cm/h	9 x 3	1	65 x 41	2
31/07/2014	20	N	small	/	7	/	10 cm/h	/	1.3	75 x 39	2.5
01/08/2014	21	N	small	/	8	/	5 cm/h	/	1.3	75 x 39	4
04/08/2014	22	N	small	/	7	/	5 cm/h	/	1.3	75 x 39	2.5
08/08/2014	23	Y 5268	small	/	7.5 cm	/	5 cm/h	/	1.3	75 x 39	2.4 cm (six 0.3 layers)
20/08/2014	24	Y 5272	small	/	6.5 cm	/	5 cm/h	/	1.3	75 x 39	2.4 cm (six 0.3 layers)
22/08/2014	25	Y 5273	big	9	4.5 (2.25 each side)	50 cm/h	12.5 cm/h	9 x 3	1	70x41cm	2.3(six 0.3 layers, last 0.5
28/08/2014	26	N	small	/	6.5 cm	/	10 cm/h	/	1.3	75 x 39	2.5

APPENDIX II

08/10/2014	27	N	big	9	4.5 (2.25 each side)	50 cm/h	12.5 cm/h	9 x 3	1 (discontinuities below)	70x41cm	2
13/10/2014	28	N	big	9	4.5 (2.25 each side)	50 cm/h	12.5 cm/h	9 x 3	1 (graben at 60° in silicone)	70x41cm	2
14/10/2014	29	N	big	9	4.5 (2.25 each side)	50 cm/h	12.5 cm/h	9 x 3	1 (graben at 20° in silicone	70x41cm	2
17/10/2014	30	Y (bad)	big	9	4.5 (2.25 each side)	50 cm/h	12.5 cm/h	9 x 3	1 (graben at 60° in silicone)	70x41cm	2
27/10/2014	31	N	big	9	4.5 (2.25 each side)	50 cm/h	12.5 cm/h	9 x 3	1 (graben at 20° in silicone	70x41cm	2
28/10/2014	32	N	big	9	4.5 (2.25 each side)	50 cm/h	12.5 cm/h	9 x 3	1 (graben at 20° in silicone	70x41cm	2
29/10/2014	33	N	big	9	4.5 (2.25 each side)	50 cm/h	12.5 cm/h	9 x 3	1 (graben at 20° in silicone	70x41cm	2
29/10/2014	34	N	big	9	4.5 (2.25 each side)	50 cm/h	12.5 cm/h	9 x 3	1 (graben at 20° in silicone	70x41cm	2
31/10/2014	35	Y 5331	big	9	4.5 (2.25 each side)	50 cm/h	12.5 cm/h	9x3	1 (graben at 20° in silicone	70x41cm	0.6+0.3(cor)+0.3+0.3(pyrex)+0.5
09/12/2014	36	N	big	/	2.25 (1.125 each side)	/	6.25 cm/h	9 x 3	1 (graben at 20° in silicone	70x41cm	2
10/12/2014	37	N	big	9	2.25 (1.125 each side)	50 cm/h	6.25 cm/h	9 x 3	1 (graben at 20° in silicone	70x41cm	2
12/10/2014	38	N	big	9	2.25 (1.125 each side)	50 cm/h	6.25 cm/h	9 x 3	1 (graben at 20° in silicone	70x41cm	2
22/01/2015	39	N	big	9	2.25 (1.125 each side)	50 cm/h	6.25 cm/h	9 x 3	1 (graben at 20° in silicone	70x41cm	1.5
28/01/2015	40	Y	big	9	2.25 (1.125 each side)	50 cm/h	6.25 cm/h	9 x 3	1 (graben at 20° in silicone	70x41cm	0.6+0.3(cor)+0.3+0.3(pyrex)+0.5
30/01/2015	41	Y	big	9	4.5 (2.25 each side)	50 cm/h	12.5 cm/h	9 x 3	1	70x41cm	0.6+0.3(cor)+0.3+0.3(pyrex)+0.6
11/04/2015	42	Y	big	9	2.25 (1.125 each side)	50 cm/h	6.25 cm/h	9 x 3	1 (graben at 20° in silicone	70x41cm	0.6+0.3(cor)+0.3+0.3(pyrex)+0.7
16/3/2015	43	N	Big	9	2.25 (1.125 each side)	5 cm/h	5 cm/h	9 x 3	1 (graben at 20° in silicone	70x41cm	2
17/4/2015	44	N	big	9	2.25 (1.125 each side)	5 cm/h	5 cm/h	9 x 3	1 (graben at 20° in silicone	70x41cm	2

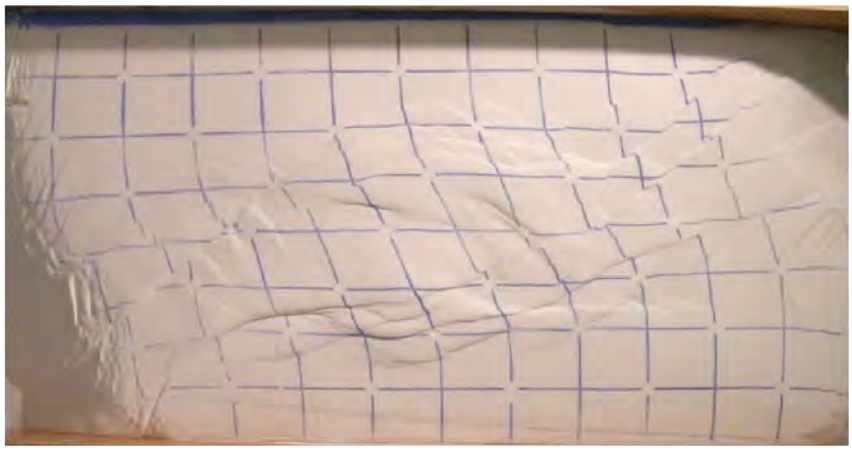

Stepover setup

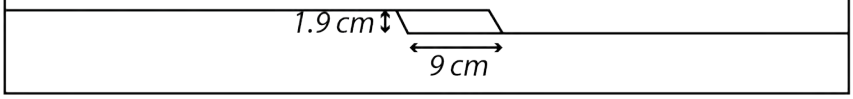

Experiment Nb: 1

Objectives:

Thickness sand: 5 cm

Thickness silicone: n/a

Velocity strike-slip: 10 cm/h

Velocity compression:2.5 cm/h

Stepover setup

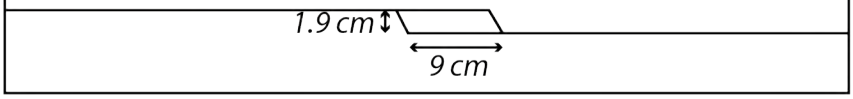

Experiment Nb: 2 (A)

Objectives: effect of compression

Thickness sand: 3 cm

Thickness silicone: n/a

Velocity strike-slip: 20 cm/h

Velocity compression: n/a

Stepover setup

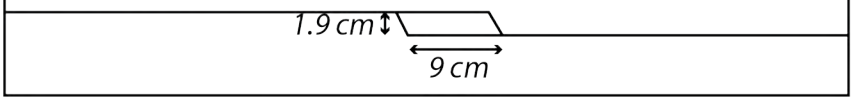

Experiment Nb: 3 (B)

Objectives: effect of compression

Thickness sand: 3 cm

Thickness silicone: n/a

Velocity strike-slip: 20 cm/h

Velocity compression: 5 cm/h

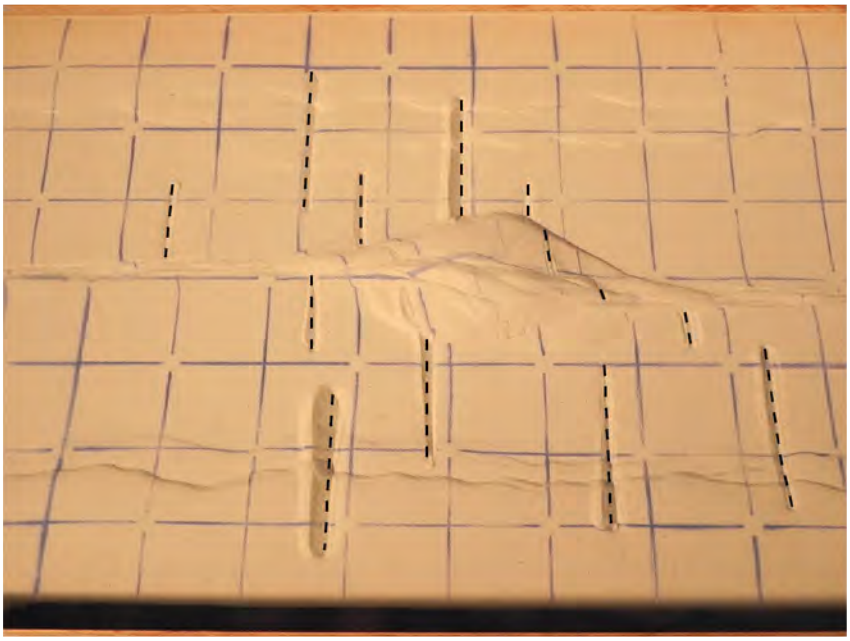

Stepover setup

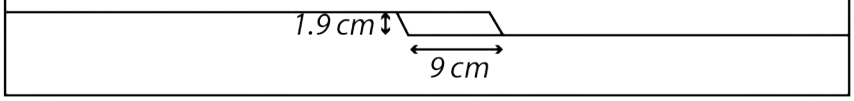

Experiment Nb: 4

Objectives: Fault reactivation in brittle medium

Thickness sand: 3 cm

Thickness silicone: n/a

Velocity strike-slip: 20 cm/h

Velocity compression: 5 cm/h

- - - - - Faults created in the sand prior to compression and after model construction

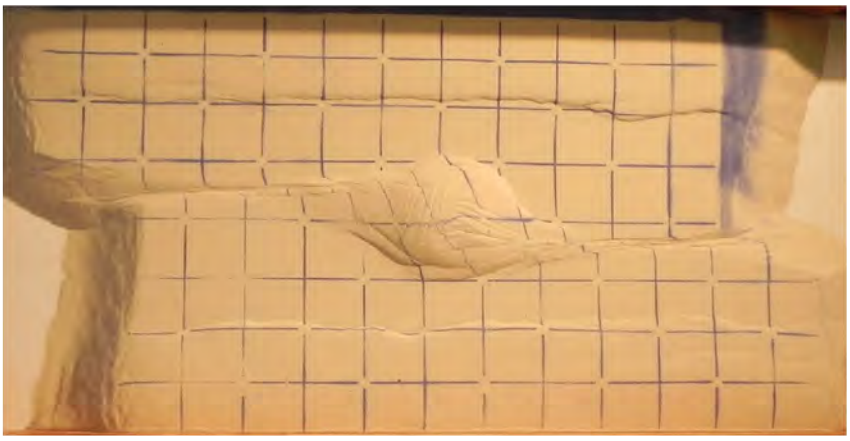

Stepover setup

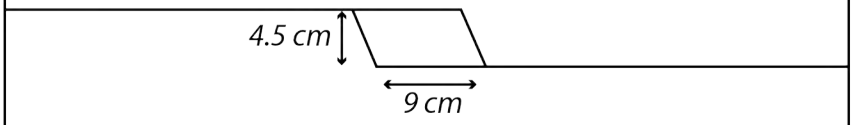

Experiment Nb: 5 (C)

Objectives: Change in stepover size

Thickness sand: 3 cm

Thickness silicone: n/a

Velocity strike-slip: 20 cm/h

Velocity compression: 5 cm/h

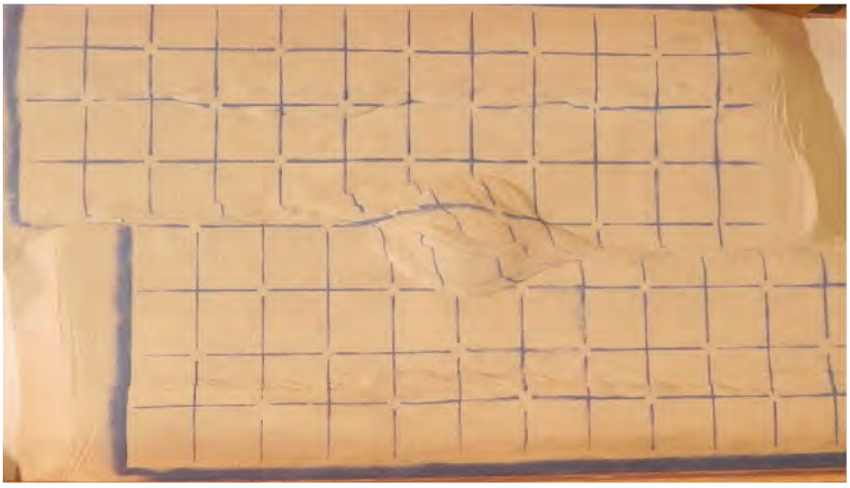

Stepover setup

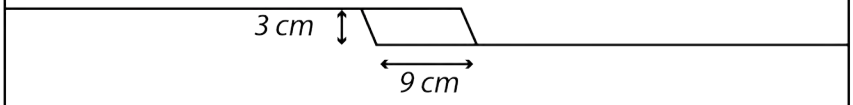

Experiment Nb: 6 (D)

Objectives: Change in stepover size

Thickness sand: 3 cm

Thickness silicone: n/a

Velocity strike-slip: 20 cm/h

Velocity compression: 5 cm/h

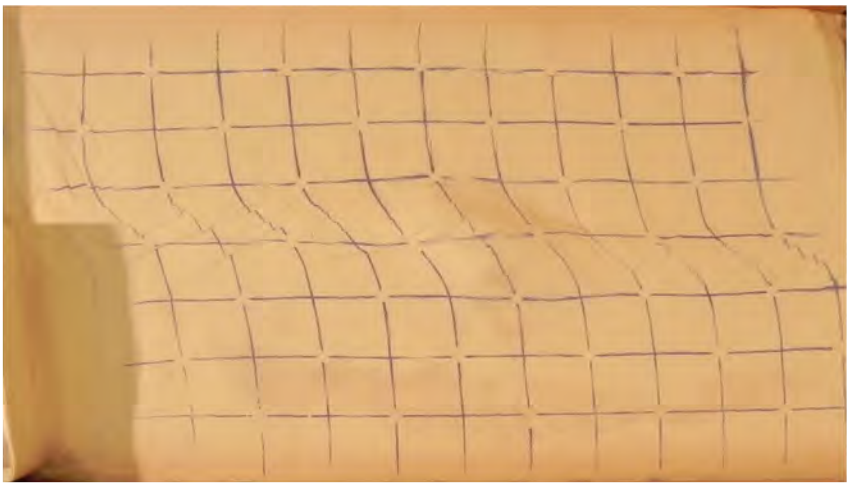

Stepover setup

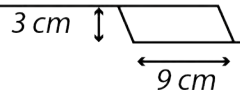

Experiment Nb: 7

Objectives: Usage of silicone

Thickness sand: 3 cm

Thickness silicone: 1 cm

Velocity strike-slip: 40 cm/h

Velocity compression: 10 cm/h

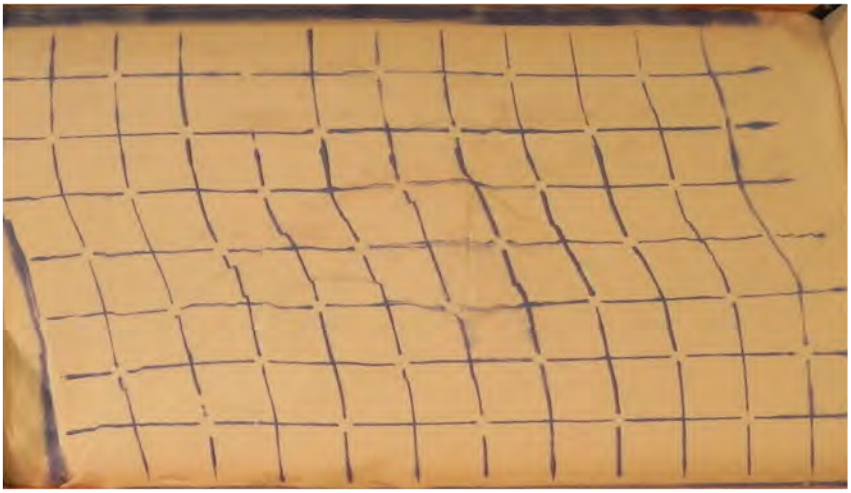

Stepover setup

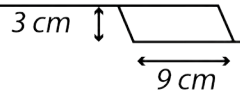

Experiment Nb: 8

Objectives: Change in silicone thickness and velocity

Thickness sand: 3 cm

Thickness silicone: 1.3 cm

Velocity strike-slip: 20 cm/h

Velocity compression: 5 cm/h

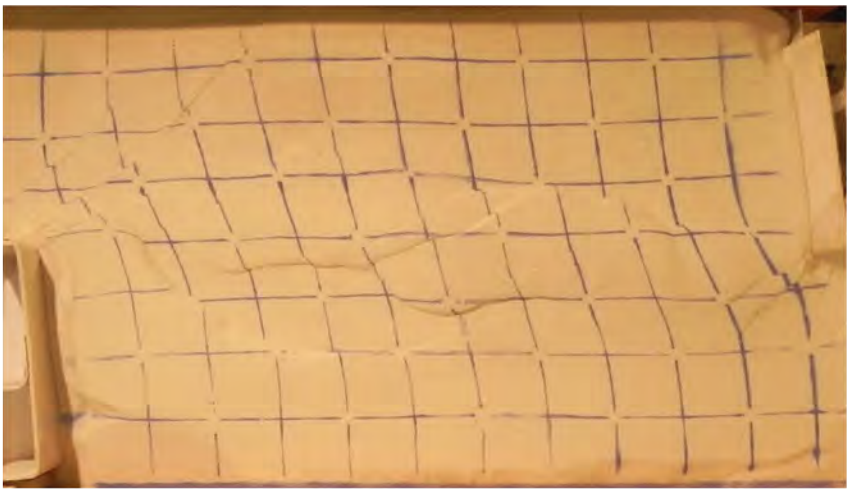

Stepover setup

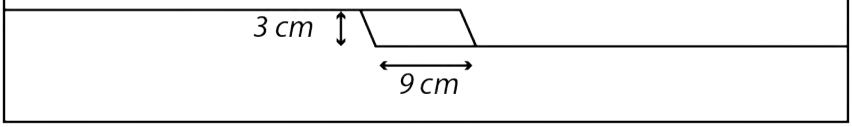

Experiment Nb: 9

Objectives: Change in velocity

Thickness sand: 3 cm

Thickness silicone: 1.5 cm

Velocity strike-slip: 10 cm/h

Velocity compression: 2.5 cm/h

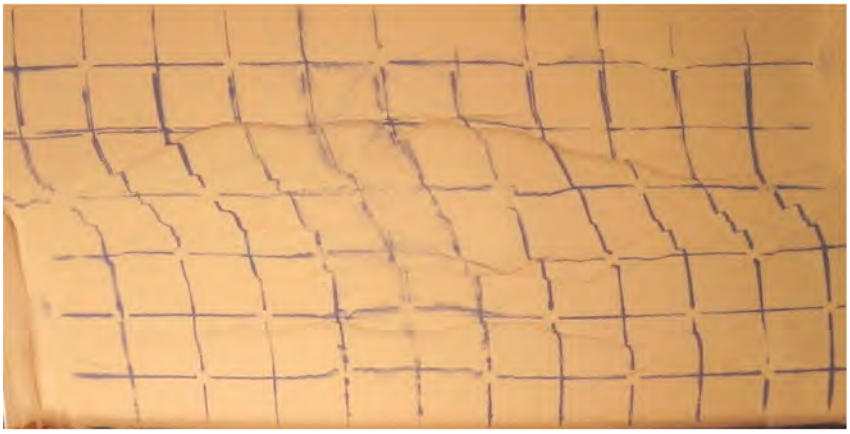

Stepover setup

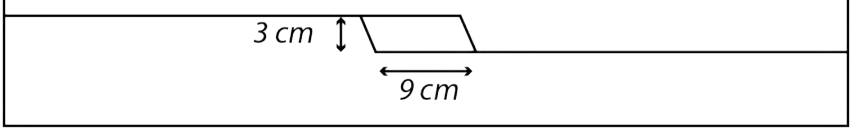

Experiment Nb: 10

Objectives: Change in silicone thickness

Thickness sand: 3 cm

Thickness silicone: 1

Velocity strike-slip: 40 cm/h

Velocity compression: 10 cm/h

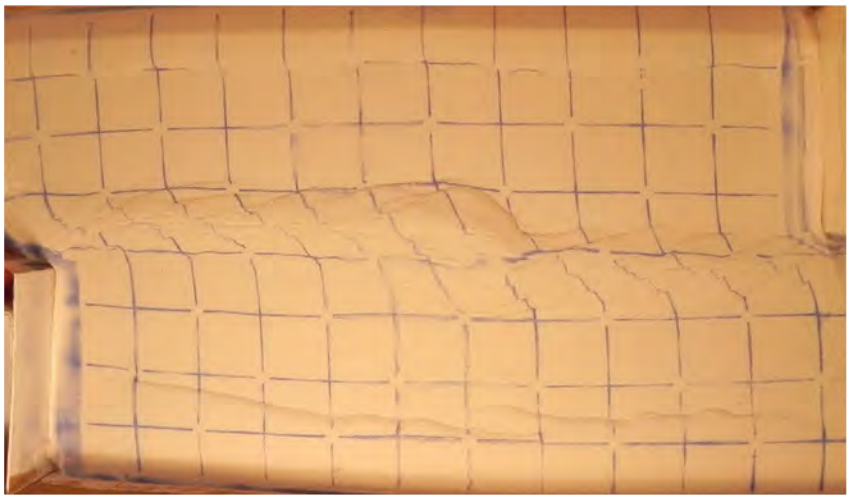

Stepover setup

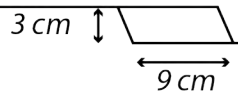

Experiment Nb: 11

Objectives: change of sand thickness

Thickness sand: 2 cm

Thickness silicone: 1 cm

Velocity strike-slip: 40 cm/h

Velocity compression: 5 cm/h

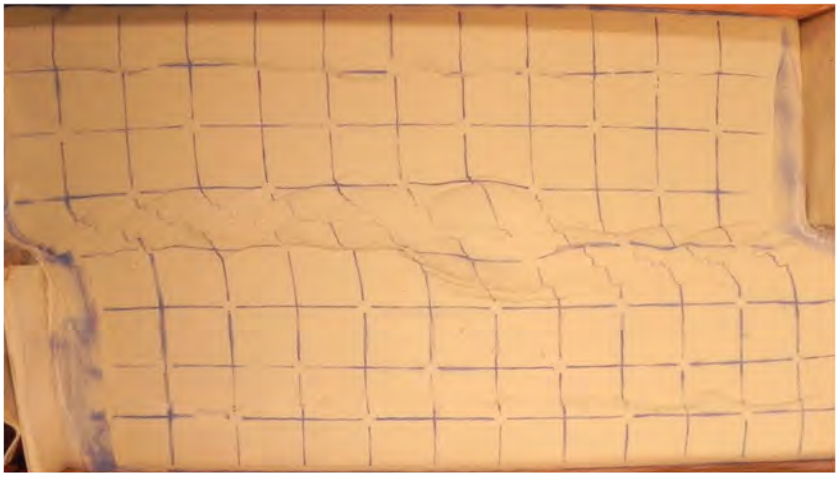

Stepover setup

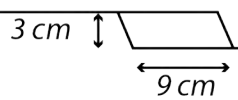

Experiment Nb: 12 (I)

Objectives: change of velocity

Thickness sand: 2 cm

Thickness silicone: 1 cm

Velocity strike-slip: 50 cm/h

Velocity compression: 12.5 cm/h

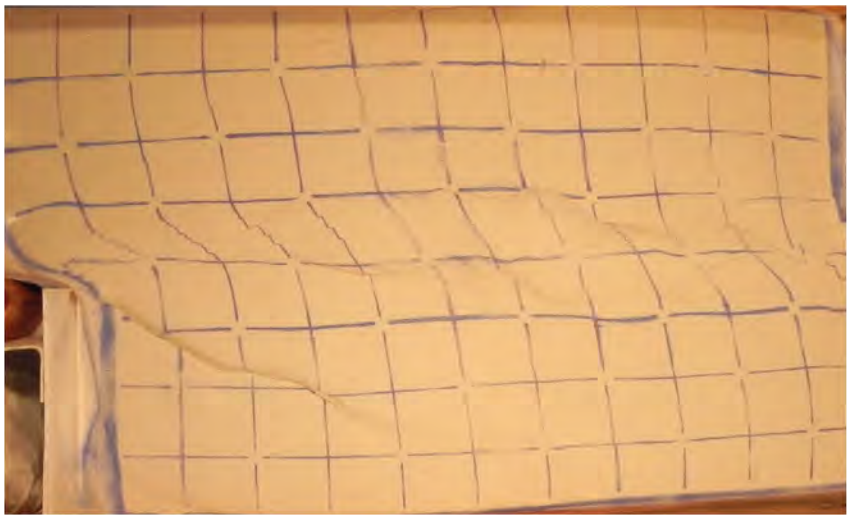

Stepover setup

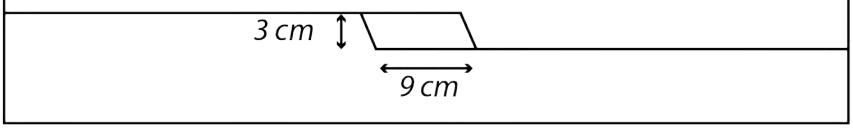

Experiment Nb: 13

Objectives: change of velocity

Thickness sand: 2 cm

Thickness silicone: 1 cm

Velocity strike-slip: 5cm/h

Velocity compression: 1.25 cm/h

Photos of experiments 14 & 15 are unavailable due to a technical difficulty

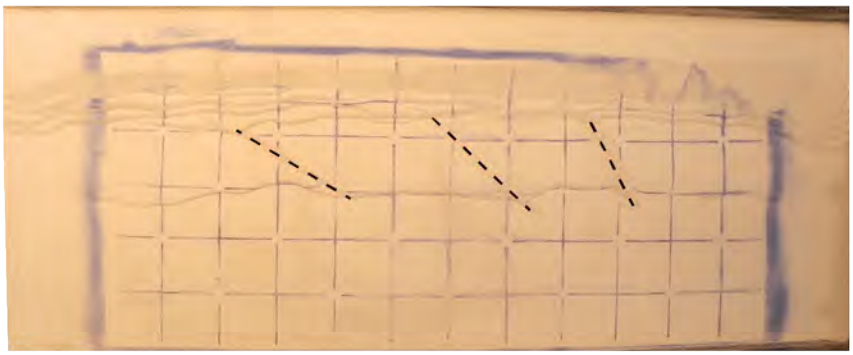

No Stepover

- - - - - Faults created in the sand prior to compression and after model construction

Experiment Nb: 16 (E)

Objectives: Fault reactivation under compression

Thickness sand: 2 cm

Thickness silicone: n/a

Velocity strike-slip: n/a

Velocity compression: 50 cm/h

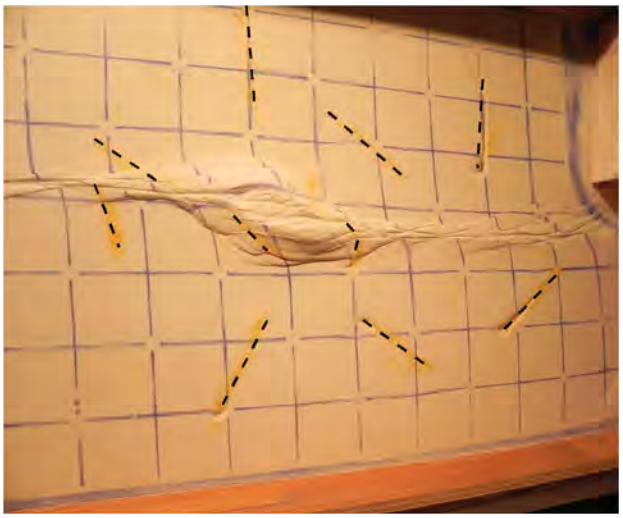

Stepover setup

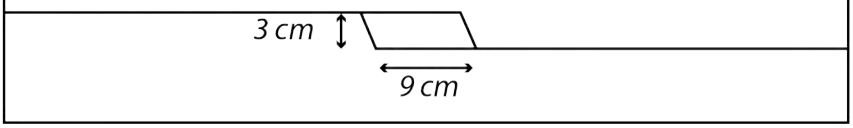

Experiment Nb: 18 (F)

Objectives: Fault reactivation in brittle medium (made in sand. Without compression, only S-S

Thickness sand: 2 cm

Thickness silicone: 1 cm

Velocity strike-slip: 50 cm/h

Velocity compression: n/a

- - - - - Faults created in the sand prior to compression and after model construction

Experiments 17 is a repetition of 12 under the CT scanner

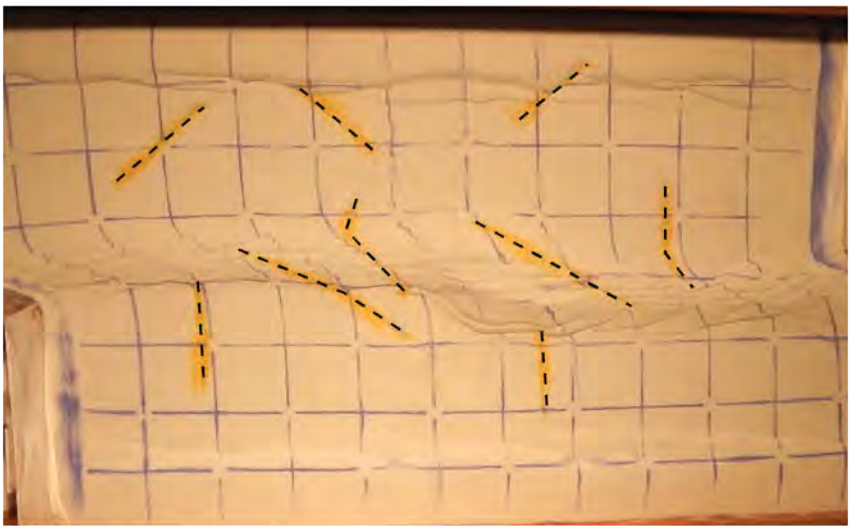

Stepover setup

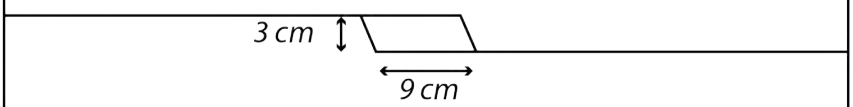

Experiment Nb: 19 (G)

Objectives: Fault reactivation in brittle medium (made in sand). With compression

Thickness sand: 2 cm

Thickness silicone: 1 cm

Velocity strike-slip: 50 cm/h

Velocity compression: 12.5 cm/h

- - - - - Faults created in the sand prior to compression and after model construction

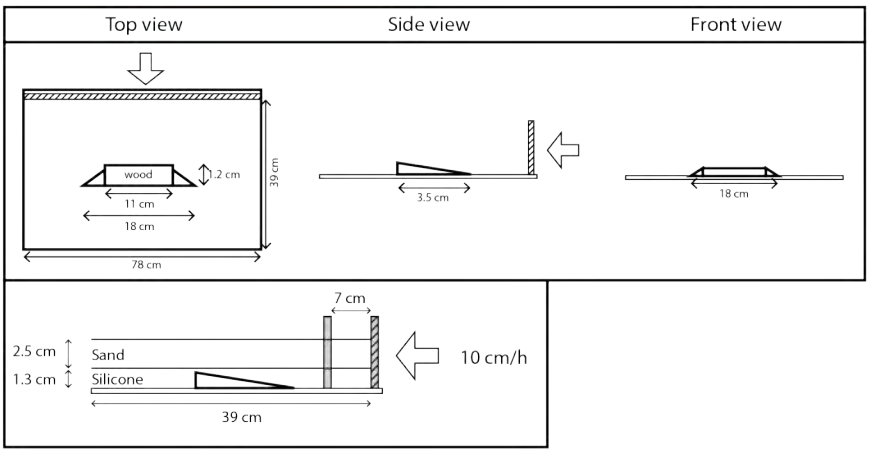

Experiment Nb: 20

Objectives: Effect of discontinuities below silicone

Thickness sand: 2.5 cm

Thickness silicone: 1.3 cm

Velocity strike-slip: n/a

Velocity compression: 10 cm/h

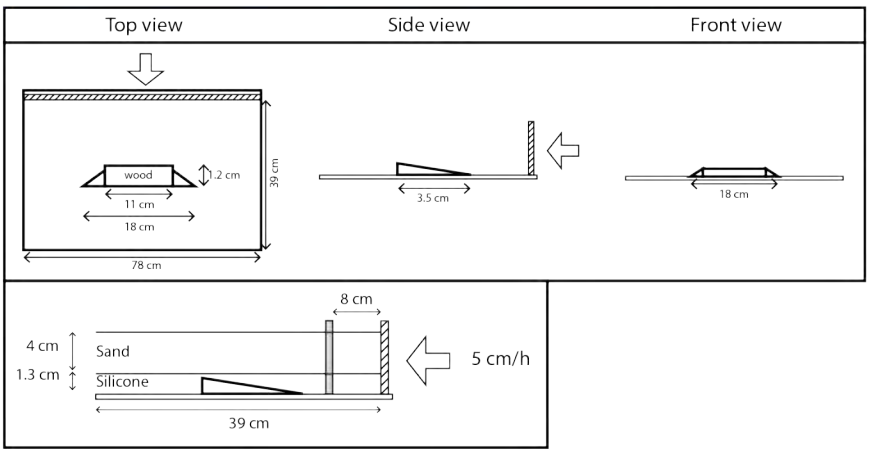

Experiment Nb: 21

Objectives: Effect of discontinuities below silicone. Change of sand thickness and velocity

Thickness sand: 4 cm

Thickness silicone: 1.5 cm

Velocity strike-slip: n/a

Velocity compression: 5 cm/h

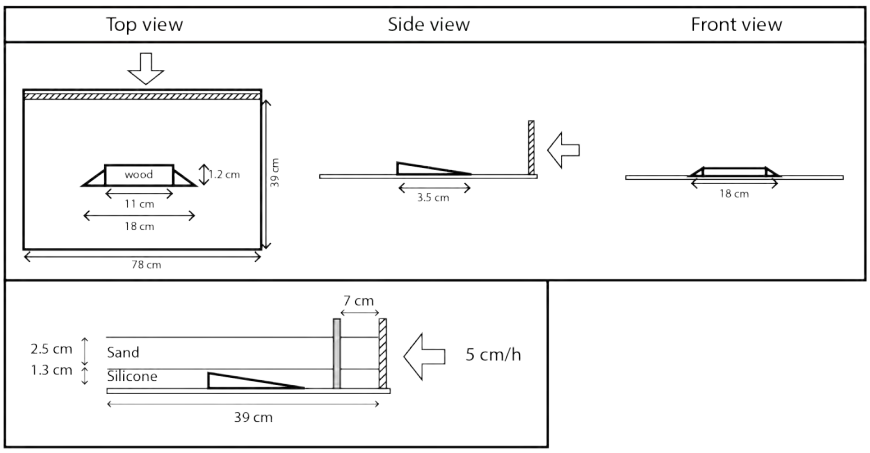

Experiment Nb: 22

Objectives: Effect of discontinuities below silicone. Change of sand thickness and velocity

Thickness sand: 2.3 cm

Thickness silicone: 1.5 cm

Velocity strike-slip: n/a

Velocity compression: 5 cm/h

Experiments 23 & 24 are a repetition of 22 under the CT scanner

Photos of experiments 25 are unavailable due to a technical difficulty

Experiments 26 is a repetition of 20

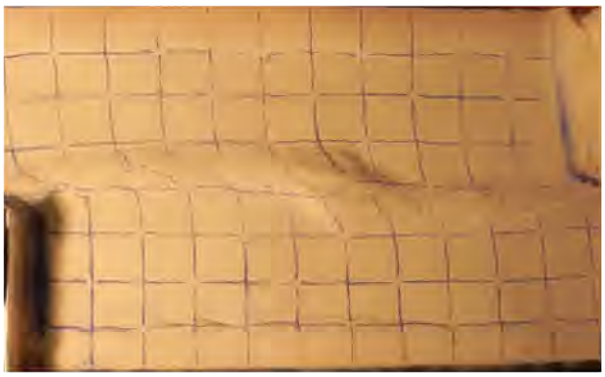

Initial setup

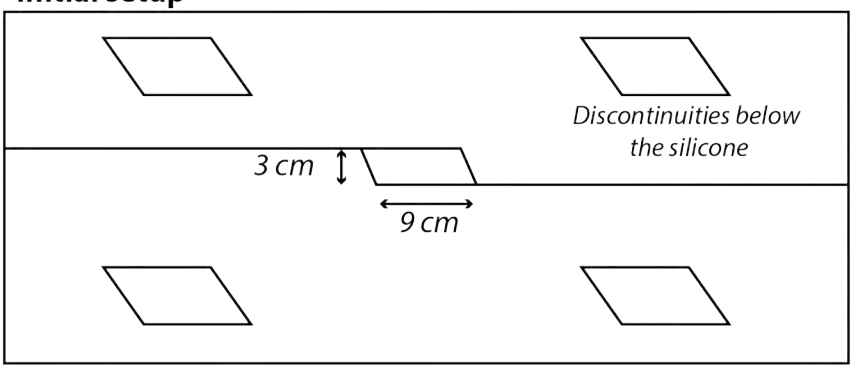

Experiment Nb: 27 (H)

Objectives: Effect of discontinuities below the silicone

Thickness sand: 2 cm

Thickness silicone: 1 cm

Velocity strike-slip: 50 cm/h

Velocity compression: 12.5 cm/h

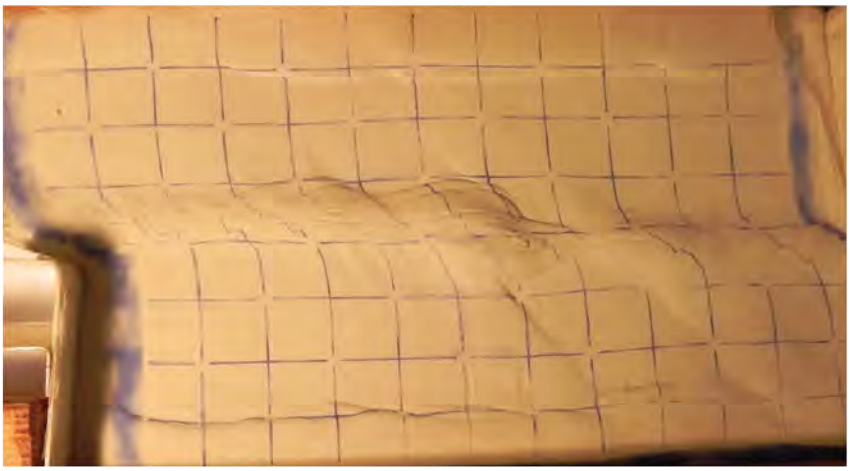

Initial setup

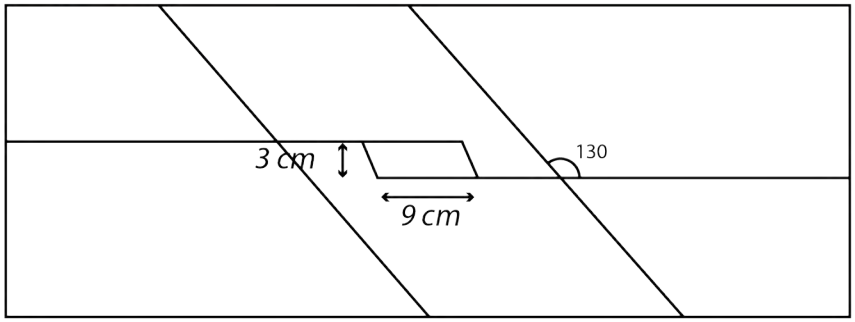

Experiment Nb: 28

Objectives: Effect of graben within the silicone below the sand

Thickness sand: 2 cm

Thickness silicone: 1 cm

Velocity strike-slip: 50 cm/h

Velocity compression: 12.5 cm/h

Graben geometry:

Experiment 30 is a repetition of 12 under the CT scanner

Experiments 29, 31, 32, 33 & 34 are a repetition of 35

Initial setup

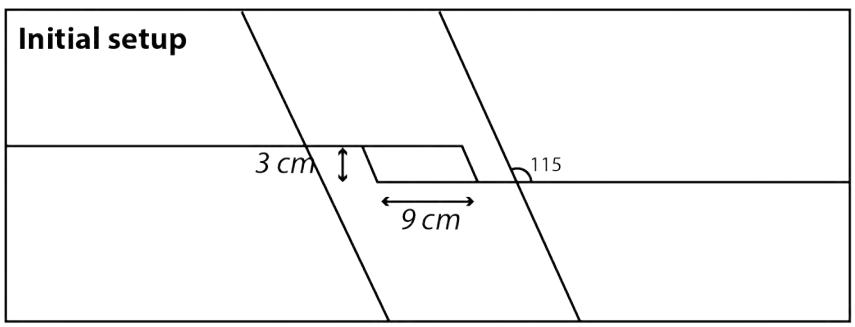

Experiment Nb: 35

Objectives: Effect of graben within the silicone below the sand. Varying graben geometry

Thickness sand: 2 cm

Thickness silicone: 1 cm

Velocity strike-slip: 50 cm/h

Velocity compression: 12.5 cm/h

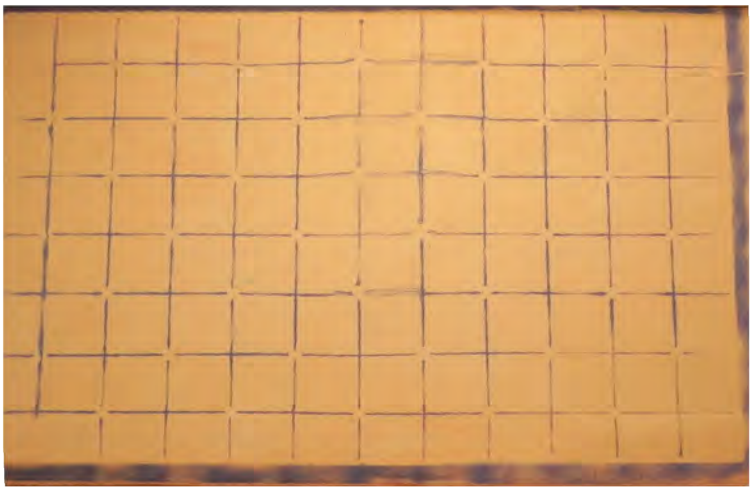

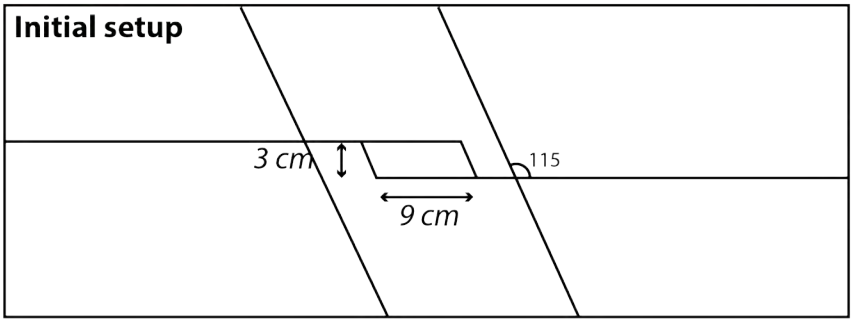

Experiment Nb: 36

Objectives: effect of compression on the graben

Thickness sand: 2 cm

Thickness silicone: 1 cm

Velocity strike-slip: n/a

Velocity compression: 6.25 cm/h

Experiments 37 & 38 are a repetition of 35

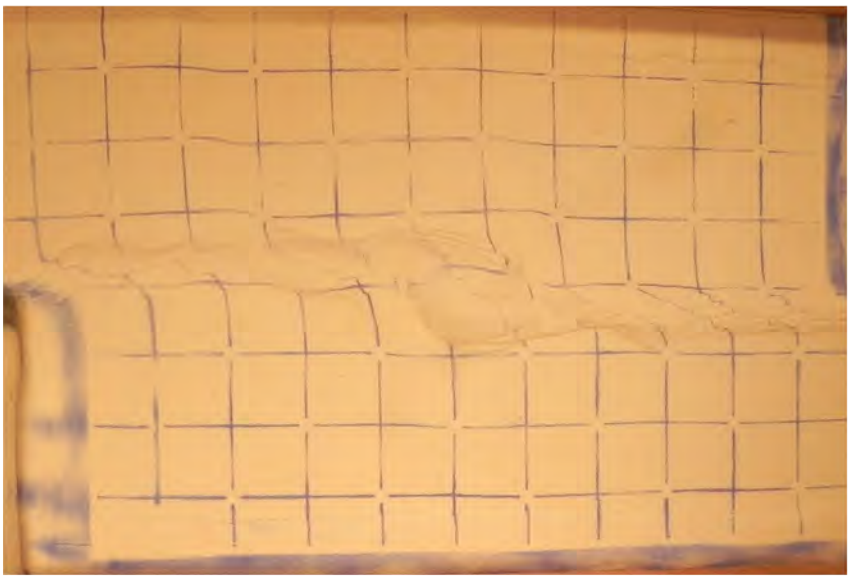

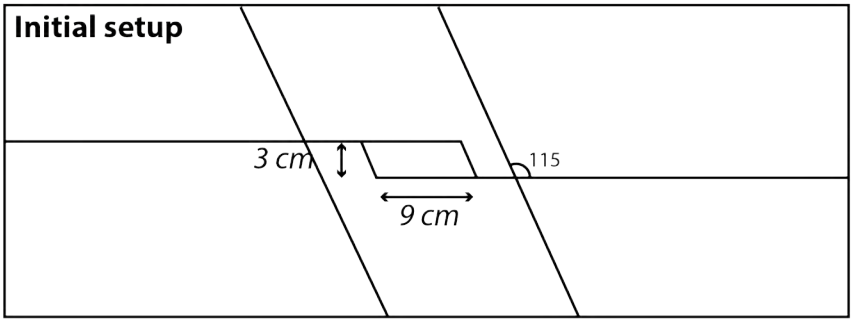

Experiment Nb: 39 (J)

Objectives: Effect of graben within the silicone below the sand. Varying sand thickness

Thickness sand: 1.5 cm

Thickness silicone: 1 cm

Velocity strike-slip: 50 cm/h

Velocity compression: 6.25 cm/h

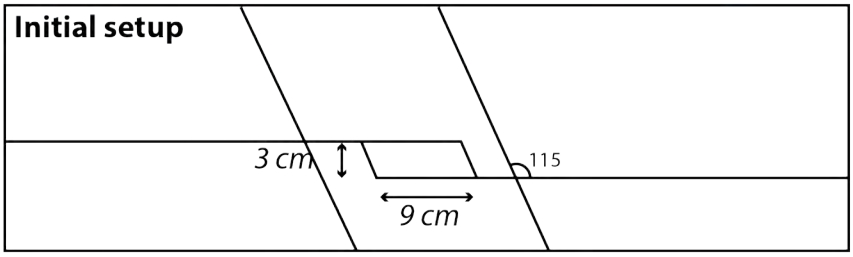

Experiment Nb: 42

Objectives: Effect of compression followed by strike-slip

Thickness sand: 2 cm

Thickness silicone: 1 cm

Velocity strike-slip: 50 cm/h

Velocity compression: 6.25 cm/h

Experiments 40 is a repetition of 39

Experiments 41 is a repetition of 19 under CT scanner

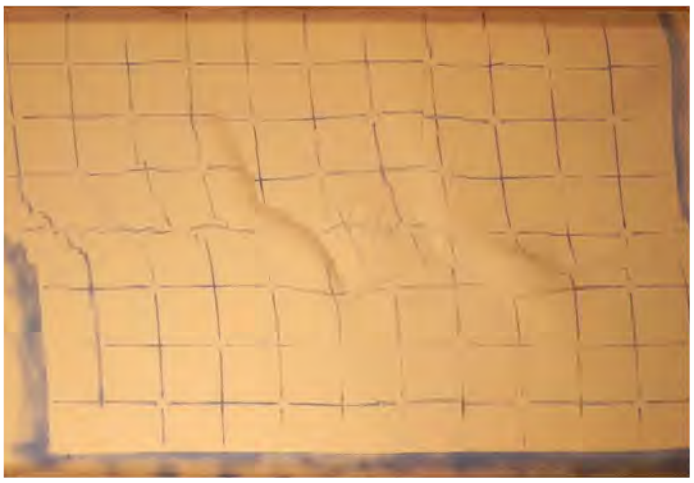

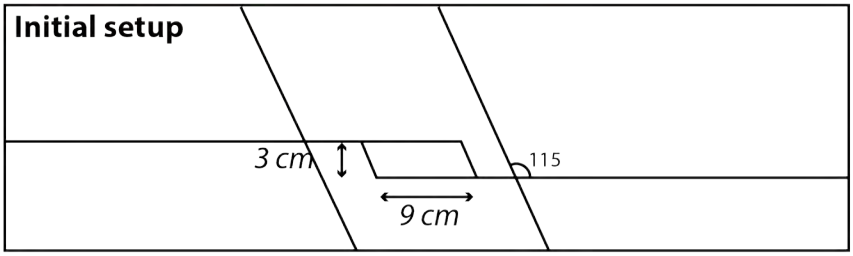

Experiment Nb: 43

Objectives: Effect of compression followed by strike-slip. Varying velocity

Thickness sand: 2 cm

Thickness silicone: 1 cm

Velocity strike-slip: 5 cm/h

Velocity compression: 5 cm/h

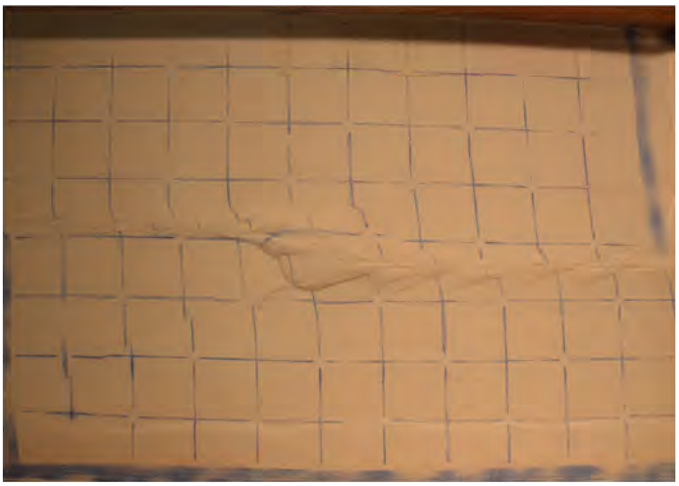

Popup dimensions

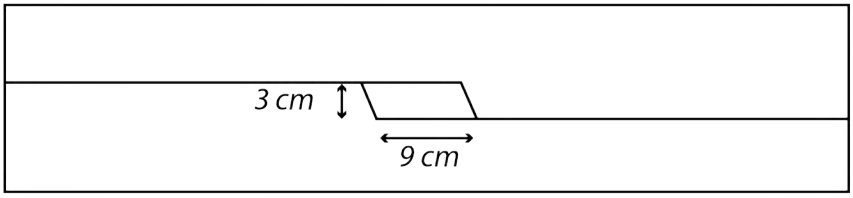

Experiment Nb: 44 (K)

Objectives: Effect of compression followed by strike-slip. Varying silicone thickness

Thickness sand: 2 cm

Thickness silicone: 0.5 cm

Velocity strike-slip: 5 cm/h

Velocity compression: 5 cm/h

ABSTRACT

The Levant Basin is located at the easternmost Mediterranean at the intersection of three major tectonic plates (Africa, Arabia, Eurasia and the smaller Anatolian microplate). The Levant Fracture System (Arabia-Africa plate boundary) borders the basin to its east and represents a 1000 km long left-lateral transform system linking rifting in the Red Sea with plate convergence along the Taurus Mountains (Arabia-Eurasia plate boundary). The Levant Basin is bordered to the north by the Cyprus Arc (Africa-Eurasia plate boundary). The interaction between these tectonic plates had important consequences on the evolution of the Levant Basin whereby its eastern boundary has been affected by deformation along the Levant Fracture System. This major plate boundary is associated with a restraining bend in Lebanon and has been active since the Late Miocene.

Until recent days, the absence of seismic data in the central Levant Basin was an obstacle against characterizing the tectonic setting of the basin. In this area, the geometry, kinematics and the age of the tectonic structures is poorly understood. A focal question thus remains on how the Levant Basin was affected by this adjacent plate boundary. Therefore, what is the impact of the deformation along the Levant Fracture System since the Late Miocene on this basin and how can we assess it? Has the latter been affected by other tectonic regimes prior to the onset of transpression? If so, how would the existing structures influence the style of modern deformation?

In this study, high quality 2D and 3D seismic reflection data (with two 4290 m3 3D seismic cubes and seven 830 km long 2D seismic lines) were interpreted allowing identification and timing of the structures in the Levant Basin offshore Lebanon. Several fault families, mapped along the margin, are remnants of a lasting and complex tectonic history since Mesozoic times. These include NNE-SSW striking thrust faults active during the early Tertiary and inactive since the Pliocene; NNE-SSW striking anticlines folded during the Late Miocene and overlying pre-existing structuresd; and ENE-WSW striking dextral strike-slip faults inherited from Mesozoic times and reactivated during the Late Miocene. Only the dextral strike-slip faults show evidence of current activity and are interpreted to be linked to transpression along the Levant Fracture System. They constitute the westward extension of the plate boundary, formed under a transpressif regime and a NW-SE compression. We have showed how this plate boundary has evolved through the Neogene with a decrease in the shortening component during the Pliocene.

The identification of pre-existing structures along the eastern Levant margin shed the light on the deep structuration affecting this area, inherited from Mesozoic tectonic events. The impact of these structures was tested through analogue modeling. Results indicated a considerable impact of pre-existing structures on the development of the restraining bend, localizing deformation at the onset of transpression and responsible of segmenting the restraining bend along an ENE direction. These ENE-WSW faults are thus major and are most likely associated with the deformation affecting the Palmyra basin since the Mesozoic, which is thus extending westward to Lebanon. This study has shown the important role of a margin on a strike-slip plate boundary. Namely, the development of antithetic faults (local dextral strike-slip faults in a regional sinistral strike-slip plate boundary) known in other similar plate boundaries is associated with a deep crustal anisotropy localizing the subsequent deformation.

On the other hand, the deep Levant Basin contains a NW-SE trending dense normal fault array, in contrast with crustal structures similar to the one described along the margin. The faults are remarkably layer-bound, contained in the Oligo-Miocene units only. Quantitative and qualitative seismic analysis of these normal faults was performed, yielding important information on their growth and evolution. Results showed that they nucleated during the Early Miocene as a result of volumetric contraction of the Oligo-Miocene host rock units. This hypothesis has consequences on our understanding of the geology of the Levant Basin as it requires that the Oligo-Miocene is formed by fine-grained sediments for faults to develop. Interpretation of fault displacement profiles also indicated that a strong mechanical stratigraphy affected their growth. The detailed 3D seismic characterization of these faults has provided insights on the growth of non-tectonic faults in sedimentary basins, most likely following the isolated fault model. This array in Lebanon provided a unique case-study whereby the interpretation results served to better understand the growth and evolution of polygonal faults, linearly oriented due to an anisotropic stress field.

__ " Yesterday i was clever, so i wanted to change the world.
Today i am wise, so i am changing myself" __ Rumi